THE ROLE OF PHOSPHOINOSITIDE 3-KINASE/AKT SIGNALING PATHWAY IN TUMOR-ASSOCIATED ANGIOGENESIS, WOUND HEALING, AND CARCINOGENESIS

Dissertation

Presented in Partial Fulfillment of the Requirements for

the Degree Doctor of Philosophy in the Graduate

School of The Ohio State University

By

Nesrine Ismail Affara, M.S.

The Ohio State University
2006

Dissertation Committee:

Dr. Fredika M. Robertson, Adviser

Dr. Robert M. Snapka

Dr. Anthony P. Young

Dr. Susheela Tridandapani

Approved by

_____

Adviser

Graduate Program in Molecular, Cellular, and Developmental Biology

ABSTRACT

The goal of the present studies was to localize two proteins known to be involved in regulation of cell proliferation and survival in specific cell populations in normal mouse skin, during multi-stage skin carcinogenesis, following skin injury, and during tumor angiogenesis. The proteins evaluated included activated Akt, as defined by phosphorylation of Akt at Serine-473 (pAkt) and mTOR, defined by phosphorylation of mTOR at Serine-2448 (pmTOR).

Our laboratory previously identified a novel murine VEGF splice variant, $VEGF_{205}$*, which was differentially expressed in mouse skin carcinomas, but not in normal skin. $VEGF_{205}$* encodes for a truncated 145 amino acid polypeptide with a unique 7 amino acid carboxyl-terminal tail, YVGAAAV, that is significantly different from the carboxyl-terminal tail of other mouse or human VEGF proteins previously identified. In the present studies, we demonstrate that $VEGF_{205}$* stimulated a significant increase in Akt phosphorylation at Serine-473 residue in human vascular endothelial cells compared to $VEGF_{120}$. Akt phosphorylation following exposure of endothelial cells to $VEGF_{205}$* was completely blocked by the PI3-K inhibitor, LY294002. Additionally, $VEGF_{205}$* induced phosphorylation of mTOR at Serine-2448 in a PI3-K-dependent manner. The selective activation of PI3-K/Akt signaling pathway in endothelial cells following exposure to $VEGF_{205}$* may provide utility as a potential molecular target for inhibiting skin tumor angiogenesis. In addition, $VEGF_{205}$* splice variant may serve as a useful diagnostic in oncology and may be used as a potential therapeutic agent in tissues whose vascular supply has been insufficient or inappropriate, including cardiovascular diseases.

One of the goals of the present study was to identify specific populations of cells, including mouse Keratinocyte stem cells (KSC) within a specific niche in hair follicles defined as “the bulge” region and preneoplastic papilloma cells that contain pAkt and

pmTOR during development of skin tumors using a murine multi-stage carcinogenesis model. The location of $CD34^+/K15^+$ KSC remained restricted to the bulge region throughout the 22-week time period examined during which pre-malignant papillomas developed and rapidly expanded. $CD34^+$ cells within the numerous hair follicles in hyperplastic skin treated with DMBA followed by repetitive exposure to 2 μg TPA were found to undergo proliferation during the process of multi-stage skin carcinogenesis. Our results also provide the first evidence for the presence of pAkt and pmTOR in $CD34^+/K15^+$ KSC localized to the ORS niche of the bulge region of mouse hair follicles. Within papillomas tissues isolated at 15 weeks following DMBA/TPA treatment, pAkt was confined to non-proliferating suprabasal cells. In addition to the presence of pmTOR in suprabasal cells within papillomas, there were fewer proliferating cells within the basal cell layer that contained pmTOR. Collectively, the present observations suggest that pAkt and pmTOR may allow the KSC cell population to evade terminal differentiation and to persist for long periods of time in their specific niche. Strategies that target pAkt and pmTOR may deplete both cells within the $CD34^+/K15^+$ KSC compartment as well as may impact the survival of non-proliferating suprabasal cells within pre-malignant papillomas.

The present studies further evaluated the temporal sequence of pAkt and pmTOR induction following acute and chronic exposure to UVB light in Skh/hr mice. Increases in pAkt staining at 24 hr and 48 hr following exposure to UVB light preceded the presence of pmTOR, which was only present at week 1 and week 20 following UVB exposure. Activation of pmTOR in epidermal keratinocytes at week 1 after exposure to UVB coincided with production of VEGF by epidermal keratinocytes and an increase in the number of blood vessels within the dermal area. The present results suggest that UVB induces a sequential activation of Akt and mTOR in epidermal and follicular keratinocytes, which may induce VEGF expression and stimulate formation of blood vessels within hyperplastic skin. Our results demonstrate the utility of targeting pAkt and pmTOR as potential anti-promoting molecules during UVB-induced skin carcinogenesis.

The temporal presence of pAkt and pmTOR in specific skin cell populations in wound tissues isolated from FVB/N mice as well as the location of $CD34^+/K15^+$ KSC were also examined over a 21-day time course of full-thickness wound healing. At 48 hr following wounding, all proliferating as well as non-proliferating epidermal keratinocytes localized to the wound edge contained pAkt, compared to the few epidermal

keratinocytes that contained pAkt in skin distal to the wound site. Following complete closure of the epithelial layer at day 5, the highest levels of pAkt immunoreactive protein were detected within proliferating and non-proliferating epidermal keratinocytes located within the wound site. At day 21 following wounding, levels of pAkt in epidermal keratinocytes along the wound healing line was comparable to that detected in keratinocytes distal to the wound site. pmTOR was only detected during the reepithelialization phase in epidermal keratinocytes located in the reepithelialized wound site, which coincided with the presence of pAkt. pAkt was also present within $CD34^+$ KSC, which remained localized to the bulge niche of hair follicles in skin tissues adjacent to the wound site at all times during cutaneous wound healing. While pAkt was present within the ORS as well as the IRS of hair follicles, pmTOR was confined specifically to cells in the ORS. The present results suggest that pAkt and pmTOR may serve as therapeutic strategies to enhance wound repair in chronic wounds that fail to heal, such as non-healing ulcers from patients with diabetes.

Using the highly invasive and metastatic human Hs578T breast tumor cell line and the slow growing and non-invasive human MCF-7 breast tumor cell line, the goal of the last series of studies was to compare the effects of the selective PI3-K inhibitor, LY294002, alone and in combination with the selective mTOR inhibitor, rapamycin, on tumor cell proliferation and phosphorylation of downstream targets of PI3-K and mTOR, including, 4E-BP1 and cyclin D1. Cell proliferation of Hs578T and MCF-7 breast tumor cells was significantly inhibited by the combination of LY294002 and rapamycin compared to the effect on proliferation by either agent alone. The combination of LY294002 and rapamycin also inhibited hyperphosphorylation of the slower migrating (δ, γ, β) species of phospho-4E-BP1, and significantly decreased cyclin D1 protein levels. These studies demonstrate that molecules downstream of IP3-K/Akt and mTOR, including hyperphosphorylated forms (δ, γ) of 4E-BP1, may provide therapeutic targets for inhibition of breast tumor cell proliferation.

Collectively, given that pAkt and pmTOR were present in KSC, skin tumor cells, as well as vascular endothelial cells undergoing angiogenesis, the present studies indicate that strategies that inhibit both Akt and mTOR signaling pathways may also be applicable for treatment of skin cancers. On the other hand, activation of Akt and mTOR signaling pathways may enhance regeneration of the vasculature in tissues whose vascular supply has been insufficient.

For my brother Habib

This dissertation is dedicated to you Habib, for the warrior that you were, for your courage and strong will to fight cancer. You did not lose the battle, you fought with hope and you refused to surrender…

You gave me strength when you needed it yourself; you gave me light when your days were surrounded by dark clouds; you made me smile and believe in myself, like you did yourself…

You will always be in my heart, an eternal candle guiding me throughout this journey….

ACKNOWLEDGMENTS

I would like to express my deep appreciation for my advisor Dr. Fredika Robertson, for the ambitious scientist she seeded in me, for her long efforts and dedication to teach me the art of scientific writing, the creativity in coming up with novel ideas and testing them, how to become an independent thinker and scientist, and for providing me with the set of survival tools that will travel with me wherever I go: patience, persistence, and confidence in oneself. I will always remember what you used to say to me, that the key to achieve things is to “Apply a seat of pants to seat of chair”, credited to Ernest Hemingway. Without your continuous training and valuable advice, it would not have been possible to achieve this dream.

I want to also express my gratitude for my committee members, Dr. Anthony Young for always believing in my abilities and supporting me, and Dr. Robert Snapka for the opportunities that you provided me and your continuous support for my career. I would like to also thank Dr. Susheela Tridandapani for serving on my committee and your critical reviews for the dissertation. I also want to thank Dr. John Bauer and Brandon Schanbacher for their help with the confocal microscopy and the use of digital image analysis softwares, and Dr. Susan Mallery for providing me with unlimited access to your lab and Ping Pei for sharing your technical expertise with me.

I also want to extend my gratitude to thank Dr. David Bisaro for believing in my potentials and giving me the chance to transfer to OSU to fulfill my dreams. I don’t know

how to convey my gratitude to Jan Zinaich, you were always there for me. I would like to also thank Edie Yamasaki, for making me feel like at home….

My deep appreciation goes for my friend Samar Al-Maalouf, for your cheerful e-mails and cards that brightened my days, for the science and troubleshooting hours that we shared over the phone, for being like my sister…. For Ihab Younis, for always being there for me… For Sama Sleiman, Nadine Bakkar, Hala Zahreddine, Joseph Stephan, and Nael Alami for your moral support.

I would like to express special thanks to Jose Saucedo, for your unlimited support and care that helped me survive the desperate moments of my brother's loss, for inciting in me the spirit of hope, success, and motivation, for the better person that you make me feel…

Special thanks to my colleague Jeni Prosperi, for laughing and crying with me throughout all these years, for your efforts to help me understand cultural differences, for sharing with me chocolate and candies, for always being there for me…..

I want to express my gratitude for my family, my mom in particular, for seeding in my character the strong ambition, the dedication, and the strong will… for giving me the opportunity to travel alone to follow my dreams, for believing in me, for your patience, for your suffering throughout the years, counting the days and years to have me in your arms…. for my dad Ismail, and my brothers Adham, Akram, Kareem, and Habib, you were with me in every step throughout my journey….

VITA

April 10, 1976……..Born- Saida, Lebanon

June 1997……Bachelor of Science-Biology, The American University of Beirut, Beirut, Lebanon

June 1999……Master of Sciences-Biology, The American University of Beirut, Beirut, Lebanon

January 2000-May 2001……...Graduate Student, Bowling Green State University, Bowling Green, Ohio, USA

June 2001-present……Graduate Student, The Ohio State University, Columbus, Ohio, USA

AWARDS

October 13, 2005 .....Society of Investigative Dermatalogy, Eugene M. Farber Endowment Travel Award, 54rd Annual Montagna Symposium on the Biology of Skin, Oregon

March 31, 2005 .....Award Winner, Graduate and Post-graduate Research Day, 4th Annual Integrated Research Day, OSU Medical Center, The Ohio State University

October 15, 2004 .....Scholar Travel Reimbursement, 53rd Annual Montagna Symposium on the Biology of Skin and 6th International Skin Carcinogenesis Conference, Oregon

April 1, 2004 .....Award Winner, Graduate and Post-graduate Research Day, 3rd Annual Integrated Research Day, OSU Medical Center, The Ohio State University

FELLOWSHIPS

July 1, 2004-June 31, 2005 .....Mary S. Muellhaupt Scholarship, through the Presidential Fellowship Competition, Spring 2004, Graduate School, The Ohio State University.

PUBLICATIONS

Research Publications

1. **Affara N.I.**,Trempus C.S., Schanbacher B.L., Pei P., Mallery S.R., Bauer J.A., and Robertson F.M. (2006) Activation of Akt and mTOR in $CD34^{+}/K15^{+}$ keratinocyte stem cells and skin tumors during multi-stage mouse skin carcinogenesis. *Anticancer Res*, **26** (4).

2. **Affara N.I.** and Robertson F.M. (2004). Vascular endothelial growth factor as a survival factor in tumor-associated angiogenesis. *In Vivo*, **18** (5): 525-42.

3. **Affara N.I.**, Schanbacher B.L., Mihm M.J., Cook A.C., Pei P., Mallery S.R., Trempus C.S., Bauer J.A., Robertson F.M. (2004). Activated Akt-1 in specific cell populations during multi-stage skin carcinogenesis. *Anticancer Res*. **24** (5A): 2773-81.

4. Farhat, G.N., **Affara, N.I.**, Gali-Muhtasib, H.U. (2001). Seasonal Changes in the Composition of the Essential Oil Extract of East Mediterranean sage (Salvia libanotica) and its Toxixity in Mice. *Toxicon*, **39** (10): 1601-5.

5. Gali-Muhtasib, H.U. and **Affara, N.I.** (2000). Chemopreventive Effects of Sage Oil on Skin Papillomas in Mice. *Phytomedicine* **7** (2): 129-136.

FIELDS OF STUDY

MAJOR FIELD: Molecular, Cellular, and Developmental Biology

TABLE OF CONTENTS

LIST OF TABLES

LIST OF FIGURES

LIST OF ACRONYMS

^{3}H-T	Methyl-[^{3}H]thymidine
4E-BP1	Eukaryotic initiation factor 4E (eIF4E)-binding protein 1
AML	Acute myeloid leukemia
Ang-1	Angiopoietin-1
ANOVA	One-way analyses of variance
BCC	Basal cell carcinoma
Bcl-2	B-cell lymphoma-2
BFGF	Basic fibroblast growth factor
Blb	Bulb
BrdU	Bromodeoxyuridine
Bu	Bulge
CCI-779	Cell cycle inhibitor-779
DAB	Diaminobenzidine
DAG	Diacylglycerol
DAPI	4', 6-diamidino-2-phenylindole
DMBA	7,12 dimethylbenz[a]anthracene
DP	Dermal papilla
eIF4E	eukaryotic initiation factor 4E
eNOS	Endothelial nitric oxide synthase
EPU	Epidermal proliferative unit
ER	Estrogen receptor
FKBP12	FK506-binding protein-12
FKHR	Forkhead transcription factor
FLIP	FLICE-inhibitory protein
Flk-1/KDR	Fetal liver kinase-1/Kinase-insert-domain-containing receptor
Flt-1	Fms-like tyrosine kinase-1
FRAP1	FK506-binding protein-rapamycin-associated protein
FRB	FKBP12-rapamycin binding
GSK-3β	Glycogen synthase kinase-3β
HIF-1α	Hypoxia-inducible factor-1
HS	Hair shaft
HUVEC	Human umbilical vein endothelial cells
IGF-1	Insulin-like growth factor-1
IKK	IκB kinase
ILK-1	Integrin-linked kinase-1
IOD	Integrated optical density
IRS	Inner root sheath
IκB	Inhibitor of nuclear factor-kappa B
K15	Cytokeratin 15

KSC	Keratinocyte stem cells
LRC	Label-retaining cells
LY294002	2-(4-morpholinyl)-8-phenylchrome
MAPK	Mitogen-activated protein kinase
mTOR	Mammalian target of rapamycin
MPO	Myeloperoxidase
NF-κB	Nuclear factor- κB
NMSC	Non-melanoma skin cancers
NP-1	Neuropilin-1
OD	Optical density
ODC	Ornithine decarboxylase
ORS	Outer root sheath
p70 S6K	70-KDa protein S6 kinase
pAkt	Phosphorylated Akt at serine 473
PBS-T	Phosphate-buffered saline containing 0.1% Tween-20
PCNA	Proliferating cell nuclear antigen
PDGFβ	Platelet derived growth factor beta
PDK-1	3-phosphoinositide-dependent protein kinase-1
PECAM-1	Platelet endothelial cell adhesion molecule-1
PH	Pleckstrin homology
PI3-K	Phosphoinositide 3-kinase
PIP_3	Phosphatidylinositol 3,4,5-triphosphate
PKB	Protein kinase B
PKC	Protein kinase C
PlGF	Placental growth factor
pmTOR	Phosphorylated mTOR at serine 2448
PPARβ	Peroxisome-proliferator-activated receptorβ
PTEN	Phosphatase and tensin homologue deleted from chromosome 10
SCC	Squamous cell carcinoma
Ser-473	Serine-473
Sgk-3	Serum and glucocorticoid responsive kinase-3
TA	Transit-amplifying cell
TAF	Tumor angiogenesis factor
Thr-308	Threonine-308
Tie	Tyrosine kinase immunoglobulin-like and epidermal growth factor homology domains receptor
TPA	12-O-tetradecanoylphorbol-13-acetate
TSP-1	Thrombospondin-1
UVB	Ultraviolet-B light
VEGF	Vascular endothelial growth factor
VEGFR-1	VEGF Receptor-1
VEGFR-2	VEGF Receptor-2
VPF	Vascular permeability factor

INTRODUCTION

Structure of the skin

The skin, being the largest organ of the body, serves as both a tough and flexible barrier to protect against water loss, invading microorganisms, wounds, and UV-induced damage. The skin is composed of three main layers, which include the epidermis, the dermis, and the hypodermis (Figure 1 A). The epidermis is composed of keratinocytes, which are specialized epithelial cells within the skin (Figure 1 A). The epidermis maintains homeostasis by proliferation of a single layer of mitotically active, undifferentiated columnar basal cells. Keratinocytes within the basal layer express cytokeratin K5 and K14 [1]. Upon proliferation, a basal cell gives rise to a daughter cell, transit-amplifying (TA) cell, which becomes committed to the process of terminal differentiation as it migrates upwards in the skin [2, 3]. As TAs detach from their underlying basement membrane, they down-regulate expression of integrins [4, 5] and stop dividing before entering the spinous layer [2]. Keratinocytes within the spinous layer develop many desmosomes that join adjacent cells, thus giving keratinocytes a spine-like appearance [6]. Keratinocytes within this layer express two new cytokeratins, K1 and K10 [7]. They also produce glutamine and involucrin, lysine-rich envelope proteins that are deposited on the inner surface of the plasma membrane. While the metabolically active keratinocytes within the next layer, the granular layer, stop expression of keratins, they synthesize a new structural protein, filaggrin, which is involved in bundling of keratin filaments. They also synthesize loricrin, a major component of the cornified envelope. They also secrete transglutaminase [8], an enzyme that cross-links loricrin and other substances to form the cornified envelope in the outer-most layer, the stratum corneum [9]. Keratinocytes in this layer, referred to as squames, are terminally differentiated, have lost their organelles and become thin and flattened [10]. While squames, now cross-

linked together with lipids, constitute an impermeable, insoluble, and protective layer, they are constantly being sloughed off the skin. However, squames are continually replaced by committed TA cells that move outwards in the skin, rendering the epidermis in a constant state of dynamic equilibrium.

Fibroblasts are the main cell type present within the dermal layer and produce the structural proteins collagen and elastin, which provide support and elasticity to the skin. The dermis also contains hair follicles, muscles, and nerves. Blood vessels are also present within the dermis to provide oxygen and nutrients. The hypodermis consists of an adipose layer, which is composed of fat-storing cells that provide thermal insulation (Figure 1 A).

The ability of the stratified skin epithelium to self-renew during normal differentiation and to regenerate following cutaneous injury is dependent upon the survival and proliferative potential of keratinocyte stem cells (KSC). Since stem cells are characterized by their lack of expression of both markers of terminal differentiation and proliferation, only a limited number of cellular markers have been found to be useful for identification and isolation of KSC. In the absence of cellular markers, initial studies that defined the specific location of cutaneous stem cells were based on the slow-cycling nature of this cell population. Using long-term pulse-chase experiments, only mouse stem skin cells that rarely entered the cell cycle retained the nucleoside analog labels methyl-[^{3}H]thymidine (^{3}H-T) and bromodeoxyuridine (BrdU), and therefore were termed "label-retaining cells" (LRC) [11-16]. An estimated 1-2% LRC have been shown to be present in the basal layer of the interfollicular epidermis, and were defined as "epidermal stem cells" [11, 14-17] (Figure 1 A). The nuclei labeled within the basal layer were distributed as single cells within the center of distinct columnar units composed of 10 basal cells and their suprabasal maturing progeny, defined as epidermal proliferative units (EPU) [13, 18] (Figure 1 B). However, the majority of LRC were present as clusters of cells that were located to a specific "growth and differentiation-restricted" niche within hair follicles [19], defined as "the bulge" (Bu) region (Figure 1 A) [11, 20]. The Bu region presents a special niche that is relatively protected from harmful environmental insults or physical injuries [21].

However, identifying bulge KSC by using label retention methods does not allow easy isolation of cutaneous stem cells for further analysis. Many attempts have recently been made to identify cellular markers to isolate bulge KSC. More recent studies have

used CD34, a cell surface glycoprotein that is expressed by hematopoietic progenitor cells and endothelial cells [22-24], as a specific marker for bulge KSC (Table 1). CD34 has recently been shown to be expressed specifically on cells in the outer root sheath of the bulge region of hair follicles in mice [25, 26] (Figure 1 A); however, CD34 was not present in this niche in skin human tissues [27]. In addition to CD34, cytokeratin 15 (K15) has been identified as a cellular marker to identify and isolate bulge KSC localized to the bulge region [28-31] (Table 1). K15 is a cytoplasmic marker that is present in the least differentiated cells of neonatal epidermis and in cells within the outer and inner root sheath of the bulge region of adult mouse and human hair follicles. Mouse KSC have also been isolated based on their high expression of cell surface adhesion molecules, such as α_6 integrin [25, 32, 33], which labels basal keratinocytes that are in contact with the basement membrane [26, 34], and β_1 integrin, which mediates adherence of keratinocytes to the underlying extracellular matrix [35, 36].

The similarity in characteristics of LRC and KSC suggested that these cell populations are equivalent. Using the combination of α_6 integrin and a proliferation-associated cell surface marker, the transferrin receptor (CD71), as well as long-term labeling with ^{3}H-T, the majority of α_6^{bright} CD71^{dim} fractions were enriched for LRC [32]. This direct correlation between LRC and KSC was further verified by the co-localization of CD34 [25] and K15 [31] with LRC in the bulge region of hair follicles.

Recent evidence suggests that KSC located to the Bu are more multipotent compared to epidermal KSC [37, 38]. Furthermore, when isolated and grown in culture, bulge KSC have been shown to possess a higher clonogenic potential compared to epidermal KSC [39]. Functionally, bulge KSC have been defined as a cell population that rarely divides, yet bulge-derived cells have been shown to possess a high proliferative potential [26, 40, 41] as well as are able to grow as holoclones [25, 26, 40]. In addition, bulge KSC persist in the specific bulge niche over the lifespan of the organism, and are multipotent, serving as precursors for all cell types within hair follicles [26].

However, evidence is conflicting regarding the contribution of KSC in the bulge region of hair follicles in skin homeostasis and regeneration following wounding. Blanpain *et al.* initially demonstrated that bulge KSC not only had the ability to give rise to functional hair follicles that underwent normal hair cycling when grafted to the back of nude mice where the skin has been surgically removed, but also were able to differentiate into all lineages of epidermis and sebaceous glands [26]. However, recent

studies have shown that although bulge KSC are responsible for regeneration of cells within hair follicles and they do participate in wound repair and regeneration, these bulge cells are not believed to be involved in renewal of the epidermis under normal conditions [42, 43]. These observations suggest that, under homeostasis, the epidermis and hair follicles contain two distinct KSC populations, the epidermal stem cells (Figure 1 A and B) and bulge stem cells (Figure 1 A), with no migration of cells from one compartment to another in the absence of environmental insults such as wounding.

The structure of hair follicles is complex (Figure 1 A). Hair follicles are composed of external concentric rings, defined as outer root sheath (ORS), which are continuous with the epidermis, an inner root sheath (IRS), and the hair shaft at the center of the hair follicle [44]. Hair follicles also contain specialized epithelial cells, the matrix cells, which localize to the bulb region at the distal end of hair follicles. Matrix cells surround specialized mesenchymal cells within the dermal papilla (DP) region, which is located at the base of the bulb (Figure 1 A). While the growth of keratinocytes within the epidermal layer is continuous, hair growth is cyclic. It is only the lower two-third of the follicle that undergoes cycles of growth (anagen), regression (catagen), and rest (telogen) [45]. The uppermost portion of hair follicles, also known as the infundibulum, which contains sebaceous glands and the bulge region, the location of KSC, is the permanent part of hair follicles [44]. Apoptosis of matrix cells during the catagen phase induce hair growth cessation and degeneration of the lower part of the hair follicle. During the resting phase telogen, interactions between mesenchymal cells within DP region and the epithelial matrix cells in the bulb stimulate matrix cells to proliferate, therefore regenerating the lower part of the hair follicle, including the IRS, as well as inducing the formation of a new hair shaft [46].

Skin cancer statistics and risk factors

Skin cancers are the most prevalent types of tumors in the United States (US) population. Human skin cancers can be divided into two types, melanoma and non-melanoma skin cancers (NMSC), which include basal cell carcinoma (BCC) and squamous cell carcinoma (SCC). While melanoma arises from the pigmented melanocytes that reside in the basal layer of the epidermis, BCC originates from basal keratinocytes in the epidermal layer and SCC originates from the upper layers of the epidermis. Although melanoma incidence accounts for only 6% of all skin cancers, it is

characterized by an aggressive growth pattern and high metastasis rates. A recent *Cancer facts and Figure* survey by the American Cancer Society indicates that, of the 62190 new cases of melanoma diagnosed this year, 7910 will be associated with death. However, more than 1 million new cases of BCC and SCC are diagnosed for the year 2006, outnumbering the incidence rate of melanoma. These numbers reflect the fact that skin cancer is the most common cancer in the US, and its incidence accounting for more than prostate, breast, lung, colon, and pancreas combined together. Although more than 80% of diagnosed NMSC are SCC and 16% are BCC, it is estimated that only 2800 cases will be associated with death for this year. In contrast to BCC, which rarely metastasize to distant organs, SCC is associated with a substantial risk of metastasis [47]. Although rarely fatal, NMSC can result in extensive local destruction of the skin tissue, leading for a severe morbidity and potential functional impairment [48, 49].

Models of skin carcinogenesis

The skin is continuously exposed to environmental insults. The more common and ubiquitous etiologic risk factor involved with the development of NMSC is ultraviolet light in the 290-320 nm wavelength, defined as UVB, which is derived from routine exposure to sunlight [50, 51]. Most of the UVB radiation is absorbed by the earth's stratospheric ozone layer; however, the rapid loss of the ozone layer and the concomitant increase in the amount of UVB light reaching the earth's surface represent an important factor leading to the dramatic increase in the incidence of NMSC [52]. Exposure to polycyclic aromatic hydrocarbons derived from the combustion of coal tar and fossil fuel by-products has been associated with development of skin malignancies as well. Exposure to environmental and chemical agents has historically been a major cause of NMSC [47]. In 1775, Sir Percival Pott was the first to report a high incidence of scrotal cancer among chimney sweeps, which was related to a continual exposure to soot [53].

Skin cancer is a multi-stage process that involves a stepwise accumulation of genetic and epigenetic alterations, leading to malignancy. One of the most commonly used animals models for the evaluation of genetic and epigenetic changes that occur during development of human skin cancers is the mouse skin model of multi-stage carcinogenesis. Distinct and sequential stages of mouse skin carcinogenesis have been recognized, which include tumor initiation, promotion, and progression.

The first experimental induction of skin cancer was achieved in 1915 by repetitive topical applications of coal tar to mouse skin [54]. The definition of skin carcinogenesis as a multi-stage process dates back to 1924. These studies demonstrated that mice previously treated with coal tar developed visible benign skin lesions, termed papillomas, only following wounding [55]. It was further demonstrated that coal tar contains an active chemical carcinogen, a polycyclic aromatic hydrocarbon, known as dibenz(a,h)anthracene. In 1940, Peyton Rous observed that treatment of rabbit skin with one topical application of coal tar results in the formation of “latent tumor cells”, which could be “promoted” to reveal themselves by further treatment of the skin with agents including wounding, turpentine, and chloroform [55]. In 1941, Berenblum reported that, while few mice developed papillomas following topical applications of dorsal skin with a carcinogen, all mice that had previously been initiated with a carcinogen developed papillomas following repetitive topical applications of croton oil extracted from *Croton triglium* [56]. Results from these previous studies demonstrated that croton oil acts as a potent promoting agent. The simplified classical method of murine two-stage skin carcinogenesis was later established by Mottram and is achieved by a single topical application of a sub-carcinogenic dose of benzo-[a]-pyrene, a process termed initiation, followed by repetitive topical applications of croton oil, a process termed promotion [54, 57].

Initiation is accomplished by a single topical application of a sub-carcinogenic dose of a skin carcinogen, 7,12 dimethylbenz[a]anthracene (DMBA), a chemical belonging to the family of polycyclic aromatic hydrocarbons. However, DMBA is not active as such, but requires metabolism by the microsomal cytochrome P-450 monooxygenase system, yielding a highly reactive intermediate, the bay-region diol epoxide [58, 59]. The electrophic nature of diol epoxides allow them to attack nucleophilic sites within nucleic acids, including oxygen and nitrogen atoms on purine and pyrimidine rings, resulting in the intercalation of the flat and planar rings of polycyclic aromatic hydrocarbons between the stacked bases of the double helical DNA, thus forming covalent bulky adducts on DNA bases and distorting the helix [60, 61]. Upon cell proliferation, DNA replication leads to a frame mutation past the point of intercalation of DMBA metabolites. On the other hand, DMBA metabolites can induce instability in the glycosidic bond between purine bases and the sugar deoxyribose, which upon cleavage by the enzyme DNA glycosylase, promotes depurination, resulting in the formation of

apurinic sites (AP). These AP sites can be repaired in an error-prone fashion and may be filled by any base during subsequent replication, most commonly adenine, resulting in the formation of base-substitution mutations [62, 63].

Cellular genes that have been recognized to contain mutations during skin carcinogenesis include activation of oncogenes, such as Harvey (Ha)-*ras*, and inactivation of tumor suppressor genes, such as *p53*. Ras proteins belong to the monomeric GTPase family. When bound to GTP, Ras protein is active. In contrast, Ras is inactive when bound to GDP. The loss of GDP and the subsequent uptake of GTP are mediated by the enzymatic activity of Guanine nucleotide releasing proteins (GNRP), therefore rendering Ras active. Inactivation of Ras occurs due to the activation of GTPase-activating proteins (GAP), which catalyzes the hydrolysis of bound GTP [64]. Extensive previous studies have demonstrated that more than 90% of skin tumors previously initiated with DMBA contain a specific A to T transversion mutation in the second position of codon 61 of the Ha-*ras* gene [65, 66]. “Initiated” cells may contain additional mutations in cellular Ha-ras gene, including specific mutations at codons 12, 13, 59 [65]. Such activating mutations result in a reduction of the intrinsic GTPase activity of GAP enzyme, therefore inhibiting the loss of bound GTP and rendering Ras constitutively active.

Mutations induced in the *ras* proto-oncogene following the initiation step are irreversible. However, these mutations are heritable, despite the fact that the epidermis itself once every 6-8 days, rendering initiated cells long-lived. There was no significant change in the number of papillomas formed with lapses in time of greater than a year between DMBA-induced initiation and TPA-induced skin tumor promotion [40, 67]. These observations suggested that carcinogen-initiated cells, which contain mutations in the Ha-*ras* gene, have characteristics similar to those of slow-cycling, long-lived KSC. Therefore, in addition to serving as a self-renewing population, KSC have been shown to serve as targets for carcinogens [17].

While cells that contain mutations in the *ras* proto-oncogene are genetically altered, they remain phenotypically indistinguishable from normal cells. However, indefinite proliferation of these initiated cells can be induced in response to exposure to appropriate proliferative stimuli. Tumor promotion stimulates these initiated keratinocytes to undergo clonal expansion, leading to outgrowth of papillomas. Application of a tumor-promoting agent to normal skin in the absence of initiation does not result in tumor

formation. In contrast to initiation, promotion is a slow and gradual process that requires a more prolonged and repetitive exposure to a promoting agent. A well-established promoting agent is croton oil, or its most active constituent, the phorbol ester 12-O-tetradecanoylphorbol-13-acetate (TPA). Tumor promoters can also include mechanical agents, such as full-thickness wounding. While TPA does not require metabolic activation to mediate its promoting effects nor does it bind covalently to DNA, TPA induces epigenetic changes that may be reversible during the earlier stages of promotion, including alterations in gene expression, signal transduction pathways, differentiation [68], and intercellular communications [69, 70].

When applied topically to mouse dorsal skin, TPA induces chronic hyperplasia [71], increased vascular permeability leading to localized edema [72], and dermal infiltration of inflammatory cells [73]. One of the immediate responses to TPA activation is up-regulation of the enzymatic activity of ornithine decarboxylase (ODC) [74, 75], which decarboxylates ornithine to form polyamine, including putrescine, spermine, and spermidine [76]. Polyamines have been shown to stimulate cellular proliferation while inhibiting differentiation [76]. Over-expression of constitutively active ODC in the epidermis of mice that have been previously initiated, led to skin tumor formation in the absence of application of any exogenous promoting agent. These previous results demonstrate the importance of ODC activity in TPA-induced mouse skin tumor promotion [74]. In addition to constitutive activation of ODC, TPA mediates its promoting effects by activation of protein kinase C (PKC) [77]. Of the 11 distinct PKC isoforms, epidermal keratinocytes express only PKC isoforms α, δ, ε, η, μ, and ζ [78, 79]. The presence of multiple PKC isoforms suggests that different isoforms may play distinct physiological roles in keratinocytes. PKC can be activated by the membrane phospholipid phosphatidylserine (PS), and diacylglycerol (DAG), a byproduct of phosphatidylinositol turnover, in the presence of Ca^{2+} [80]. Interestingly, TPA has been shown to directly activate PKC in the absence of DAG [77]. PKC activation has been shown to result in dephosphorylation of c-jun, leading to enhanced activity of AP-1 DNA binding activity and transactivation [81]. PKC also mediates the transcription of TPA-induced genes, including ODC [82].

Migration of peripheral leukocytes [73] following topical exposure to TPA has been shown to be dependent upon the release chemotactic factors, including tumor necrosis factor-α (TNF-α) [83] as well as the pro-inflammatory cytokines interleukin-

1α (IL-1α) [84, 85] and granulocyte-macrophage colony-stimulating factor (GMC-SF) [86]. TPA not only induces dermal leukocyte infiltration but also induces activation of infiltrating leukocytes as well as epidermal keratinocytes to produce reactive oxygen species [87]. In addition, infiltrating leukocytes, neutrophils in particular, have been shown to produce nitric oxide and superoxide anion, which interact to form the reactive nitrogen intermediate peroxynitrite [88]. Production of peroxynitrite has been shown to induce formation of DNA adducts such as 8-hydroxydeoxyguanosine [89] and 8-nitroguanine [90], resulting in base-pair mutations [89, 91]. Upon decomposition into reactive intermediates, including nitrogen dioxide and tyrosyl radicals, peroxynitrites can further induce nitration of aromatic amino acids, including tyrosine [92].

UVB light serves as both an initiating and a promoting agent. Absorption of UVB light by DNA induces covalent links between adjacent pyrimidines bases, resulting in the formation of pyrimidine photoproducts, cyclobutane pyrimidine dimer [93] and pyrimidine-(6-4)-pyrimidone lesion [94]. Formation of pyrimidine photoproducts has been shown to induce “UV signature mutations”, including C to T and CC to TT transitions [95] commonly found at CC nucleotides [96]. Following exposure to UVB, dipyrimidine photoproducts are excised by the nucleotide excision repair system. However, patients with xeroderma pigmentosum are deficient in nucleotide excision repair, and therefore, are extremely sensitive to UV-induced DNA damage, and develop skin cancer in sun-exposed areas [97].

While exposure to UVB has been shown to induce such UV-signature mutations in the *p53* tumor suppressor gene, leading to loss of function [98], some UV-induced skin cancers have been shown to contain low frequency of activating mutations in the *ras* oncogene compared to the high frequency of mutations in *p53* gene, including mutations at codon 61 of N-*ras* [99] and Kristen (Ki)-*ras* genes [100]. Repeated exposure to UVB light results in the clonal expansion of initiated keratinocytes that contain *p53* mutations, given their acquired resistance to UV-induced apoptosis as well as their proliferative advantage over normal keratinocytes [101, 102].

Progression represents a step of acquisition of an invasive phenotype of tumor cells in a small subset of preneoplastic papillomas. This step of conversion of mouse benign skin tumors to malignancy represents a stage of additional genetic instability, which has been shown to be associated with trisomy of chromosomes 6 and 7, with concomitant loss of the normal Ha-*ras* allele [103], and amplification of mutant Ha-*ras*

allele [104]. In addition, inactivation of the tumor suppressor p53 has been detected in SCC [105]. Progression of SCC to spindle cell carcinomas has been associated with the loss of expression of the cell adhesion protein E-cadherin [106].

While some benign papillomas regress or remain dormant for the lifetime of the organism using the murine model of multi-stage skin carcinogenesis, less than 10% of papillomas progress into carcinomas [107]. These observations suggest the presence of additional alterations that enhance the malignant conversion of papillomas into SCC. In order to survive, expand in size, and progress to form carcinomas, skin tumors require the development of new blood vessels (Figure 2).

Tumor-Associated Angiogenesis

The development of blood vessels has been defined as neovascularization and is a fundamental and highly regulated process necessary for appropriate embryonic development [108]. In adult mammals, this activity occurs only during normal physiological processes such as the female reproductive cycle [109] and wound healing [110]. While tumors that are relatively small (< 200 μm) use existing vasculature as a source of oxygen and nutrients, in a process termed vessel co-option [111], tumors that are beyond this size have increased nutritional requirements and exist within a hypoxic, metabolically-deficient microenvironment. Studies over the last four decades have demonstrated that actively growing tumors have an absolute requirement for development of new blood vessels, which support increases in tumor mass, tumor survival, and provide an avenue for tumor invasion and metastasis (Figure 2). Without this process, defined as tumor-associated angiogenesis [112, 113], developing tumors are in a prevascular state and exist in a state of equilibrium between proliferation and apoptosis, where tumor growth is restricted [114] and tumors become dormant [115].

As tumor cells proliferate and their layers accumulate, the distance between malignant cells within the expanding tumor mass and the nearest blood vessel increases. When tumors reach a size of 1-2 mm, tumor cells located at a distance greater than 200 μm from the nearest blood vessel become hypoxic, and are deficient in critical nutrients [116]. To allow for tumor expansion, survival, and metastasis, tumors undergo what has been defined as the “angiogenic switch”, which results from a shift in the balance of anti-angiogenic growth factors that inhibit formation of new vasculature to

favor the production of pro-angiogenic growth factors which induce tumor-associated angiogenesis (Figure 2) [117, 118].

Early studies demonstrated the presence of tumor angiogenesis factor (TAF), which was initially defined as a soluble growth factor that diffuses into the tumor microenvironment [119]. Although the first pro-angiogenic growth factor identified was basic fibroblast growth factor (bFGF, FGF-2) [120], this protein lacks a signal sequence for secretion, and therefore bFGF remains intracellular and cannot diffuse into the tumor microenvironment. Despite recent evidence demonstrating the presence of a selective export of bFGF in tumor cells isolated from dermal fibrosarcomas and not by normal dermal fibroblasts cells [121], this protein is now believed to be a general angiogenic growth factor that is not critical for angiogenesis based on studies demonstrating that the loss of bFGF does not result in any significant phenotypic alteration in the vasculature during embryonic development [122].

The second angiogenic growth factor was identified based on its ability to induce vascular permeability in guinea pig skin and was named vascular permeability factor (VPF) [123]. VPF was later found to have identity with proteins purified from pituitary folliculostellate cells that stimulated proliferation of cultured endothelial cells and was therefore defined as vascular endothelial growth factor-A (VEGF-A) [124-126]. Studies using knock-out mice demonstrated that the loss of only one VEGF-A allele resulted in early embryonic lethality, indicating that VEGF-A was critical to angiogenesis during development [127, 128]. Studies have revealed that VEGF-A is part of a family of VEGF-related molecules consisting of other members including VEGF-B [129], VEGF-C [130], VEGF-D [131], VEGF-E [132] and placental-derived growth factor (PlGF) [133]. For the purpose of the present studies, VEGF-A will be designated as VEGF.

VEGF production is stimulated following activation or mutation of oncogenes such as Bcr-Abl, ras, and erbB-2/HER-2/neu [134, 135]. In addition, the hypoxic tumor microenvironment and activation of survival pathways work synergistically with oncogenes to increase VEGF production [136, 137]. VEGF is recognized as a pivotal growth factor in tumor-associated angiogenesis [138]. Since it can activate and recruit vascular endothelial cells to undergo all of the necessary activities required to form new capillary beds, VEGF has been defined as a complete angiogenic growth factor [139]. VEGF stimulates vasodilation and increases permeability of pre-existing capillaries, leading to leakage of plasma proteins [140] and deposition of an extravascular fibrin gel

around developing vasculature. This provides a matrix to support the subsequent proliferation and migration of vascular endothelial cells [141]. As an additional critical component of its activity as a complete angiogenic growth factor, VEGF activates signal transduction pathways that regulate survival of tumor cells [142-144], vascular endothelial cells [145, 146], and pericytes [147], which exist in the tumor microenvironment that is hypoxic and deprived of nutrients. The pivotal nature of VEGF to tumor-associated angiogenesis is demonstrated by the detection of its presence in all tumors thus far examined and by the correlation between production of VEGF with tumor stage and tumor progression [148-151].

In addition to bFGF and VEGF-related proteins, other pro-angiogenic growth factor families have been identified, which have distinct activities in tumor-associated angiogenesis and act in concert with VEGF. Angiopoietin-1 (Ang-1) [152, 153], Ang-2 [154], Ang-3, and Ang-4 [155] are members of the Angiopoietin family of proteins which bind to receptors within the tyrosine kinase immunoglobulin-like and epidermal growth factor homology domains (Tie) receptor family that are expressed by tumor cells, vascular endothelial cells, and pericytes. During embryonic development, ligand binding of Ang-1 to the Tie-2 receptor tyrosine kinase increases adherence of vascular endothelial cells to pericytes, resulting in stabilization of newly formed blood vessels [156]. In addition, Ang-1 regulates vascular endothelial cell survival, sprouting, and organization into tubules [157]. Ang-1 can also inhibit VEGF-induced permeability and reduce inflammation [158]. Despite the fact that each of ligands bind to the same receptor, Ang-2 and Ang-3 inhibit the Tie-2 tyrosine phosphorylation induced by Ang-1, therefore counteracting the stabilizing effects of Ang-1 [112]. Molecular profiling studies have demonstrated that VEGF up-regulates Ang-2 during tumor-associated angiogenesis, resulting in destabilization of existing vasculature, loss of pericytes, and subsequent enhancement of tumor vessel formation [159, 160]. The co-operative activities of VEGF and Ang-2 may, in part, account for the morphologically distinct tortuous blood vessels formed during tumor-associated angiogenesis and may also be responsible for the less stable, leaky vessels that develop adjacent to expanding tumors [161]. Although the members of the Angiopoietin family and their associated Tie-2 receptor have opposing roles in angiogenesis, it is clear that the balance in production of these growth factors plays a key role in regulating tumor vessel formation [162]. Disruption of this delicate balance in relative amounts of Ang-1 or Ang-2 has been

observed to result in significant defects in tumor-associated angiogenesis [163]. Recent evidence suggests that VEGF, Tie-2, Ang-1, and Ang-2 are simultaneously expressed during tumor growth, yet are differentially expressed spatially within the tumor microenvironment as well as temporally expressed during tumor vessel development [161]. It is clear that further studies which continue to define the roles of the members of this family of proteins will provide insight into their use as therapeutics and as targets for therapeutics in not only VEGF-induced tumor-associated angiogenesis but also in disorders associated with enhanced inflammatory responses.

Tumor-associated angiogenesis is a complex process that involves the coordinated activity of a number of different cell types within the tumor microenvironment, including tumor cells and stromal cell populations of vascular endothelial cells and pericytes [164]. While the literature is replete with studies that define the role of tumor cells during tumor-associated angiogenesis, the role of vascular endothelial cells is currently being elucidated. In contrast, the role of pericytes during this process has only recently been recognized and remains to be completely defined. Figure 2 provides a schematic representation of tumor-associated angiogenesis and the role of these individual cell types in this process. Following the angiogenic switch, tumors acquire an angiogenic phenotype, produce pro-angiogenic growth factors such as VEGF and express the associated VEGF receptors, which confers the ability to respond to these proteins in an autocrine manner. As a pro-angiogenic growth factor, VEGF activates vascular endothelial cells within the capillaries adjacent to expanding tumors. Once activated by VEGF, vascular endothelial cells secrete proteolytic enzymes that degrade basement membranes and the extracellular matrix surrounding the pre-existing blood vessel. Digestion of these elements allows the vascular endothelial cells to detach from pericytes that reside beneath the vascular endothelial cells. Following their detachment, vascular endothelial cells proliferate, and migrate toward the source of pro-angiogenic growth factor production by invasion through spaces created by enzyme degradation (Figure 2). These recruited vascular endothelial cells then secrete extracellular matrix proteins which provide the building blocks for development of new basement membranes that support the tumor vessels. The vascular endothelial cells then change from an actively proliferating population of cells to subsequently undergo differentiation and organization into hollow tubes that connect the expanding tumor mass to nearby vascular beds. Furthermore, vascular endothelial cells secrete VEGF and an

additional protein, platelet derived growth factor beta (PDGFβ), which induce migration of pericytes into the area of active tumor vessel formation (Figure 2 B) [165]. Pericytes respond to PDGFβ via expression of the associated receptor tyrosine kinase, platelet derived growth factor receptor beta (PDGFR-β). Direct interactions between pericytes and vascular endothelial cells stimulate differentiation of pericytes into vascular smooth muscle cells that stabilize and maintain the newly formed tumor vasculature [166]. Blood flow is then initiated which inhibits the rate of apoptosis within tumors, providing both a source of oxygen and nutrients and a route for tumor invasion and metastasis to distant organ sites.

VEGF also acts as a chemotactic factor which results in recruitment and activation of non-vascular cells, including inflammatory mast cells, macrophages, and neutrophils (Figure 2 B) [167-169]. Recruited inflammatory cells produce pro-angiogenic products as well as synthesize matrix metalloproteinases [170-173], which has led to these cells being defined as “co-conspirators” in tumor-associated angiogenesis [171]. Other cell types have also been identified as playing a role in tumor-associated angiogenesis such as bone marrow-derived stromal cells, which respond to pro-angiogenic growth factors, migrate from the bone marrow to the tumor site, and differentiate into capillary-like structures [174]. Further studies are required to more completely define the interactions of pro-angiogenic growth factors with each of the cell types involved in tumor-associated angiogenesis.

Additionally, in a unique process defined as vasculogenic mimicry, tumor cells within aggressively growing malignancies such as melanomas trans-differentiate into cells with phenotypic and functional characteristics of vascular endothelial cells [175]. These cells form a vascular network rich in extracellular matrix proteins without the need to activate endothelial cells that are usually required for angiogenesis. It is clear that further investigation will reveal additional cell types that contribute to tumor vessel formation as well as will elucidate previously undefined contributions of cells that are known to play a role in tumor-associated angiogenesis.

Although one gene encodes for both rodent and human VEGF, a number of different VEGF proteins with specific activities can be produced through the alternative splicing of the 8 exons within the single VEGF gene. Alternative splicing generates distinct peptides named for the number of amino acids contained within them. In humans, the most abundantly produced VEGF splice variants are $VEGF_{121}$, $VEGF_{165}$,

and $VEGF_{189}$ [176] (Figure 3 A). Less abundantly produced human VEGF splice variants identified to date are $VEGF_{145}$ [177], $VEGF_{183}$ [178], and $VEGF_{206}$ [179]. Although the majority of human VEGF splice variants are pro-angiogenic, an anti-angiogenic splice variant $VEGF_{165}b$, was found to be down-regulated in renal tumors, and the loss of $VEGF_{165}b$ coincided with induction of the angiogenic switch in this tissue [180]. $VEGF_{165}b$ lacks exon 8, which is replaced by exon 9, resulting in production of a protein with the same length as $VEGF_{165}$ but with a carboxyl-terminal tail composed of 6 unique amino acids, SLTRKD (Figure 3 A). A very recent study reported that $VEGF_{165}b$ is present in differentiated renal podocytes but was not present in this cell type undergoing active proliferation, suggesting that alternative splicing of VEGF pre-mRNA is an integral part of regulating neovascularization [181]. Further studies may reveal the existence of other human VEGF splice variants with functional activities that vary from those described to date. Elucidation of the activities of the distinct VEGF splice variants may provide insight into their utility as both therapeutics and therapeutic targets.

In contrast to human VEGF splice variants, murine VEGF variants are one amino acid shorter than the analogous human splice variants, but in most cases the mouse VEGF proteins possess biological activities similar to human VEGF splice variants (Figure 3 B). Murine VEGF splice variants identified to date include $VEGF_{120}$, $VEGF_{144}$, $VEGF_{164}$, and $VEGF_{188}$ [182]. In addition to these murine proteins, our laboratory identified, sequenced, and characterized the activities of a novel murine splice variant designated as $VEGF_{205}$* (Genbank Accession AY120866) (Figure 3 B). This VEGF splice variant was first identified by detection of its mRNA and protein only in mouse skin papillomas and squamous cell carcinomas, which was completely undetectable in normal skin (85). $VEGF_{205}$* contains exons 1-6, and lacks exons 7 and 8. In place of these exons is a 61 bp extension to exon 6a, defined as exon 6' (Figure 3 B). Due to the presence of a stop codon in exon 6', translation of murine $VEGF_{205}$* mRNA results in the production of a truncated 145 amino acid protein containing a carboxyl-terminal tail consisting of 7 unique amino acids, YVGAAAV. The exon structure of murine $VEGF_{205}$* and the resultant VEGF splice variant protein are significantly different from any other human or mouse VEGF splice variant described to date, including human $VEGF_{206}$ (Figure 3 A and B). The size, amino acid sequence of the carboxyl-terminal tail, and biological activities of $VEGF_{205}$* are unique. The biological activity of VEGF splice variants occurs following receptor-ligand binding and subsequent transduction of specific

signals. Identification of VEGF receptor families has been crucial to understanding the functions of the individual VEGF splice variants. Thus far, there have been two distinct VEGF receptor families identified, which include the VEGF receptor tyrosine kinase family and the Neuropilin family. The VEGF receptor tyrosine kinase family includes VEGF Receptor-1 (VEGFR-1), which was first isolated and characterized as fms-like tyrosine kinase-1 (Flt-1) [183-185], VEGFR-2, also defined as Fetal Liver Kinase 1/Kinase-insert- Domain-containing Receptor (Flk-1/KDR) [186, 187], and VEGFR-3, first defined as Flt-4 [188].

Despite their structural homology and the ability of VEGFR-1 and VEGFR-2 to bind VEGF and induce receptor auto-phosphorylation at specific tyrosine residues, these receptors have distinct expression patterns within different organs, which may overlap, and they also activate specific signal transduction pathways [189]. The loss of VEGFR-2 in homozygous mice was lethal due to impaired development of hematopoietic precursors and lack of differentiated endothelial cells [190]. The loss of VEGFR-1 gene was lethal as well, however, these mice developed large blood vessels that lacked organization and contained overgrowth of endothelial cells within the vascular lumen [191]. These observations confirmed the distinct roles of VEGFR-1 and VEGFR-2 in regulating endothelial cell proliferation and differentiation.

The differential ability of VEGF receptor-ligand binding to induce selective biological activities including increased vascular permeability as well as proliferation, migration, differentiation, and organization of vascular endothelial cells into vascular tubules during tumor-associated angiogenesis is due to phosphorylation of specific VEGFR-associated tyrosine residues. For example, following binding of VEGF to VEGFR-2, vascular endothelial cells undergo proliferation which is due to phosphorylation of tyrosine residues 1054/1059 [192], while migration of these cells is stimulated following phosphorylation of tyrosine residue 951 [192, 193]. Conversely, binding of VEGF to VEGFR-1 inhibits VEGFR-2-mediated endothelial cell proliferation, but not migration [194]. Although VEGFR-1 has a ten-fold higher affinity for VEGF than VEGFR-2 [194], VEGFR-1 tyrosine kinase activity is ten-fold weaker than VEGFR-2 [195]. Furthermore, mice carrying the extracellular domain of VEGFR-1 gene that lacked the tyrosine kinase domain developed normal vessels and survived [196]. These unique characteristics of VEGFR-1 suggest that only the extracellular domain of VEGFR-1 may function as a ligand-trapping molecule that negatively regulates levels of VEGF. Indeed,

recent studies reported that alternative splicing produces a shorter and a soluble form of VEGFR-1 (sVEGFR-1), which acts as a decoy receptor that sequesters VEGF, preventing it from binding to VEGFR-2 [197].

While VEGF splice variants bind differentially to VEGFR-1 and VEGFR-2, VEGF-C and VEGF-D bind only to VEGFR-3, a VEGF receptor that is critical to appropriate development of lymphatic vessels [198]. In addition, VEGFR-3 is expressed on a variety of tumor cells of different origins and may be useful as a marker of early stages of tumor progression [130, 199]. Although further studies are required to completely define the roles of these VEGF receptors in tumor-associated angiogenesis, there are a number of therapeutic approaches that are based on the interactions of VEGF and VEGFR-2 currently being developed that target tumor vessels [200-202].

Neuropilins are a second family of VEGF receptors whose members identified thus far include neuropilin-1 (NP-1) [203], and neuropilin-2 (NP-2) [204]. NP-1 and NP-2 belong to a family of collapsins/semaphorins receptors first described as neuronal axon guidance factors present in developing embryos [205, 206]. These receptors are now known to be expressed not only by vascular endothelial cells and pericytes [203, 204], but by tumor cells as well. One of the primary functions of NP-1 and NP-2 is to act as receptors for specific VEGF splice variants. NP-1 and NP-2 bind $VEGF_{165}$ as well as the heparin-binding form of placental growth factor (PlGF), PlGF-2 [207], and VEGF-B [208]. Only NP-2 can bind $VEGF_{145}$ [204]. In contrast, neither NP-1 nor NP-2 binds $VEGF_{121}$, a VEGF splice variant that lacks the ability to bind heparin and heparan sulfate proteoglycans [204]. Both NP-1 and NP-2 are alternatively spliced [209] and contain short intracellular domains which lack tyrosine kinase domains [210]. To mediate VEGF signaling, NP-1 acts as a co-receptor for VEGFR-2 [203], resulting in enhanced binding affinity of $VEGF_{165}$ to VEGFR-2, and effectively increasing the local concentration of VEGFR-2 at the cell surface [211, 212]. Taken together with a recent report that blockade of NP-1 effectively inhibits angiogenesis in murine retinal neovascularization [213], these studies suggest that the Neuropilin receptors may serve as targets for development of VEGF splice variant specific anti-angiogenic therapies [212]. Further studies are necessary to determine if there are other members of this receptor family, to fully elucidate the role of these receptors in tumor-associated angiogenesis, and to determine if these receptors can be used to target this process.

Production of multiple VEGF splice variants allows this one group of proteins to regulate specific functions of tumor cells, vascular endothelial cells and pericytes, resulting in precise regulation of tumor-associated angiogenesis. In part, distinct biological activities of VEGF splice variants are determined by the exons present within the splice variant pre-mRNA (Figure 3 A and B). Exon 1 encodes for the signal sequence common to all VEGF splice variants. The presence of Exon 1 indicates that each of the splice variant proteins can be secreted. Exon 2 encodes for a specific N-terminal sequence, which is also common to all known human and rodent VEGF splice variants. Exon 3 is also contained within all known VEGF splice variants and encodes for VEGF dimerization sites and for binding to VEGFR-1 [184, 185]. Exon 4 encodes for binding of VEGF alternative splice variants to VEGFR-2 [186, 187]. Exon 5 encodes for a plasmin cleavage site, which allows production of smaller VEGF peptide fragments through proteolytic cleavage [214, 215]. Exon 6 encodes for binding of VEGF splice variants to heparin and heparan sulfate proteoglycans on the surface of cells [216]. Exon 6 is either not present, as occurs with murine $VEGF_{120}$ and $VEGF_{164}$ (Figure 3 B), and human $VEGF_{165}$b (Figure 3 A), or is significantly altered by loss of part of exon 6 designated as exon 6b, which occurs in murine $VEGF_{188}$ and $VEGF_{144}$ (Figure 3 B). Exon 6 is also altered by extension of 6a, designated as exon 6', which occurs in $VEGF_{205}$* (Figure 3 B). Exon 7 encodes for an additional heparin binding domain [216] and it is also lost in a number of VEGF splice variants including murine $VEGF_{120}$, $VEGF_{144}$, and $VEGF_{205}$*. The presence or absence of exons 6 and 7 determines the ability of the specific VEGF splice variants to either freely diffuse within the tumor microenvironment or to bind heparin and heparan sulfate proteoglycans, therefore remaining sequestered and acting as slow release molecules. For example, $VEGF_{121}$ lacks the charged basic amino acids encoded by exons 6 and 7, and therefore, is a soluble growth factor that does not bind heparin (Figure 3 A) [214]. In contrast, $VEGF_{189}$ contains exons 6 and 7, has a high affinity for binding heparin, resulting in sequestration of this splice variant by the extracellular matrix and heparan sulfate proteoglycans on the cell surface [215]. Other VEGF splice variants that contain either exon 6 or exon 7 but not both possess only one of the two heparin-binding domains (Figure 3 B). VEGF splice variants with this exon configuration, such as $VEGF_{164}$, can both freely diffuse in the area surrounding of the tumor as well as remain bound to the cell surface and extracellular matrix. The number of VEGF splice variants which have deletions, insertions, or

alterations in either exon 6 and/or exon 7 suggests that production of VEGF splice variants that differentially bind heparin or freely diffuse is tightly regulated during angiogenesis. For example, the exon structure of the unique murine $VEGF_{205}$* splice variant predicts that it is actively secreted based on the presence of exon 1, that it can dimerize and bind both VEGFR-1 and VEGFR-2 based on the presence of exons 3 and 4. Additionally, $VEGF_{205}$* is predicted to bind heparin and heparan sulfate proteoglycans based on the presence of exon 6, resulting in its retention within the local tumor microenvironment. Since $VEGF_{205}$* contains an extension of exon 6a, designated as 6', that encodes for a protein with a novel carboxyl-terminus tail, this VEGF splice variant is expected to have activities that differ from other VEGF splice variants. We have defined one such activity of $VEGF_{205}$*, which is stimulation of survival pathways of vascular endothelial cells.

Akt Signal Transduction Pathway

Akt (also known as Protein kinase B) is a serine/threonine kinase with homology to both protein kinase C (PKC) and cyclic-AMP-dependent protein kinase A (PKA) [217, 218]. Akt was first identified as the cellular homolog of the v-*akt* oncogene derived from the murine AKT8 retrovirus [219, 220]. Although AKT8 virus was replication defective, the virus was able to induce malignant transformation of the CCL 64 mink lung epithelial cell line [219]. The oncogenic potential of AKT8 virus has been shown to occur due to the acquisition of the cellular sequence of the proto-oncogene c-*akt*, which was fused downstream to the viral *gag* gene [220]. As a consequence, mature v-Akt protein contains a Gag sequence that is myristylated, which constitutively targets v-Akt to the plasma membrane in close vicinity to upstream kinase activators [221]. To date, there are three mammalian c-Akt (Akt) isoforms that have been identified, including Akt-1 [218], Akt-2 [222], and Akt-3 [223, 224], with each isoform encoded by a separate gene. There is a differential expression of the three isoforms within various tissues. While the loss of Akt-1 gene resulted in growth retardation and increased rate of apoptosis in testis and thymus of mutant mice [225], the loss of Akt-2 resulted in a diabetic phenotype, with impaired regulation of insulin [226, 227]. Loss of Akt-3 has recently been shown to impair normal brain development [228]. Interestingly, knock-out mice with targeted loss of both Akt-1 and Akt-2 genes have impaired skin development which is characterized by the presence of a thin epidermis with very few cells in each layer of the skin [229].

These observations support a role for Akt-1 and Akt-2 isoforms in skin development and homeostasis.

Akt is a core component of the phosphoinositide 3-kinase (PI3-K) signaling pathway [230] (Figure 4 A). Akt is composed of an amino-terminal pleckstrin homology (PH) domain that binds phospholipids [231], a kinase domain, and a proline-rich carboxyl-terminal regulatory domain. In response to growth factors including VEGF splice variants, PI3-K is recruited to the inner surface of the plasma membrane resulting in the generation of the membrane-bound lipid phosphatidylinositol 3,4,5-triphosphate (PIP_3). Following binding of PIP_3 to the PH domain, Akt is translocated from the cytoplasm to the inner surface of the plasma membrane [232]. This results in conformational changes rendering Akt accessible to phosphorylation at two amino acid residues, threonine-308 (Thr-308), which lies within the Akt kinase domain, and serine-473 (Ser-473), which is located within the Akt regulatory domain [233] (Figure 4 A). Phosphorylation of Akt at Thr-308 and Ser-473 is carried out by two distinct kinases: 3-phosphoinositide-dependent protein kinase-1 (PDK-1) which phosphorylates Thr-308 [234], and integrin-linked kinase-1 (ILK-1), which phosphorylates Ser-473 [234-236]. Akt activation can be negatively regulated by the phosphatase activity of the tumor suppressor protein, phosphatase and tensin homologue deleted from chromosome 10 (PTEN), which acts by reversing the production of PIP_3 by PI3-K [237, 238]. 2-(4-morpholinyl)-8-phenylchrome (LY294002) is a competitive synthetic inhibitor for the ATP binding site of PI3-K and leads to inhibition of Akt phosphorylation [239, 240].

Akt acts primarily as a survival factor (Figure 4 B), resulting in protection of cells against programmed cell death, apoptosis. The inhibition of apoptosis by Akt may be mediated by multiple mechanisms, some of which may be cell-specific. Akt has been shown to protect vascular endothelial cells from Fas (CD95)-induced apoptosis by inducing the expression of the anti-apoptotic FLICE-inhibitory protein (FLIP), a caspase 8 (FLICE) inhibitor [241]. Akt has also been shown to induce survival of endothelial cells by phosphorylating and inactivating pro-apoptotic proteins within the family of Forkhead transcription factors (FKHR) [242, 243], resulting in their translocation from the nucleus into the cytoplasm, therefore inhibiting transcription of genes that would otherwise promote apoptosis, including Fas ligand, TNF-related apoptosis-inducing ligand), TRAIL, and TNF receptor type 1 associated death domain, TRADD [244]. Akt has been shown to phosphorylate and inactivate the pro-apoptotic B-cell lymphoma-2 (Bcl-2) family

member BAD on Ser-136 as well, which frees the Bcl-2/Bcl-X complex to promote cell survival [245-247]. Akt may also promote cell survival by phosphorylating and inactivating Caspase 9, the effector of apoptosis [248]. Not only does Akt induce survival by inactivating pro-apoptotic proteins, but by inducing transcription of genes that promote survival as well [249]. Activated Akt has been shown to induce degradation of the inhibitor of nuclear factor-kappa B (IκB) by directly phosphorylating and activating IκB kinase (IKK). Degradation of IκB frees NF-κB to translocate to nucleus and initiate transcription of pro-survival genes, including the Bcl-2 family member Bfl-1/A1 [250] and the caspase inhibitors c-IAP1 and c-IAP2 [251].

Although the majority of studies to date have focused on the role of Akt as a survival factor, Akt can also act as a multi-functional protein kinase which regulates both cell proliferation and increases in cell mass [252] (Figure 4 C). Akt phosphorylates and consequently blocks the activity of glycogen synthase kinase-3β (GSK-3β), thereby preventing degradation of cyclin D1 which is a protein required for progression of cells from the G_1 phase of the cell cycle into the S phase [253]. In addition, Akt regulates cell proliferation by phosphorylating the cell cycle inhibitory protein, $p21^{Cip1/WAF1}$, which inhibits interactions between $p21^{Cip1/WAF1}$ and proliferating cell nuclear antigen (PCNA), thereby reversing repression of DNA replication [254, 255].

On the other hand, Akt has been shown to stimulate cell proliferation by directly phosphorylating and activating the mammalian target of rapamycin (mTOR), also known as FK506-binding protein-rapamycin-associated protein (FRAP1), on Ser-2448 residue [256] (Figure 4 C). mTOR was identified through characterization of the activity of pharmacological agent Rapamycin [257], also known as Sirolimus or Rapamune [258, 259], a macrolide antibiotic isolated from a strain of *Streptomyces hygroscopicus* contained in a soil sample collected on Easter Island, Rapa Nui [260]. Rapamycin has been shown to inhibit mTOR kinase activity by binding and activating the cytoplasmic receptor, FK506-binding protein-12 (FKBP12) [261], which interacts with FKBP12-rapamycin binding (FRB) domain of mTOR, and consequently inhibiting mTOR activity [262].

Although Akt acts as a key activator of mTOR, recent evidence suggests that signaling molecules, including PKCη, can activate Akt and mTOR in parallel [263, 264] (Figure 4 C). Furthermore, activation of mTOR in transformed B lymphocytes has recently been shown to occur independent of Akt activation [265]. In addition,

accumulation of phosphatidic acid (PA) following activation of phospholipase D has been shown to induce mTOR activation independently of PI3K/Akt signaling pathway [266] (Figure 4 C). Although phosphorylation of mTOR at Ser-2448 has previously been shown to be directly phosphorylated by Akt [256, 267], the nature of upstream kinase(s) that phosphorylate mTOR at this site remains elusive and requires further investigation [268-272].

mTOR controls cell cycle progression by phosphorylating and activating 70-KDa protein S6 kinase (p70 S6K), which by phosphorylating the 40 S ribosomal protein S6, stimulates translation of mRNA that possess a 5'-terminal oligopyrimidine (5'-TOP), including that encode ribosomal proteins and translation elongation factors [273, 274]. Although mTOR has been reported as the major kinase activator upstream of p70 S6K, PDK-1 has been shown to directly phosphorylate p70 S6K as well [275]. Despite the critical role of p70 S6K in inducing entry of cells into the S-phase of the cell cycle [276], loss of p70 S6K in embryonic stem cells did not result in significant reduction in cell proliferation [277].

In addition to phosphorylating p70 S6K, mTOR has been found to phosphorylate in parallel the eukaryotic initiation factor 4E (eIF4E)-binding protein 1 (4E-BP1) [278, 279] (Figure 4 C). mTOR stimulates eIF4E activity by phosphorylating 4E-BP1 at Thr-37 and Thr-46 residues [279]. When 4E-BP1 is in its α form, which is hypophosphorylated, 4E-BP1 binds with high affinity to eIF4E. As a consequence, the α form of 4E-BP1 inhibits eIF4E-dependent mRNA translation, including translation of proteins that are required for entry into the G1-phase of the cell cycle, such as cyclin D1 [280]. The presence of δ and γ forms of 4E-BP1, which are hyperphosphorylated, inhibits the association between 4E-BP1 and eIF4E. This release of eIF4E by the δ and γ forms of 4E-BP1 leaves eIF4E free to assemble with other translation initiation factors to initiate protein translation [281].

Not only does mTOR stimulate cell cycle progression, but recent studies have shown that mTOR regulates cell size as well [282]. In yeast systems where proliferation is correlated with nutrient availability, mTOR acts a sensor for ATP and amino acids within the environment, thus coupling the physical size of yeasts to the availability of extracellular nutrients [283]. Under nutrient-deprived conditions, activation of mTOR stimulates cells to maintain their mass and cellular size, thus preventing cells from undergoing proliferation and the subsequent loss of cell mass with each cycle of cell

division. Therefore, mTOR acts as a survival factor under adverse conditions by conferring the cells with the ability to evade apoptosis [284]. Taken together, mTOR acts by integrating the availability of amino acids, energy, and growth factors to ensure proper control of expansion in cell size and progression through the cell cycle.

In addition to its ability to regulate cell survival, mass, and proliferation, recent evidence documented a role of Akt in tumor-associated angiogenesis. Activation of Akt in vascular endothelial cells has been shown to directly phosphorylate and activate endothelial nitric oxide synthase (eNOS) on Ser-1177 [285], stimulating production and accumulation of nitric oxide (NO) [286]. Akt-dependent release of NO has been shown to induce vasodilation of vascular blood vessels, which suggests that Akt may regulate the initial critical steps of vascular wall remodeling and angiogenesis [287].

In summary, it is evident that Akt can be placed at the center of several signaling pathways involved in cell survival, growth, proliferation, as well as tumor-associated angiogenesis. These facts highlight the utility of Akt signaling pathway as a major therapeutic target.

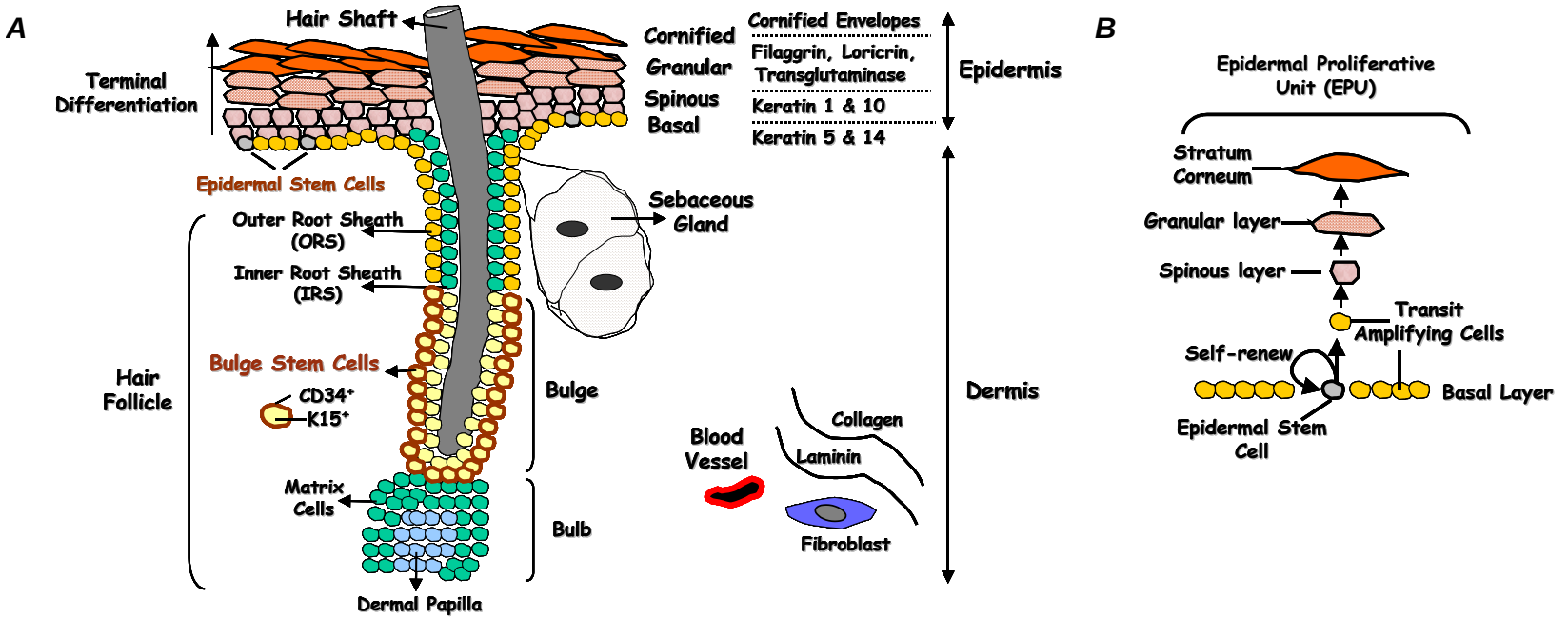

Figure 1. Shematic diagram illustrating the structure of the skin. (A) Epidermal keratinocytes undergo limited proliferation in the basal layer, then commit to terminal differentiation as they move upwards through the different layers of the skin. Although a small percentage of keratinocytes stem cells (KSC) are located within the basal layer of interfollicular epidermis (Epidermal stem cells), the majority of KSC are located in a specific niche within hair follicles, defined as “the bulge” region (Bulge stem cells). KSC localized to the bulge region are multipotent, serving as precursors for all cell types within hair follicles. Bulge stem cells are not believed to be involved in renewal of the epidermis under normal conditions; however, bulge stem cells do participate in wound repair and regeneration. ***(B)*** Epidermal stem cells are located at the center of distinct columnar units composed of 10 basal cells and their suprabasal maturing progeny, defined as epidermal proliferative unit (EPU).

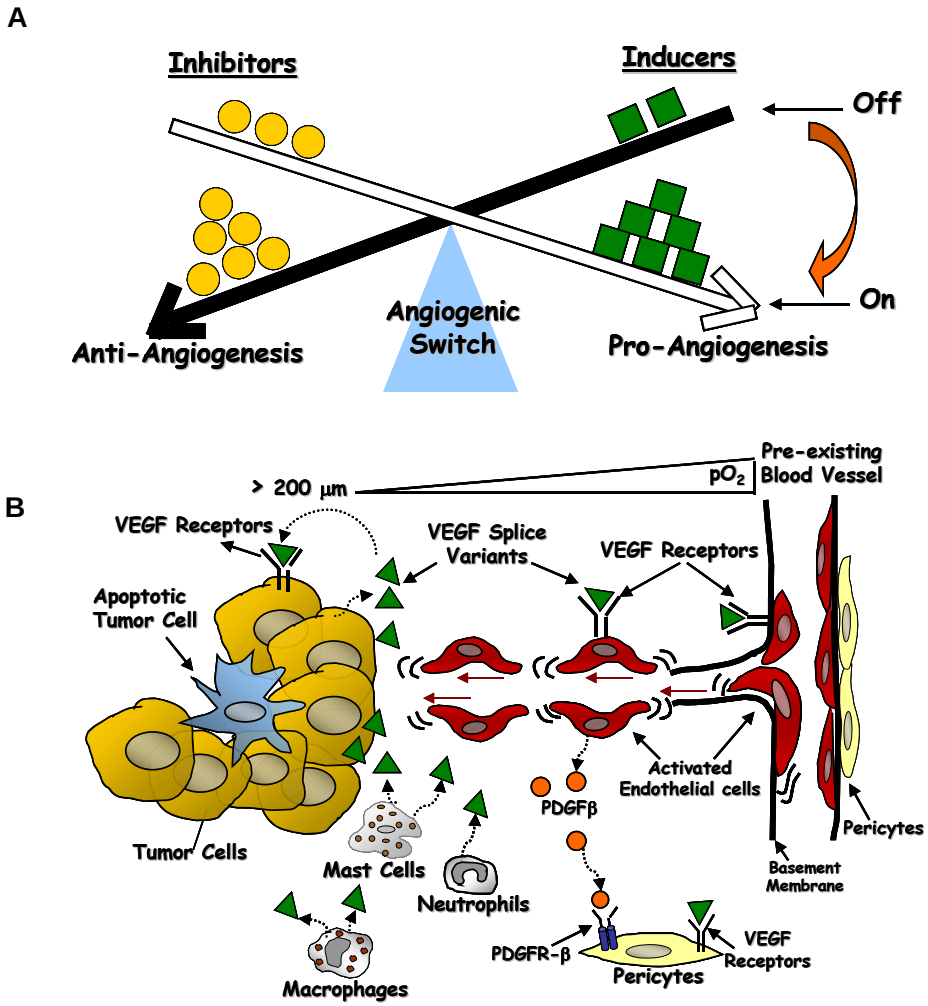

Figure 2. Schematic of tumor-associated angiogenesis. (A) "The angiogenic switch" results from production of inducers of angiogenesis which are pro-angiogenic growth factors with a simultaneous down-regulation of inhibitors of angiogenesis. ***(B)*** Tumor cells and infiltrating inflammatory cells, including mast cells, neutrophils, and macrophages, produce VEGF splice variants that activate vascular endothelial cells lining adjacent blood vessels. The endothelial cells then detach from the underlying pericytes and extracellular matrix, proliferate, migrate, and then organize and differentiate into capillary tubes which provide oxygen and nutrients to expanding tumors.

Figure 3. Structure and functions of human and murine VEGF Exons. (A) The human VEGF gene gives rise to 7 distinct VEGF splice variants, including $VEGF_{121}$, $VEGF_{145}$, $VEGF_{165}$, $VEGF_{165}$b, $VEGF_{183}$, $VEGF_{189}$, and $VEGF_{206}$. $VEGF_{165b}$, which has inhibitory activity, lacks exons 6 and 8, and contains a novel 6 amino acid sequence SLTRKD, designated as exon 9. ***(B)*** The mouse VEGF gene gives rise to splice variants that are all one amino acid shorter than the corresponding human splice variants. Mouse splice variants include $VEGF_{120}$, $VEGF_{144}$, $VEGF_{164}$, and $VEGF_{188}$. The unique mouse splice variant $VEGF_{205}$* lacks exons 7 and 8, and contains exon 6 which includes a 61 bp extension of exon 6a, designated as exon 6', which encodes a unique 7 amino acid carboxyl-terminal tail, YVGAAAV, that is significantly different from the carboxyl-terminal tail of any VEGF protein identified to date.

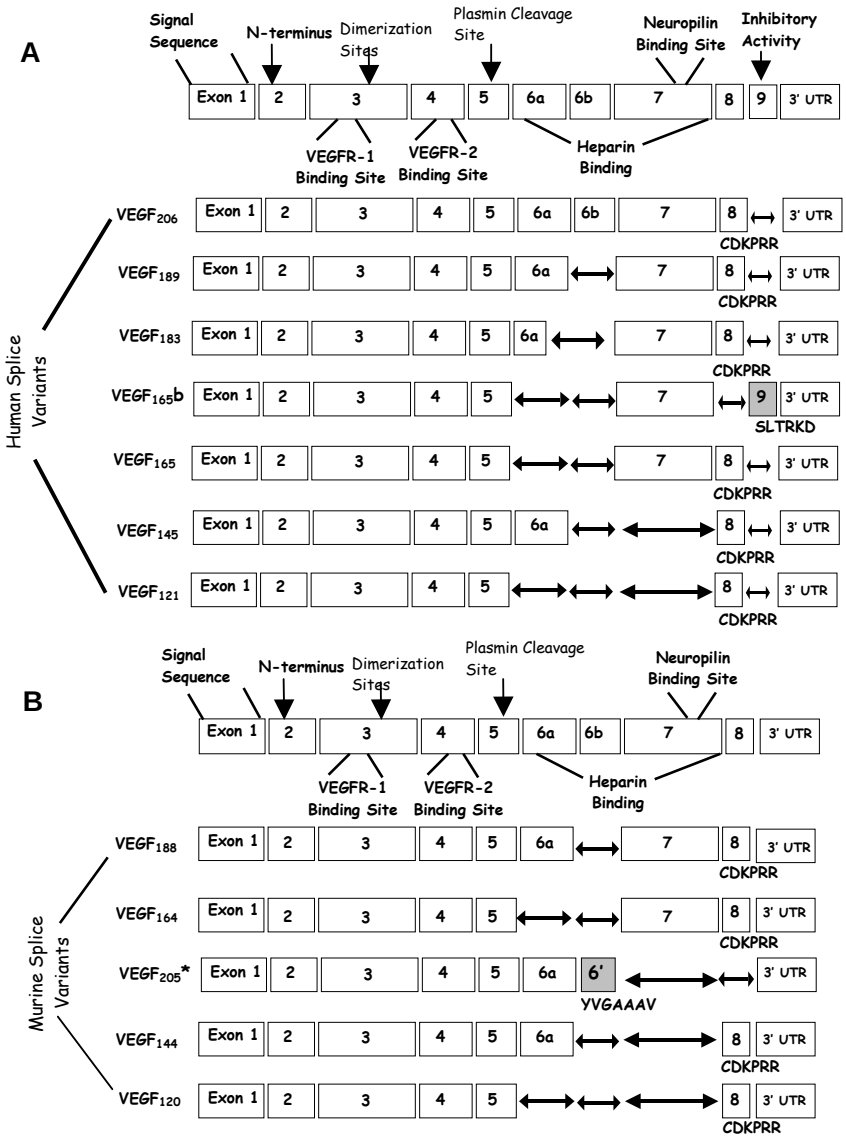
A
Signal Sequence
N-terminus
Dimerization Sites
Plasmin Cleavage Site
Neuropilin Binding Site
Inhibitory Activity
Exon 1
2
3
4
5
6a
6b
7
8
9
3' UTR
VEGFR-1 Binding Site
VEGFR-2 Binding Site
Heparin Binding
Human Splice Variants
VEGF206
VEGF189
VEGF183
VEGF165b
VEGF165
VEGF145
VEGF121
CDKPRR
SLTRKD
B
Signal Sequence
N-terminus
Dimerization Sites
Plasmin Cleavage Site
Neuropilin Binding Site
VEGFR-1 Binding Site
VEGFR-2 Binding Site
Heparin Binding
Murine Splice Variants
VEGF188
VEGF164
VEGF205*
VEGF144
VEGF120
6'
YVGAAAV
CDKPRR

Figure 3

Figure 4. Akt acts as a multi-functional protein. (A) Activation of Ak (pAkt). Binding of growth factors, including vascular endothelial growth factor (VEGF) to tyrosine (Y) kinase receptors activates PI3-K. Activated PI3-K then catalyzes the production of phosphatidylinositol 3,4,5,-triphosphate (PI-3,4,5,-P_3), which binds to the pleckstrin homology domain (PH) domain of Akt and PDK-1. Akt is then translocated from the cytoplasm to the plasma membrane and undergoes conformational changes. Akt can then be phosphorylated at Thr-308 by PDK-1 and at Ser-473 by ILK. ***(B) pAkt acts as a survival factor.*** pAkt promotes cell survival by phosphorylating and inhibiting the pro-apoptotic proteins BAD, caspase 9, and the Forkhead transcription factors (FKHR) and by inducing the expression of the anti-apoptotic FLICE-inhibitory protein (FLIP). pAkt also phosphorylates and activates IKK, which results in the phosphorylation and degradation of IκB, an inhibitor of nuclear factor- κB (NF-κB), freeing NF-κB to induce transcription of survival genes. ***(C) pAkt induces cell cycle progression.*** Akt stimulates entry into the cell cycle by activation the mammalian target of rapamycin (mTOR). pAkt also induces cell cycle entry by inactivating glycogen synthase kinase-3 beta (GSK-3β), which results in the stabilization of Cyclin D1 and by inhibiting $p21^{Cip1/WAF1}$. LY294002 is a specific inhibitor of PI3-K, while rapamycin is a selective inhibitor of mTOR.

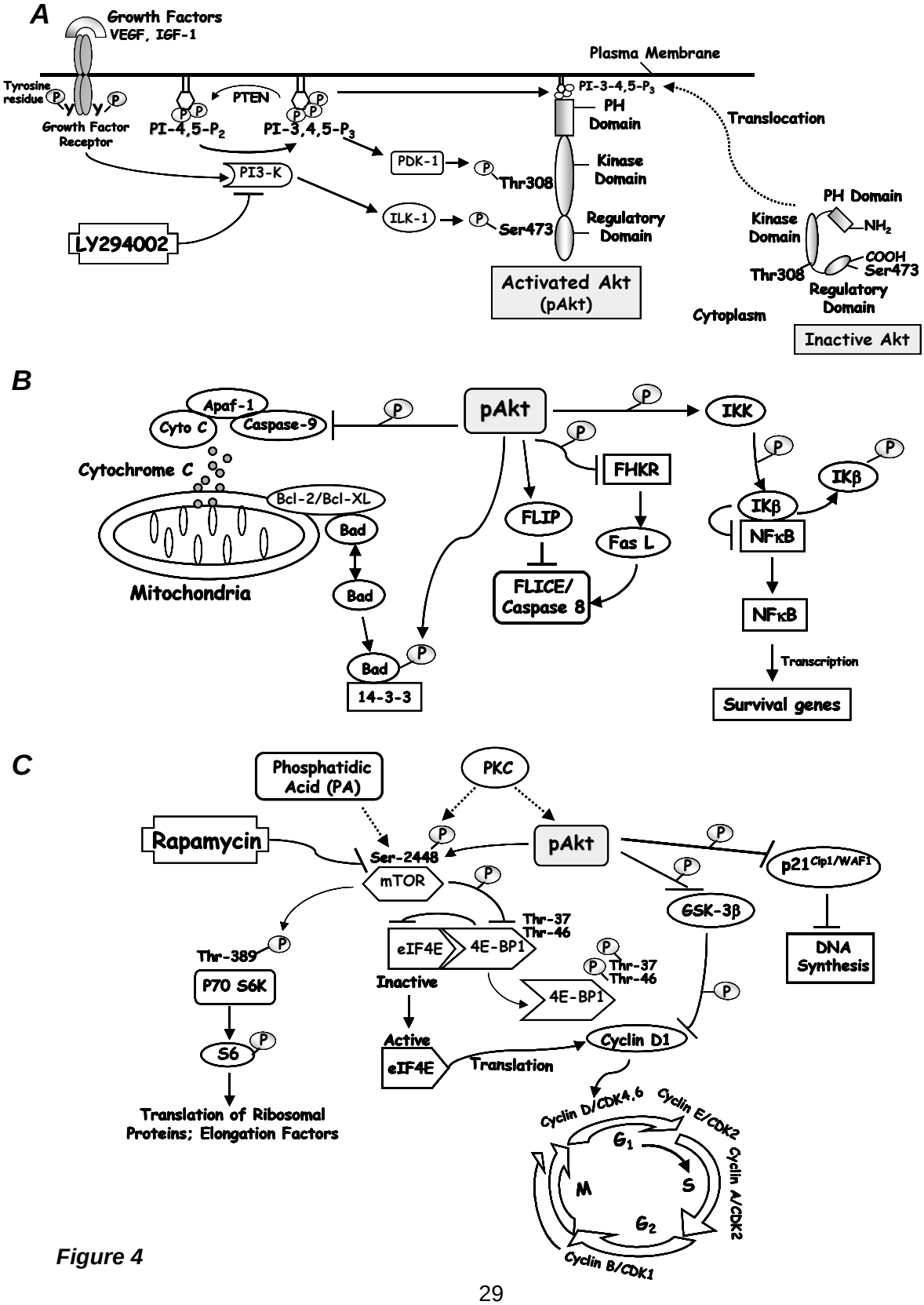
A
Growth Factors
VEGF, IGF-1
Plasma Membrane
Tyrosine residue
Growth Factor Receptor
PTEN
PI-4,5-P2
PI-3,4,5-P3
PI-3-4,5-P3
PH Domain
Translocation
PDK-1
Thr308
Kinase Domain
PI3-K
ILK-1
Ser473
Regulatory Domain
LY294002
Activated Akt (pAkt)
PH Domain
Kinase Domain
NH2
COOH
Ser473
Thr308
Regulatory Domain
Cytoplasm
Inactive Akt
B
Apaf-1
Cyto C
Caspase-9
pAkt
IKK
Cytochrome C
FHKR
IKβ
Bcl-2/Bcl-XL
FLIP
NFκB
Bad
Fas L
Mitochondria
FLICE/ Caspase 8
Transcription
14-3-3
Survival genes
C
Phosphatidic Acid (PA)
PKC
Rapamycin
Ser-2448
pAkt
p21Cip1/WAF1
mTOR
GSK-3β
Thr-37
Thr-46
Thr-389
eIF4E
4E-BP1
DNA Synthesis
P70 S6K
Inactive
Thr-37
Thr-46
4E-BP1
S6
Active
eIF4E
Translation
Cyclin D1
Translation of Ribosomal Proteins; Elongation Factors
Cyclin D/CDK4,6
Cyclin E/CDK2
G1
S
M
G2
Cyclin A/CDK2
Cyclin B/CDK1

Figure 4

Table 1. List of markers used to identify specific populations of cells.

Name of Marker	Cell population
CD34	Keratinocytes located to the ORS of the bulge region of hair follicles
CD31/PECAM-1	Endothelial cells
Giemsa	Mast cells
Gr-1	Activated neutrophils
K15	Keratinocytes located to both the ORS and IRS of the bulge region of hair follicles
MPO	Activated neutrophils
PCNA	Proliferating cells in the G_1/S and G_2 phase of the cell cycle
Toluidine Blue	Mast cells

CHAPTER 1

FUNCTIONAL CHARACTERIZATION OF NOVEL MURINE $VEGF_{205}$* PROTEIN WHICH STIMULATES MIGRATION AND PHOSPHORYLATION OF AKT AND MTOR IN HUMAN ENDOTHELIAL CELLS

1.1. Abstract

The present study describes the identification, cloning, sequencing, and characterization of the biological activities of murine $VEGF_{205}$*, which encodes for a truncated 145 amino acid polypeptide with a unique 7 amino acid carboxyl-terminal tail, YVGAAAV, that is significantly different from the carboxyl-terminal tail of other mouse or human vascular endothelial growth factor-A (VEGF-A) proteins previously identified. $VEGF_{205}$* binds to VEGF receptor 2 (VEGFR-2; Flk-1/KDR) of human umbilical vein endothelial cells (HUVEC), leading to phosphorylation of VEGFR-2 at both tyrosines (Y) Y-951 and Y-1054/1059. Recombinant $VEGF_{205}$* protein stimulated human endothelial cells to form tubules with large luminal spaces and greater numbers of terminal branch points compared to the smaller, more organized tubules formed by endothelial cells exposed to $VEGF_{120}$. Although $VEGF_{205}$* was not as mitogenic as $VEGF_{120}$, this novel VEGF splice variant stimulated significantly greater wound closure using an *in vitro* model compared to $VEGF_{120}$. $VEGF_{205}$* stimulated a significant increase in Akt phosphorylation at Serine-473 residue (Akt-Ser-473-P) compared to $VEGF_{120}$. The $VEGF_{205}$*-induced Akt activation was completely blocked by the phosphoinositide 3-kinase (PI3-K) inhibitor, LY294002. While both $VEGF_{205}$* and $VEGF_{120}$ induced phosphorylation of Akt at Thr-308 residue (Akt-Thr-308-P) compared to unstimulated cells, there was no significant difference in phosphorylation levels of Akt-Thr-308-P following exposure of HUVEC to $VEGF_{205}$* compared to $VEGF_{120}$. These results suggest that $VEGF_{205}$* differentially activated integrin-linked kinase-1 (ILK-1) compared to $VEGF_{120}$. Additionally, $VEGF_{205}$* induced phosphorylation of mammalian target of rapamycin (mTOR) at Serine-2448, which was

also inhibited by LY294002. Taken together, identification of $VEGF_{205}$* splice variant may serve as a useful diagnostic in oncology and may be used as a potential therapeutic agent in tissues whose vascular supply has been insufficient or inappropriate, including cardiovascular diseases. $VEGF_{205}$*-induced PI3-K/Akt signaling pathway may further serve as a molecular target for inhibiting skin tumor angiogenesis.

1.2. Introduction

The development of blood vessels has been defined as neovascularization, a highly regulated and necessary process for appropriate embryonic development [108]. With the exception of tumor growth [288], neovascularization in adult mammals occurs only during normal physiological processes such as the female reproductive cycle [109] and wound healing [110, 289]. As tumor cells proliferate and their layers accumulate, the distance between malignant cells within the expanding tumor mass and the nearest blood vessel increases. When tumors reach a size of 1-2 mm, tumor cells located at a distance greater than 200 μm from the nearest blood vessel become hypoxic and are deficient in critical nutrients [116]. At this stage, tumor cells are in a state of equilibrium between proliferation and apoptosis. In order to expand beyond this critical size, actively growing tumors have an absolute requirement for development of new blood vessels [114], which has been defined as tumor angiogenesis. During the point at which tumors are expanding in size, tumors undergo what has been defined as the “angiogenic switch” [117], which results from the shift in the balance of anti-angiogenic growth factors that inhibit formation of new vasculature to favor the production of pro-angiogenic growth factors that diffuse into the surrounding of the tumor. One family of pro-angiogenic proteins that has been identified is vascular endothelial growth factor-A (VEGF-A) [118].

Although one gene encodes for both rodent and human VEGF-A, a number of different VEGF proteins with specific activities can be produced through the alternative splicing of the 8 exons within the single VEGF gene. In humans, the most abundantly produced VEGF splice variants are $VEGF_{121}$, $VEGF_{165}$, and $VEGF_{189}$ [176], with less abundantly produced VEGF splice variants including $VEGF_{145}$ [177], $VEGF_{183}$ [178], and $VEGF_{206}$ [179]. Although the majority of human VEGF splice variants are pro-angiogenic, an anti-angiogenic splice variant $VEGF_{165}b$ has been identified [181] which has been shown to be down-regulated in renal tumors, with the loss of $VEGF_{165}b$ coinciding with activation of the angiogenic switch [180]. $VEGF_{165}b$ lacks exon 8, which is replaced by exon 9, resulting in production of a protein with the same length as $VEGF_{165}$ but with a carboxyl-terminal tail composed of 6 unique amino acids, SLTRKD [181].

Murine VEGF variants are one amino acid shorter than the analogous human splice variants, but in most cases the mouse VEGF proteins possess biological activities similar to human VEGF splice variants. Murine VEGF splice variants identified to date include $VEGF_{120}$, $VEGF_{144}$, $VEGF_{164}$, and $VEGF_{188}$ [182]. In addition to these murine

VEGF proteins, we first identified a novel murine VEGF splice variant designated as $VEGF_{205}$*, which was present in carcinomas isolated of FVB/N mice but was completely undetectable in normal skin [290]. This study was the first to identify and examine the importance of differential expression of mouse VEGF splice variants in murine skin tumor promotion and progression [290].

The biological activities of VEGF splice variants occurs following binding to the VEGF receptor tyrosine kinase family, which include VEGF Receptor-1 (VEGFR-1), which was first isolated and characterized as fms-like tyrosine kinase-1 (Flt-1) [183-185] and VEGFR-2, also defined as fetal liver kinase-1/Kinase-insert-domain-containing receptor (Flk-1/KDR) [186, 187]. The differential ability of VEGF receptors to induce selective biological activities including increased vascular permeability as well as proliferation, migration, differentiation, and organization of vascular endothelial cells into vascular tubules during tumor-associated angiogenesis is due to phosphorylation of specific VEGFR-associated tyrosine residues. For example, following binding of VEGF to VEGFR-2, vascular endothelial cells undergo proliferation which is due to phosphorylation of tyrosine residues 1054/1059 [192], while migration of these cells is stimulated following phosphorylation of tyrosine residue 951 [192, 193]. Conversely, VEGFR-1 is a kinase-defective receptor tyrosine kinase, which negatively modulates angiogenesis [291, 292]. Binding of VEGF to VEGFR-1 inhibits VEGFR-2-mediated endothelial cell proliferation, but does not inhibit migration that occurs following VEGF binding to VEGFR-2 on endothelial cells [194]. VEGFR-1 can also act as a decoy receptor that sequesters VEGF, preventing it from binding to VEGFR-2 [197]. Given that VEGFR-1 acts as endogenous inhibitor of VEGF-induced angiogenic activities, strategies to block VEGF-induced VEGFR-2 activation are being developed to examine the anti-angiogenic [293, 294] and anti-tumor effects of VEGFR-1 [295-299].

Since VEGF can activate and recruit vascular endothelial cells to undergo all of the necessary activities required to form new capillary beds, the VEGF-A family of proteins have been defined as complete angiogenic growth factors [139, 300]. VEGF splice variants not only stimulate tumor blood vessel formation, but may also act as a survival factor by preventing tumor-associated endothelium, which exist in the tumor microenvironment that is hypoxic and deprived of nutrients, from undergoing apoptosis and senescence [145, 146, 301]. Akt, also known as protein kinase B (PKB), is a core component of the phosphoinositide 3-kinase (PI3-K) signaling pathway [302, 303]. Akt is

composed of an amino-terminal pleckstrin homology (PH) domain that binds phospholipids [231], a kinase domain, and a proline-rich carboxyl-terminal regulatory domain. In response to growth factors such as $VEGF_{205}$*, PI3-K is recruited to the inner surface of the plasma membrane resulting in the generation of the membrane-bound lipid, phosphatidylinositol 3,4,5-triphosphate (PI-3,4,5-P_3) [304, 305]. Following binding of PI-3,4,5-P_3 to the PH domain, Akt is recruited to the inner surface of the plasma membrane [232], where Akt becomes fully activated by phosphorylation at two amino acid residues, serine-473 (Ser-473) and threonine-308 (Thr-308). Phosphorylation of Akt at Thr-308 and Ser-473 residues is carried out by two distinct kinases, 3-phosphoinositide-dependent protein kinase-1 (PDK-1) which phosphorylates Thr-308 residue [234], and integrin-linked kinase-1 (ILK-1), which phosphorylates Ser-473 residue [236, 306, 307]. 2-(4-morpholinyl)-8-phenylchrome (LY294002) is a competitive inhibitor for the ATP binding site of PI3-K and leads to inhibition of Akt phosphorylation [239, 240].

Although the majority of studies have focused on the role of Akt as a survival factor, Akt can also act as a multi-functional protein kinase which regulates both cell proliferation and increase in cell mass [252, 308]. Akt has been shown to directly phosphorylate the mammalian target of rapamycin (mTOR) at Ser-2448 residue [256, 267, 309]. mTOR was initially identified as the cellular target of the pharmacological agent rapamycin [257], also known as sirolimus or Rapamune [258, 259], a lipophilic macrolide antibiotic which was first isolated from a strain of *Streptomyces hygroscopicus* that is indigenous to Easter Island (also known as Rapa Nui) [260].

mTOR couples increases in cell mass and size to the availability of extracellular nutrients. mTOR has been shown to serve as a sensor for ATP and amino acids [283] and to regulate cellular responses during nutrient deprivation [310]. mTOR-dependent increases in cell mass has been further shown to be tightly coupled to cell cycle progression, which allows cells to proliferate continuously while maintaining their size [282]. Following its activation, mTOR stimulates phosphorylation of 70 KDa ribosomal protein S6 kinase (p70 S6K) enzyme at Thr-389 residue. Once activated, p70 S6K stimulates entry of cells into the S-phase of the cell cycle by phosphorylating the 40S ribosomal protein, S6. This sequence of events leads to an increased rate of initiation of translation of mRNAs that encode ribosomal proteins and translation elongation factors [311, 312]. In addition, mTOR initiates translation of proteins that are required for entry

into the G1-phase of the cell cycle, including cyclin D1, by phosphorylating eukaryotic translation initiation factor 4E-binding protein 1 (4E-BP1) at Thr-37 and Thr-46 residues [278, 279, 313]. 4E-BP1 negatively regulates the activity of the eukaryotic initiation factor 4E (eIF4E), thus relieving the translation inhibitory effects of 4E-BP1 leaves eIF4E free for initiation of protein translation [281]. Taken together, Akt induces signal transduction pathways critical to survival, expansion in cell mass, and proliferation.

The present studies reported the cloning, sequencing, production of purified recombinant $VEGF_{205}$* protein, and characterized the functional activities of $VEGF_{205}$*, which activates Akt and mTOR and selectively induces human umbilical endothelial cells to undergo migration and tubule formation.

1.3. Materials and Methods

1.3.1. Cloning of $VEGF_{205}$* cDNA. $VEGF_{205}$* cDNA was generated from total RNA isolated from Tg.AC mouse lung and was obtained in two parts. The 5'-end was amplified using an exon 2/exon 3 forward primer (bp 101-123, 5'-GAA GTC CCA TGA AGT GAT CAA G-3') and a reverse primer specific for the region downstream of exon 6a (bp 507-525, 5'-TCC AGG GCA TTA GAC AGC A-3'), under the conditions of 95^{o}C for 20 sec, 59^{o}C for 20 sec, and 72^{o}C for 60 sec, for a total of 38 cycles, which yielded a 424 bp product. To obtain the 3'-end, a primer spanning the exon 6a boundary into the immediate downstream region (bp 481-498, 5'-TTC TGG AGC GTG TAC GTT-3') and a 3'UTR reverse primer (5'-AAA CCC TGA GGA GGC TCC TT-3') were used under conditions of 95^{o}C for 20 sec, 54^{o}C for 20 sec, and 72^{o}C for 60 sec, for a total of 38 cycles, which yielded a 250 bp PCR product that was gel-purified before re-amplification using a nested forward primer (bp 484-501, 5'-TGG AGC GTG TAC GTT GGT-3'). DNA fragments were cloned into pcDNA4/HisMax-TOPO and pCR2.1 (Invitrogen, Carlsbad Ca), and the DNA sequence of at least two clones was determined for each construct. The DNA fragments generated included overlap of cDNA sequence that was unique and not primer encoded.

1.3.2. Expression, purification, and refolding of His-tagged $VEGF_{205}$* and $VEGF_{120}$. DNA fragments encoding the mature VEGF polypeptides were amplified by PCR using a common exon 2 forward primer (5'-GGC AGC CAT ATG GCA CCC ACG ACA GAA GGA-3'). $VEGF_{120}$ was amplified using exon 8 specific reverse primer (5'-AGA CTC GAA TTC CTC ACC GCC TTG GCT TGT-3'). $VEGF_{205}$* was amplified using reverse primer that is specific to the novel exon 6' sequence (5'-AGA CTC GAA TTC CAG GAA GGC TCC AAG GAA-3'). Following amplification, the DNA fragments were cloned into pCR4-TOPO vector (Invitrogen) for verification by automated DNA sequencing. DNA fragments were then subcloned into the *Nde*I-*Eco*RI restriction sites of pET-28a (Novagen, Madison, WI), which fuses an additional 21 amino acids and a His-Tag to the amino-terminus. Expression of recombinant protein was induced with 0.5 mM isopropyl β-D-1-thiogalactopyranoside in cultures of transformed *E. coli* BL21 (DE3) cells (Stratagene, La Jolla, CA) grown to an optical density of 0.6 at 650 nm for 2 hr. Bacterial cells were harvested, resuspended in 10 ml of TIN buffer (100 mM Tris-HCl, pH 8.0, 5 mM imidazole and 300 mM NaCl), and lysed by sonication. Inclusion bodies were washed

with 40 ml of 2 M urea-TIN buffer and recombinant protein was extracted with 25 ml of 8 M urea-TIN buffer at 4^{o}C overnight. Clarified supernatant was applied to a 5 ml Ni^{2+}-Sepharose column (Amersham Pharmacia Biotech, Uppsala, Sweden), washed with 60 mM imidazole, and eluted with 120 mM imidazole. Recombinant protein was diluted to 90-140 ng/ml in 10 mM Tris-HCl, pH 8.5, 6 M urea, 0.1 M NaH_2PO_4, 20 mM dithiothreitol, 1 mM EDTA, then dialysed against 100 mM Tris-HCl, pH 8.5, 0.5 M Guanidine hydrochloride (GdCl), 2 mM EDTA, 5 mM cysteine, and 1 mM cystine at 4^{o}C overnight with gentle stirring, which was followed by dialysis against 0.1 M acetic acid for 24 hr, and finally dialyzed against PBS. Clarified protein was concentrated using Centriplus YM-10 (Millipore, Bedford, MA). Protein concentrations were determined using the BIO-RAD Protein Assay (BIO-RAD, Hercules, CA) and BSA (Sigma, St. Louis, MO) was used as a standard. Protein concentrations were further verified by Commassie-blue staining of 600 ng of reduced VEGF proteins separated by SDS-polyacrylamide gel (SDS-PAGE).

1.3.3. Western blot analysis of recombinant VEGF proteins. To confirm the identity of recombinant VEGF proteins, equal aliquots of recombinant VEGF proteins (200 ng) were separated by 12% SDS-PAGE and blotted to nitrocellulose membrane. Membranes were incubated with polyclonal goat anti-mouse VEGF (1:1000, R&D Systems, Minneapolis, MN) for 1 hr at room temperature. Blots were then incubated for 1 hr at room temperature with horseradish peroxidase (HRP)-linked donkey anti-goat IgG (1:5000, Jackson ImmunoResearch Laboratories, West Grove, PA) in 5% non-fat dried milk powder and 1% BSA in phosphate-buffered saline containing 0.1% Tween-20 (PBST). The signal was developed using ECL+plus Western Blotting Detection System (Amersham).

1.3.4. Cell culture. Human umbilical vein endothelial cells (HUVEC) (Clonetics, San Diego, CA) were maintained in a 37^{o}C humidified atmosphere (95% air and 5 %CO_2) in Endothelial Basic Medium-2 (EBM-2) supplemented with Endothelial Growth Medium-2 (EGM-2) SingleQuots as recommended by the manufacturer (Clonetics). HUVEC up to 6 passages were used for all experiments.

1.3.5. Proliferation assay. HUVEC were grown in 96-well tissue culture plates (2000 cells per well) in Dulbecco's modified Eagle's minimal essential medium (DMEM; high glucose) supplemented with 10% fetal bovine serum (Invitrogen) and antibiotics (penicillin G/streptomycin sulfate) in a 37^{o}C humidified atmosphere with 5% CO_2 for 24 hr. Recombinant VEGF proteins (0.01-100 ng/ml) and Alamar blue (10%; Biosource International, Carmarillo, CA) were added to the media. Following 24 hr of incubation of cells with Alamar blue, absorbance was measured as optical density (OD) at 570 nm and 600 nm. The percent of Alamar blue dye reduction was used as a measure of cell proliferation and was calculated according to manufacturer's instructions. Cell number was evaluated in at least 6 samples.

1.3.6. Cell treatment and protein isolation. HUVEC (1x 10^5 cells) were plated on 100 mm plates and grown to 80% confluency. HUVEC were starved for 6 hr in EMB-2 supplemented with 10 units /ml heparin and 2 mM glutamine, and pre-treated for the last hour with 1 mM sodium orthovanadate (Na_3VO_4, Sigma). The PI3-K specific inhibitor LY294002 (40 μM; Sigma) was added at 3 hr following serum starvation. HUVECs were then stimulated at 37^{o}C with 50 ng/ml of the individual recombinant VEGF proteins for 2, 5, 15, 30, or 60 minutes. Cells were lysed with cold lysis buffer (150 mM NaCl, 10 mM Tris-HCl pH 7.5, 1% Triton X-100, 1 mM Na_3VO_4, 10 μg/ml aprotinin, 10 μg/ml leupeptin, and 1 mM PMSF). Cells were scraped and lysates were clarified by centrifugation. Proteins were normalized using the BIO-RAD protein assay. Samples were stored at -80^{o}C until Western blot analysis was performed.

1.3.7. Western blot analysis. Equal aliquots of protein extracts (22 μg/sample) were analyzed by Western blot analysis using 8% SDS-PAGE and then blotted to Hybond-P polyvinylidene difluoride membrane (PVDF; Amersham, Piscataway, NJ). The blots were blocked by incubation in 5% non-fat dried milk powder in PBST. Blots were then incubated with polyclonal rabbit anti-phospho-VEGF Receptor-2 (Tyr-951) (1:500; Cell Signaling), polyclonal rabbit anti-phospho-VEGF Receptor-2/3 (Ab-1) (1:2500; Oncogene, San Diego, CA), polyclonal rabbit anti-phospho-Akt-Ser-473 (1:500; Cell Signaling), polyclonal rabbit anti-phospho-Akt-Thr-308 (1:500; Cell Signaling), polyclonal rabbit anti-phospho-mTOR-Ser-2448 (1:500; Cell Signaling) in 5% BSA in PBST overnight at 4^{o}C. Blots were then incubated for 1 hr at room temperature with

horseradish peroxidase (HRP)-linked goat anti-rabbit IgG (1:2000; Amersham) in PBST containing 5% non-fat dried milk powder. Signals were visualized using the ECL+Plus Western Blotting Detection System (Amersham). Blots were subsequently stripped and re-probed with polyclonal mouse anti-Flk-1 (A-3) (1:200; Santa Cruz Biotechnology, Santa Cruz, CA), polyclonal rabbit anti-Akt (1:1000; Cell Signaling), or polyclonal rabbit anti-mTOR (1:500; Cell Signaling). Blots were then incubated for 1 hr at room temperature with HRP-linked sheep anti-mouse or goat anti-rabbit IgG (1:2000; Amersham) in PBST containing 5% non-fat dried milk powder. Controls for Akt phosphorylation at Ser-473 residue included whole cell lysates isolated from serum starved NIH3T3 cells with (+) and without (-) PDGF treatment, at 100 mg/ml for 10 minutes (Cell Signaling). To verify equal loading of protein samples, blots were re-probed with monoclonal mouse anti-β-actin (1:5000; Sigma) for 1 hr, then incubated with anti-mouse IgG (1:4000; Amersham) for 30 min. Images were scanned and band intensities were analyzed using NIH Image 1.62f analysis software.

1.3.8. Wound migration assay. HUVEC (4×10^5 cells) were seeded into 6-well plates and grown to confluence in EBM-2 medium containing 10% FBS. Cells were then washed once with PBS, and incubated in the presence of DMEM supplemented with 2% FBS for 4 hr. A linear scar was drawn then across the cells monolayer using a sterile plastic tip. Media was then replaced with DMEM containing 1% FBS, in the presence or absence of VEGF isoforms (10 ng/ml) for 20 hr. To determine wound width at time 0 hr, scars were drawn in one well just before staining with Diff-Quick (Dade Behring Ag, Newark, DE) (Figure 5 A). Digital images of wounds were captured using 10x objective on an inverted microscope (Olympus, Melville, NY) with an attached digital camera (Diagnostic Instruments, Sterling Heights, MI). Image analysis was performed using Image Pro Plus software (Media Cybernetics, Silver Springs, MD) and a custom-written macro. A line intensity histogram was measured perpendicular to wound and spanning full height of image, which resulted in an intensity profile curve on which the following parameters were measured (Figure 1.5 A): Baseline intensity, which was determined on a per-image basis by using the average intensity of confluent regions; Wound width, defined as the width where intensity curve crosses the baseline; Peak Height, the maximum intensity peak within the wound; Wound width at 1/2 height, the width of the

wound at 1/2 the maximum peak height within the wound; and Area under curve, the area under the curve of intensity histogram.

1.3.9. Tubule assay. HUVEC were incubated in DMEM supplemented with 5% FBS for 16 hr, then harvested, washed twice with EMB-2, and resuspended at a concentration of 4x 10^5 cells/ml. Recombinant VEGF proteins were diluted in DMEM supplemented with 0.1% de-lipidated BSA (BD Biosciences, Bedford, MA), which was then combined with an equal volume of HUVEC and plated (200 μl) into 96 well plates coated with 10 μg/ml mouse type IV collagen (BD Biosciences), resulting in a final concentration of 4 x 10^4 cells/well. Following 30 hr of incubation, cells were stained with Diff-Quik (Dade Behring Ag). Digital images were captured using a CCD camera (Diagnostic Instruments) mounted on an Olympus BX40 microscope. Endothelial cell-derived tubule formation was quantitated using Image Pro Plus analysis software (Media Cybernetics). Images were captured under identical lighting and optical settings, and color segmentation was used to eliminate non-specific background staining. Once segmented, a mask of the image was filtered to delineate the cell connections and cell masses. The image was then filtered and skeletonized. The skeleton was superimposed on the mask of the connections. The length of the terminal branches within the skeleton, which represent cellular projections, was measured (Figure 1.6 A, panel F). Terminal branches that were <15 μm in width were counted. The number of terminal branches was normalized to the number of cells in the field of view.

1.3.10. Statistical analysis. Statistical analyses were performed using the unpaired, one-tailed Student's *t* test or one way analyses of variance (ANOVA) on ranks for non-parametric comparison, with *post-hoc* Dunnet test to evaluate significant comparisons between treatment groups and control samples. Comparisons of three or more groups were conducted using one-way ANOVA, with Student-Newman-Keuls *post-hoc* analysis (GraphPad Prism). In all cases, results are expressed as mean ± SEM, and statistical significance was defined as $p<0.05$, unless otherwise described.

1.4. Results

1.4.1. Identification of a novel murine $VEGF_{205}$* splice variant of 145 amino acids. Although we initially believed that murine $VEGF_{205}$* was analogous to human $VEGF_{206}$, through cloning, sequencing, production of recombinant protein and verification of amino acid sequence, we demonstrated that $VEGF_{205}$* mRNA is composed of only the first 6 exons (exon 1-exon 6a) of murine VEGF-A, with an extension of exon 6a, consisting of an additional 61 bases designated as exon 6' (Figure 1.1 A), with the loss of exons 7 and 8 (Figure 1.1 B). The 3'-end of the 61 bp insertion in $VEGF_{205}$* contains a novel consensus sequence encoding the 5'-splice donor site required for $VEGF_{205}$* processing. In addition, a novel splice acceptor site is present within the intronic sequence of exon 7, which is located 120 bp upstream of exon 8. The 7 amino acids encoding the novel exon 6' include Tyr-Val-Gly-Ala-Ala-Ala-Val (YVGAAAV) (Figure 1.1 C), followed by the in-frame stop codon TAA, resulting in a unique carboxyl-terminal amino acid sequence. This is in direct contrast to $VEGF_{120}$, $VEGF_{144}$, $VEGF_{188}$, and $VEGF_{164}$, which share the 6 amino acids encoding exon 8, Cys-Asp-Lys-Pro-Arg-Arg (CDKPRR) (Figure 1.1 C). $VEGF_{205}$* is therefore unlike any of the other murine VEGF-A splice variant proteins that have been identified to date.

Termination of protein synthesis within exon 6' of $VEGF_{205}$* yields a mature polypeptide consisting of 145 amino acid residues following cleavage of the 26-amino acid signal peptide (Genbank Accession no. **AY120866**) (Figure 1.1 C). To indicate that this novel VEGF protein differs from human $VEGF_{206}$ and to avoid confusion with the human $VEGF_{145}$, this unique murine VEGF splice variant is referred to as $VEGF_{205}$*.

1.4.2. Expression and refolding of recombinant $VEGF_{205}$*. To assess the biological functions of $VEGF_{205}$*, recombinant His-tagged $VEGF_{205}$* protein was produced. For functional comparison, $VEGF_{120}$, which was previously shown to induce both proliferation and migration of endothelial cells [314, 315], was generated as a His-tagged protein. To illustrate that that recombinant VEGF proteins efficiently formed dimers, purified refolded proteins (600 ng) were separated on a 12% SDS-PAGE gel under non-reducing conditions (-βME; β-mercaptoethanol) (Figure 1.2). Under reducing conditions (+βME), both $VEGF_{205}$* and $VEGF_{120}$ migrated as monomers. $VEGF_{205}$* migrated as two bands, representing both the glycosylated and unglycosylated forms of the proteins, as has been previously reported with other VEGF splice variants [316].

For Western blot analysis of $VEGF_{205}$* and $VEGF_{120}$, aliquots of 200 ng of purified recombinant VEGF splice variants were analyzed. Recombinant $VEGF_{205}$* and $VEGF_{120}$ were detected using a commercially available polyclonal mouse anti-$VEGF_{164}$ antibody. To confirm the position of purified recombinant VEGF proteins, a commercially available recombinant $VEGF_{120}$ ($rVEGF_{120}$) (R&D Systems) was used a positive control.

1.4.3. Differential phosphorylation of VEGF receptors by $VEGF_{205}$* and $VEGF_{120}$ on human umbilical vein endothelial cells. VEGF binding to VEGFR-2 leads to phosphorylation of VEGFR-2 at multiple tyrosine (Y) residues [317]. Using human umbilical vein endothelial cells (HUVEC), we examined the ability of $VEGF_{120}$ and $VEGF_{205}$* to phosphorylate VEGFR-2 at Y951, a residue associated with endothelial cells migration [192, 193], and Y-1054/Y1059, which is associated with endothelial cells proliferation [192] (Figure 1.3). Phosphorylation of VEGFR-2 at both Y-951 and Y-1054/Y-1059 residues was not detected in control HUVEC or in HUVEC treated with 10% FBS for 2 min (Figure 1.3 A). Treatment of HUVEC with 50 ng/ml of $VEGF_{205}$* for 2 min induced a significant ($p<0.05$) increase in VEGFR-2 phosphorylation at Y-951 compared to the lower levels of VEGFR-2 phosphorylation at Y-951 in HUVEC treated with 50 ng/ml $VEGF_{120}$ for 2 min (Figure 1.3 B). On the other hand, treatment of HUVEC with $VEGF_{205}$* induced significantly ($p<0.05$) lower levels of VEGFR-2 phosphorylation at Y-1054/Y1059 compared to $VEGF_{120}$.

1.4.4. Recombinant $VEGF_{205}$* induces proliferation of endothelial cells. The purified recombinant $VEGF_{120}$ produced in our laboratory using methods as described, induced HUVEC proliferation to similar levels as commercially purchased recombinant murine $VEGF_{120}$ ($rVEGF_{120}$) (R&D Systems) (Figure 1.4 A), confirming the functional activity of purified recombinant $VEGF_{120}$ that we produced. $VEGF_{205}$* induced a dose dependent mitogenesis of HUVEC, which was 10-fold lower than that induced by recombinant $VEGF_{120}$ protein, previously characterized as highly mitogenic [315] (Figure 1.4 B). These results suggested that the role of $VEGF_{205}$* in skin tumor angiogenesis was not primarily stimulation of vascular endothelial cell proliferation and prompted our further studies to characterize the spectrum of molecular activities of murine $VEGF_{205}$*.

1.4.5. Recombinant $VEGF_{205}$* stimulates endothelial cell migration. To determine the effect of $VEGF_{205}$* on vascular endothelial cell migration, a cell-based wound healing model was used, as previously described [318-320]. Wounds were artificially created by drawing a linear scar across HUVEC grown in monolayer cultures using a sterile plastic tip (Figure 1.5 A). HUVEC were then incubated in the presence or absence of VEGF splice variants (10 ng/ml) for 20 hr. $VEGF_{205}$* induced significant ($p<0.05$) migration of HUVEC into the wounded space compared to unstimulated cells as demonstrated by the significant ($p<0.05$) wound closure following incubation of HUVEC with $VEGF_{205}$* compared to control HUVEC (Figure 1.5 B). There was no significant difference in migration of HUVEC into the wounded space following incubation with $VEGF_{120}$ compared to control HUVEC.

1.4.6. Recombinant $VEGF_{205}$* stimulates formation of tubules with large luminal spaces. Studies were performed to evaluate the ability of $VEGF_{205}$* to induce HUVEC to organize into tubules, which are precursors to mature blood vessels. Tubule formation by HUVEC grown on collagen coated plates was examined following incubation of HUVEC for 30 hr at 37^{o}C in the absence of serum (Figure 1.6 A, panel A), in the presence of 5% fetal calf serum (Figure 1.6 A, panel B), 50 ng/ml of recombinant $VEGF_{120}$ (Figure 1.6 A, panel C), 50 ng/ml of recombinant $VEGF_{205}$* (Figure 1.6 A, panel D), or the combination of 50 ng/ml of recombinant $VEGF_{120}$ and 2 ng/ml of recombinant $VEGF_{205}$* (Figure 1.6 A, panel E).

In the absence of serum, HUVEC did not form organized structures (Figure 1.6 A, panel A). When grown in 5% fetal calf serum (Figure 1.6 A, panel B), HUVEC formed a mat of uniformly-shaped proliferating cells. $VEGF_{205}$* stimulated formation of tubes with large luminal spaces (Figure 1.6 A, panel D) compared to the small luminal spaces formed by HUVEC following incubation with $VEGF_{120}$ (Figure 1.6 A, panel C). The ability of $VEGF_{205}$* to induce large luminal spaces was a dominant activity in the presence of greater doses of recombinant $VEGF_{120}$ protein (50 ng/ml) and significantly lower doses of $VEGF_{205}$* (2 ng/ml) (Figure 1.6 A, panel E).

Digital image analysis of terminal branch points in cultured HUVEC treated with either 50 ng/ml $VEGF_{205}$* or $VEGF_{120}$ was performed (Figure 1.6 A, panel F). $VEGF_{205}$* induced significantly ($p<0.01$) more terminal branch points formed on a per cell basis compared to $VEGF_{120}$ (Figure 1.6 B).

1.4.7. Recombinant $VEGF_{205}$* activates the PI3-K/Akt signal transduction pathway. Western blotting was performed to examine the effects of $VEGF_{205}$* on the kinetics of Akt phosphorylation at Ser-473 in HUVEC cultured under serum-free conditions (Figure 1.7). No significant change in the ratio of phospho-Akt-Ser-473/Akt was observed in HUVEC incubated in the presence of 10% FBS for 15 min compared to unstimulated cells (Data not shown). Similarly, no significant change in the ratio of phospho-Akt-Ser-473/Akt was observed following incubation of HUVEC with 50 ng/ml $VEGF_{120}$ compared to unstimulated HUVEC (Figure 1.7 A and B). $VEGF_{205}$* at the same concentration of 50 ng/ml stimulated a significantly ($p<0.01$) greater time-dependent increase in the ratio of phospho-Akt-Ser-473/Akt compared to unstimulated control HUVEC (Figure 1.7 B). Phosphorylation of Akt at Ser-473 was maximal at 30 min following exposure to $VEGF_{205}$*, which did not significantly change at 60 min following exposure of HUVEC to $VEGF_{205}$* (Figure 1.7 B). Treatment of HUVEC with the specific PI3-K inhibitor, LY294002, completely inhibited $VEGF_{205}$* induced Akt phosphorylation at Ser-473 (Figure 1.7 C and D), demonstrating that recombinant $VEGF_{205}$* protein selectively stimulates the PI3-K/Akt signal transduction pathway in vascular endothelial cells. $VEGF_{205}$* induced phosphorylation of Akt at Ser-473 to similar levels in HUVEC purchased from a different source, American Type Culture Collection (ATCC, Manassas, VA), which was completely inhibited following treatment of endothelial cells with LY294002 (Data not shown), confirming the specificity of $VEGF_{205}$*-induced activation of PI3-K/Akt signaling pathway.

Exposure of HUVEC to $VEGF_{120}$ or $VEGF_{205}$* (50 ng/ml) induced phosphorylation of Akt at Thr-308 compared to unstimulated cells, which was completely inhibited following treatment of endothelial cells with LY294002 (Figure 1.7 E and F). However, there was no significant difference in the ratio of phospho-Akt-Thr-308/Akt following incubation of HUVEC with 50 ng/ml $VEGF_{205}$* compared to $VEGF_{120}$ (Figure 1.7 F).

1.4.8. Recombinant $VEGF_{205}$* stimulates phospho-mTOR-Ser-2448. Western blotting was performed to examine the effects of $VEGF_{205}$* on phospho-mTOR-Ser-2448 in HUVEC cultured under serum-free conditions (Figure 1.8). No significant change in the ratio of phospho-mTOR-Ser-2448/mTOR was observed following incubation of HUVEC with 50 ng/ml $VEGF_{120}$ compared to unstimulated HUVEC (Figure 1.8 A and B). There were no inhibitory effects of LY294002 on baseline levels of phospho-mTOR-Ser-2448 in

unstimulated cells or HUVEC incubated with $VEGF_{120}$ (Figure 1.8 B). In contrast, treatment of HUVEC with 50 ng/ml $VEGF_{205}$* resulted in a significant ($p<0.05$) increase in the ratio of phospho-mTOR-Ser-2448/mTOR compared to unstimulated cells. Incubation of HUVEC with LY294002 in the presence of $VEGF_{205}$* resulted in a low but significant ($p<0.05$) 0.5-fold decrease in the ratio of phospho-mTOR-Ser-2448/mTOR compared to levels of phospho-mTOR-Ser-2448/mTOR in HUVEC stimulated with $VEGF_{205}$* in the absence of LY294002 (Figure 1.8 B).

1.5. Discussion

Prior to our first studies, only 3 murine VEGF splice variants had been widely studied, which included $VEGF_{120}$, $VEGF_{164}$, and $VEGF_{188}$ [182]. Our studies were among the very first to report the existence of a cDNA containing an extended exon 6a, $VEGF_{205}$*, that was preferentially expressed in mouse skin carcinomas [290]. These observations predicted that specific VEGF splice variants are differentially expressed at specific times during tumor-associated angiogenesis and may stimulate unique and specific functions of endothelial cells within the tumor mass. In the present study, we cloned and sequenced $VEGF_{205}$* cDNA and evaluated its biological functions on human vascular endothelial cells.

The exon structure, the size, and amino acid sequence of the carboxyl-terminal tail of murine $VEGF_{205}$* are different from any other human or mouse VEGF splice variants described to date, including $VEGF_{206}$. The exon structure of $VEGF_{205}$* mRNA includes exons 1-6a, with exon 6a extended by an additional 61 bases that we have designated as exon 6'. Due to the presence of a stop codon in exon 6', protein translation of this open reading frame yielded a novel VEGF splice variant of 145 amino acids following the cleavage of the 26 amino acid residues encoding the secretory signal peptide. In contrast to $VEGF_{120}$, $VEGF_{144}$, $VEGF_{188}$, and $VEGF_{164}$, which share the 6 amino acids encoding exon 8, CDKPRR, $VEGF_{205}$* contains 7 unique amino acid residues, YVGAAAV, encoding the novel exon 6'. Thus, the positively charged and potentially kinked carboxyl-terminus found in the majority of VEGF splice variants [180] is replaced with hydrophobic amino acids in $VEGF_{205}$*.

The potential molecular activities of $VEGF_{205}$* may in part be predicted based on its exon structure (Figure 1.1 C). The presence of exon 1 predicts that it is actively secreted. The presence of exons 3 and 4 predicts that $VEGF_{205}$* can dimerize and binds to both VEGFR-1 and VEGFR-2 based on Additionally, $VEGF_{205}$* is predicted to bind heparin and heparin sulfate proteoglycans based on the presence of exon 6a, resulting in its retention within the local tumor microenvironment. Since $VEGF_{205}$* contains an extension of exon 6a, exon 6', that encodes for a protein with a novel carboxyl-terminal tail, $VEGF_{205}$* is expected to have activities that significantly differ from other VEGF splice variants. To analyze the functional activities of the novel $VEGF_{205}$* splice variant, recombinant $VEGF_{205}$* was purified from *E. coli* and subsequently refolded.

The differential ability of $VEGF_{205}$* to induce selective biological activities is due to its ability to phosphorylate specific VEGFR-2 tyrosine residues. Following binding of VEGF splice variant proteins to VEGFR-2 receptor, vascular endothelial cells undergo proliferation, which is due to phosphorylation of tyrosine residue Y-1059/1054 [192], while migration of these cells is stimulated following phosphorylation of tyrosine residue Y-951 within the VEGFR-2 receptor tyrosine kinase [192, 193]. Conversely, binding of VEGF to VEGFR-1 inhibits VEGFR-2 induced proliferation by acting as a decoy receptor [197]. While $VEGF_{205}$* bound efficiently to VEGFR-2 (data not shown), $VEGF_{205}$* induced significantly lower levels of VEGFR-2 phosphorylation at Y-1054/1059 compared to $VEGF_{120}$, thus suggesting that $VEGF_{205}$* is less mitogenic compared to $VEGF_{120}$. This data is consistent with our results of $VEGF_{205}$*-induced proliferation as described below. On the other hand, $VEGF_{205}$* induced a significant increase in VEGFR-2 phosphorylation at Y-951 in vascular endothelial cells compared to $VEGF_{120}$. These results suggest that $VEGF_{205}$* induces migration of vascular endothelial cells through selective phosphorylation of Y-951 of VEGFR-2.

We evaluated the ability of $VEGF_{205}$* to induce proliferation of vascular endothelial cells, which is one of the first steps in the process of tumor-associated blood vessel development. Although $VEGF_{205}$* stimulated proliferation of HUVEC, the concentration of $VEGF_{205}$* to induce half-maximal proliferation was 10-fold greater compared to that of $VEGF_{120}$, which has been previously characterized as highly mitogenic [314]. These results suggest that the role of $VEGF_{205}$* is not primarily stimulation of vascular endothelial cell proliferation and prompted further studies to characterize the biological effect(s) of $VEGF_{205}$*.

During angiogenesis, endothelial cells of existing small blood vessels are activated to migrate and organize into hollow tubes that ultimately form new capillaries. Using a wound healing assay [318-320], we demonstrated that $VEGF_{205}$* induced significant migration of vascular endothelial cells into the wounded space compared to $VEGF_{120}$. These results support a potential role of $VEGF_{205}$* in mobilizing vascular endothelial cells from pre-existing blood vessels to organize into new vessels adjacent to tumors.

In addition to promoting vascular endothelial cells migration, $VEGF_{205}$* stimulated formation of tubules with large luminal spaces, which was distinct from the pattern of migration and organization of endothelial cells into tubule-like structures following

exposure to the more ubiquitously expressed $VEGF_{120}$. $VEGF_{205}$*-induced organization of vascular endothelial cells into large tubules was a dominant characteristic, since a combination of 50 ng/ml $VEGF_{120}$ and a significantly 25-fold lower doses of $VEGF_{205}$ stimulated endothelial cells to form tubes with large luminal spaces as well. These results suggest that the presence of very low levels of local $VEGF_{205}$* within the tumor microenvironment can significantly impact the process of neovascularization. In contrast to normal blood vessels, recent studies have shown that tumor vasculature is highly disorganized, characterized by blood vessels that are tortuous and dilated, and containing significantly increased terminal branches [321]. The current finding that $VEGF_{205}$* stimulated formation of tubules with large luminal spaces could explain the tortuous and large blood vessels that have been observed in advanced papillomas and carcinomas [322]. In addition, $VEGF_{205}$* induced significantly more terminal branch points compared to $VEGF_{120}$. Evaluation of the number of tubule branches has been previously used to examine formation of tubule-like structures by vascular endothelial cells [323]. The increase in the number of terminal branches in endothelial cells following exposure to $VEGF_{205}$* suggests the formation of higher number of tubule-like structures compared to $VEGF_{120}$, resulting in the formation of vasculature composed of a high number of tubule-like structures with large luminal spaces.

Persistence of new blood vessels depends on the survival of the newly recruited vascular endothelial cells; however, until tumor angiogenesis is completed, endothelial cells are present within a hypoxic and nutrient-deprived microenvironment, and consequently are at risk of undergoing apoptosis. Exposure of vascular endothelial cells to $VEGF_{205}$* selectively stimulated phosphorylation of Akt at Ser-473 compared to vascular endothelial cells following exposure to $VEGF_{120}$. $VEGF_{205}$*-induced increase in phospho-Akt-Ser-473 levels was inhibited by the specific PI3-K inhibitor, LY294002. These results suggest that activation of PI3-K/Akt signaling pathway in vascular endothelial cells is dependent upon the tumor microenvironment during which specific VEGF splice variants, such as $VEGF_{205}$*, stimulates phosphorylation of Akt at Ser-473. These results further support a model for differential functions of VEGF splice variants during tumor angiogenesis [324]. Collectively, activation of Akt following exposure to $VEGF_{205}$* may selectively block apoptosis in vascular endothelial cells undergoing angiogenesis in newly formed blood vessels.

While both $VEGF_{205}$* and $VEGF_{120}$ induced phosphorylation of Akt at Thr-308 residue compared to unstimulated cells, there was no significant difference in phosphorylation levels of Akt at Thr-308 following exposure of HUVEC to $VEGF_{205}$* compared to $VEGF_{120}$. These results suggest that $VEGF_{120}$ only stimulated activation of PDK-1 in endothelial cells, whereas $VEGF_{205}$* differentially activated ILK-1 compared to $VEGF_{120}$, resulting in selective phosphorylation of Akt at Ser-473. The definition of the role(s) of ILK-1 in angiogenesis is only now emerging. Recent studies have demonstrated that ILK is required for VEGF-mediated endothelial cell migration and formation of blood vessels [325]. Although the majority of studies to date have focused on the role of Akt as a survival factor, there is a growing evidence supporting a role of Akt in inducing cell motility [326, 327]. Recent studies have demonstrated that loss of Akt inhibited migration of endothelial cells [328]. Taken together with results from the current study, $VEGF_{205}$* may induce mobilization of endothelial cells by the selective activation of PI3-K/ILK-1/Akt signaling pathway.

Additionally, $VEGF_{205}$* induced phosphorylation of mTOR at Ser-2448, which was also inhibited by LY294002. Akt has been shown to act as an upstream kinase activator of mTOR, by directly phosphorylating mTOR at Ser-2448 residue [267, 309, 329]. Given the observation that $VEGF_{205}$*-induced phosphorylation of mTOR at Ser-2448 was significantly reduced but not completely inhibited in the presence of LY294002 suggests that phosphorylation of mTOR following exposure of endothelial cells to $VEGF_{205}$* is mediated only via PI3-K/Akt signaling pathway. The decrease in levels of $VEGF_{205}$*-induced phospho-mTOR in the presence of LY294002 further confirms the selective activation of Akt signaling pathway in endothelial cells when exposed to $VEGF_{205}$*. Taken together, these results suggest that $VEGF_{205}$* not only induces PI3-K/Akt signal transduction pathway, leading to survival of vascular endothelial cells, but also stimulates Akt-dependent phosphorylation of mTOR at Ser-2448, thus regulating expansion in cell mass and proliferation of endothelial cells undergoing angiogenesis. Collectively, the present studies suggest that activation of PI3-K/Akt/mTOR signaling pathway is critical for $VEGF_{205}$*-mediated angiogenesis.

In summary, we have cloned and sequenced a novel murine VEGF isoform, $VEGF_{205}$*, produced recombinant protein and characterized its biological activities. $VEGF_{205}$*, which is expressed at specific stages of skin carcinogenesis and contains a novel carboxyl-terminal tail, differentially activates PI3-K/Akt/mTOR signaling pathway.

As demonstrated by the identification of the inhibitory $VEGF_{165}b$ splice variant [180, 181] and the results of the present studies, identification of novel VEGF splice variants with specific biological functions may advance the development of effective therapeutics and diagnostics for use in both oncology and cardiovascular diseases. The ability of $VEGF_{205}$* to activate PI3-K/Akt signaling pathway through ILK-1-associated selective activities and to stimulate migration and tubule formation of endothelial cells suggests that $VEGF_{205}$* have utility in treating diseases in which the lack of appropriate development of vascular architecture has been delayed or damaged.

Figure 1.1. Sequence and exon structure of $VEGF_{205}$*. (A) *Nucleotide sequence of $VEGF_{205}$* cDNA.* $VEGF_{205}$* mRNA contains an extended region of exon 6a, which consists of an additional 61 bp of the intronic sequence of exon 6a, that we have termed exon 6' (marked by ***solid*** underlining). This sequence is followed by 120 bp of the intronic sequence upstream of exon 8 (marked by ***dotted*** underlining). However, the presence of an in-frame stop codon TAA within the novel sequence of exon 6' results in the generation of a novel COOH-terminal exon structure, consisting of 7 unique amino acids, which include YVGAAAV. In addition, termination of protein synthesis within exon 6' yields a mature polypeptide which consists of 145 amino acid residues following cleavage of the 26-amino acid signal sequence (*Highlighted* nucleotides). ***(B)*** *Exon structure of $VEGF_{205}$*, illustrating the novel $VEGF_{205}$* alternative mRNA splicing sites.* The 3'-end of the exon 6' contains a novel consensus sequence encoding the 5'-splice donor site required for $VEGF_{205}$* mRNA processing. In addition, a novel splice acceptor site is present within the intronic sequence of exon 7, and is located 120 bp upstream of exon 8. Exons are presented in *boxes* and introns by *solid* lines ***(C)*** *Exon structure of murine VEGF.* The murine VEGF gene, through alternative mRNA splicing, gives rise to 4 VEGF splice variants, which include $VEGF_{188}$, $VEGF_{164}$, and $VEGF_{120}$. The unique mouse splice variant $VEGF_{205}$* lacks exons 7 and 8, and contains the novel exon 6', which encodes a unique carboxyl-tail consisting of 7 unique amino acid, YVGAAAV.

A

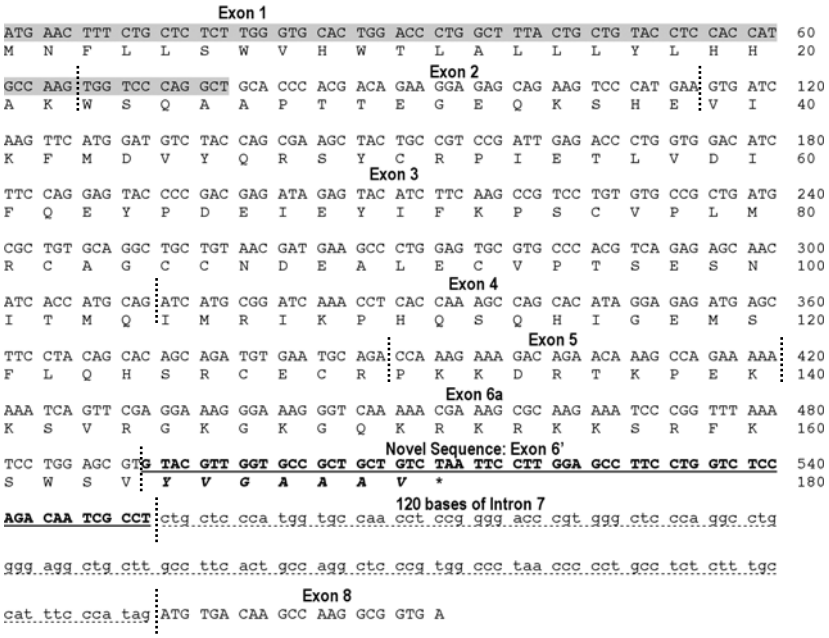

B

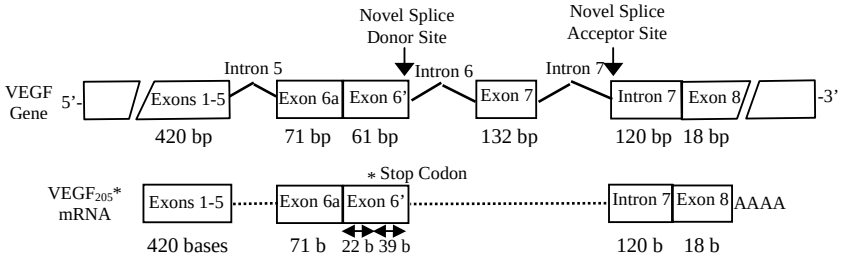

C

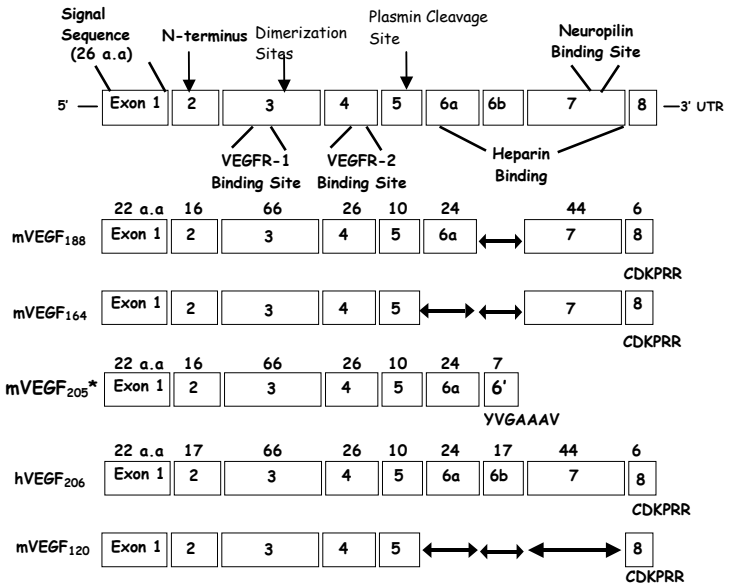

Figure 1.1

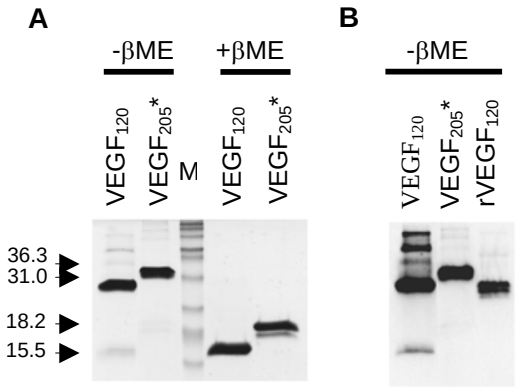

Figure 1.2. Expression and refolding of recombinant VEGF$_{205}$*. (A) Recombinant VEGF$_{205}$* and VEGF$_{120}$ were purified from overexpressing *E. coli* and refolded into homodimers. Equal aliquots of refolded proteins (600 ng) were separated on 12% SDS-PAGE gel under non-reducing (-βME) conditions to show VEGF dimers formation and reducing (+βME) conditions to show monomers formation. The gel was Commassie-blue-stained and photographed. Arrowheads indicate the position of recombinant VEGF proteins. Size marker is indicated as (M). ***(B)*** Aliquots of recombinant VEGF splice variants (200 ng) were separated on 12% SDS-PAGE gel and immunoblotted with anti-VEGF$_{164}$ antibody to detect recombinant VEGF$_{205}$* and VEGF$_{120}$. To confirm the position of recombinant VEGF proteins, a commercially available recombinant VEGF$_{120}$ (rVEGF$_{120}$) (R&D Systems) was used a positive control.

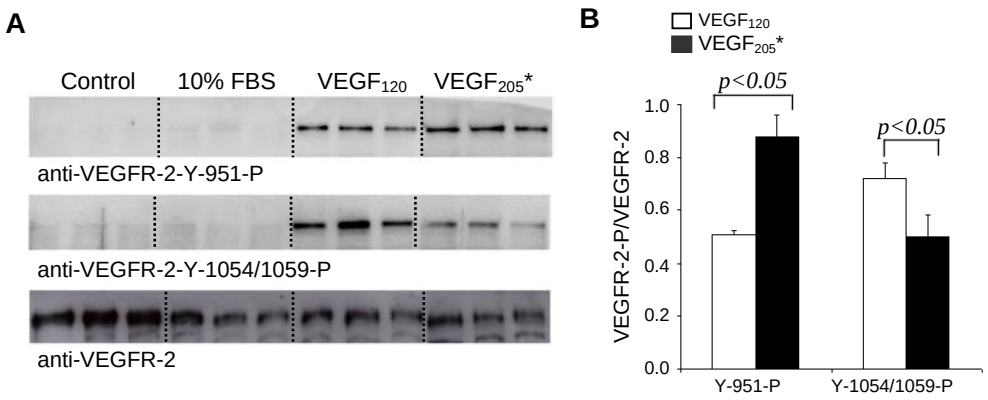

Figure 1.3. VEGF$_{205}$* induces phosphorylation of VEGFR-2 at Y-951 and Y-1054/1059 in HUVEC. ***(A)*** Confluent cultures of HUVEC were serum-deprived for 6 hr and were left either untreated (Control), treated with 50 ng/ml VEGF$_{120}$, VEGF$_{205}$*, or 10% FBS for 2 min. Equal aliquots of total proteins (22 μg) were resolved by 8% SDS-PAGE gel and immunoblotted with either anti-phospho-VEGFR-2-Y-951 or anti-phospho-VEGFR-2-Y-1054/1059 antibodies, stripped and then re-probed with anti-VEGFR-2 antibody. ***(B)*** Densitometric analysis of the ratio of phospho-VEGFR-2-Y-951/VEGFR-2 and phospho-VEGFR-2-Y-1054/1059/VEGFR-2 in response to stimulation with VEGF$_{120}$ or VEGF$_{205}$*. Data represent mean ± SEM, n=3.

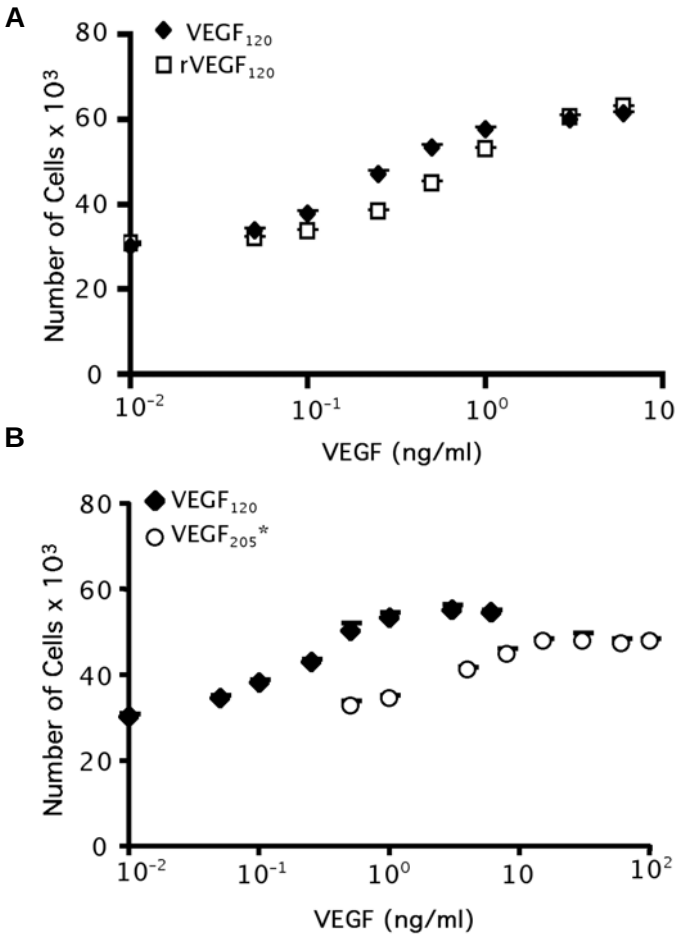

Figure 1.4. VEGF$_{205}$* induces proliferation of HUVEC. (A) *Recombinant VEGF$_{120}$ induced HUVEC proliferation to similar levels as commercially purchased recombinant murine VEGF$_{120}$ (rVEGF$_{120}$) (R&D Systems).* HUVEC were seeded at a density of 2000 cells per well and stimulated with increasing concentrations of recombinant VEGF$_{120}$ and rVEGF$_{120}$ in the presence of 10% Alamar blue, and the percent of dye reduction was determined at 24 hr. ***(B)*** Recombinant VEGF$_{205}$* was not as mitogenic as VEGF$_{120}$. HUVEC were seeded at a density of 2000 cells per well and stimulated with increasing concentrations of recombinant VEGF$_{205}$* or VEGF$_{120}$. VEGF$_{205}$* induced a dose dependent mitogenesis of HUVEC, which was 10-fold lower than that induced by recombinant VEGF$_{120}$ protein. Data represent mean ± SEM, n=6.

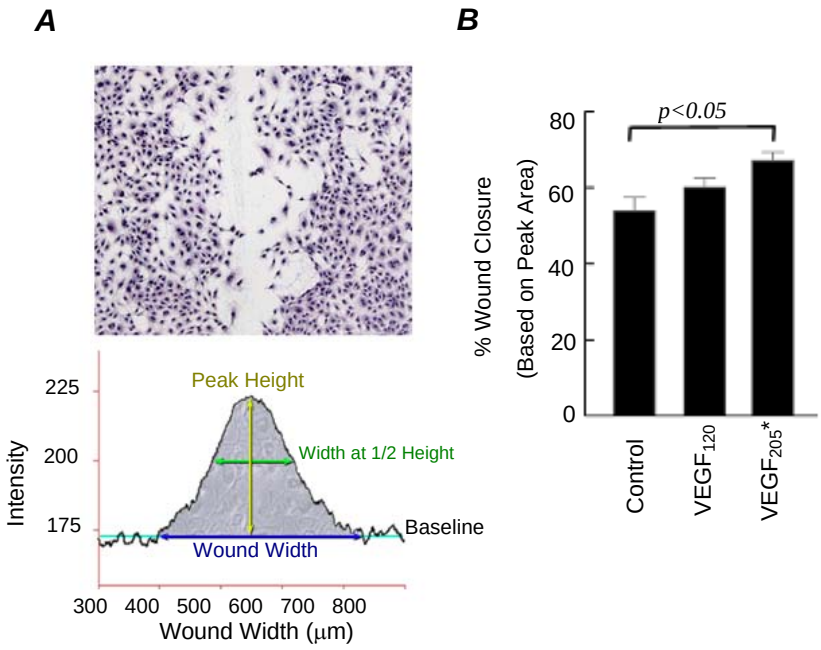

Figure 1.5. $VEGF_{205}$* induces migration of HUVEC in vitro. (A) A cell-based wound healing model was used to determine the effect of $VEGF_{205}$* on vascular endothelial cell migration. Wounds were artificially created by drawing a linear scar across HUVEC grown in monolayer cultures in the presence of 10 ng/ml of $VEGF_{120}$ or $VEGF_{205}$* for 20 hr. An intensity profile curve perpendicular to the wound and including the full height of the wound was calculated. A representative intensity histogram is shown at the bottom. ***(B)*** Migration of HUVEC into the wounded area was quantitated by calculating the wound width at 1/2 peak height based on peak area. Data are plotted as percentage of wound closure at 0 hr.

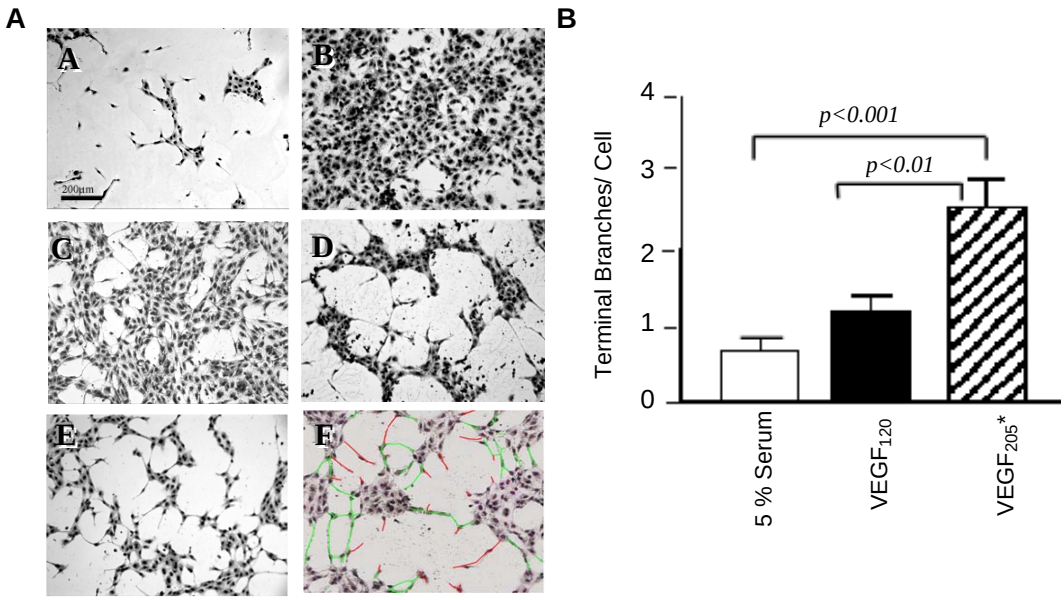

Figure 1.6. VEGF$_{205}$* induces vessel-like structures in vitro. (A) HUVEC were plated on collagen-coated 96-well plates and tube formation was evaluated at 30 hr following incubation of HUVEC in the absence of serum *(panel A)*, in the presence of 5% fetal calf serum *(panel B)*, 50 ng/ml of recombinant VEGF$_{120}$ *(panel C)*, 50 ng/ml of recombinant VEGF$_{205}$* *(panel D)*, 50 ng/ml of VEGF$_{120}$ and 2 ng/ml of VEGF$_{205}$* *(panel E)*. *(Panel F)* Images of hematoxylin-stained HUVEC were captured and cellular projections which are <15 μm in length were delineated (*in red*) and designated as terminal branch points. ***(B)*** Number of terminal branch points was calculated and normalized to the number of cells in each field of view. Data represent mean ± SEM, n=4.

Figure 1.7. Recombinant $VEGF_{205}$* activates PI3-K/Akt signal transduction pathway. (A) HUVEC were serum-starved for 6 hr and were left untreated (Control), or treated with 50 ng/ml of either $VEGF_{120}$ or $VEGF_{205}$* for 0-60 min. Equal aliquots of total proteins were resolved by 8% SDS-PAGE and immunoblotted with anti-Akt-Ser-473-P antibody. Blots were stripped and re-probed with anti-Akt antibody. ***(B)*** Densitometric analysis of the ratio of Akt-Ser-473-P/Akt in response to stimulation with $VEGF_{120}$ or $VEGF_{205}$*. Results are expressed as fold increase with respect to Control. Data represent mean ± SEM. ***(C and E)*** HUVEC were serum-starved for 6 hr, followed by incubation for 3 hr in the presence (+) or absence (-) of 40 μM LY294002. Cells were then left untreated (Control), or treated with 50 ng/ml of either $VEGF_{120}$ or $VEGF_{205}$* for 2 min. Equal aliquots of total proteins were resolved by 8% SDS-PAGE and immunobloted with anti-Akt-Ser-473-P ***(C)*** or anti-Akt-Thr-308-P antibody ***(D)***. Blots were re-probed with anti-Akt antibody. The blot was then re-probed for β-actin to verify equal loading of samples. ***(D)*** Densitometric analysis of the ratio of Akt-Ser-473-P/Akt. Results are expressed as above. ***(F)*** Densitometric analysis of the ratio of Akt-Thr-308-P/Akt. Data are expressed as mean ± SEM.

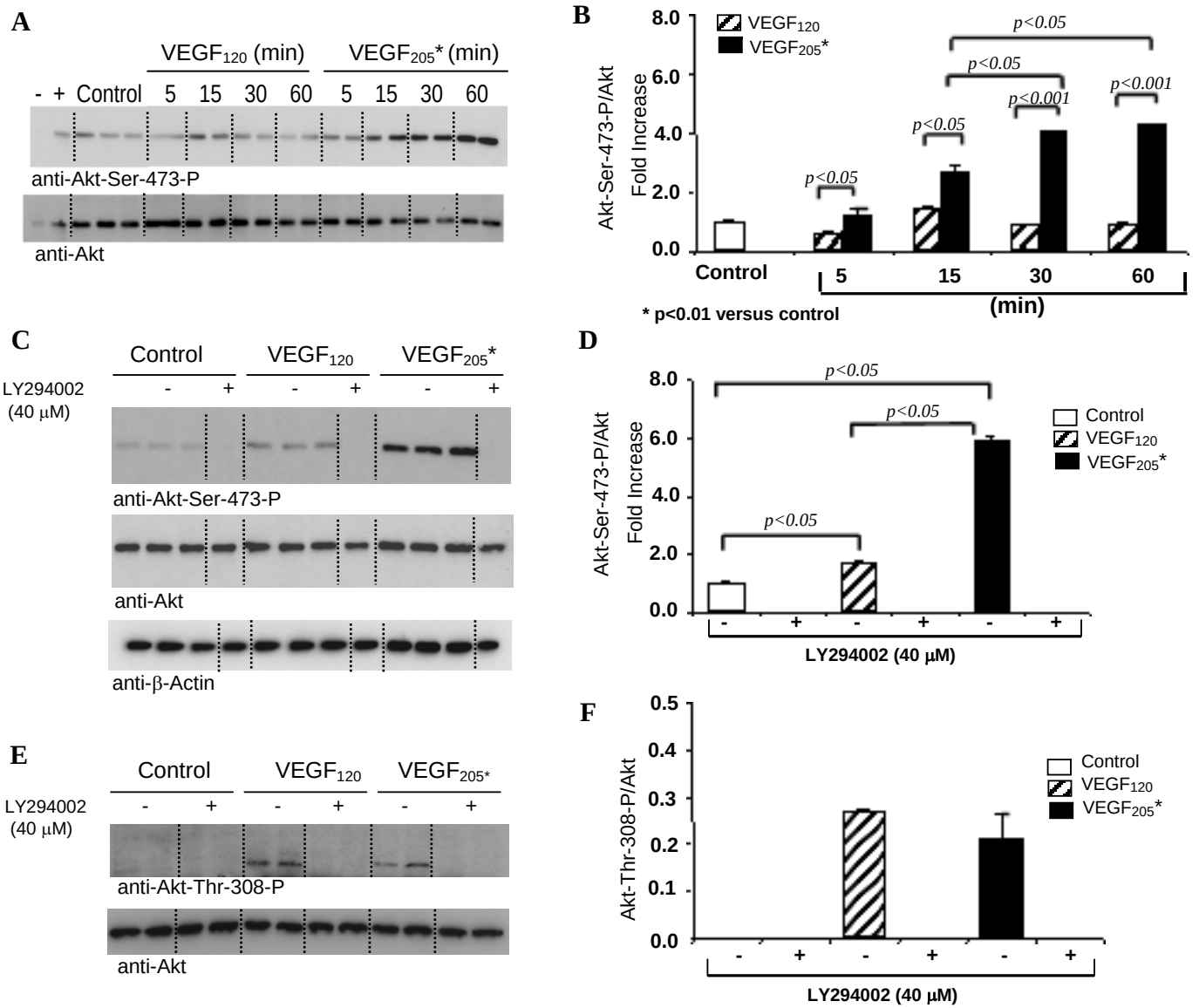
A
VEGF120 (min)
VEGF205* (min)
- + Control 5 15 30 60 5 15 30 60
anti-Akt-Ser-473-P
anti-Akt
B
VEGF120
VEGF205*
Akt-Ser-473-P/Akt
Fold Increase
8.0
6.0
4.0
2.0
0.0
p<0.05
p<0.05
p<0.05
p<0.001
p<0.05
p<0.001
Control
5
15
30
60
(min)
* p<0.01 versus control
C
Control
VEGF120
VEGF205*
LY294002
(40 μM)
- + - + - +
anti-Akt-Ser-473-P
anti-Akt
anti-β-Actin
D
p<0.05
p<0.05
p<0.05
Control
VEGF120
VEGF205*
Akt-Ser-473-P/Akt
Fold Increase
8.0
6.0
4.0
2.0
0.0
- + - + - +
LY294002 (40 μM)
E
Control
VEGF120
VEGF205*
LY294002
(40 μM)
- + - + - +
anti-Akt-Thr-308-P
anti-Akt
F
Control
VEGF120
VEGF205*
Akt-Thr-308-P/Akt
0.5
0.4
0.3
0.2
0.1
0.0
- + - + - +
LY294002 (40 μM)

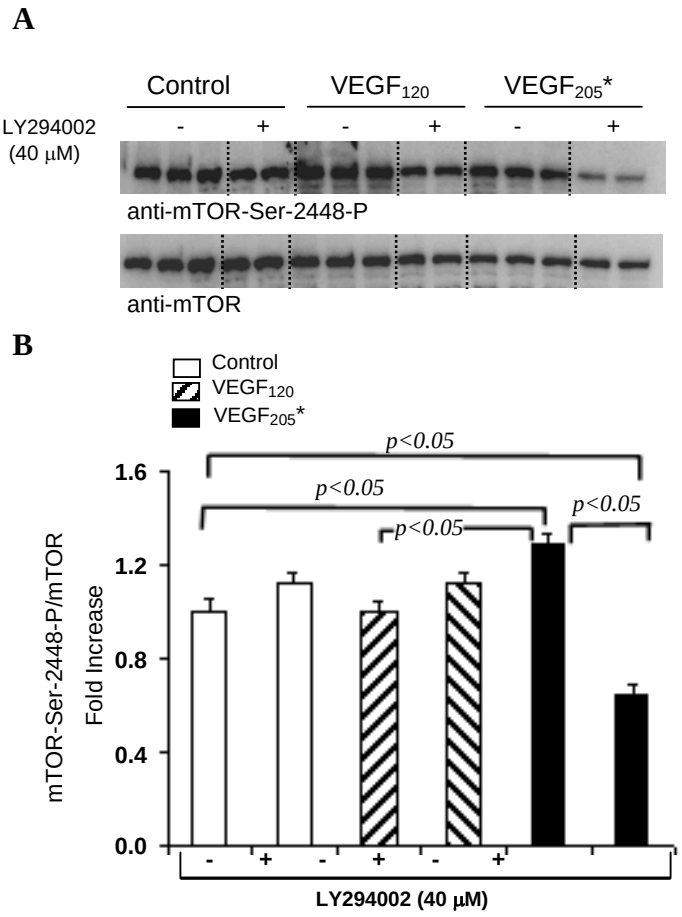

Figure 1.8. Recombinant VEGF$_{205}$* stimulates phospho-mTOR-Ser-2448. (A) HUVEC were serum-starved for 6 hr, followed by incubation for 3 hr in the presence (+) or absence (-) of 40 μM LY294002. Cells were then left untreated (Control), or treated with 50 ng/ml of either VEGF$_{120}$ or VEGF$_{205}$* for 2 min before harvest. Equal aliquots of total proteins were resolved by 8% SDS-PAGE and immunobloted with anti-phospho-mTOR-Ser-2448 antibody. Blots were stripped and re-probed with anti-mTOR. ***(B)*** Densitometric analysis of the ratio of mTOR-Ser-2448-P/mTOR in response to stimulation with VEGF$_{120}$ or VEGF$_{205}$*. Results are expressed as fold increase with respect to Control. Data represent mean ± SEM.

CHAPTER 2

ACTIVATED AKT IN SPECIFIC CELL POPULATIONS DURING MULTI-STAGE SKIN CARCINOGENESIS

2.1. Abstract

The goal of the present study was to identify specific populations of cells that contain activated Akt, as determined by the presence of phosphorylated Akt at serine 473 (p-Akt), during development of skin tumors using a murine multi-stage carcinogenesis model. Nucleated papillomas cells as well as both epidermal and follicular keratinocytes in hyperplastic skin contained increased pAkt compared to skin treated only with acetone or 7, 12 dimethylbenz[a]anthracene (DMBA). Although the numbers of both mast cells and neutrophils were significantly increased in the stroma of papillomas ($p<0.0005$; $p<0.0001$, respectively), only mast cells contained pAkt. The amount of total Akt protein was similar regardless of time or treatment group examined. The present results suggest that activation of Akt may provide specific populations of epidermal keratinocytes that develop into skin tumors with the ability to resist terminal differentiation and have enhanced proliferation during multi-stage skin carcinogenesis. In addition, mast cells which contain activated Akt may persist within the stroma of papillomas during skin tumor development and progression through this signaling pathway, thereby contributing to a pro-oxidant and pro-angiogenic microenvironment.

2.2. Introduction

Under normal conditions, keratinocytes, which are the specialized epithelial cells of the skin, undergo limited proliferation. As these cells migrate into the upper layers of the epidermis, they subsequently undergo terminal differentiation, which is a form of apoptosis. During multi-stage skin carcinogenesis, keratinocytes that contain mutations in the Ha-*ras* oncogene induced by exposure to 7, 12 dimethylbenz[a]anthracene (DMBA) undergo successive rounds of proliferation in response to a tumor promoter such as 12-0-tetradecanoylphorbol-13-acetate (TPA) [330, 331]. This leads to clonal expansion of these Ha-*ras* mutated cells which also have significant alterations in their pattern of differentiation and a decreased level of apoptotic death [332, 333]. An initial study demonstrated that transgenic mice expressing insulin-like growth factor-1 (IGF-1) selectively targeted to the basal compartment of epidermis responded to exposure to ultraviolet (UV) light with a decreased epidermal apoptosis compared to the skin of non-transgenic mice, which was associated with significantly elevated Akt kinase activity [334]. In addition, IGF-1 transgenic mice developed greater numbers of papillomas when treated with a mouse skin carcinogenesis protocol. These results suggested that IGF-1 expression in the basal epidermis activated the inositidylphosphate-3-kinase PI3-K/Akt (protein kinase B) pathway, which was associated with both resistance of keratinocytes to apoptosis and with a tumorigenic phenotype [334]. Another study demonstrated that transfection of PB keratinocytes, which usually have low rates of tumor formation when grown *in vivo,* with wild-type Akt resulted in rapidly growing, undifferentiated, and highly invasive skin tumors [335]. These observations were consistent with studies demonstrating that Akt acted as an oncogene when transfected into NIH 3T3 fibroblasts [336] and also confirmed a previous report that Akt null mice had significant defects in differentiation of the skin [229].

Although previous studies have demonstrated an association between increased Akt kinase activity and development of skin tumors [334, 335, 337], the specific cell populations that contain activated Akt during multi-stage skin carcinogenesis are unknown. The present study used digital image analysis in conjunction with immunochemistry and immunofluorescence to identify cell populations within epidermis, dermis, papillomas, and stromal tissue that contained activated Akt, as determined by detection of phosphorylation of Akt at serine 473 (pAkt).

2.3. Materials and Methods

2.3.1. Treatment of SENCAR mice with DMBA and TPA. Female SENCAR mice (6-8 weeks old, 22-28 g; NCI, Bethesda, MD) were housed in vivarium facilities at The Ohio State University that meet American Association for Accreditation of Laboratory Animal Care requirements. All procedures were approved by The Ohio State University Institutional Animal Care Utilization Committee prior to beginning the study. Animals were fed basal Teklad 22/5 rodent diet (Harland Industries, Indianapolis, IN) *ad libitum* and kept in rooms maintained on a 12 hr light/dark cycle. At 24 hr prior to initial treatment with HPLC grade acetone, DMBA or TPA, the dorsal skin of mice was carefully shaved. Mice treated topically with 0.2 ml acetone served as the solvent control. DMBA (Sigma, St. Louis, MO) was dissolved in acetone and applied at a final concentration of 25 nmol DMBA in 0.2 ml acetone to cover the entire back of mice. TPA (Alexis Biochemicals, San Diego, CA), at a final concentration of 2 μg, was dissolved in acetone and applied in a volume of 0.2 ml to the dorsal skin of mice. SENCAR mice were treated with one of two protocols. For short term experiments, the dorsal skin of SENCAR mice was treated with two topical applications of either 0.2 ml acetone or 25 nmol DMBA, with a 48 hr time interval between treatments with acetone or DMBA, followed at 7 days by a single topical application of either 0.2 ml acetone or 2 μg TPA in 0.2 ml acetone. At 24 hr after the final application of either acetone or TPA, mice were sacrificed by carbon dioxide euthanasia. Dorsal hair was removed using a depilatory agent, skin was isolated, and tissue samples were either fixed in 10% neutral buffered formalin and embedded in paraffin prior to sectioning for histological and immunohistochemical analysis as described previously [338], or used to isolate protein for Western blotting analysis of total Akt protein, as described below.

For studies in which skin and papillomas were isolated at 15 weeks and 22 weeks of multi-stage carcinogenesis, SENCAR mice were either initiated with a single topical application of 25 nmol DMBA or treated with a single topical application of 0.2 ml acetone and at 7 days later, mice were treated topically twice weekly with either 0.2 ml acetone or 2 μg of TPA in 0.2 ml acetone. Dorsal skin samples and papillomas were isolated at 15 weeks and 22 weeks. At 4 hr following the final topical application of 2 μg TPA, mice were then sacrificed by carbon dioxide euthanasia. Skin and papillomas were isolated, and tissue samples were processed for immunohistochemical and Western blotting analysis.

2.3.2. Immunochemical staining methods. Following processing and paraffin embeddment, 4 μm serial sections of skin tissues were placed on histological glass slides. Immunohistochemical staining was performed using a DAKO Autostaining system, as previously described [339]. Briefly, cross-sections of tissues were dewaxed, rehydrated, and treated with preheated citrate buffer (pH 6.0) to recover antigenicity. Endogenous peroxidase activity was blocked with a 3% H_2O_2/methanol solution, followed by incubation in 10% goat serum/PBS blocking solution (Vector Laboratories, Burlingame, CA). Skin sections were stained with rabbit anti-phospho-Serine-473-Akt antibody (polyclonal anti-pAkt [pAkt], 0.031 μg/mL, Santa Cruz Biotechnology, Santa Cruz, CA). The presence of the pAkt antigen was visualized using diaminobenzidine (DAB; 0.06% w/v, DAKO, Carpinteria, CA) and tissues were counterstained with methyl green. The specificity of antibody staining was verified using pre-immune rabbit IgG (0.031 μg/ml, Santa Cruz Biotechnology). Using polyclonal anti-myeloperoxidase (MPO) antibody (0.4 μg/ml, Neomarkers, Fremont, CA) and nuclear morphology, similar methods were used to identify and quantitate the numbers of activated neutrophils within the dermal compartment and within the stroma of papillomas. Mast cells were identified and quantitated based on staining with 0.2% toluidine blue (in 0.7N HCl) (Sigma) using Vital New Red as a counterstain (Pfaltz & Bauer, Inc., Waterbury, CT), as previously described [171].

2.3.3. Immunofluorescent staining methods. Sections of fixed, paraffin-embedded skin samples (4 μm) were mounted onto glass sides (SuperFrost/Plus, Fischer Scientific, Pittsburgh, PA). Tissue sections were then deparaffinized using Histo-Clear (National Diagonistics, Atlanta, GA) and rehydrated in a graded series of alcohols. Antigen was unmasked by heating samples in 10 mM citrate buffer (pH 6.0) in a microwave oven. To reduce autofluorescence, sections were treated in 3 changes of freshly prepared solutions of sodium borohydride ($NaBH_4$, 1 mg/ml in PBS, Sigma) for 10 min each. To block background staining, tissue sections were incubated for 30 min at room temperature with Image-iT^{TM} FX Signal Enhancer (Molecular Probes, Eugene, OR). Tissues sections were then incubated overnight at room temperature in a humidified chamber with rabbit polyclonal anti-phospho-Serine-473-Akt (1:50 in PBS, Santa Cruz Biotechnology) and were then incubated at room temperature in the dark for 1 hr with Alexa Fluor-633-conjugated goat anti-rabbit IgG (1:500 in PBS, Molecular Probes). After

incubation with secondary antibody, tissues were washed in PBS, dehydrated, and mounted using VectaShield Mounting Medium (Vector Laboratories) which contains the DNA dye 4', 6-diamidino-2-phenylindole (DAPI) that fluoresces in the 405 nm (blue) range and specifically stains nucleated cells. Specificity of antibody binding was determined by incubation with only secondary antibodies followed by placement of coverslips using Vectashield with DAPI.

2.3.4. Digital photomicroscopy and image analysis. Fluorescent images were obtained using a laser scanning confocal microscope (Zeiss LSM 510 Meta), with excitation wavelengths of 633 nm for Alexa Fluor-633 (red) fluorescence and 405 nm for DAPI-associated (blue) fluorescence. Images were obtained using 40x objective lens at identical settings of illumination. To quantitate pAkt immunohistochemical staining within specific cell populations, digital images of tissue sections were captured using a Diagnostic Instruments digital camera (Insight camera; 1600x 1200 resolution) mounted on an Olympus research microscope. Images were then transferred to digital image analysis software (Image Pro Plus, Media Cybernetics, Silver Spring, MD). Multiple images were captured from each tissue section using a 40x objective in order to encompass the entire tissue sectional area. Images were captured under identical lighting and optical settings, and color segmentation was used to eliminate non-specific background staining and counterstaining. Epidermal and follicular compartments within the skin were delineated in each image, and pAkt immunostaining was quantitated within each compartment of the skin by calculation of integrated optical densities (IOD), which is a proportional measure of brown signal, based on DAB staining, as previously described [340-342]. The capture and processing of digital images were performed by investigators who were unaware of the treatment group assignments. Intra-observer variability (coefficient of variation for 5 images made by one blinded observer) and inter-observer variability (three blinded observers, 5 images each) for these imaging procedures was less than 2% and 5%, respectively. In parallel experiments, serial sections of skin were also evaluated for the presence of neutrophils and mast cells using histochemical and immunochemical stains, as well as nuclear morphology, as described above. Multiple digital images of these leukocyte populations were captured and calibrated, as described above using an 80x objective. Populations of neutrophils and mast cells were quantitated using a segmentation-based approach, as described above.

2.3.5. Protein extracts. Dorsal skin and papillomas were homogenized on ice in 2.5 ml homogenation buffer, pH 8.6 (Tris-HCl, 60 mM; EDTA, 5 mM, EGTA; 5 mM, sucrose, 300 mM; DTT, 5 mM; leupetin, 200 μg/ml; PMSF, 2 mM; aprotinin, 20 μg/ml; sodium molybdate, 10 mM), followed by sonication for 10 seconds. Samples were clarified by centrifugation at maximum speed on a microcentrifuge at 4^{o}C for 15 min. Supernatants were collected and then centrifuged again for 5 min at maximum speed. Protein concentrations were determined using the BIO-RAD protein assay (BIO-RAD, Hercules, CA) and bovine albumin serum (BSA) (Sigma) was used as a standard**.** Samples were stored at -80^{o} C until Western blot analysis was performed.

2.3.6. Western blot analysis. Equal aliquots of protein extracts (35 μg/sample) were analyzed by Western blot analysis using 10% SDS-polyacrylamide gel and then blotted to Hybond-P polyvinylidene difluoride membrane (Amersham, Piscataway, NJ) during an overnight transfer. The blots were blocked by incubation in 5% non-fat dried milk powder in phosphate-buffered saline containing 0.1% Tween-20 (PBS-T), and then washed with PBS-T. Blots were then incubated with rabbit polyclonal anti-Akt antibody (1:500 dilution) (Cell Signaling Technology, Beverly, MA) in 1% BSA in PBS-T overnight at 4^{o}C with constant shaking. After extensive washing with PBS-T, blots were incubated for 1 hr at room temperature with 1:2000 dilution of horseradish peroxidase-conjugated goat anti-rabbit IgG secondary antibody (Jackson ImmunoResearch Laboratories, West Grove, PA) in PBS-T containing 5% non-fat dried milk powder. The enhanced chemiluminescence (ECL plus) Western Blotting Detection System (Amersham) was used to detect the signal, with exposure to Hyperfilm^{TM} ECL (Amersham). To verify equal loading of protein samples, blots were re-probed with 1:5000 dilution of mouse monoclonal anti-β-actin (Sigma) for 1 hr at room temperature, followed by extensive washing with PBS-T. Blots were subsequently incubated for 30 min at room temperature with 1:4000 dilution of peroxidase-linked sheep anti-mouse IgG (Amersham) and detection of the signal was processed as described above.

2.3.7. Statistical analysis. Significant differences in pAkt in specific regions of skin and in papillomas were determined using two-tailed Student's *t* -test (SigmaStat; Jandel Scientific, San Rafael, CA) or one-way analyses of variance (ANOVA) on ranks for non-

parametric comparisons (relative pAkt staining), with post-hoc Dunnet test to evaluate significant comparisons between treatment groups and acetone control skin. Comparisons of three or more groups were conducted using one-way ANOVA, with Student-Newman-Keuls post-hoc analysis. In all cases, results are expressed as mean ± SEM, and significance was defined as $p<0.05$, unless otherwise described.

2.4. Results

2.4.1. Histology of mouse skin. Dorsal SENCAR mouse skin treated with acetone (Figure 2.1 A) or DMBA (Figure 2.1 B) had a uniform epidermal thickness of 1-2 epidermal cell layers, with few cells in the dermis. At 24 hr after a single topical application of 2 μg TPA, the epidermal thickness had increased to 3-5 cell layers and there was also an increase in inflammatory cells within the dermis. Both changes were present regardless of previous topical treatment with either acetone or DMBA (Figure 2.1 C and D).

Skin treated for 15 weeks with either acetone alone (Figure 2.2 A) or with DMBA (Figure 2.2 B) followed by twice weekly applications of acetone was of uniform epidermal thickness, with 1-2 epidermal layers and low numbers of cells within the dermis. Skin isolated from mice treated once with DMBA followed by twice weekly applications of 2 μg TPA for 15 weeks (Figure 2.2 D) was hyperplastic, with a significantly increased epidermal thickness and visible increases in the numbers of cells within the dermis. Comparatively, at 15 weeks, the hyperplasia in skin treated with acetone followed by twice weekly application of 2 μg TPA (Figure 2.2 C) was not as great as that observed in skin treated once with DMBA followed by twice weekly treatments of TPA (Figure 2.2 D).

2.4.2. Quantitation of pAkt in compartments of skin at 24 hr and 15 weeks. Sections of skin isolated from SENCAR mice at 24 hr and 15 weeks were stained with anti-pAkt antibody and relative immunohistochemical staining intensities of pAkt within the epidermal and follicular compartments were quantitated using digital image analysis (Figure 2.1 F, Figure 2.2 E). In general, regardless of the time at which skin samples were isolated, the epidermal compartment contained more cells than the follicular compartment of the skin, and more epidermal cells that contained pAkt (Figure 2.1 F and Figure 2.2 E). At the 24 hr time point, there was a 3-fold increase in pAkt in the epidermis of skin treated with a single topical application of 2 μg TPA, regardless of pre-treatment of the dorsal skin with acetone or DMBA, ($p<0.01$) (Figures 2.1 C and D compared to Figures 2.1 A and B; Figure 2.1 F).

At 15 weeks, the highest pAkt levels in both epidermal and follicular compartments were in keratinocytes in skin treated with a single initiating dose of DMBA followed by twice weekly application of 2 μg TPA (Figures 2.2 D and E). At 15 weeks, the levels of pAkt in both compartments of the skin following treatment with DMBA/TPA

were 2-fold higher than the levels of pAkt at the earlier time point of 24 hr after treatment with DMBA/TPA (Figures 2.1 D and F compared to Figures 2.2 D and E).

2.4.3. Quantitation of pAkt in papillomas. The DNA dye DAPI in combination with immunofluorescence and confocal microscopy were used to identify the nucleated cells (blue fluorescence) that contained pAkt (red fluorescence) in papillomas isolated from SENCAR mice at 22 weeks of tumor promotion (Figure 2.3 A). Digital imaging analysis showed statistically significant increases ($p<0.0001$) in pAkt immunohistochemical staining in nucleated papilloma cells compared to pAkt in epidermal keratinocytes from the dorsal skin of mice treated topically with acetone (Figure 2.3 C). The level of pAkt in papillomas was similar to the level of pAkt staining detected in both the epidermal compartment of skin isolated at 15 weeks after treatment with DMBA/TPA (Figure 2.2 E and Figure 2.3 C) and in hyperplastic epidermis adjacent to papillomas isolated at 15 weeks and 22 weeks following DMBA/TPA treatment (data not shown).

2.4.4. Identification and quantitation of specific leukocytes in the dermal compartment of the skin and stroma. Dermal mast cells were identified and quantitated based on toluidine blue staining (Figure 2.4 A, arrows; inset, arrow). Regardless of the type of treatment of the dorsal skin, all dermal mast cells contained pAkt (Figure 2.4 B, arrows, inset, arrow). There were low numbers of dermal mast cells in skin isolated at 24 hr regardless of the type of topical treatment. The numbers of mast cells were significantly increased in the dermis of skin isolated at 15 weeks from mice treated once with DMBA followed by twice weekly treatments with acetone ($p<0.05$) and in the dermis of skin isolated from mice treated once with acetone followed by twice weekly treatments with TPA ($p<0.01$). The stromal tissue of papillomas isolated at 22 weeks had the greatest numbers of mast cells ($p<0.0005$) (Table 2.1).

Dermal neutrophils were identified and quantitated based on anti-MPO antibody staining (Figure 2.4 C, inset, arrow), which has previously been used as a marker of activated neutrophils [343]. Although the numbers of dermal neutrophils were significantly increased in skin treated with either TPA or DMBA/TPA at the 24 hr time point ($p<0.0001$) and in the stroma of papillomas ($p<0.0001$) (Table 2.1), these cells did not contain pAkt (Figure 2.4 D, arrow; inset, arrow).

2.4.5. Western blot of total Akt protein. The amount of total Akt protein levels in dorsal mouse skin and papillomas was constant, regardless of treatment of skin or time evaluated (Figure 2.5). To verify equal loading of protein, blots were reprobed with mouse anti-β-actin antibody.

2.5. Discussion

The present study identified specific cell populations in the epidermal, follicular, and dermal compartments of the skin during multi-stage carcinogenesis which contained pAkt. The use of specific antibodies, immunochemistry, multi-color immunofluorescent probes, and computer assisted digital image analysis methods allowed quantitation and statistical analysis of pAkt in specific cell populations and provided a high degree of reproducibility (inter- and intra-observer variabilities were < 5%).

Akt (protein kinase B) is one signal transduction molecule that is activated during multi-stage skin carcinogenesis [334, 335, 337, 344]. Akt has been associated with enhanced keratinocytes survival, a proliferative phenotype, and with altered and/or diminished keratinocytes differentiation [334, 335]. Previous studies reported that lapses in time of greater than a year between tumor initiation and tumor promotion do not significantly change the number of papillomas formed [345]. These observations suggest that initiated keratinocytes have a survival advantage which allows them to persist in the skin for long periods of time despite the presence of apoptotic mechanisms, which, under normal conditions, would result in elimination of these mutated cells. The present study did not detect an increase in pAkt in skin treated only with DMBA which may be due to the very low number of initiated cells that contained pAkt that have not undergone clonal expansion. Akt appears to become constitutively activated during tumor promotion, which was demonstrated in the present studies by the detection of pAkt in skin isolated at 15 weeks after a single exposure to DMBA and successive twice weekly treatment with TPA compared to the lack of significant elevation in pAkt in skin isolated at 15 weeks after treatment with TPA in the absence of tumor initiation with DMBA. Additional evidence supporting the constitutive activation of pAkt during tumor promotion comes from studies performed in our laboratory which found no significant difference in pAkt levels between skin treated topically with a single exposure or multiple treatments with DMBA (unpublished observations). Taken together, these results suggest that one of the critical factors in stimulating constitutive activation of Akt is the clonal expansion of Ha-*ras* mutated cells during tumor promotion.

Although the numbers of activated neutrophils were significantly increased at early times (24 hr) after exposure to TPA and in the stroma of papillomas, this cell type did not contain pAkt. This observation is consistent with the known 3-7 day life span of this cell type. Our earlier studies demonstrated that the numbers of circulating peripheral

blood neutrophils were elevated over the time of tumor promotion and that they produce elevated levels of reactive oxygen intermediates while in the circulation following topical application of dorsal epidermis with TPA [346, 347]. The amounts of reactive oxygen intermediates produced by neutrophils isolated from mice treated with either TPA or with DMBA followed by TPA was sufficient to induce DNA damage and mutation [346]. Taken together with the present observations, it appears that during skin carcinogenesis, bone marrow derived neutrophils are continually produced, are activated, and then migrate from the peripheral circulation into the dermal microenvironment of hyperplastic skin and papillomas, however, they are not a cell type that undergoes active proliferation nor do they have a prolonged life-span through Akt activation during skin carcinogenesis.

In contrast, we found that mast cells were prevalent within the stroma of papillomas and did contain pAkt. These cells have been suggested to act as “co-conspirators” in skin carcinogenesis by their ability to release matrix metalloproteinases, which triggers the “angiogenic switch” leading to neovascularization [88, 171]. The present studies demonstrate that mast cells contain pAkt, which would both provide a survival advantage and would support their involvement in the pro-angiogenic microenvironment within hyperplastic skin and in papillomas over a prolonged period of time.

Infiltrating inflammatory cells have been suggested to have a role in inducing epigenetic alterations that occur during multi-stage carcinogenesis through their ability to produce a “pro-oxidant environment”. Treatment of skin with either TPA or DMBA stimulates production of both oxygen and nitrogen reactive intermediates [88, 338, 347-350], resulting in formation of oxidative DNA adducts. Furthermore, we previously reported that both inflammatory leukocytes as well as epidermal keratinocytes release cytokines and other inflammatory mediators during tumor promotion, which in turn stimulates production of free radicals [84, 86, 338]. Recent studies reported the reactive oxygen species, such as H_2O_2 [351-354], and reactive nitrogen species, such as peroxynitrite [355], can directly activate Akt. Taken together, it appears that there may be cross-talk between keratinocytes and inflammatory leukocytes through their production of reactive oxygen and nitrogen intermediates and production of cytokines, which may activate Akt leading to enhanced survival of these cell populations and stimulating sustained proliferation of specific epidermal and follicular keratinocytes during multi-stage skin carcinogenesis.

The present results suggest that specific populations of epidermal and follicular keratinocytes, which have been shown to ultimately form papillomas and carcinomas [17, 29, 356, 357], contain constitutively activated Akt during multi-stage skin carcinogenesis. In addition, mast cells within the dermis of hyperplastic skin and in the stroma of papillomas contain activated Akt, suggesting that this molecular pathway may provide these inflammatory cells and keratinocytes populations with the ability to persist in the tissue during skin carcinogenesis, which maintains a tumorigenic, pro-oxidant and pro-angiogenic microenvironment. Further studies are necessary to determine the effects of inhibiting Akt activation in development of papillomas and their progression to malignant carcinomas.

Figure 2.1. Localization and quantitation of pAkt in skin at 24 hr after topical treatment with acetone, DMBA, or TPA. There were few cells with pAkt in dorsal skin treated once topically with acetone ***(A)***, or DMBA ***(B)*****,** with significantly higher number of cells with pAkt in skin treated with acetone followed at 7 days later by a single topical application of 2 μg TPA (acetone/TPA) ***(C)*** and in skin treated once with 25 nmol DMBA followed at 7 days later by a single topical treatment with 2 μg TPA (DMBA/TPA) ***(D)***. Specificity of pAkt antibody binding was determined by evaluation of the lack of binding of non-immune IgG ***(E)***. (A-E, 400x magnification). ***(F)*** Dorsal skin treated with either acetone/TPA or DMBA/TPA had significantly increased pAkt in the epidermal compartment ***(C, D, and F)***. Only skin treated with acetone/TPA had significantly increased pAkt in cells in the follicular compartment ***(D and F)***. Data are expressed as mean ± SEM; Quantitation of pAkt is expressed as integrated optical density (IOD). n = 3-4 mice for each group; ** statistically significant difference from acetone control group, $p<0.01$.

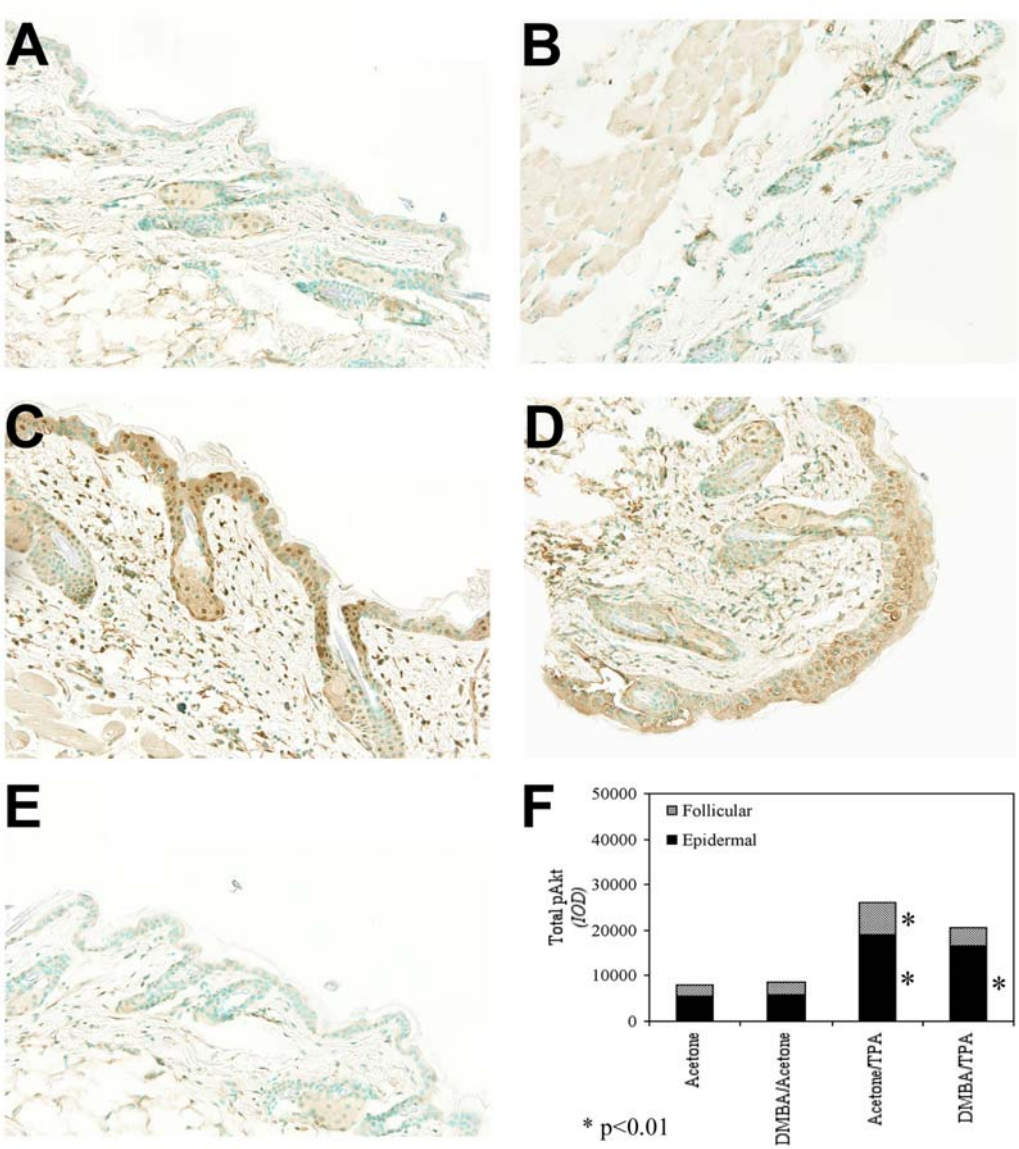
A
B
C
D
E
F
Follicular
Epidermal
Total pAkt (IOD)
50000
40000
30000
20000
10000
0
Acetone
DMBA/Acetone
Acetone/TPA
DMBA/TPA
* p<0.01

Figure 2.1

Figure 2.2. Quantitation of pAkt in epidermal and follicular compartments of the skin at 15 weeks of tumor promotion. In skin isolated at 15 weeks, few cells within the epidermal and follicular compartments contained pAkt in skin treated topically with acetone ***(A)***, DMBA/acetone ***(B)***, or acetone/TPA ***(C)***. Numerous cells in both the epidermal and follicular compartments contained pAkt in skin treated topically with DMBA/TPA ***(D)***. (A-D, 400x magnification) ***(E)*** Skin isolated from the DMBA/TPA treatment group had significantly increased pAkt in the epidermal and follicular compartments of the skin compared to any of the other treatment groups. n = 3 mice for each group; **, $p<0.01$ DMBA/TPA versus acetone control skin.

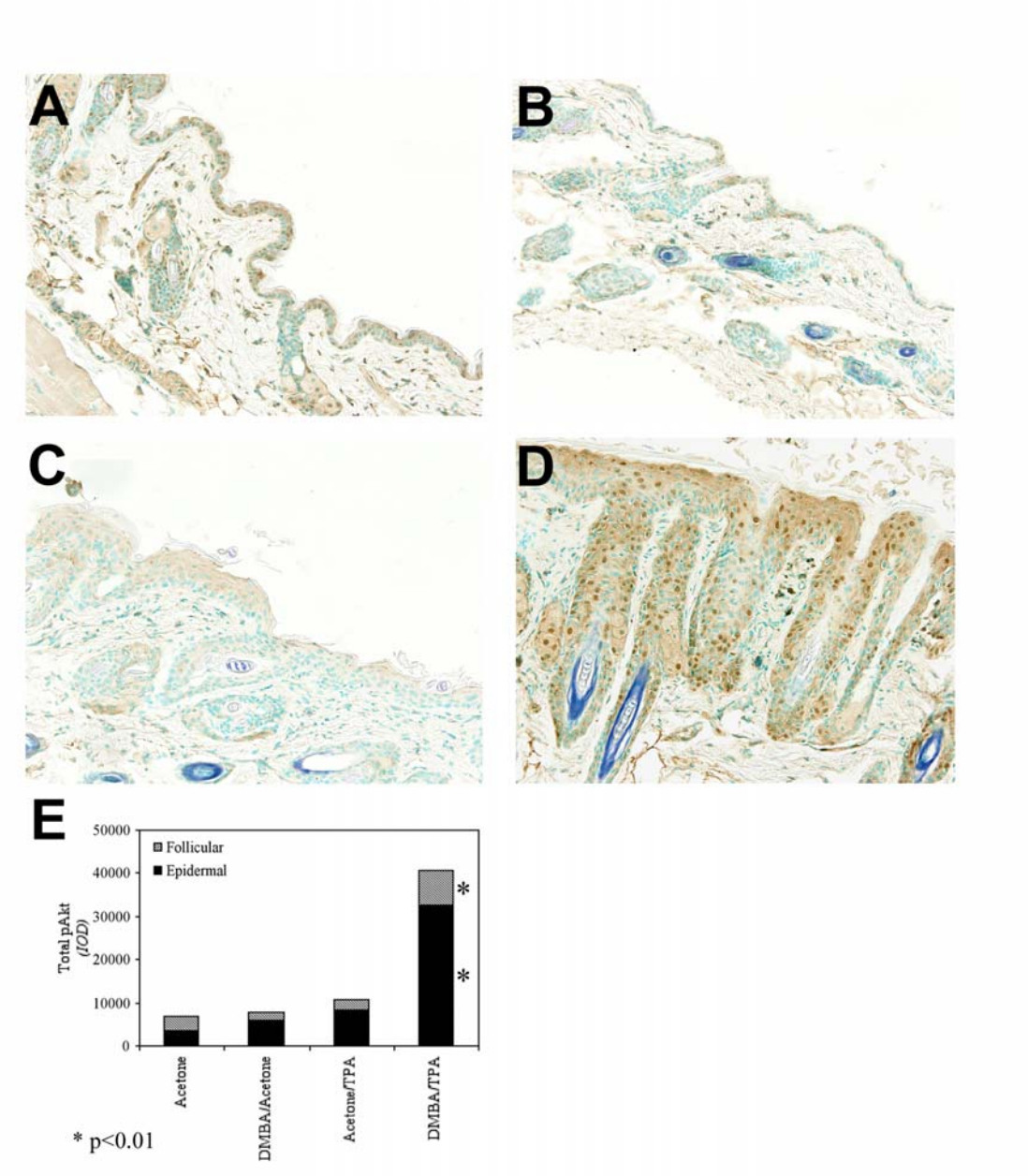
A
B
C
D
E
Follicular
Epidermal
Total pAkt (IOD)
50000
40000
30000
20000
10000
0
Acetone
DMBA/Acetone
Acetone/TPA
DMBA/TPA
*
*
* p<0.01

Figure 2.2

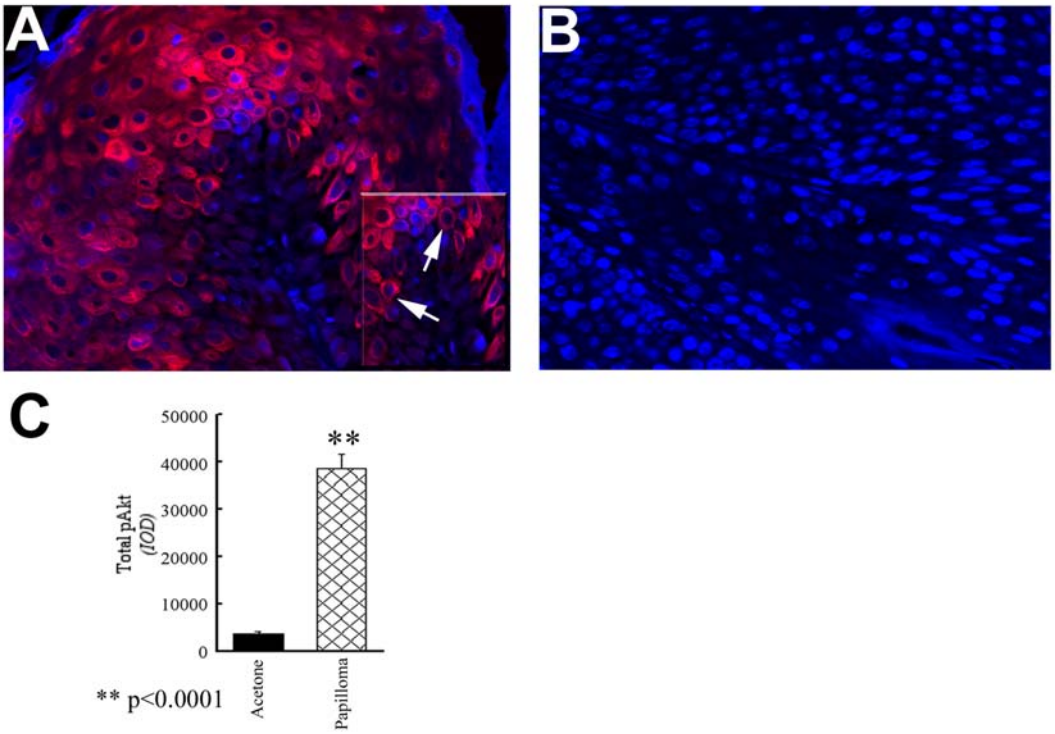

Figure 2.3. Localization and quantitation of pAkt in papillomas. (A) Representative immunofluorescence photomicrograph of nucleated cells (DAPI-associated blue fluorescence) that contain pAkt (Alexa-633-associated red fluourescence) in papillomas tissue isolated from SENCAR mice at 22 weeks of tumor promotion (inset, arrows). ***(B)*** Photomicrograph of DAPI-associated blue fluorescence showing nucleated cells within papillomas tissue (A-B, 400x magnification). ***(C)*** Quantitative analysis of pAkt immunohistochemical staining in papillomas. n = 2-3 mice for each group; **, $p<0.0001$ papillomas versus acetone control skin, unpaired *t*-test.

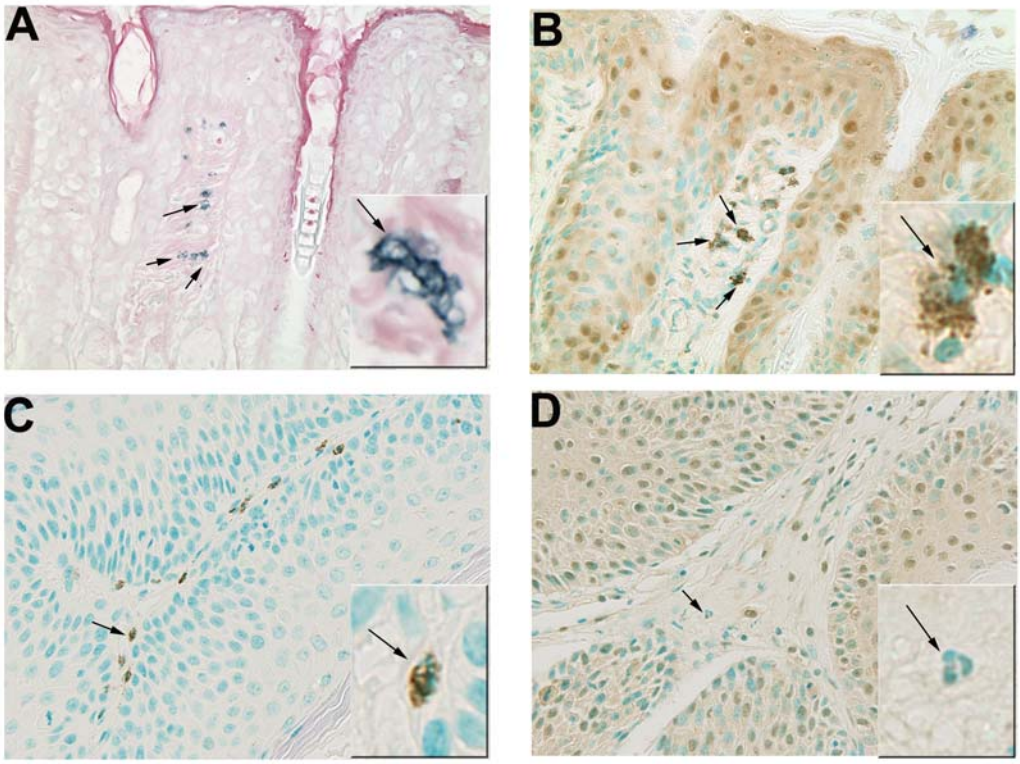

Figure 2.4. Identification and localization of pAkt in dermal inflammatory leukocytes of dorsal SENCAR mouse skin. Mast cells in serial sections of skin treated with DMBA/TPA for 15 weeks were identified by toluidine blue staining **(*A*, arrows, inset, arrow)** and were found to contain pAkt **(*B*, arrows, inset, arrow)**. Neutrophils were identified in serial sections of papillomas isolated from SENCAR mice at 22 weeks of tumor promotion using anti-myeloperoxidase (MPO) antibody staining **(*C*, arrow, inset, arrow)** and did not contain pAkt **(*D*, arrow; inset, arrow)**. (A-D, 400x magnification).

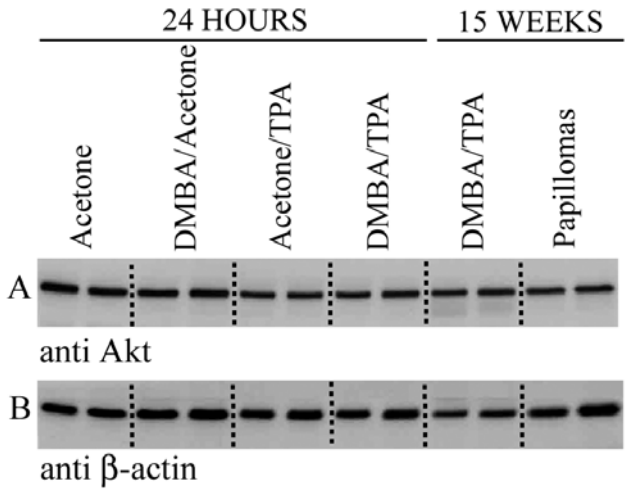

Figure 2.5. Western blot analysis of total Akt potein. (A) Analysis of total Akt protein in extracts of dorsal SENCAR mouse skin at 24 hr and in skin and papillomas isolated at 15 weeks demonstrated no change in total Akt protein. Samples were run in duplicate. ***(B)*** To verify the equal loading of proteins, the blot was re-probed for β-actin.

Table 2.1. Quantitation of mast cells and neutrophils in SENCAR skin and papillomas

	Mast Cells/Treatment Group ± SEM		Neutrophils/Treatment Group ± SEM	
Treatment	24 hr	15 Weeks	24 hr	15 Weeks
Acetone/Acetone	5 ± 1	6 ± 1	4 ± 1	3 ± 1
DMBA/Acetone	5 ± 0	9 ± 1*	7 ± 1*	4 ± 1
Acetone/TPA	5 ± 0	12 ± 2**	189 ± 21‡	4 ± 1
DMBA/TPA	5 ± 0	8 ± 1	78 ± 6‡	3 ± 1
Papillomas	N/A	14 ± 2***	N/A	21 ± 3‡

* $p < 0.05$; ** $p < 0.01$; *** $p < 0.0005$; ‡ $p < 0.0001$ versus Acetone control group.

CHAPTER 3

ACTIVATION OF AKT AND MTOR IN $CD34^+/K15^+$ KERATINOCYTE STEM CELLS AND SKIN TUMORS DURING MULTI-STAGE MOUSE SKIN CARCINOGENESIS

3.1. Abstract

The goal of the present studies was to localize two proteins known to be involved in regulation of cell proliferation and survival in specific cell populations in normal SENCAR mouse skin and during multi-stage skin carcinogenesis. The proteins evaluated included activated Akt, as defined by phosphorylation of Akt at Serine-473 (pAkt), and mammalian target of rapamycin (pmTOR), defined by phosphorylation of mTOR at Serine-2448 (pmTOR). The cell populations examined included mouse keratinocyte stem cells (KSC) within hair follicles and preneoplastic papilloma cells. The present studies used immunochemical staining analysis as well as triple color immunofluorescence in combination with confocal microscopy to evaluate the presence of activated Akt and mTOR in KSC within the bulge niche of hair follicles, as identified by expression of the specific markers of mouse KSC, CD34 and cytokeratin 15 (K15). Western blot analysis was used to examine CD34 and K15 protein levels in dorsal skin isolated of SENCAR mice during multi-stage skin carcinogenesis. $CD34^+/K15^+$ KSC were located only in the outer root sheath (ORS) of a specific niche within hair follicles defined as “the bulge”. The location of $CD34^+/K15^+$ KSC remained restricted to the bulge region throughout the 22-week time period examined during which pre-malignant papillomas developed and rapidly expanded. There was significant decrease in K15 protein levels at 24 hr and 15 weeks in dorsal skin treated with DMBA/TPA compared to CD34 protein levels. $CD34^+$ cells within the numerous hair follicles in hyperplastic skin were found to undergo proliferation during the process of multi-stage skin carcinogenesis based on their staining with antibodies directed against proliferating cell nuclear antigen (PCNA). While pAkt was present within the bulge region of hair follicles,

pmTOR was present in cells in the ORS of the bulge region as well as the upper infundibulum of hair follicles in dorsal skin treated with acetone. Within papillomas tissues isolated at 15 weeks following DMBA/TPA treatment, pAkt was localized to suprabasal cells with nominal staining of pAkt in the basal cell layer. There were fewer cells within the basal cell layer that contained pmTOR, in addition to the presence of pmTOR in suprabasal cells within papillomas. These results provide first time evidence for pAkt and pmTOR in $CD34^{+}/K15^{+}$ KSC localized to the outer root sheath niche of the bulge region of mouse hair follicles. Taken together, the present observations suggest that pAkt and mTOR may allow this cell population to evade terminal differentiation and to persist for long periods of time in their specific niche. Strategies that target pAkt and pmTOR may deplete both cells within the $CD34^{+}/K15^{+}$ KSC compartment as well as may impact the survival of non-proliferating suprabasal cells within pre-malignant papillomas.

3.2. Introduction

Early studies defined the location of cutaneous stem cells based only on their slow-cycling nature. Using long-term pulse-chase experiments, only mouse skin cells that rarely entered the cell cycle and therefore have a very slow turn-over rate, retained the nucleoside analog labels methyl-[^{3}H]thymidine (^{3}H-T) and bromodeoxyuridine (BrdU) [11-16]. Results of these initial studies led to the definition of these cells in mouse skin as "label-retaining cells" (LRC). Although studies have demonstrated that the majority of LRC are located within the bulge region of mouse hair follicles, an estimated 1-2% LRC have also been shown to be present in the basal layer of the interfollicular epidermis [11, 13-16]. The nuclei labeled within the basal layer were distributed as single cells within distinct columnar units composed of 10 basal cells and their suprabasal maturing progeny, defined as epidermal proliferative units (EPU) [13, 18, 31, 358].

Using transgenic approaches not previously available, more recent studies have demonstrated that the majority of LRC reside in a specific "growth and differentiation-restricted" niche within hair follicles [19], defined as "the bulge" region [11, 20]. Since this specific niche is relatively protected from harmful environmental insults [21], and these cells have been shown to have a high proliferative potential [26, 40, 41] as well as are able to grow as clones [25, 26, 40], these cells have been defined as mouse keratinocyte stem cells (KSC) [22, 25, 26, 29].

More recent studies have used CD34 [25] and Cytokeratin 15 (K15) [28] as markers to identify and isolate KSCs localized to the bulge region. CD34 is a cell surface glycoprotein that is expressed by hematopoietic progenitor cells and endothelial cells [22-24]. While CD34 is present specifically on cells in the outer root sheath of the bulge region of hair follicles in mice [25], it is not present in this niche in human tissue [27, 359]. Cytokeratin 15 (K15) is a cytoplasmic marker that is present in the least differentiated cells of neonatal epidermis and in cells within the outer and inner root sheath of the bulge region of adult mouse and human hair follicles [28-31].

In addition to CD34 and K15, mouse KSC have also been isolated based on their high expression of cell surface adhesion molecules, such as α_6 integrin [25, 32, 33], which labels basal keratinocytes that are in contact with the basement membrane [4, 26, 34], and β_1 integrin, which mediates adherence of keratinocytes to the underlying extracellular matrix [35, 36].

Using the combination of α_6 integrin and a proliferation-associated cell surface marker, the transferrin receptor (CD71), KSC were defined as α_6^{bright} and $CD71^{dim}$ that localized to the bulge region of hair follicles [32]. Using cell sorting experiments, the majority of α_6^{bright} $CD71^{dim}$ fractions were enriched for LRC at 14 weeks post-labeling of mice with ^{3}H-T [32]. This direct correlation between LRC and KSC was further verified by the co-localization of CD34 [25] and K15 [31] with LRC in the bulge region of hair follicles. Thus, the similarity in characteristics of LRC and KSC suggested that these cell populations are equivalent. Functionally, KSC have been defined as a cell population that rarely divides, persist in the specific bulge niche over the lifespan of the organism [11, 25, 26, 29, 360, 361], and serve as precursors for all cell types within hair follicles [362]. Although KSC are responsible for regeneration of cells within the hair follicle and they do participate in wound repair and regeneration, these cells are not believed to be involved in normal epidermal renewal [38, 42].

One mechanism by which KSC may persist in the skin over long periods of time is by activation of survival pathways that allow cells to resist apoptotic signals. Akt/Protein kinase B is a molecule that is activated through the phosphoinositide 3-kinase (PI3-K) signaling pathway and has been shown to be associated with cell survival [302, 303]. Following its activation, PI3-K is recruited to the inner surface of the plasma membrane resulting in the generation of the membrane-bound lipid, phosphatidylinositol 3,4,5-triphosphate (PI-3,4,5-P_3). Binding of PI-3,4,5-P_3 to Akt amino-terminal pleckstrin homology (PH) domain results in its recruitment to the inner surface of the plasma membrane [231, 232], where Akt becomes activated by phosphorylation at two amino acid residues, serine-473 (Ser-473) [235, 306] and threonine-308 (Thr-308) [234].

Knock-out mice with targeted loss of both Akt-1 and Akt-2 genes have impaired skin development which is characterized by the presence of a thin epidermis with very few cells in each layer of the skin [229]. Deficiency in Akt-1 and Akt-2 leads to a significant decrease in both the size and number of hair follicles, suggesting that Akt may contribute to the ability of KSC to persist in a quiescent state over the lifetime of the organism [229]. In an earlier study, we reported that during skin carcinogenesis, epidermal and follicular keratinocytes in hyperplastic skin and papillomas contain activated Akt, as determined by phosphorylation of Akt at serine 473 (pAkt) [363]. These results suggested that activated Akt may provide specific populations of cells that

participate in the process of mouse skin carcinogenesis with the ability to resist undergoing terminal differentiation.

An additional molecule that has recently become of interest is the mammalian target of rapamycin (mTOR), which is an effector molecule downstream of Akt. Following Akt activation, mTOR becomes phosphorylated at serine 2448 residue [256, 267, 309]. mTOR is a sensor for ATP and amino acids within the environment [283]. In yeast systems, mTOR is known to regulate cellular responses during nutrient deprivation [310], thus coupling the physical size of yeast to the availability of extracellular nutrients. mTOR has also been shown to induce survival of primary acute myeloid leukemia (AML) cells [364], suggesting a potential role of mTOR in regulating cell survival as well. Interestingly, mTOR also regulates entry of cells into the cell cycle, specifically by stimulating the initiation of protein translation of cyclin D1 [365, 366]. Since cyclin D1 has been shown to be involved in multi-stage skin carcinogenesis [367-369], mTOR may act as an upstream molecule that be involved in skin tumor development and progression.

The present studies used triple color immunofluorescence, immunostaining, and confocal microscopy to provide first time evidence for the presence of activated Akt and mTOR in $CD34^{+}/K15^{+}$ KSC within the bulge niche of hair follicles as well as in non-proliferative $CD34^{-}/K15^{-}$ cells within pre-malignant papillomas. $CD34^{+}/K15^{+}$ KSC remained localized within their bulge niche during skin tumor development. Although normally quiescent, we found that KSC undergo proliferation during multi-stage carcinogenesis. Taken together, pAkt and pmTOR may coordinate survival of KCS, contributing to the persistence of KSC in the skin over long periods of time during multi-stage skin carcinogenesis. In addition, Akt/mTOR signaling pathway may confer longevity to suprabasal keratinocytes and also may be involved in the sustained proliferation of suprabasal keratinocytes within papillomas tissues.

3.3. Materials and Methods

3.3.1. Treatment of SENCAR mice with DMBA and TPA. Female SENCAR mice (6-8 weeks old, 22-28 g; NCI, Bethesda, MD) were housed in vivarium facilities at The Ohio State University that meet American Association for Accreditation of Laboratory Animal Care requirements. All procedures were approved by The Ohio State University Institutional Animal Care Utilization Committee. Animals were fed basal Teklad 22/5 rodent diet (Harland Industries, Indianapolis, IN) *ad libitum* and kept in rooms maintained on a 12 hr light/dark cycle. Mice treated topically with 0.2 ml HPLC grade acetone (Aldrich, Milwaukee, WI) served as the solvent control. DMBA (Sigma, St. Louis, MO) was dissolved in acetone and applied at a final concentration of 25 nmol DMBA in 0.2 ml acetone. TPA (Alexis Biochemicals, San Diego, CA), at a final concentration of 2 μg, was dissolved in acetone and applied in a volume of 0.2 ml. Dorsal skin was carefully shaved 24 hr prior to initial treatment. For short-term experiments, dorsal skin of SENCAR mice was treated with two topical applications of acetone or 25 nmol DMBA, with a 48 hr time interval between treatments with acetone or DMBA, followed at 7 days by a single topical application of acetone or TPA. At 24 hr after the final application of acetone or TPA, mice were sacrificed by carbon dioxide euthanasia. Dorsal hair was removed using a depilatory agent, skin was isolated, and tissue samples were fixed in 10 % neutral buffered formalin and embedded in paraffin for immunostaining analysis or used to isolate protein for Western blotting analysis.

For studies in which papillomas and hyperplastic skin were analyzed, mice were initiated with a single topical application of 25 nmol DMBA or treated with a single topical application of acetone and at 7 days later, mice were treated topically twice weekly with acetone or 2 μg TPA. At 4 hr following the final application of TPA at either 15 or 22 weeks, mice were sacrificed by carbon dioxide euthanasia. Dorsal skin and papillomas were isolated and processed as described above.

3.3.2. Immunochemical staining methods. Sections of formalin-fixed and paraffin-embedded skin samples (4 μm) were cut and mounted onto SuperFrost/Plus slides (Fisher Scientific, Pittsburgh, PA). Tissues sections were deparaffinized using Histo-Clear (National Diagnostics, Atlanta, GA), and rehydrated in a graded series of alcohol. Endogenous peroxidase activity was quenched using 3% H2O2 in methanol. Following antigen retrieval by steam heating in 10 mM citrate buffer (pH 6.0), non-specific binding

was blocked with 1% bovine serum albumin (BSA) (Sigma) in 1X TBS containing 0.05% Tween 20 (TBST). Sections were then incubated with goat anti-CD34 (1:150; Santa Cruz Biotechnology, Santa Cruz, CA), chicken anti-keratin 15 (K15; 1:2000; Covance, Berkley, CA) for 1 hr at room temperature, or rabbit anti-Akt-Ser-473-P (pAkt, 1:50; Santa Cruz), rabbit anti-phospho-mTOR-Ser-2448 (pmTOR; 1:50; Cell Signaling Technology, Beverly, MA) overnight at 4^{o}C in 1% BSA in TBST. Sections were incubated for 20 min with biotinylated horse anti-goat IgG, goat anti-chicken, or goat anti-rabbit IgG (1:200; Vector Laboratories, Burlingame, CA), followed by incubation for 30 min with avidin-biotinylated horseradish peroxidase complex (ABC Elite) (Vector Laboratories). The presence of CD34, K15, pAkt, and pmTOR antigens was visualized with the chromagen VIP substrate (Vector Laboratories) or 3,3-diaminobenzidine (DAB; Vector Laboratories). The specificity of pAkt staining was determined by examining the extent of binding of anti-pAkt antibody by tissue sections that had been pre-incubated with Akt-Ser-473-P Blocking Peptide (Cell Signaling Technology) for 2 hr. Tissues were counterstained with preheated Methyl Green (Vector Laboratories) for 5 min, dehydrated, mounted, viewed, and photographed.

For double immunochemical labeling (Figure 3.1), sections were incubated with goat anti-CD34 antibody, followed by incubation with the biotinylated horse anti-goat IgG. Slides were incubated with avidin-biotinylated alkaline phosphatase complex (Vector Laboratories). CD34 staining was visualized by incubation with the chromagen Vector Red alkaline phosphatase substrate (Vector Laboratories). Samples were then treated with Avidin/Biotin blocking kit (Vector Laboratories) prior to incubation overnight at 4^{o}C with rabbit anti-PCNA antibody (1:50, Santa Cruz). Slides were incubated with biotinylated goat anti-rabbit IgG, followed with avidin-biotinylated horseradish peroxidase complex. Tissues were then incubated with the chromagen DAB, dehydrated, mounted, viewed, and photographed.

Quantitation of $CD34^{+}$ cells that stained with anti-PCNA antibody was evaluated by counting the number of $CD34^{+}$ cells, then counting the number of $CD34^{+}$ cells which co-expressed PCNA within 10-20 consecutive high-power fields (800x). Data was represented as the ratio of the number of $CD34^{+}$ cells that stained positive for PCNA to the total number of $CD34^{+}$ cells ($PCNA^{+}/CD34^{+}$), and expressed as mean $\pm$ standard error of mean (SEM).

3.3.3. Immunofluorescent staining. Sections of paraffin-embedded skin samples (4 μm) were rehydrated as described above. To reduce autofluorescence, sections were treated with sodium borohydride (1 mg/ml; Sigma) in TBST. For double immunofluorescence staining, to block background staining, sections were incubated for 30 min at room temperature with Image-iT^{TM} FX Signal Enhancer (Molecular Probes, Eugene, OR). Sections were incubated overnight at 4^{o}C with both anti-pAkt and anti-CD34 (1:50, Santa Cruz). Tissues were then incubated at room temperature for 1 hr with Alexa Fluor-647-conjugated donkey anti-goat IgG, followed by Alexa Fluor-555-conjugated donkey anti-rabbit for 1 hr (1:500, Molecular Probes). Tissues were mounted using VectaShield Mounting Medium (Vector Laboratories) containing 4', 6-diamidino-2-phenylindole (DAPI), a DNA dye that specifically stains nucleated cells. Specificity of antibody binding was determined by incubation with only secondary antibodies followed by placement of coverslips using Vectashield containing DAPI.

For serial immunofluorescent staining, serial tissue sections were incubated with goat anti-CD34 antibody (1:150) or chicken anti-K15 (1:2000) for 1 hr at room temperature. Sections were incubated with horse anti-goat or goat anti-chicken IgG, followed by incubation with avidin-biotinylated alkaline phosphatase complex. The slides were then incubated with the chromagen Vector Red alkaline phosphatase substrate, which was visualized as red fluorescence. Tissue sections were mounted using VectaShield containing DAPI.

3.3.4. Confocal microscopy and digital imaging. Digital images of stained tissues were captured using a Diagnostic Instruments digital camera (Insight camera; 1600 x 1200 resolution) mounted on an Olympus research microscope, using identical lighting and optical settings. Images were then transferred to digital image analysis software (Image Pro Plus, Media Cybernetics, Silver Spring, MD). Fluorescent images were obtained using a laser scanning confocal microscope (Zeiss LSM 510 Meta), with excitation wavelengths of 543 nm for Alexa Fluor-555 and Vector Red, 633 nm for Alexa Fluor-647, and 405 nm for DAPI-associated fluorescence. Emission signals were observed using a set of band-pass filters. Images were merged using Adobe Photoshop software (Adobe Systems, Inc., San Jose, CA).

3.3.5. Cell proliferation measured by autoradiography. Methods to identify cells incorporating [methyl-3H]/thymidine were as previously described [84]. Mice were injected intraperitoneally (i.p.) with 30 μCi of [methyl-3H]/thymidine (70-90 Ci/mmol) in 0.5 ml PBS at 1 hr prior to death. Sections were cut, immersed in Kodak NTB-2 nuclear tracking emulsion (Eastman Kodak, Rochester, NY), and incubated at 40-45^{o}C in darkness. Slides were then placed on a chilled glass plate for 10 min. Slides were dried and placed vertically in a light-tight box containing silica gel desiccant, followed at 16-18 days by placement of individual slides for 5 min in Kodak D-19 developer at 18^{o}C. Slides were fixed for 5 min in Kodak fixer and stained with Harris' acid hematoxylin for 2 min. Slides were rinsed with cold water, incubated with ammonia water, and washed with 70% ethanol prior to incubation with eosin stain for 1 min. Slides were dehydrated, viewed, and photographed.

3.3.6. Protein extraction. Dorsal skin and papillomas were homogenized on ice in homogenation buffer, pH 8.6 (Tris-HCl, 60 mM; EDTA, 5 mM, EGTA, 5 mM; sucrose, 300 mM; DTT, 5 mM; leupetin, 200 μg/ml; PMSF, 2 mM; aprotinin, 20 μg/ml; sodium molybdate, 10 mM), followed by sonication for 10 sec. Samples were clarified by centrifugation and supernatants were collected. Protein concentrations were determined using BIO-RAD assay (BIO-RAD, Hercules, CA) and BSA (Sigma) was used as a standard.

3.3.7. Western blot analysis. Methods to analyze equal aliquots of protein extracts (35 μg) by Western blotting were as previously described [363]. Blots were incubated for 1 hr at room temperature with goat anti-CD34 (1:150) or chicken anti-K15 (1:1000) in TBST containing 5% non-fat dried milk. Blots were then incubated for 1 hr with peroxidase-linked anti-goat or anti-chicken IgG (1:2000; Jackson ImmunoResearch Laboratories, West Grove, PA) in TBST containing 5% milk. The signal was developed using ECL+Plus (Amersham Pharmacia Biotech, Piscataway, NJ). To verify equal loading of protein samples, blots were reprobed with mouse anti-β-actin (1:5000; Sigma) for 1 hr, and then incubated with anti-mouse IgG (1:4000; Amersham) for 30 min. Images were scanned and bands intensity was analyzed using NIH Image 1.62f software.

3.3.8. Statistical analysis. Significant differences in the number of $PCNA^{+}/CD34^{+}$ KSCs and western blot analysis of CD34, and K15 proteins of mouse skin treated with either acetone, DMBA, TPA, or DMBA/TPA were determined using one way analysis of variance (ANOVA) on ranks for non-parametric comparisons (GraphPad Prism Software, San Diego, CA), with Student-Newman-Keuls *post-hoc* analysis to evaluate significant comparisons between three or more groups. Results were expressed as mean $\pm$ SEM, with $p<0.05$ being statistically significant.

3.4. Results

3.4.1. Histology of mouse skin. Dorsal skin isolated from SENCAR mice treated once with 200 μl acetone (Figure 3.2 A) or with a single topical application of 25 nmol DMBA (Figure 3.2 B) followed by twice weekly applications of 200 μl acetone (DMBA/acetone) for 15 weeks had a uniform epidermal thickness of 1-2 keratinocytes and low numbers of cells within the dermis. There was no difference in the histology of dorsal epidermis treated with acetone compared to skin of untreated mice (not shown). Epidermal hyperplasia was evident in skin treated once with acetone followed by twice weekly applications of 2 μg TPA for 15 weeks (acetone/TPA) (Figure 3.2 C), and in skin treated once with 25 nmol DMBA followed by twice weekly treatments of TPA (DMBA/TPA) (Figure 3.2 D), with epidermal thickness increased to 5-6 cell layers. In addition, hair follicles in skin treated with either DMBA/TPA or acetone/TPA were also hyperplastic and elongated, indicating that the follicles were in the anagen phase of the hair follicle cycle (Figure 3.2 D, arrows).

3.4.2. Localization of $CD34^+$ and $K15^+$ KSC to the bulge region of hair follicles. To localize $CD34^+$ cells and $K15^+$ cells within the skin, consecutive serial sections of dorsal skin isolated from SENCAR mice treated topically with acetone were stained with anti-CD34 antibody (Figure 3.3 A-C) or anti-K15 antibody (Figure 3.3 D-F). The DNA dye DAPI was used in combination with confocal microscopy to identify nucleated cells (blue fluorescence) in hair follicles that contained CD34 (Vector red-associated fluorescence) (Figure 3.3 C) or K15 (Vector red-associated fluorescence) (Figure 3.3 F). $CD34^+$ staining in the ORS of the Bulge (Bu) region of hair follicles (Figure 3.3 C) coincided with the location of $K15^+$ cells in consecutive serial sections of control skin (Figure 3.3 F). While $CD34^+$ cells were located only in the outer root sheath (ORS) of the Bu region (Figure 3.3 A-C), $K15^+$ cells were present in both the inner root sheath (IRS) and ORS of the Bu (Figure 3.3 D-F).

3.4.3. $CD34^+$ KSC remain localized to the bulge niche during all stages of development of hair follicle. Hair follicle cycling comprises numerous structural reorganizations. Each hair follicle cycles through 3 different stages of growth, which include catagen, also known as hair follicle regression, telogen, which is the resting phase, followed by anagen, known as the growth phase. During all stages of hair follicle

cycling, only the lower portion of the hair follicle undergoes cycles of destruction and restoration, while the upper portion of the hair follicle, also known as the permanent portion, remains intact. During early anagen, the hair follicle grows downward to regenerate the lower portion of the hair follicle (Figure 3.4 A). During this stage, $CD34^+$ KSC cells localized to the bulge region (Figure 3.4 A). No $CD34^+$ cells were present within the bulb or the infundibulum region of hair follicles. In addition, there was a notable absence of $CD34^+$ staining cells within the epidermal compartment of the skin. While a new hair follicle develops adjacent to the old one at the onset of anagen (Figure 3.4 B), $CD34^+$ cells remained localized to the new bulge region of the new hair follicle that is generated. During the telogen phase (Figure 3.4 C), $CD34^+$ cells remain located to the bulge niche, despite the degeneration of the lower portion of the hair follicle.

3.4.4. Differential location of $CD34^+$ cells and $K15^+$ cells in hyperplastic skin, endothelial cells, mast cells, but not in papillomas. Only cells within the ORS of the Bu region of hair follicles were $CD34^+$ (Figure 3.5 A, arrowheads), while cells within both the ORS and IRS of hair follicles were $K15^+$ (Figure 3.5 B, arrowheads). Papilloma cells in pre-malignant lesions isolated at 22 weeks after DMBA/TPA skin carcinogenesis were neither $CD34^+$ nor $K15^+$ (Figure 3.5 C and D, respectively). In contrast, both endothelial cells as well as mast cells within papillomas were $CD34^+$ (Figure 3.5 C, insets).

3.4.5. Western blot analysis of total CD34 protein and K15 protein. Analysis of CD34 protein in extracts of dorsal skin isolated from SENCAR mice demonstrated that CD34 protein was present in skin at 24 hr after treatment with two topical applications of 200 μl acetone or 25 nmol DMBA followed at 7 days by a single topical application of acetone or 2 μg TPA (Figure 3.6 A-C). There was a significant increase in CD34 protein in skin treated with DMBA/acetone ($p<0.01$) or DMBA/TPA ($p<0.05$) (Figure 3.6 B). In contrast to the relatively high levels of CD34 protein in hyperplastic skin isolated from mice treated with DMBA/TPA at 15 weeks of tumor promotion, CD34 protein was not present in protein extracts isolated from papillomas at 15 weeks of skin carcinogenesis (Figure 3.6 A and C). K15 protein was present in all skin samples isolated at 24 hr, regardless of treatment group (Figure 3.6 A and D), with the highest level of K15 in skin isolated at 24 hr from mice treated topically with DMBA/acetone ($p<0.05$). While K15 protein was

present in skin treated with DMBA/TPA isolated at 15 weeks, protein isolated from papillomas did not contain detectable K15 (Figure 3.6 A and E).

Comparatively, there was a significant ($p<0.05$) decrease in the amount of K15 protein in hyperplastic skin isolated from SENCAR mice at 15 weeks that have been treated with DMBA/TPA (Figure 3.6 E) compared to the amount of CD34 protein isolated from the same skin tissues (Figure 3.6 C). The decrease in K15 protein levels compared to CD34 protein levels in skin isolated at 15 weeks after treatment with DMBA/TPA (Figure 3.6 E and C) was similar to the significant ($p<0.05$) decrease in the amount of K15 protein (Figure 3.6 D) in DMBA-initiated dorsal skin of mice isolated at 24 hr following a single topical application of TPA compared to the amount of CD34 protein (Figure 3.6 B). To verify equal loading of proteins, blots were re-probed with mouse anti-β-actin antibody, which was unchanged regardless of time or treatment group (Figure 3.6 A).

3.4.6. Co-localization of $CD34^+$ and pAkt in cells within the bulge niche. Double-immunofluorescence and confocal microscopy were used to identify $CD34^+$ cells (Alexa-647 red-associated fluorescence) within the ORS of the Bu (Figure 3.7 A) which contained pAkt (Alexa-555 green-associated fluorescence) (Figure 3.7 B). Nucleated cells within the entire hair follicle were defined by DAPI-associated blue fluorescence (Figure 3.7 C). Figure 3.7 D is a representative merged image of CD34, pAkt, and DAPI staining in hair follicles of dorsal skin isolated from mice treated topically with acetone showing the co-localization of $CD34^+$/Akt^+ nucleated cells within the Bu niche of a hair follicle. Nucleated $CD34^+$ cells in hyperplastic skin isolated from mice at 15 weeks that had been treated with DMBA/TPA also contained activated Akt (Data not shown).

3.4.7. Analysis of CD34 and PCNA in specific regions of hair follicles during skin carcinogenesis. Double immunohistochemical staining was used to co-localize cells within skin isolated during multi-stage carcinogenesis that stained with anti-CD34 antibody (*red*; membrane localization) and anti-PCNA antibody (*brown*; nuclear staining) (Figure 3.8). In skin isolated at 15 weeks after treatment with acetone, $CD34^+$ cells were visible within the ORS of the Bu, however they were $PCNA^-$, indicating that these cells were quiescent and non-cycling (Figure 3.8 A, inset). Note the numerous $PCNA^+$ cells in the upper portion of the hair follicle, defined as the infundibulum (arrowheads). In skin

isolated at 15 weeks following a single exposure to 25 nmol DMBA followed by twice weekly application of acetone, there were $CD34^+$ cells within the BU that are also $PCNA^+$ (Figure 3.8 B, inset, arrows). In addition, there were $CD34^-/PCNA^+$ cells in the bulb (Blb) region as well as the infundibulum of hair follicles (Figure 3.8 B, arrowheads). These observations were similar to the location of $CD34^+/PCNA^+$ and $CD34^-/PCNA^+$ cells in skin isolated from mice at 15 weeks following a single exposure to acetone followed by twice weekly applications of 2 μg TPA (Figure 3.8 C, arrowheads and inset, arrows). Skin isolated at 15 weeks following treatment with DMBA/TPA contained elongated and hyperplastic hair follicles, with numerous $CD34^-/PCNA^+$ cells in the Blb and infundibulum and $CD34^+/PCNA^+$ cells in the ORS of the Bu niche (Figure 3.8 D, arrowheads and inset, arrows, respectively). Quantitation of the number of $PCNA^+/CD34^+$ cells in hair follicles of skin treated with DMBA or TPA revealed that there was no statistical difference between the numbers of $PCNA^+/CD34^+$ cells in the skin treated with acetone, DMBA/acetone or acetone/TPA (Figure 3.8 E). Twice weekly applications of 2 μg TPA to DMBA-initiated skin stimulated proliferation of $CD34^+$ cells, as determined by the significant increase ($p<0.001$) in the number of $PCNA^+/CD34^+$ cells compared to the numbers of $PCNA^+/CD34^+$ cells in skin treated with acetone, DMBA/acetone, or acetone/TPA (Figure 3.8 E).

3.4.8. Identification of non-proliferating $pAkt^+$ cells in papillomas. Suprabasal cells within papillomas isolated at 22 weeks of skin carcinogenesis that contained pAkt (Figure 3.9 A, inset arrows) were not located within the proliferative compartment, as shown by their lack of incorporation of [methyl-^{3}H] thymidine (^{3}H-T) (Figure 3.9 C, inset, arrow) and their lack of PCNA staining (Figure 3.9 D, inset, arrow). The specificity of the pAkt staining is demonstrated by the lack of staining in sections of papillomas pre-incubated with phospho-Akt-Ser-473 blocking peptide and anti-pAkt antibody (Figure 3.9 B).

3.4.9. Comparative localization of pAkt and pmTOR in mouse skin and papillomas. While pAkt was present within the bulge region of hair follicles (Figure 3.10 A, inset, arrowhead), pmTOR was present in cells in the ORS of the Bu (Figure 3.10 B, inset, arrowhead) as well as the upper infundibulum of hair follicles (Figure 3.10 B, inset, arrow) in consecutive serial sections of SENCAR mice treated with acetone.

pAkt was localized to suprabasal cells within papillomas isolated at 15 weeks following DMBA/TPA treatment (Figure 3.10 C, inset, white arrowheads) with lack of staining of pAkt in the basal cell layer, as indicated by the visible methyl green counterstain (Figure 3.10 C, inset, black arrows). While suprabasal cells within papillomas contained pmTOR (Figure 3.10 D, inset, white arrowheads), there were fewer cells within the basal cell layer (Figure 3.10 D, inset, black arrows) that contained pmTOR.

The pattern of pAkt (Figure 3.10 E) and pmTOR (Figure 3.10 F) staining detected in hyperplastic epidermis adjacent to papillomas isolated from SENCAR mice at 15 weeks of tumor promotion was similar to the staining pattern of pAkt (Figure 3.10 C) and pmTOR (Figure 3.10 D) staining in papillomas.

3.5. Discussion

Although KSC are slow cycling cells [25, 29], they have been found to possess the potential to undergo proliferation giving rise to transit amplifying cells, as demonstrated by the ability of *in vitro* cultures of pure populations of $CD34^+$ cells isolated by cell sorting techniques to divide and form large colonies containing keratinocytes of small size and undifferentiated morphology [25, 26]. These colonies, which are defined as holoclones, represent the clonal expansion of a single KSC [2]. Previous studies showed that KSC proliferate only during the anagen growth phase of hair follicles in normal unwounded skin [19, 28]. The present study localized KSC to the ORS of the bulge region of hair follicles in normal skin and demonstrated that the location of KSC within this specific niche was not altered during multi-stage skin carcinogenesis. $CD34^+/K15^+$ cells were not detected within skin papillomas, which is consistent with the composition of these pre-malignant lesions recognized as being primarily differentiated suprabasal keratinocytes. $CD34^+/K15^+$ cells remained localized only within the ORS of the Bu region of hair follicles in hyperplastic skin adjacent to pre-malignant papillomas. The present study also demonstrates that $CD34^+$ cells do undergo proliferation during multi-stage skin carcinogenesis. Taken together, the present observations demonstrate evidence for the proliferative capacity of $CD34^+$ cells during skin carcinogenesis and confirm that this cell population persists within their specific niche of the ORS of the Bu region of hair follicles during multi-stage skin carcinogenesis.

In addition to identification of proliferative KSC during multi-stage carcinogenesis, $CD34^+$ cells within the ORS of the Bu niche were also observed to contained activated pAkt, as defined by phosphorylation of Akt at serine-473 residue (pAkt) (Figure 3.11). Previous studies have reported that deletion of the Akt-1 gene leads to retardation in morphogenesis of postnatal hair follicles [370] and loss of both Akt-1 and Akt-2 has been reported to lead to depletion of putative bulge stem cells in hair follicles [229]. Akt activation has recently been shown to induce long-term maintenance of human embryonic stem cells in their undifferentiated state [371, 372], suggesting that Akt activation in KSC may represent one mechanism by which KSCs resist undergoing differentiation in normal skin (Figure 3.11). The importance of pAkt in conferring $CD34^+$ KSC with the ability to persist in the bulge region of hair follicles over the lifetime of the organism may be similar to the reported role of an Akt-related family member, serum and glucocorticoid responsive kinase-3 (Sgk-3). Loss of function of Sgk-3 reduced the

supply of transit amplifying cells in the bulb region in the lower portion of hair follicles, thus causing their premature entry into the apoptotic catagen phase of hair follicle cyclic morphogenesis [373].

In addition to the presence of pAkt in $CD34^+$ cells within the ORS of the Bu niche, these cells contained pmTOR as well (Figure 3.11). mTOR, an effector molecule downstream of Akt [256], not only plays a role in conferring cells with survival signals [364], but also regulates cellular size [309]. mTOR-dependent-increase in cell size and cell cycle progression have been shown to be tightly coupled and coordinated [260]. Previous studies reported that quiescent KSCs exhibit a smaller diameter and cellular area compared to the larger size of actively cycling transit amplifying cells [32]. The presence of pmTOR in KSC suggests that pmTOR may play a role in controlling the size of KSC, therefore tightly regulating the entry of KSC into the cell cycle.

Previous studies have demonstrated that KSC can serve as targets for skin carcinogens [374]. The administration of DMBA was found to have no effect on either latency and multiplicity of skin tumors following exposure of mice to topical administration of 5-fluorouracil (5-FU) [375], which kills rapidly cycling transit amplifying cells and spares quiescent cells. These authors concluded from these studies that quiescent KSC may be targets for initiation of mutations in the v-Ha-*ras* oncogene by DMBA [375]. Taken together with the present observations, these results suggest that the intrinsic activation of Akt in $CD34^+$ cells may contribute to the persistence of initiated keratinocyte populations containing Ha-*ras* mutations which, under normal conditions, would be eliminated by apoptotic mechanisms. Therefore, Akt activation may block depletion of KSC during multi-stage skin carcinogenesis.

While $CD34^+/K15^+$ cells that were localized to the ORS of the bulge region of hair follicles contained pAkt, $CD34^-/K15^+$ cells localized to the IRS of hair follicles lacked the presence of pAkt (Figure 3.11). Furthermore, the present study demonstrates a significant decrease in K15 protein levels at 24 hr and 15 weeks in dorsal skin treated with DMBA/TPA compared to CD34 protein levels. The present observations further confirm that the differential presence of pAkt in $CD34^+/K15^+$ cells may maintain the survival of KSCs in their specific niche, thus preventing their depletion during multi-stage skin carcinogenesis. In contrast, $CD34^-/K15^+$ cells did not contain pAkt, therefore, may be sensitive to skin carcinogenesis (Figure 3.11). Taken together, the present

observations indicate that K15 may serve as a marker of sensitivity to multi-stage skin carcinogenesis.

The current studies demonstrate that pAkt was not only restricted to $CD34^+/K15^+$ cells in the bulge region of hair follicles, but was also present in suprabasal keratinocytes in papillomas. Loss of Akt-1 in primary human keratinocytes grown as organotypic skin cultures resulted in cell death of keratinocytes, demonstrating that Akt-1 may provide an essential survival signal in suprabasal cells during normal stratification of skin [376]. Taken together, the present results indicate that pAkt may provide differentiated suprabasal cells in papillomas with the ability to evade the normal process of terminal differentiation, thus conferring them with the ability to persist within the skin over long periods of time.

While pAkt staining was nominal in the basal cell layer within papillomas tissues, fewer cells within the basal layer of papillomas contained pmTOR. pmTOR has been previously shown to stimulate entry of cells into the cell cycle by phosphorylating in parallel the 70 KDa ribosomal protein S6 kinase (p70 S6K) [273, 311, 312] and eukaryotic initiation factor 4E (eIF4E)-binding protein 1 (4E-BP1). Once activated, p70 S6K induces phosphorylation of the 40S ribosomal protein, S6, leading to an increased rate of initiation of translation of mRNAs that encode ribosomal proteins and translation elongation factors [273, 311, 312]. On the other hand, mTOR initiates translation of protein that are required for entry into the G1-phase of the cell cycle, such as cyclin D1, by phosphorylating 4E-BP1 at Thr-37/Thr-46 residues [279, 377], thus inhibiting the association between 4E-BP1 and eIF4E and freeing eIF4E for initiation of protein translation [281]. The location of pmTOR to fewer cells within the basal layer of papillomas suggests that pmTOR may be essential for the proliferation of basal cells during multi-stage skin carcinogenesis. The current observations correlate with previous studies demonstrating that localization of nuclear immunostaining of Cyclin D1 was confined only to the basal proliferative compartments of skin tumors [378].

Localization of pAkt in suprabasal keratinocytes within papillomas tissues coincided with the location of pmTOR. However, localization of pmTOR in suprabasal keratinocytes did not correlate with PCNA expression, a proliferative marker that is expressed in the G_1/S and G_2 phases of the cell cycle [379]. pmTOR not only stimulates entry into the cell cycle, but has been recently shown to induce survival of primary AML cells, suggesting that pmTOR may regulate cell survival as well. These results suggest a

model in which Akt and its downstream effector, mTOR, may act together or separately to induce long-term maintenance and survival of non-proliferating $CD34^-/K15^-$ suprabasal keratinocytes within papillomas tissues. Taken together, the present observations indicate that pmTOR may differentially induce survival or proliferation of cells depending on its localization to specific keratinocytes within papillomas tissues. When transfected into PB keratinocytes, which usually have low rates of tumor formation when grown *in vivo*, wild-type Akt resulted in rapidly growing, undifferentiated, and highly invasive skin tumors [335]. In contrast, these mice did not develop skin tumors following implantation of subcutaneous pumps which allowed continuous delivery of rapamycin [368], indicating that pmTOR may mediate Akt-dependent activities during multi-stage skin carcinogenesis.

Further investigations may provide evidence for the utility of pAkt and pmTOR as novel therapeutic targets in the basal as well as suprabasal cells layers within skin tumor tissues. In addition, strategies targeting pAkt and pmTOR may deplete the $CD34^+/K15^+$ KSC compartment and may also block the persistence of non-proliferative pre-malignant papilloma cells. The approach of targeting both pAkt and pmTOR within the bulge region of hair follicles may have utility in inhibiting development and progression of any skin lesions that have $CD34^+/K15^+$ KSC as its origin, including both squamous cell carcinomas and basal cell carcinomas.

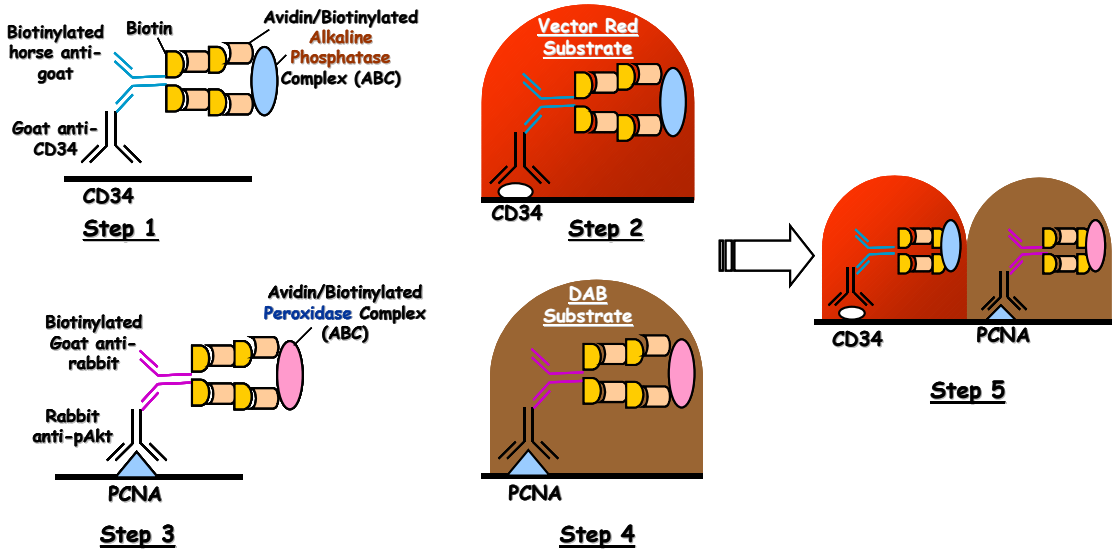

Figure 3.1. Schematic of strategies used for double-immunolabeling of bulge cells for CD34 and PCNA. Sections of formalin-fixed and paraffin embedded sections (4 μm) were incubated with goat anti-CD34, followed with biotinylated horse anti-goat IgG. Slides were then incubated with avidin-biotinylated alkaline phosphatase complex. CD34 antigen was visualized with the chromagen Vector Red alkaline phosphatase substrate (*red*). Skin sections were then incubated with rabbit anti-PCNA antibody, followed by incubation with biotinylated goat anti-rabbit IgG. Slides were then incubated with avidin-biotinylated horseradish peroxidase complex. The presence of PCNA antigen was visualized with the chromagen 3,3-diaminobenzidine (DAB, *brown*).

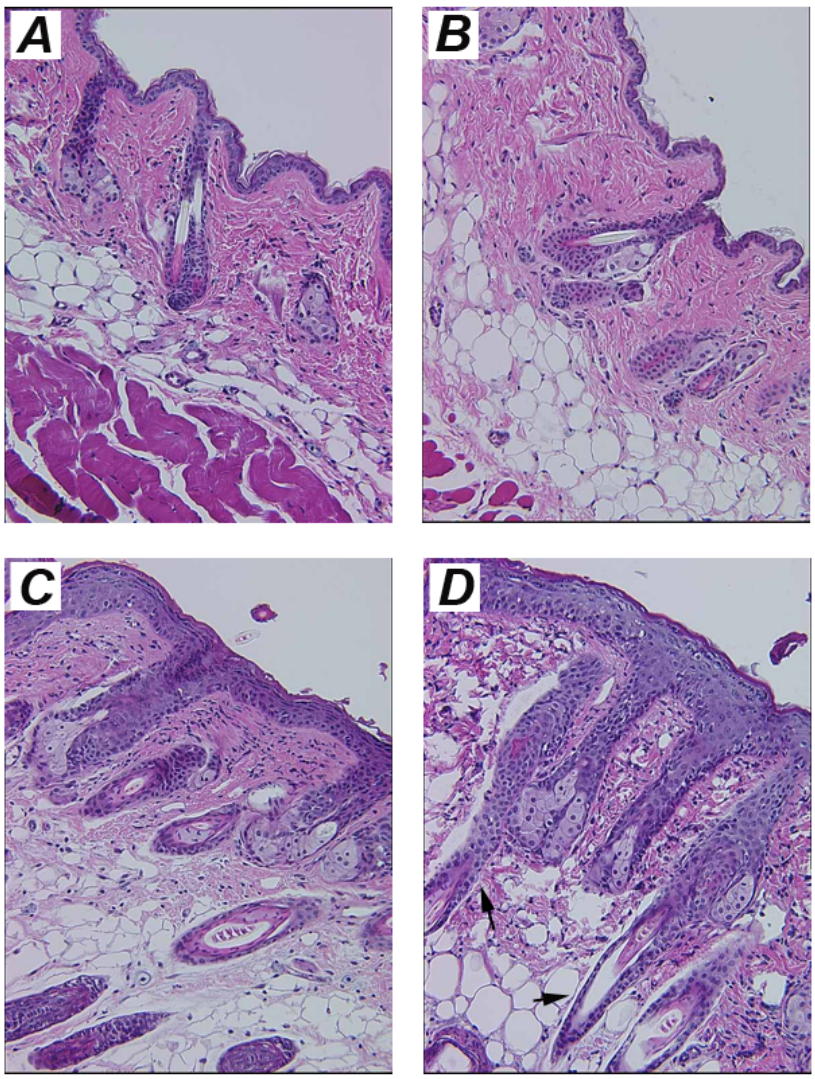

Figure 3.2. Histology of mouse skin. Hematoxylin & Eosin of paraffin-embedded dorsal skin tissues isolated from SENCAR mice treated topically twice weekly for 15 weeks with acetone alone ***(A)***, a single topical application of 25 nmol DMBA followed by twice weekly applications of acetone ***(B)***, a single topical treatment with acetone followed by twice weekly topical applications of 2 μg TPA ***(C)***, and skin treated topically with a single dose of 25 nmol DMBA followed by twice weekly topical applications of 2 μg TPA for 15 weeks ***(D)***. Hair follicles in dorsal skin isolated from mice treated once with DMBA followed by twice weekly topical applications of TPA for 15 weeks were hyperplastic and elongated ***(D, arrows)***.

Figure 3.3. Immunofluorescent localization of CD34$^+$ and K15$^+$ cells in hair follicles. Representative immunofluorescent photomicrographs of nucleated cells (DAPI-associated blue fluorescence) ***(B and E)*** that contain either CD34 ***(A)*** or K15 ***(D)*** (vector red-associated red fluorescence) in consecutive sections of dorsal skin isolated from SENCAR mice treated with acetone for 15 weeks and subjected to confocal microscopy for imaging. ***(C)*** represents CD34 staining merged with DAPI to highlight the location of nucleated cells in the outer root sheath of the Bu which contained CD34. ***(F)*** represents K15 staining merged with DAPI to highlight the location of nucleated cells in both the IRS and ORS of the bulge which contained K15. Abbreviations: Bu, bulge; Blb, bulb; HS, hair shaft; ORS/IRS, outer/inner root sheath. (A-F 400x magnification).

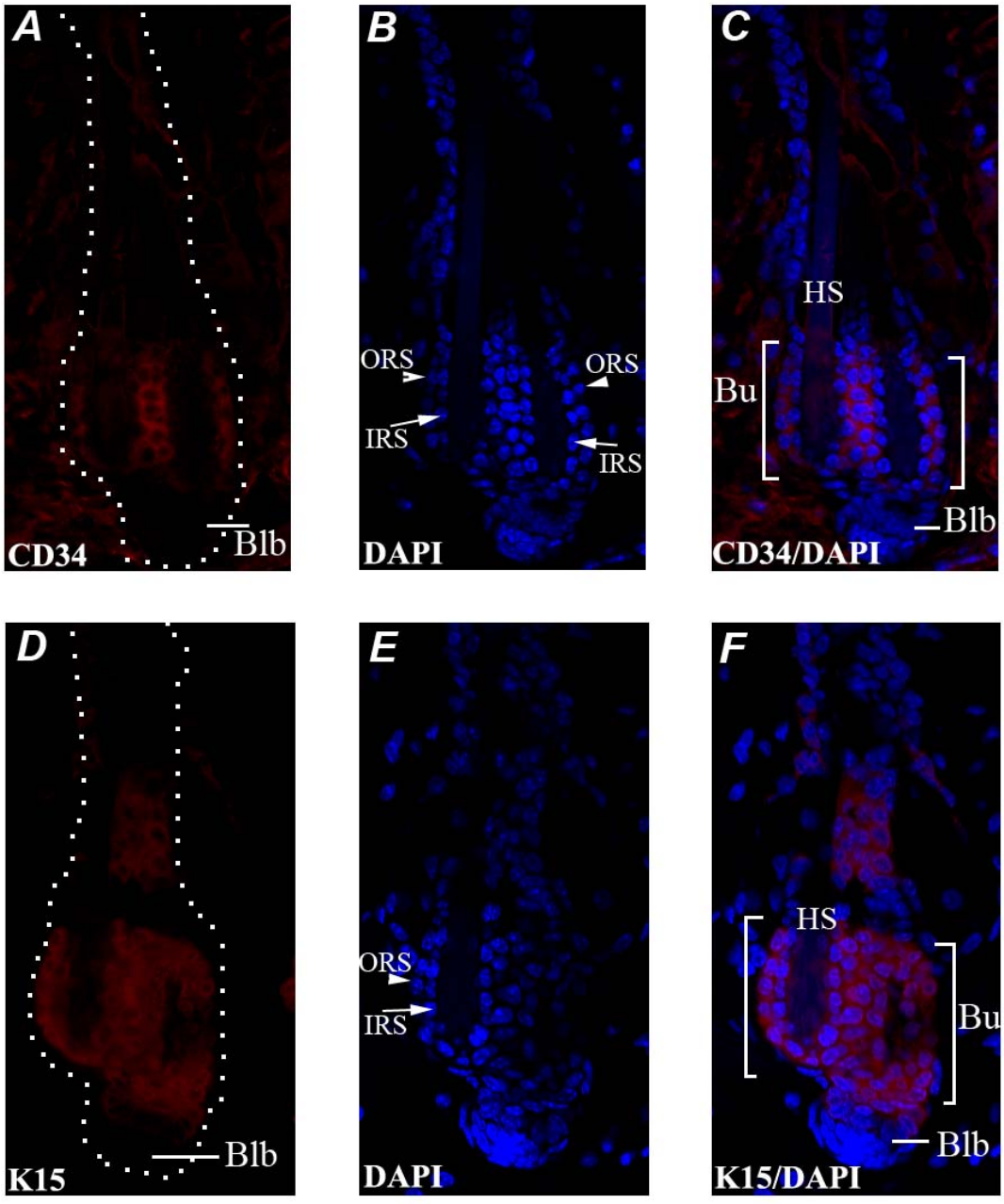
A
CD34
Blb
B
ORS
ORS
IRS
IRS
DAPI
C
HS
Bu
Blb
CD34/DAPI
D
K15
Blb
E
ORS
IRS
DAPI
F
HS
Bu
Blb
K15/DAPI

Figure 3.3

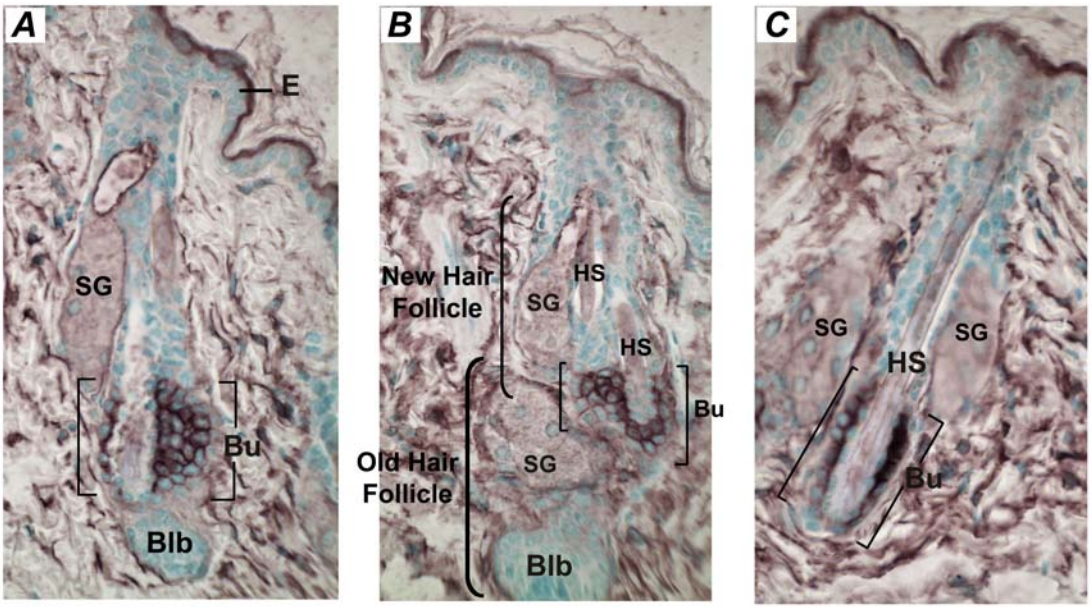

Figure 3.4. CD34+ cells remain localized to the Bu of hair follicles, regardless of the hair growth cycle. Sections of control dorsal skin treated with acetone and isolated at 15 weeks were immunostained with anti-CD34 antibody (CD34, *violet*). CD34+ putative stem cells localized to the Bu of hair follicles, located just below the sebaceous gland in early anagen ***(A)***, anagen ***(B)***, and telogen ***(C)*** phase of hair follicle growth cycle. Note that during anagen *(B)*, CD34+ cells localized to the newly developed Bu of the new hair follicle generated to the old one. Arrows indicate $CD34^{+}$ cells. Abbreviations: Bu, bulge; Blb, bulb; HS, hair shaft; SG, sebaceous gland. (A-C 600x magnification).

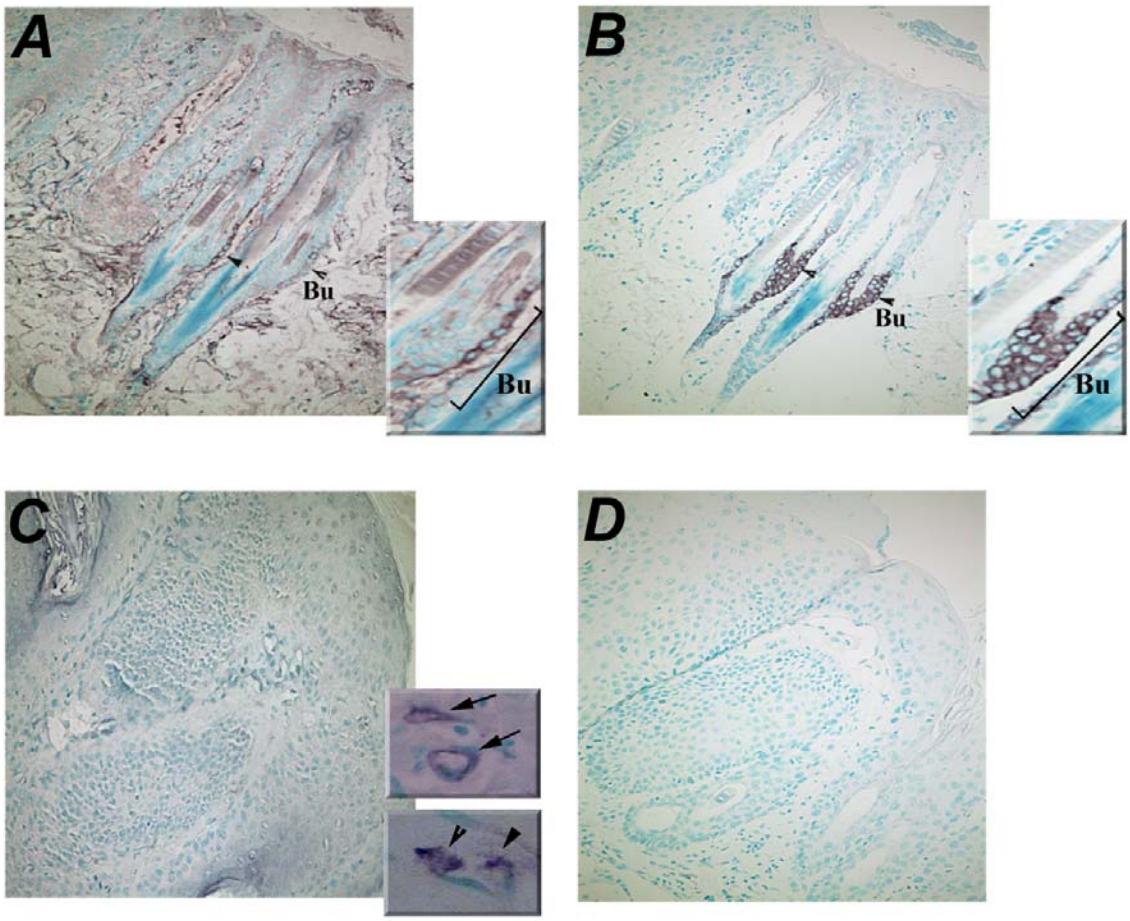

Figure 3.5. Localization of CD34 and K15 within papilloma tissue. CD34^{+} ***(A)*** and K15^{+} ***(B)*** cells remain localized to the Bu of hair follicles (arrowheads) in hyperplastic skin adjacent to papilloma isolated from SENCAR mice at 22 weeks of tumor promotion. CD34 ***(C)*** and K15 ***(D)*** staining was not present within papilloma tissue. Specific cell types within stroma of papilloma expressed CD34, including endothelial cells (*C*, inset, arrows) and mast cells (*C*, inset, arrowheads). *Abbreviations*: Bu: bulge.

Figure 3.6. Western blot analysis of CD34 and K15 proteins. (A) Analysis of CD34 and K15 proteins in extracts of dorsal SENCAR mouse skin treated with two topical applications of acetone or DMBA and isolated at 24 hr following a single topical application of acetone or TPA (24 hours) and in skin and papillomas isolated of SENCAR mice initiated with DMBA followed by twice weekly topical applications of TPA for 15 weeks (15 weeks). Expression of CD34 and K15 was absent in papillomas protein extracts. To verify the equal loading of proteins, the blots were re-probed for β-actin. ***(B-C and D-E)*** Densitometric analysis of CD34 and K15 expression, respectively, expressed as arbitrary units. ‡ *p<0.05*, CD34 versus K15 expression in dorsal skin of SENCAR mice treated with two topical applications of DMBA and isolated at 24 hr following a single topical application of TPA. ✱ *p<0.05*, CD34 versus K15 expression in dorsal skin of SENCAR mice treated with a single topical application of DMBA followed by twice weekly topical applications of TPA for 15 weeks.

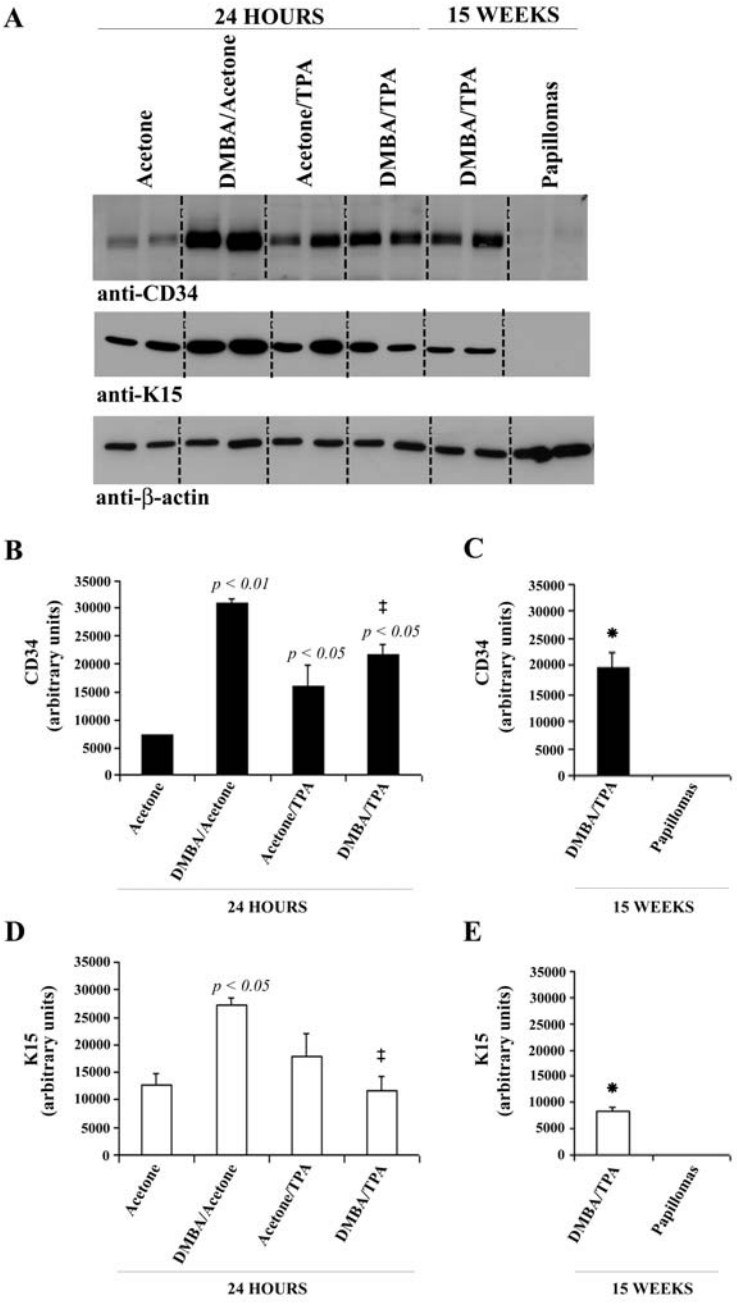
A
24 HOURS
15 WEEKS
Acetone
DMBA/Acetone
Acetone/TPA
DMBA/TPA
DMBA/TPA
Papillomas
anti-CD34
anti-K15
anti-β-actin
B
CD34 (arbitrary units)
p < 0.01
p < 0.05
p < 0.05
‡
Acetone
DMBA/Acetone
Acetone/TPA
DMBA/TPA
24 HOURS
C
CD34 (arbitrary units)
*
DMBA/TPA
Papillomas
15 WEEKS
D
K15 (arbitrary units)
p < 0.05
‡
Acetone
DMBA/Acetone
Acetone/TPA
DMBA/TPA
24 HOURS
E
K15 (arbitrary units)
*
DMBA/TPA
Papillomas
15 WEEKS

Figure 3.6

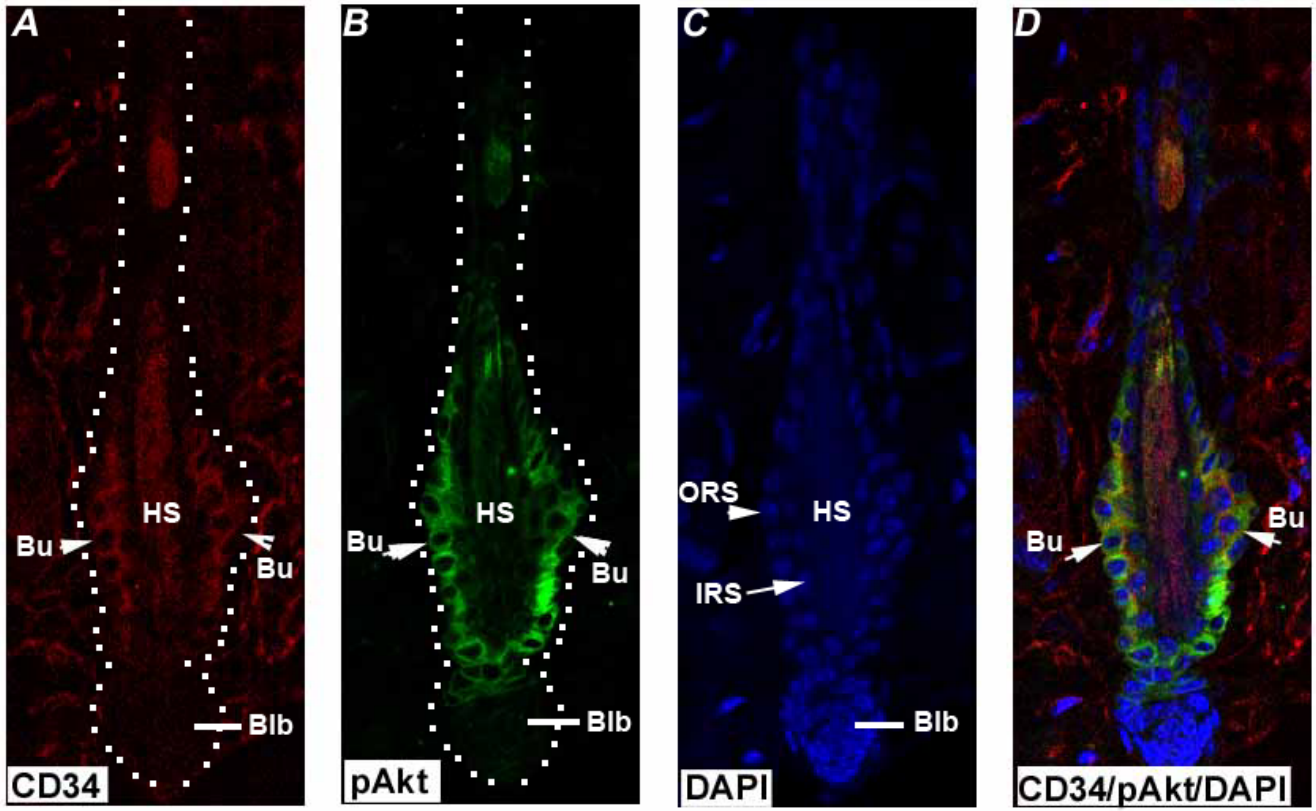

Figure 3.7. Immunofluorescent co-localization of CD34 and pAkt in KSC. Double immunofluorescence and confocal microscopy were used to identify nucleated cells (***C***; DAPI-associated blue fluorescence) that contained both CD34 (***A***; Alexa-647-associated red fluorescence) and pAkt (***B***, Alexa-555-associated green fluorescence) in dorsal skin isolated from SENCAR mice treated with acetone only. ***(D)*** CD34 (red) staining was merged with pAkt (green) and DAPI (blue) to reveal co-localization of CD34 and pAkt in KSC located in the ORS of the Bu. (A-D 400x magnification). *Abbreviations:* Bu: bulge; Blb: bulb; HS: hair shaft; ORS/IRS: outer/inner root sheath.

Figure 3.8. Co-localization of CD34 and PCNA in the bulge region of hair follicles. Double immunostaining was performed to localize CD34 (*red*/membrane staining) and PCNA (*brown*/nuclear staining) in skin sections isolated at 15 weeks of SENCAR mice treated topically with the control vehicle acetone ***(A)***, DMBA/Acetone ***(B)***, Acetone/TPA ***(C)***, and DMBA/TPA ***(D)***. Regardless of the treatment group, $CD34^+$ KSCs remained localized to the outer root sheath in the Bu of hair follicles ***(A-D)***. Numerous $CD34^-$ cells located in the infundibulum and the blb of hair follicles were $PCNA^+$ ***(A-D***, *arrowheads**)***. $CD34^+$ bulge cells co-expressed PCNA proliferating antigen in skin treated with DMBA/TPA ***(D***, inset; arrows indicate double-labeled cells***)***. (A-D 600x magnification). ***(E)*** Dorsal skin treated with DMBA/TPA had significantly increased number of $CD34^+$ cells co-expressing PCNA compared to any of the other treatment groups. ** $p<0.001$, DMBA/TPA versus acetone control skin. *Abbreviations:* Bu: bulge; Blb, bulb.

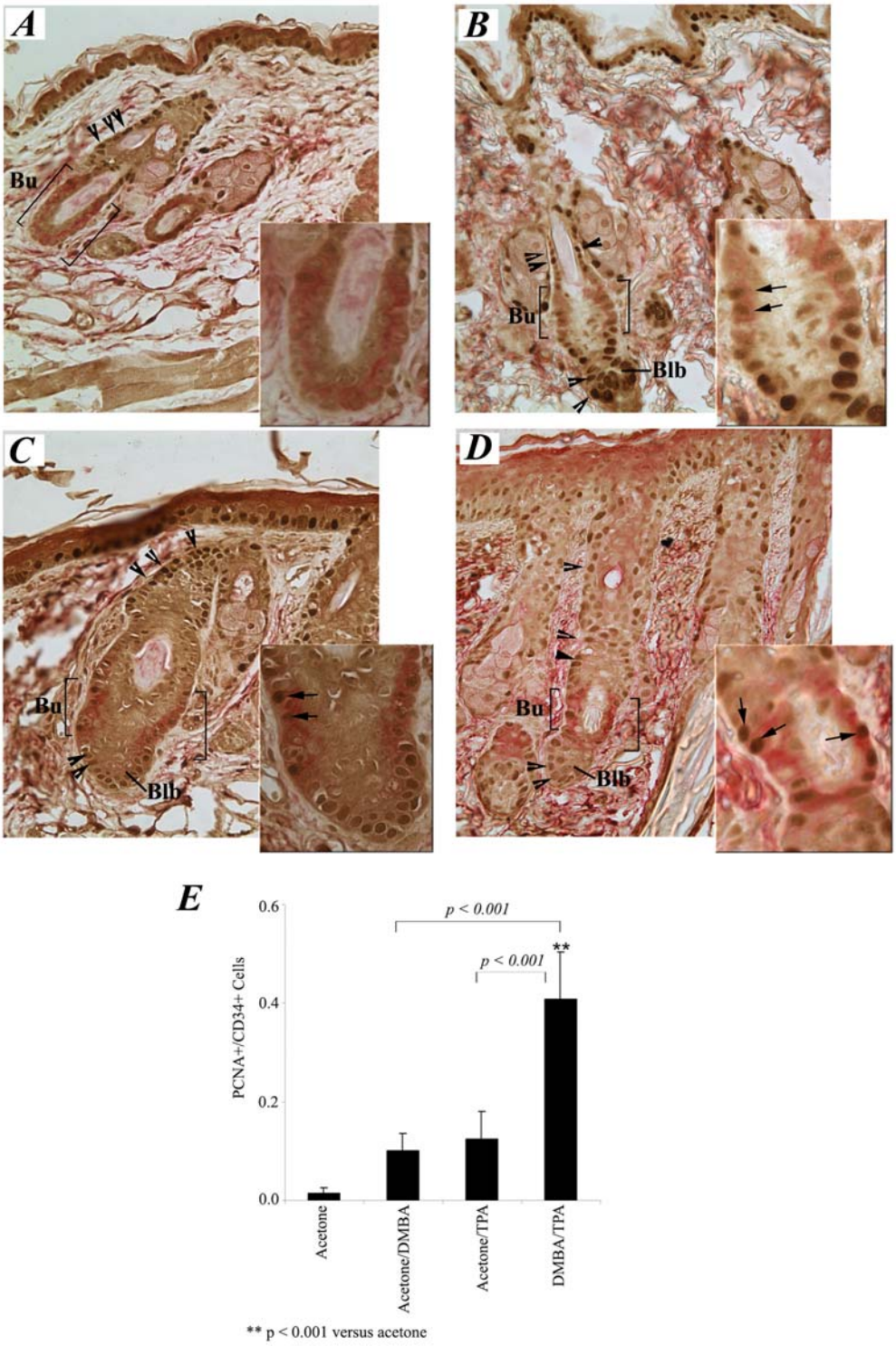
A
Bu
B
Bu
Blb
C
Bu
Blb
D
Bu
Blb
E
p < 0.001
p < 0.001
**
PCNA+/CD34+ Cells
0.6
0.4
0.2
0.0
Acetone
Acetone/DMBA
Acetone/TPA
DMBA/TPA
** p < 0.001 versus acetone

Figure 3.8

Figure 3.9. Localization of pAkt in papillomas. (A) is a representative photomicrograph of pAkt staining in papilloma isolated from SENCAR mice at 22 weeks of tumor promotion. pAkt staining was localized to suprabasal keratinocytes (inset, arrowhead), with nominal staining of pAkt in basal cells of papilloma ***(A****, inset, arrow)*. ***(B)*** Immunostaining of papilloma using pAkt antibody pre-incubated with phospho-Akt-473 Blocking Peptide confirmed the specificity of the immunochemical localization of pAkt protein within the suprabasal keratinocytes in papilloma. ***(C)*** Basal keratinocytes within papilloma tissue were found within the proliferative compartment, as determined by autoradiographic detection of [methyl-^{3}H]thymidine incorporation ***(****inset, arrow, silver grains****)***. ***(D)*** Basal keratinocytes within papilloma tissue were positive for PCNA staining ***(****inset, arrow****)***.

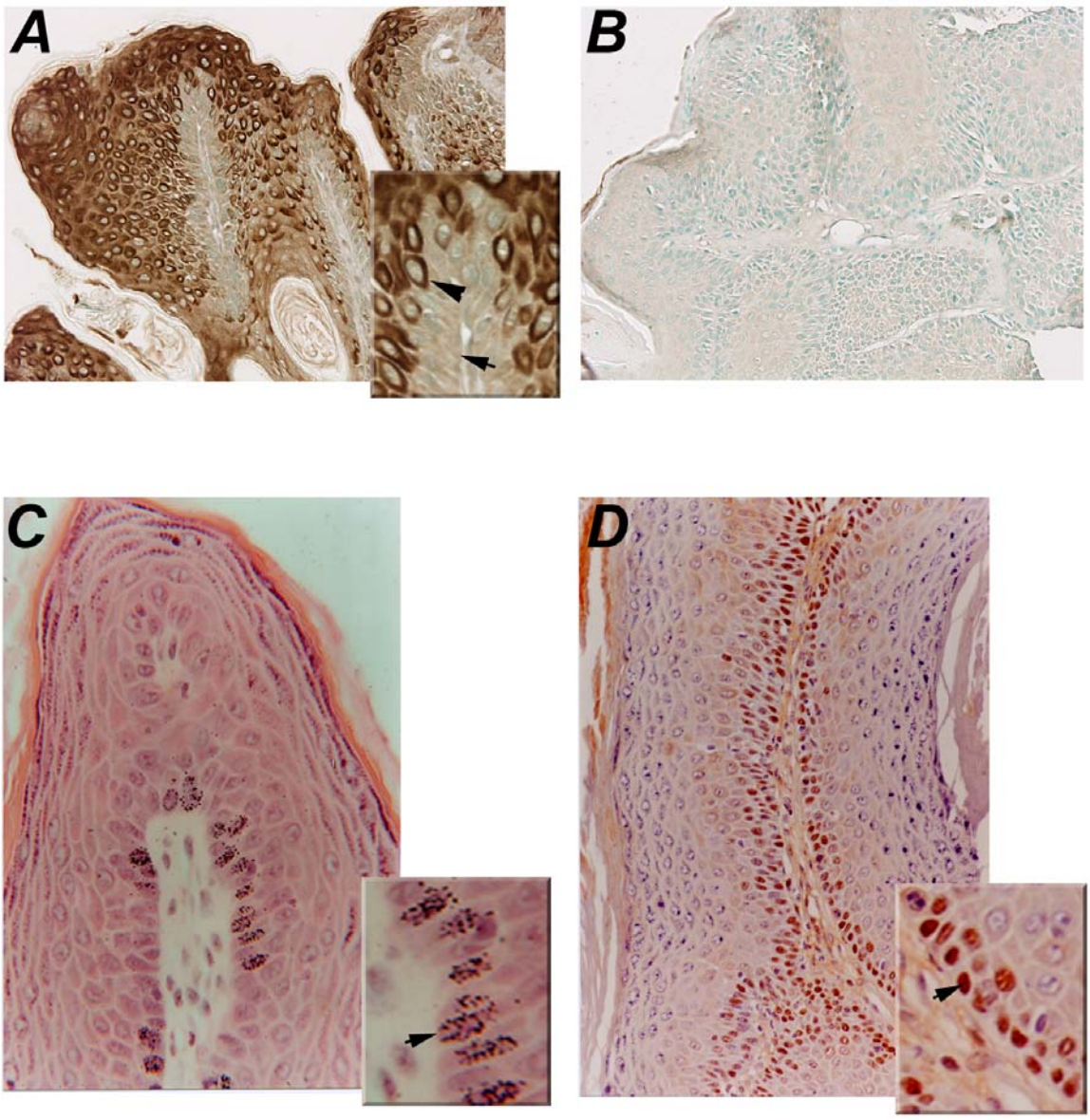

Figure 3.9

Figure 3.10. Comparative localization of pAkt and mTOR in mouse skin and papillomas. (A) and ***(B)*** represent pAkt and pmTOR staining, respectively, in serial sections of SENCAR skin treated with acetone for 15 weeks ***(****insets, arrowheads****)***. ***(C)*** and ***(D)*** represent pAkt and pmTOR staining, respectively, in serial sections of papillomas isolated from SENCAR mice at 15 weeks of tumor promotion. ***(E)*** and ***(F)*** represent pAkt and pmTOR staining in serial sections of skin adjacent to papillomas isolated from SENCAR mice at 15 weeks of tumor promotion. pAkt and pmTOR staining were localized to suprabasal keratinocytes (***C***-***F****, inset, white arrowheads)*, with nominal staining of pAkt in basal cells of papilloma (***C***-***F****, inset, black arrows****)***. (A and B, 400x magnification; C-F, 125x magnification).

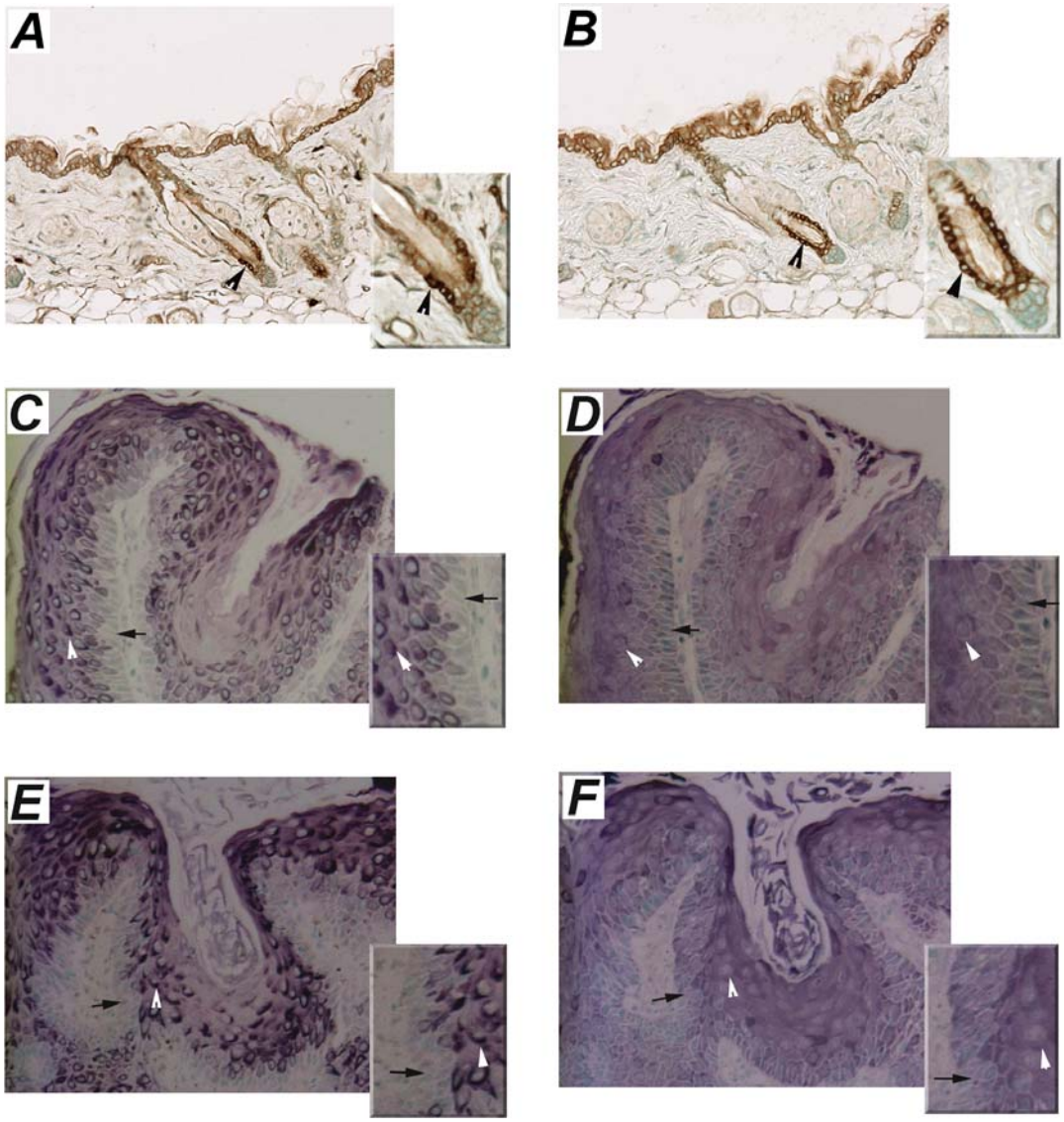

Figure 3.10

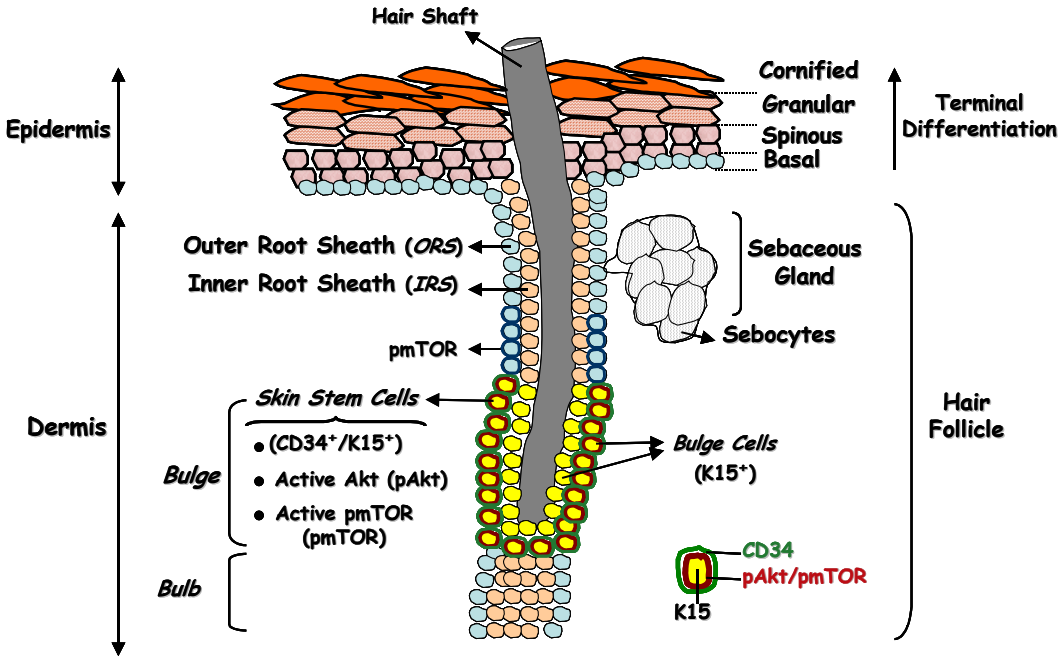

Figure 3.11. Schematic illustration of intrinsic activation of Akt and mTOR in CD34$^+$ cells putative skin stem cells. While CD34$^+$ cells were located only in the outer root sheath *(ORS)* of the bulge region in hair follicles, K15$^+$ cells were present in both the inner and outer layers of the bulge *(ORS/IRS)*. CD34$^+$/K15$^+$ KSC located in the ORS of the bulge of hair follicles in both normal and hyperplastic skin isolated at 15 weeks during multi-stage skin carcinogenesis contained pAkt and pmTOR. Activated Akt/mTOR may be one survival pathway by which CD34$^+$/K15$^+$ KSC persist in their respective niche of the skin, thus maintaining their ability to serve as a self-renewing population of cells over the life time of the organism and during multi-stage skin carcinogenesis.

CHAPTER 4

KINETICS OF ULTRAVIOLET LIGHT B-INDUCED SKIN INFLAMMATION, ANGIOGENESIS AND AKT/MAMMALIAN TARGET OF RAPAMYCIN (MTOR) ACTIVATION

4.1. Abstract

Exposure to ultraviolet radiation B (UVB) (290-320 nm) has been recognized as the most common and significant environmental factor in inducing skin cancers. The mechanisms by which survival signaling pathways are induced in response to UVB light exposure have only began to be examined. The present studies evaluated the temporal sequence of pAkt and pmTOR induction as well as described the localization of pAkt and pmTOR following acute and chronic exposure to UVB light in Skh/hr mice. Increases in pAkt staining at 24 hr and 48 hr following exposure to UVB light preceded the induction of pmTOR, which was only present at week 1 and week 20 following UVB exposure. pAkt was present in all the proliferating cell layers in papillomas isolated from Skh/hr mice at week 20 following a regimen of 3 times weekly of exposure to 2240 J/m^2 UVB light, in contrast to the presence of pAkt in non-proliferating suprabasal cells within papillomas isolated from SENCAR mice at week 22 following initiation with 25 nmol dimethylbenz[a]anthracene (DMBA) and repetitive topical applications of 2 μg 12-O-tetradecanoylphorbol-13-acetate (TPA). The presence of pmTOR was nominal within UVB-induced papillomas tissues while pmTOR staining coincided with pAkt staining in chemically-induced papillomas. Activation of pmTOR in epidermal keratinocytes at week 1 after exposure to UVB coincided with production of VEGF by epidermal keratinocytes and an increase in the number of blood vessels within the dermal area. UVB also induced a potent cutaneous inflammatory response that involved the temporal sequence of infiltration of neutrophils at the early stages of UVB-induced skin carcinogenesis followed by mast cells infiltration at the late stages following chronic exposure to UVB. Mast cells were in close association with dermal blood vessels following chronic

exposure to UVB light. The present results suggest that UVB induces a sequential activation of Akt and mTOR in epidermal and follicular keratinocytes, which may work in concert to induce VEGF expression and stimulate formation of blood vessels within hyperplastic skin. Agents that inhibit Akt and mTOR signaling pathways alone and in combination may be useful in defining the differential roles of pAkt and pmTOR in epidermal hyperplasia, cutaneous angiogenesis, and inflammation during UVB-induced skin carcinogenesis. The present studies also demonstrate the utility of targeting pAkt and pmTOR as potential anti-promoting molecules.

4.2. Introduction

Non-melanoma skin cancers (NMSC), including basal cell carcinomas (BCC) and squamous cell carcinomas (SCC), are the most commonly diagnosed type of skin malignancies [380]. There are several experimental models of multi-stage skin carcinogenesis that mimic the multi-step process that is observed to occur during development and progression of human NMSC [55, 381]. Exposure to chemicals such as polycyclic hydrocarbons, which are derived from incomplete combustion of fossil fuels, has been shown to induce human NMSC. However, a more common and ubiquitous environmental agent for development of NMSC is the routine exposure to ultraviolet light in the 290-320 nm wavelength, defined as UVB [50, 51, 382, 383]. Most of the UVB radiation is absorbed by the earth's stratospheric ozone layer; however, the rapid loss of the ozone layer and the concomitant increase in the amount of UVB light reaching the earth's surface represent an important environmental risk factor leading to the dramatic increase in the incidence of NMSC [52].

UVB light is a well-characterized complete skin carcinogen and acts as a tumor initiator and tumor promoter, thus inducing DNA damage and epigenetic changes [384]. A number of studies have demonstrated that mutations in p53 tumor suppressor gene leading to a loss of p53 function are present in the majority of UVB-induced skin tumors [96, 385-387], resulting in persistence of keratinocytes which contain DNA damage. However, in the presence of high levels of DNA damage, apoptotic pathways are induced in keratinocytes following exposure to UVB light, thus stimulating the removal of DNA-damaged cells [388]. Activation of anti-apoptotic molecules and survival signaling pathways may confer DNA-damaged cells with the ability to resist UVB-induced apoptosis and persist in the skin following exposure to UVB light, thus contributing to UVB-induced skin carcinogenesis. While the majority of studies have focused on evaluating UVB-induced DNA damage and activation of apoptotic signaling pathways during UVB-induced skin carcinogenesis, identification of survival signal transduction pathways as well as other factors that may be involved in UVB-induced skin carcinogenesis, including inflammatory mediators and angiogenic growth factors, remain to be completely characterized.

One mechanism by which keratinocytes may persist in the skin following exposure to UVB is by activation of Akt, also known as protein kinase B (PKB), a core component of the phosphoinositide 3-kinase (PI3-K) signaling pathway [302, 303]. Following its activation, PI3-K catalyzes the phosphorylation of phosphoinositides (PI) at the 3-position of the inositol ring, generating the membrane-bound lipid, phosphatidylinositol 3,4,5-triphosphate (PI-3,4,5-P_3), which binds with high affinity to the amino-terminal pleckstrin homology (PH) domain of Akt [232]. While inactive Akt is localized to the cytoplasm, binding of PI-3,4,5-P_3 to Akt PH domain results in recruitment of Akt to the inner surface of the plasma membrane. Binding of PI-3,4,5-P_3 to Akt PH domain not only induces translocation of Akt to the plasma membrane, but also confers a conformational change that renders Akt accessible to phosphorylation at two amino acid residues, serine-473 (Ser-473) [306, 307] and threonine-308 (Thr-308) [234].

Several lines of evidence suggest a role of Akt in UVB-induced skin tumors. The primary studies that have implicated the Akt signaling pathway in UVB-induced skin carcinogenesis reported that transgenic mice expressing insulin-like growth factor-1 (IGF-1) selectively targeted to the basal compartment of epidermis responded to exposure to UVB light with a decreased epidermal apoptosis compared to the skin of non-transgenic mice, which was associated as well with significantly elevated Akt kinase activity [334]. In addition, treatment of IGF-1 transgenic mice with topical applications of the selective PI3-K inhibitor, LY294002, inhibited IGF-1-mediated PI3-K/Akt signaling in the epidermis, resulting in reduced epidermal proliferation and skin tumor development [389]. These results suggested that IGF-1 expression in the basal epidermis induced activation of PI3-K/Akt signaling pathway, which was associated with both resistance of keratinocytes to apoptosis and a tumorigenic phenotype. Using cultured epidermal cells, previous studies further demonstrated that Akt can be directly activated by UVB-generated reactive oxygen species, H_2O_2 [352, 353]. Although previous studies have demonstrated an association between increased Akt kinase activity and development of UVB-induced skin tumors [334, 389], the specific cell populations that contain activated Akt during UVB-induced skin carcinogenesis are unknown.

Although the majority of studies have focused on the role of Akt as a survival factor, Akt has also been shown to induce entry of cells into the G_1-phase of the cell cycle. Akt directly phosphorylates the mammalian target of rapamycin (mTOR) at Ser-2448 residue [256, 267, 309], thus stimulating synthesis of proteins required for cell

cycle progression. mTOR was identified in yeast as the cellular target of the lipophilic macrolide rapamycin [257], which was initially isolated from a strain of bacterium, *Streptomyces hygroscopicus*, that is indigenous to Easter Island [260]. Following its activation, mTOR initiates mRNA translation by phosphorylating in parallel two signaling molecules: 70 KDa ribosomal protein S6 kinase (p70 S6K) enzyme at Thr-389 [273, 311] and eukaryotic initiation factor 4E (eIF4E)-binding protein 1 (4E-BP1). There is little information available on the activation of mTOR following exposure to UVB light. Exposure of cultured human dermal fibroblasts to UVB light resulted in phosphorylation of p70 S6K, which was reduced in the presence of rapamycin [390]. Results of these previous studies provided indirect evidence for the activation of mTOR following exposure to UVB light. However, there are no studies to date that have evaluated phosphorylation and localization of mTOR during UVB-induced skin carcinogenesis.

Akt may also be involved in regulating tumor-associated angiogenesis [391], the process of new capillary formation from pre-existing vasculature. Induction of tumor-associated angiogenesis is an early event that occurs in actively growing skin tumors [322, 392]. The acquisition of an angiogenic phenotype during skin tumor development is induced by the “angiogenic switch” [117, 118], which results from the shift in the balance of anti-angiogenic growth factors that inhibit formation of new vasculature to favor the production of pro-angiogenic growth factors that diffuse into the surrounding of the tumor. Using microarray analysis following UVB irradiation of human normal epidermal keratinocytes, a recent study identified thrombospondin-1 (TSP-1), which is an endogenous inhibitor of angiogenesis, as one of the genes that was down-regulated following exposure of keratinocytes to UVB light [393]. This decrease in TSP-1 expression occurred at very early times following exposure to UVB light and persisted over 18 hr [393]. However, the process of tumor angiogenesis is not only dependent on the inhibition of negative regulators of angiogenesis, but rather on the balance between anti-angiogenic and pro-angiogenic factors [394]. Recent studies demonstrated that the pro-angiogenic fibroblast growth factor (FGF) was not a primary angiogenic growth factor during UVB light-induced skin carcinogenesis [395]. In contrast, one family of pro-angiogenic proteins that has been shown to play a role in UVB-induced skin carcinogenesis is vascular endothelial growth factor-A (VEGF-A) [396-398]. Exposure to UVB light induced a significant increase in VEGF mRNA and protein levels in human epidermal keratinocytes *in vitro* [397]. In addition to the production of VEGF by cultured

human epidermal keratinocytes, a number of studies have linked the infiltration of mast cells with activation of angiogenesis and have defined these cells as “co-conspirators” of skin tumor-associated angiogenesis [171]. However, neither the kinetics of VEGF protein production nor the specific cells that produce this pro-angiogenic growth factor have been defined in models of UVB light-induced skin tumor growth.

When transfected into PB keratinocytes, which usually have low rates of tumor formation when grown *in vivo*, wild-type Akt resulted in rapidly growing, undifferentiated, and highly invasive skin tumors [335]. These Akt-induced tumors contained an increased number of blood vessels, which was concomitant with an increase in VEGF protein levels [337]. In contrast, implantation of subcutaneous pumps which allowed continuous delivery of rapamycin completely inhibited development of Akt-induced skin tumors [368]. VEGF expression has previously been shown to be regulated at the translational level through mTOR-dependent activation of p70 S6K and suppression of 4E-BP1, leading to increases in VEGF protein levels [395, 399, 400]. Taken together, these previous results suggest that pmTOR may mediate Akt-dependent signaling during skin carcinogenesis.

Since there is little information available on the role of Akt-dependent signaling during UVB-induced skin carcinogenesis, the goal of the present studies was to characterize the effects of acute and chronic exposure to UVB light on phosphorylation of Akt and mTOR, epidermal proliferation, VEGF protein production, and formation of blood vessels and to examine infiltration of neutrophils and mast cells over the time-period of UVB-induced skin carcinogenesis. The time points examined in these studies were 24 hr after a single dose of 1 minimal erythemic dose of UVB light, 48 hr after a single exposure to UVB light, 1 week after 3 exposures to UVB light and at 20 weeks of a regimen of 3 times weekly exposure to UVB light.

4.3. Materials and Methods

4.3.1. Treatment of Skh/hr mice: Skh/hr hairless mice (8-10 weeks old) (Taconics Farms, Germantown, NY) were irradiated dorsally, three times weekly, with Phillips F40UVB lamps (American Ultraviolet Company, Lebannon, IN), which emit primarily UVB light (290-320 nm). The total UVB dose per irradiation was 2240 J/m^2, as measured with a UVX digital radiometer (UVP Inc., San Gabriel, CA), and in this system is equivalent to one minimal erythemic dose. Tissues samples (0.5 cm^2) were isolated from the dorsal skin of Skh/hr mice at 24 hr, 48 hr, week 1, and week 20 following exposure to UVB light, fixed in 10% neutral buffered formalin (Shandon, Pittsburgh, PA), and embedded in paraffin for immunohistochemical analysis.

4.3.2. Immunochemical localization of pAkt and pmTOR: Sections of formalin-fixed and paraffin-embedded skin samples (4 μm) were cut and mounted onto SuperFrost/Plus slides (Fisher Scientific, Pittsburgh, PA). Tissues sections were deparaffinized using Histo-Clear (National Diagnostics, Atlanta, GA), and rehydrated in a graded series of alcohol. Endogenous peroxidase activity was quenched using 3% H_2O_2 in methanol for 20 min. Following antigen retrieval by steam heating in 10 mM citrate buffer (pH 6.0) for 15 min, non-specific binding was blocked with 1% bovine serum albumin (BSA) (Sigma, St. Louis, MO) in 1X TBS containing 0.05% Tween 20 (TBST). Sections were then incubated with either rabbit anti-phospho-Akt-Ser-473 (pAkt, Santa Cruz Biotechnology, Santa Cruz, Ca) or rabbit anti-phospho-mTOR-Ser-2448 (pmTOR; 1:50; Cell Signaling Technology, Beverly, MA) in a humidified chamber overnight at 4^oC in 1% BSA in TBST. Sections were then incubated for 20 min with biotinylated goat anti-rabbit IgG (1:200; Vector Laboratories, Burlingame, CA), followed by incubation for 30 min with avidin-biotinylated horseradish peroxidase complex (ABC Elite) (Vector Laboratories). The presence of pmTOR antigen was visualized using VIP substrate as the chromagen (Vector Laboratories). The specificity of pAkt staining was determined by examining the extent of binding of anti-pAkt antibody by tissue sections that had been pre-incubated with Akt-Ser-473-P Blocking Peptide (Cell Signaling Technology, Beverly, MA) for 2 hr. Tissues were counterstained with preheated Methyl Green (Vector Laboratories) for 5 min, dehydrated, mounted, viewed, and photographed.

4.3.3. Detection of cell proliferation measured by immunohistochemical detection of proliferating cell nuclear antigen: Sections were processed as described above with the following modifications. Non-specific binding was blocked with 1% BSA in TBST. Sections were incubated with rabbit anti-PCNA antibody (1:50, Santa Cruz Biotechnology) in 1% BSA in TBST for 1 hr at room temperature. Sections were then incubated with the biotinylated secondary antibody goat anti-rabbit IgG (1:200, Vector laboratories) in 1% BSA in TBST for 20 min. Slides were then incubated with the horseradish peroxidase conjugated avidin complex (ABC Elite, Vector Laboratories) for 30 min, and then incubated with 3,3-diaminobenzidine (DAB; Vector Laboratories). Tissues were counterstained with preheated Methyl Green (Vector Laboratories) for 5 min, dehydrated, mounted, viewed, and photographed. The amount of cell proliferation was quantitated by counting PCNA-positive cells in at least 5 random 250x fields.

4.3.4. Detection of infiltrating neutrophils: To detect infiltrating neutrophils within the dermis of Skh/hr mice, tissue sections were incubated with the primary antibody rat anti-Ly-6G (Gr-1) (1:400, Pharmingen, San Diego, CA) for 1 hr at room temperature. Non-specific binding was blocked with 1% BSA in TBST. Sections were then incubated with the biotinylated rabbit anti-rat IgG secondary antibody (1:200, Vector Laboratories) for 20 min. Slides were then incubated with the horseradish peroxidase conjugated avidin complex (ABC Elite, Vector Laboratories) for 30 min, and then incubated with the chromagen DAB (Vector Laboratories). The specificity of the immunoreactive anti-Gr-1 localization was verified using pre-immune isotypic rat $IgG_{2b,\kappa}$ (1:400, Pharmingen). Tissues were counterstained with preheated Methyl Green (Vector Laboratories) for 5 min, dehydrated, mounted, viewed, and photographed. The dermal neutrophils were counted in 10 random 200x fields.

4.3.4. Detection of mast cells: 4 μm sections of paraffin-embedded skin tissues were mounted mounted onto SuperFrost/Plus slides (Fisher Scientific, Pittsburgh, PA). Tissues sections were then deparaffinized using Histo-Clear (National Diagonistics, Atlanta, GA), and rehydrated in a graded series of alcohol. To identify mast cells in cutaneous dorsal skin isolated of Skh/hr mice, the May Grunwald Giemsa staining kit (Poly Scientific R & D Corp., Bay Shore, NY) was used. In brief, tissue sections were incubated with Jenner Stain Working solution for 6 min, followed by incubation with 5%

Giemsa solution diluted in distilled water for 45 min. Tissue sections were then rinsed quickly in distilled water, then incubated briefly with 2 consecutive applications of Acetic Acid 1% Aqueous. Following rinsing with water, the slides were then dehydrated, mounted, viewed, and photographed. Mast cells stained blue and the background stained pink. The number of mast cells was quantitated within 10 200x fields.

4.3.5. Evaluation of angiogenesis: Following tissue rehydration and antigen retrieval, as described above, tissue sections were incubated with either goat anti-VEGF antibody (15 μg/ml, R & D Systems, Minneapolis, MN) overnight at 4^{o}C or rabbit anti-CD31 (1:250, Santa Cruz Biotechnology) for 1 hr at room temperature. Tissue sections were then incubated with biotinylated goat anti-rabbit or horse anti-goat IgG (1:200, Vector Laboratories) for 20 min followed by incubation with the horseradish peroxidase conjugated avidin complex (ABC Elite, Vector Laboratories) for 30 min, with an additional incubation with VIP (Vector Laboratories). Tissues were counterstained with preheated Methyl Green (Vector Laboratories) for 5 min, dehydrated, mounted, viewed, and photographed.

4.3.6. Digital microscopy: Digital images of tissue sections were captured using a Diagnostic Instruments digital camera (Insight camera; 1600 x 1200 resolution) mounted on an Olympus research microscope. Images were captured using identical lighting and optical settings and transferred to digital image analysis software (Image Pro Plus, Media Cybernetics, Silver Spring, MD).

4.3.7. Statistical analysis: Significant differences in numbers of mast cells, neutrophils, and PCNA-positive cells in skin isolated from non-irradiated control Skh/hr mice and skin isolated at 24 hr, 48 hr, week 1, and week 20 following UVB exposure were analyzed using two-tailed Student's *t*-test or one way analysis of variance (ANOVA) on ranks for non-parametric comparisons (GraphPad Prism Software, San Diego, CA), with Student-Newman-Keuls *post-hoc* analysis was used. Results were expressed as mean ± standard error of mean (SEM), with $p<0.05$ being statistically significant.

4.4. Results

4.4.1. Histologic evaluation of cutaneous alterations following exposure to UVB. Dorsal skin was isolated from Skh/hr mice at 24 hr, 48 hr, and at week 1 and 20 after exposure to 3 weekly doses of 2240 J/m^2 UVB light. To evaluate alterations in the epidermis and dermis, tissue sections were stained with hematoxylin and eosin. Dorsal skin of non-irradiated Skh/hr mice had a uniform epidermal thickness of 1-2 epidermal cell layers, with few cells visible in the dermis. Dorsal skin of Skh/hr mice had abnormal hair follicles morphology, including a lack of hair shafts and widened hair canals (Figure 4.1 A, inset). Although sebaceous glands retained their normal structures, they were positioned at the end of hair follicles. There was a noticeable absence of bulb region tissue, which was replaced with a small cluster of keratinocytes (Figure 4.1 A, inset, arrowhead), previously identified as “putative bulge-derived cells” [401].

Exposure to UVB light resulted in a time-dependent increase in epidermal thickness. At 24 hr after a single exposure to UVB (Figure 4.1 B), there was an increase in epidermal thickness to 2-3 cell layers while dorsal skin isolated at 48 hr following exposure to UVB was hyperplastic (Figure 4.1 C) compared to non-irradiated skin (Figure 4.1 A). At week 1 following exposure to UVB, the epidermal thickness had increased to 13-14 cell layers and hair follicles were hyperplastic (Figure 4.1 D; arrows). The hyperplasia in skin exposed to UVB light for 1 week was similar to that observed in skin at week 20 following UVB light exposure (Figure 4.1 F). A significant number of mast cells infiltrating the dermal area of the skin was observed at week 20 following exposure to UVB (Figure 4.1 F, arrows).

4.4.2. Immunohistochemical localization of pAkt following exposure to UVB light. Immunohistochemical analysis was used to identify and localize cells within the epidermal and follicular compartments that contained pAkt in response to UVB exposure (Figure 4.2). pAkt was present in few cells within the epidermal and follicular compartments of non-irradiated dorsal skin (Figure 4.2 A). In addition, pAkt was present within the putative bulge-derived cells of hair follicles (Figure 4.2 A, arrow). All epidermal and follicular keratinocytes contained pAkt in dorsal skin of Skh/hr mice at 24 hr in response to UVB light (Figure 4.2 B). At 48 hr following exposure of mice to UVB light (Figure 4.2 C), pAkt levels within the epidermis were significantly higher than pAkt levels present in skin isolated at 24 hr from UVB-irradiated mice (Figure 4.2 B). Both the epidermal and follicular keratinocytes within hyperplastic skin isolated at week 1

following exposure to UVB light contained pAkt (Figure 4.2 D). The level of pAkt in skin isolated at week 20 following exposure to UVB light (Figure 4.2 E) was similar to the level of pAkt staining detected in skin isolated at week 1 after exposure to UVB (Figure 4.2 D). The specificity of the immunoreactive pAkt localization was demonstrated by the lack of staining in skin tissue sections pre-incubated with phospho-Akt-Ser-473 Blocking Peptide and anti-pAkt antibody (Figure 4.2 F).

4.4.3. Immunochemical localization of pAkt and proliferating cells in skin following exposure to UVB light. Serial sections of skin isolated at 24 hr, 48 hr, week 1, and week 20 following exposure to UVB were examined to identify proliferating and/or non-proliferating keratinocytes which contained pAkt (Figure 4.3). In normal non-irradiated skin, PCNA-positive cells were present within the basal cells of the epidermis (Figure 4.3 A', inset). At week 1 and 20 following exposure to UVB light, PCNA-positive cells were present in basal layers of the epidermis, but were absent within suprabasal layers, as indicated by the lack of PCNA staining and the visible methyl green counterstain (Figure 4.3 D' and E', insets).

Comparative analysis of serial sections at early time points (24 hr and 48 hr) following exposure of mice to UVB demonstrated that cells which contained pAkt (Figure 4.3 B and C) were present within both the proliferative compartment, as defined by immunochemical detection of PCNA-positive populations, and within the non-proliferating cell populations, which were PCNA-negative and localized to epidermal suprabasal cells (Figure 4.3 B' and C'). pAkt immunoreactive protein (Figure 4.3 D and E) was also present within proliferating as well as non-proliferating epidermal keratinocytes within hyperplastic skin isolated at week 1 and week 20 following exposure to UVB light (Figure 4.3 D' and E').

4.4.4. PCNA analysis of epidermal proliferation. Exposure of Skh/hr dorsal skin to UVB light induced significant hyperplasia in the epidermal layer. To identify epidermal cell populations undergoing proliferation and to examine the extent of hyperplasia following exposure of the skin to UVB light, immunolocalization of anti-PCNA antibody was evaluated (Figure 4.4). The number of PCNA-positive cells within the epidermal layer of Skh/hr mice significantly ($p<0.0001$) increased at 24 hr following exposure to UVB as compared with the number of PCNA-positive cells in non-UVB irradiated skin. UVB-induced increases in the number of PCNA-positive cells persisted for 48 hr

($p<0.01$), 1 week ($p<0.0001$), and 20 weeks ($p<0.0001$) compared to non-irradiated skin. Exposure of mice to 3 doses of UVB light for 1 week resulted in the most significant increase in the number of PCNA-positive cells throughout the epidermis compared to UVB-irradiated skin at earlier time points ($p<0.001$) and week 20 ($p<0.01$).

4.4.5. Immunohistochemical localization of pmTOR in skin following exposure to UVB light. At 24 hr and 48 hr following exposure to UVB light (Figure 4.5 B), only few cells scattered within the epidermal compartment contained pmTOR, which was similar to pmTOR staining pattern within the epidermal layer of non-irradiated mice (Figure 4.5 A). All epidermal and follicular keratinocytes within hyperplastic skin isolated at week 1 following exposure to UVB light contained pmTOR (Figure 4.5 D). In contrast to the high levels of pmTOR present within epidermal and follicular keratinocytes at week 1 following exposure to UVB light (Figure 4.5 D), pmTOR staining had a patchy distribution within the hyperplastic skin at week 20 following exposure to UVB light, with less numbers of epidermal and follicular keratinocytes that contained pmTOR (Figure 4.5 E).

4.4.6. Comparative analysis of immunochemical localization of pAkt, pmTOR, and PCNA in UVB-induced and chemically-induced papillomas. Evaluation of the immunochemical localizations of pAkt, pmTOR, and PCNA was examined in serial consecutive sections of papillomas isolated from Skh/hr mice at 20 weeks of a regimen of 3 times weekly exposure to 2240 J/m^2 UVB light (Figure 4.6 D-F). Chemically-induced papillomas were isolated of SENCAR mice initiated with a single topical application of 25 nmol dimethylbenz[a]anthracene (DMBA) and at 7 days later, SENCAR mice were treated topically twice weekly with 2 μg of 12-O-tetradecanoylphorbol-13-acetate (TPA) in 0.2 ml acetone for 22 weeks (Figure 4.6 A-C).

The pattern of pAkt, pmTOR, and PCNA staining in papillomas isolated of Skh/hr mice following UVB exposure (Figure 4.6 D-F) differed significantly compared to papillomas isolated of SENCAR mice at 22 weeks following DMBA/TPA treatment (Figure 4.6 A-C). While suprabasal cells within papillomas isolated from SENCAR mice at 22 weeks of chemically-induced skin carcinogenesis were the major type of keratinocytes which contained pAkt (Figure 4.6 A), pAkt was present in all cell layers in papillomas isolated of Skh/hr mice following UVB exposure (Figure 4.6 D). Suprabasal $pAkt^+$ keratinocytes in chemically-induced papillomas isolated of SENCAR mice (Figure

4.6 A) were not located within the proliferative compartment, as shown by their lack of PCNA staining (Figure 4.6 C). In contrast, pAkt staining in UVB-induced papillomas (Figure 4.6 D) coincided with PCNA localization in consecutive serial sections (Figure 4.6 F).

Localization of pAkt to suprabasal keratinocytes in papillomas isolated of SENCAR mice following DMBA/TPA treatment (Figure 4.6 A) coincided with pmTOR localization (Figure 4.6 B). However, the presence of pAkt within papilloma tissue isolated from Skh/hr mice at week 20 following exposure to UVB (Figure 4.6 D) did not correlate with pmTOR staining within these papillomas since pmTOR presence was nominal (Figure 4.6 E).

These significant differences in the localization patterns of pAkt and pmTOR in papillomas isolated from SENCAR mice at 22 weeks of tumor promotion and in papillomas isolated from Skh/hr mice at 20 weeks following UVB exposure were further verified within the hyperplastic hair follicles and epidermis of skin adjacent to papillomas (Figure 4.6 G-J). While pAkt localization (Figure 4.6 G) coincided with pmTOR staining (Figure 4.6 H) in consecutive serial sections of skin adjacent to DMBA/TPA-induced papillomas, there was a nominal staining of pmTOR (Figure 4.6 J) in skin adjacent to UVB-induced papillomas, which did not correlate with pAkt localization (Figure 4.6 I).

4.4.7. Immunochemical localization of VEGF in skin following exposure to UVB light. Immunochemical studies were performed to identify the cell types within the dermis and epidermis that produced VEGF immunoreactive protein following exposure to UVB. There was no detectable VEGF protein present in skin isolated from non-irradiated Skh/hr mice (Figure 4.7 A). At 24 hr and 48 hr following exposure to UVB light (Figure 4.7 B), VEGF was not present within the epidermal and follicular compartments of the skin. At week 1 following exposure to UVB, few suprabasal cells produced VEGF protein (Figure 4.7 D). At week 20 following exposure to UVB, a large number of cells produced VEGF immunoreactive protein, including suprabasal and basal keratinocytes as well as follicular keratinocytes (Figure 4.7 E).

4.4.8. Immunochemical localization of CD31 in skin following exposure to UVB light. Immunochemical localization of CD31/platelet endothelial cell adhesion molecule-1 (PECAM-1), an endothelial cell-specific marker [402], was performed to examine the

effect of UVB light on the number, size, and location of blood vessels within the dermis of Skh/hr mice (Figure 4.8). There were infrequent blood vessels in non-irradiated mice, which localized deep within the dermis (Figure 4.8 A). At 24 hr and 48 hr following exposure to UVB light (Figure 4.8 B and C), there were fewer blood vessels within the dermis of Skh/hr mice compared to the lower number of blood vessels in non-irradiated mice (Figure 4.8 A). At week 1 following exposure to UVB light (Figure 4.8 D), not only there was a noticeable increase in the number of blood vessels compared to earlier time points (Figure 4.8 B and C), but there were increases in the size and diameter of blood vessels as well compared to blood vessels in skin isolated at 24 hr and 48 hr following exposure to UVB (Figure 4.8 B and C). Examination of tissue sections isolated from Skh/hr mice at week 20 following exposure to UVB light (Figure 4.8 E, arrows) revealed the presence of higher number of widely dilated blood vessels compared to any of the earlier time points. A significant number of blood vessels within the dermis of skin isolated from Skh/hr mice at week 20 were located at the dermal-epidermal junction (Figure 4.8 E, arrows). Blood vessels present within the lower part of the dermis (Figure 4.8 E, inset, arrows) were in close association with mast cells (Figure 4.8 E, inset, arrowheads).

4.4.9. Quantitation of infiltrating mast cells in the dermis following exposure to UVB light. Mast cells within the dermis were identified by Giemsa staining in non-irradiated dorsal skin (Figure 4.9 A) and skin isolated at 24 hr (Figure 4.9 B), 48 hr (Figure 4.9 C), week 1 (Figure 4.9 D), and week 20 (Figure 4.9 E) following exposure to 2240 J/m^2 UVB light. The number of mast cells within the dermis was quantitated by enumeration of mast cells within at least 10 high-power (200x) fields (Figure 4.9 F). Regardless of the time at which skin samples were isolated following UVB exposure, there were no significant differences in the number of mast cells detected in non-irradiated control skin.

The number of mast cells was significantly ($p<0.0001$) elevated at week 1 following exposure to UVB light compared to the number of mast cells within the corresponding dermis of non-irradiated control skin (Figure 4.9 F). The number of mast cells remained elevated at week 20 following exposure to UVB ($p<0.0001$). Dorsal skin isolated at week 1 and week 20 had significantly increased mast cells infiltration

compared to any of the earlier time points ($p<0.001$). The highest number of mast cells was observed at week 20 following exposure of mice to UVB light (Figure 4.9 F).

4.4.10. Quantitation of infiltrating neutrophils in the dermis following exposure to UVB light. Dermal neutrophils were identified and quantitated based on anti-Gr-1 staining (Figure 4.10), an antibody directed against a myeloid differentiation antigen that is restricted to mature neutrophils. The number of infiltrating neutrophils within the dermis was significantly ($p<0.001$) increased as early as 24 hr (Figure 4.10 B and G) in skin isolated of Skh/hr following UVB exposure compared with the number of neutrophils within the dermis of non-UVB irradiated mice (Figure 4.10 A and G). The number of infiltrating neutrophils significantly ($p<0.001$) increased at 48 hr following a single exposure of mice to UVB light (Figure 4.10 C and G) compared to the number of neutrophils in dorsal skin at 24 hr after UVB exposure (Figure 4.10 B). The number of dermal neutrophils significantly ($p<0.001$) decreased in a gradual manner at week 1 (Figure 4.10 D and G) and week 20 (Figure 4.10 E and G) following exposure to UVB light compared to the number of neutrophils at 48 hr following treatment with UVB (Figure 4.10 C and G). The low level of isotypic antibody binding within the dermal area 48 hr following exposure to UVB light (Figure 4.10 F) demonstrated the specificity of the immunoreactive Gr-1 localization.

4.5. Discussion

The skin is continuously exposed to environmental insults, with UVB light being the most ubiquitous etiological factor in human skin cancers and responsible for most cutaneous damage following both acute and long-term exposure [403]. Although previous studies showed a role for Akt in UVB-induced skin carcinogenesis [334, 352, 353, 404], thus far no studies have defined either the kinetics or immunochemical localization of pAkt and pmTOR over the time course of UVB-induced skin carcinogenesis. The current studies provide first time evidence of the early time of induction of pAkt and pmTOR as well as described the localization of pAkt and pmTOR during UVB-induced skin carcinogenesis.

Results of the present studies demonstrate an increase in pAkt immunoreactive protein in epidermal keratinocytes as early as 24 hr following exposure to UVB light compared to untreated skin, which gradually increased over the 20-week time course of UVB-induced skin carcinogenesis examined, suggesting a persistent activation of Akt following chronic exposure of the skin to UVB light. UVB acts as a tumor initiator, therefore, inducing DNA damage, including the formation of pyrimidine photoproducts, cyclobutane pyrimidine dimer [93] and pyrimidine-(6-4)-pyrimidone lesions [94]. Formation of pyrimidine photoproducts has been shown to induce mutations, including C to T and CC to TT transitions [95], commonly found in the *p53* tumor suppressor gene leading to a loss of function [98]. However, apoptotic pathways are activated in the presence of high levels of DNA damage in keratinocytes after exposure to UVB light. The induction of phosphorylation of Akt within epidermal keratinocytes following acute exposure to UVB light may confer initiated keratinocytes with the ability to resist apoptotic pathways that would eliminate cells containing UVB-induced DNA damage. Repeated exposure to UVB light also acts as a tumor promoter, resulting in the clonal expansion of keratinocytes that contain both *p53* mutations and pAkt. In addition, given the self-renewal nature of the skin, the persistence of pAkt in non-proliferating suprabasal keratinocytes, in particular, at week 1 and week 20 following chronic exposure to UVB suggests that activation of Akt may confer a survival advantage to suprabasal keratinocytes, allowing them to resist the commitment to differentiate.

The present results also provide first evidence for a specific temporal sequence of mTOR phosphorylation at Ser-2448 during UVB-induced skin carcinogenesis. Increases in pAkt staining at 24 hr and 48 hr following exposure to UVB preceded the

induction of pmTOR, which was only prevalent at week 1 and week 20 following UVB exposure. The temporal regulation of pAkt and pmTOR suggests that during UVB-induced skin carcinogenesis, pAkt may activate mTOR in a time-dependent manner following chronic exposure to UVB light. On the other hand, although mTOR has been shown to act as a direct substrate for Akt [256], the identity of upstream activator(s) of mTOR remains elusive [268]. Signaling molecules that have recently been shown to activate Akt and mTOR in parallel include protein kinase C-η (PKC-η) [263], a calcium-independent PKC isoform that is activated by the membrane bound lipids PI-3,4,5-P_3 following activation of PI3-K. pmTOR has been previously shown to initiate translation of protein that are required for entry into the G1-phase of the cell cycle, such as cyclin D1, by phosphorylating in parallel p70 S6K and 4E-BP1. The localization of pmTOR to basal keratinocytes within the epidermal layer at week 1 and 20 following exposure to UVB light suggests that pmTOR stimulates proliferation of basal cells following exposure to UVB light. However, pmTOR localized to non-proliferating suprabasal keratinocytes as well, suggesting a role of pmTOR in regulating cell survival. pmTOR not only stimulates entry into the cell cycle, but has recently been shown to induce survival of primary acute myeloid leukemia (AML) cells [364]. Taken together, the present results suggest a model in which the Akt and mTOR signaling pathway may serve as an essential mechanism in inducing proliferation of basal keratinocytes as well as long-term maintenance and survival of non-proliferating suprabasal cells during UVB-induced skin carcinogenesis.

The present studies are one of the first to characterize differences in localization of pAkt and pmTOR in papillomas isolated from Skh/hr mice at week 20 following a regimen of 3 times weekly exposure to 2240 J/m^2 UVB light compared to localization of pAkt and pmTOR in papillomas isolated from SENCAR mice at week 22 following initiation with 25 nmol DMBA and repetitive topical applications of 2 μg TPA. While non-proliferating suprabasal cells within papillomas isolated from SENCAR mice at 22 weeks of chemically-induced skin carcinogenesis were the major type of keratinocytes that contained pAkt, pAkt was present in all the proliferating cell layers in papillomas isolated from Skh/hr mice following UVB exposure. In contrast to chemically-induced papillomas, the presence of pAkt in UVB-induced papillomas did not correlate with pmTOR staining. The present results extend previous studies which reported significant differences in gene expression alterations in skin tumors following exposure to UVB light compared to skin tumors induced by treatment with DMBA and TPA. While more than 90% of skin

tumors have been shown to contain activating mutation at codon 61 of the Harvey (Ha)-*ras* proto-oncogene when mouse skin tumors are induced by a standard multi-stage skin carcinogenesis DMBA and TPA protocol [65], chronic exposure to UVB light has been shown to induce mutations in the p53 tumor suppressor gene leading to a loss of function [405]. In the present study, we document differences in expression and localization of pAkt and pmTOR in UVB-induced papillomas compared to chemically-induced skin tumors, suggesting differential activation of Akt and mTOR signaling pathways during both processes. Akt has previously been shown to regulate cell proliferation independently of mTOR activation by phosphorylating and consequently blocking the activity of glycogen synthase kinase-3β (GSK-3β) [406], thereby preventing phosphorylation and subsequent proteolytic degradation of cyclin D1 [253], an essential key regulator protein that is required for progression of cells into the G1-phase of the cell cycle. Taken together, the present results suggest a model in which pAkt/pmTOR signaling pathway may induce survival of suprabasal keratinocytes in chemically-induced papillomas [363], while the presence of pAkt may stimulate proliferation of the less-differentiated keratinocytes in UVB-induced papillomas.

The present results are one of only a few studies that document the presence and cellular location of VEGF in specific populations of keratinocytes over the time course of UVB-induced skin carcinogenesis. Previous studies reported up-regulation of VEGF mRNA expression within suprabasal keratinocytes in hyperplastic epidermis following long-term UVB irradiation, with nominal expression of VEGF mRNA detected in the skin of non-UVB-irradiated mice [407]. In the present immunochemical studies, VEGF protein expression localized to selective keratinocytes within the epidermal compartment of skin at week 1 following UVB exposure and to selective keratinocytes in both the epidermal and follicular compartments of the skin at week 20 following exposure to UVB light. These results suggest that VEGF protein is produced locally by few keratinocytes within the epidermal and follicular compartment of the skin during UVB-induced skin carcinogenesis.

VEGF protein expression coincided with the induction of pmTOR at week 1 and week 20 following exposure to UVB light. In addition to regulating VEGF expression at the transcription level, pmTOR has been also shown to regulate VEGF expression at the translation level. The transcriptional activation of VEGF is mediated by the pmTOR-dependent translation of hypoxia-inducible factor-1 (HIF-1α) [182]. HIF-1α acts as a

transcription factor by binding to an oxygen-regulated element within the VEGF gene enhancer region, leading to the transcription activation of VEGF [408]. On the other hand, VEGF mRNA translation may be regulated by the mTOR-dependent activation of p70 S6K and inactivation of the translational repressor, 4EB-P1 [399, 400]. Taken together, the present results suggest that mTOR is activated in a specific temporal manner during UVB-induced skin carcinogenesis and is associated with VEGF expression within epidermal keratinocytes at week 1 following exposure to UVB light. Therefore, pmTOR may be an important mediator of the angiogenic switch during UVB-induced skin carcinogenesis.

There was a gradual increase in the number of blood vessels within the dermal area of skin at week 1 and week 20 following UVB exposure which occurred coincident with the production of VEGF protein. At week 20 following exposure to UVB light, blood vessels were dilated and localized proximal to the epidermal/dermal junction. These observations are consistent with previous studies that have shown that chronic UVB irradiation resulted in an increase in the number of enlarged blood vessels [407]. Chronic exposure to UVB also induced endothelial cell proliferation within large blood vessels in particular [409]. Collectively, the present results demonstrate that following chronic exposure to UVB light, epithelial cells within hyperplastic skin have an absolute requirement for dermal blood supply.

UVB light has also been shown to have important effects on the immune system. The present studies demonstrate a temporal sequence of infiltration of mast cells and neutrophils into the dermal area of the skin of Skh/hr mice over the 20-week time course of UVB-induced skin carcinogenesis. While the number of mast cells started to significantly increase at week 1, with the highest number of infiltrating mast cells detected at week 20, the number of infiltrating neutrophils was maximum at 48 hr following exposure of mice to UVB light, which was accompanied with a gradual decrease in the number of infiltrating neutrophils at week 1 and week 20 in UVB-treated skin. The current observations suggest a role of infiltrating neutrophils in mediating inflammatory signals at the early stages rather than at the late stages during UVB-induced skin carcinogenesis. Previous studies in our laboratory have shown that infiltrating neutrophils produced inducible nitric oxide synthase (iNOS) and the reactive nitrogen intermediate, peroxynitrite, during the tumor promotion process [88]. These results suggest that neutrophils may play role in inducing epigenetic alterations that

occur following UVB-induced skin carcinogenesis through their ability to produce a “pro-oxidant” microenvironment.

The presence of enlarged and densely granulated mast cells in the dermal area of skin isolated at week 20 following chronic exposure to UVB light coincided with their intimate association with blood vessels within the dermal area. The present results suggest a potential interaction between mast cells and endothelial cells lining blood vessels in UVB-irradiated skin. Absence of mast cells have previously been shown to attenuate tumor-associated angiogenesis in papillomavirus-infected transgenic mice that are deficient in mast cells compared to their wild type littermates [171]. Indeed, mast cells have been shown to release diverse factors known to enhance angiogenesis, including VEGF [410], which may act as a proliferative and survival factor for newly recruited endothelial cells. Furthermore, mast cells have been shown to induce stromal remodeling by secreting heparinase and metalloproteinases [411, 412], which not only release and activate latent VEGF splice variants sequestered by the extracellular matrix and heparin sulfate proteoglycans on cell surfaces in the skin, but also facilitate endothelial cell migration [413]. Endothelial cells, on the other hand, have been recently shown to regulate survival and proliferation of human mast cells [414]. Given the tight association of mast cells with blood vessels which was observed only at the late stages of UVB-skin carcinogenesis, the present observations confirm previous studies which linked the presence of mast cells with angiogenesis and have defined these cells as “co-conspirators” of tumor associated angiogenesis [171].

While most studies have focused on characterizing apoptotic pathways that are activated following exposure to UVB light, the mechanisms by which survival signaling pathways are induced in response to UVB exposure have only began to be examined. The present results documented the sequential activation of pAkt and pmTOR over the 20-week time course of UVB-induced skin carcinogenesis and in papillomas. Activation of pmTOR in epidermal keratinocytes within hyperplastic skin at week 1 following UVB exposure coincided with production of VEGF by epidermal keratinocytes and an increase in the number of blood vessels within the dermal area. The present studies also demonstrate the accumulation of mast cells around blood vessels within the dermis of mice following chronic exposure to UVB light. Taken together with the results of previous studies, our results suggest that the use of agents capable of blocking Akt and mTOR signaling pathways, including the use of the IP3K selective inhibitor, LY294002, and the

selective mTOR inhibitor, rapamycin, may be effective anti-promoting and anti-progressing agents, preventing the development of UVB-induced NMSC. The close association of mast cells with newly recruited blood vessels may also provide a potential anti-angiogenic therapeutic intervention during UVB-induced skin carcinogenesis.

Figure 4.1. Histological evaluation of UVB-induced skin carcinogenesis using H & E staining. Hematoxylin & Eosin of paraffin-embedded dorsal skin tissues isolated from non-irradiated control Skh/hr hairless mice ***(A)***, skin isolated from Skh/h mice at 24 hr after a single dose of 1 minimal erythemic dose of UVB light ***(B)***, 48 hrs after a single exposure to UVB light ***(C)***, 1 week after 3 exposures to UVB light ***(D)***, and at 20 weeks of a regimen of 3 times weekly exposure to UVB light ***(E)***. (A-E) original magnification 320x. Hair shaft was not present in hair follicles isolated from Skh/h hairless mice ***(A, inset, arrow)***. A small cluster of keratinocytes occupied the lower part of the hair follicle ***(A, inset, arrowhead)***. There was a significant epidermal and follicular hyperplasia in skin isolated of Skh/hr mice at week 1 and week 20 following exposure to UVB light ***(D and E, arrows)***. Mast cells infiltrating the dermal area of the skin were observed at week 20 following exposure to UVB ***(F, arrows)***.

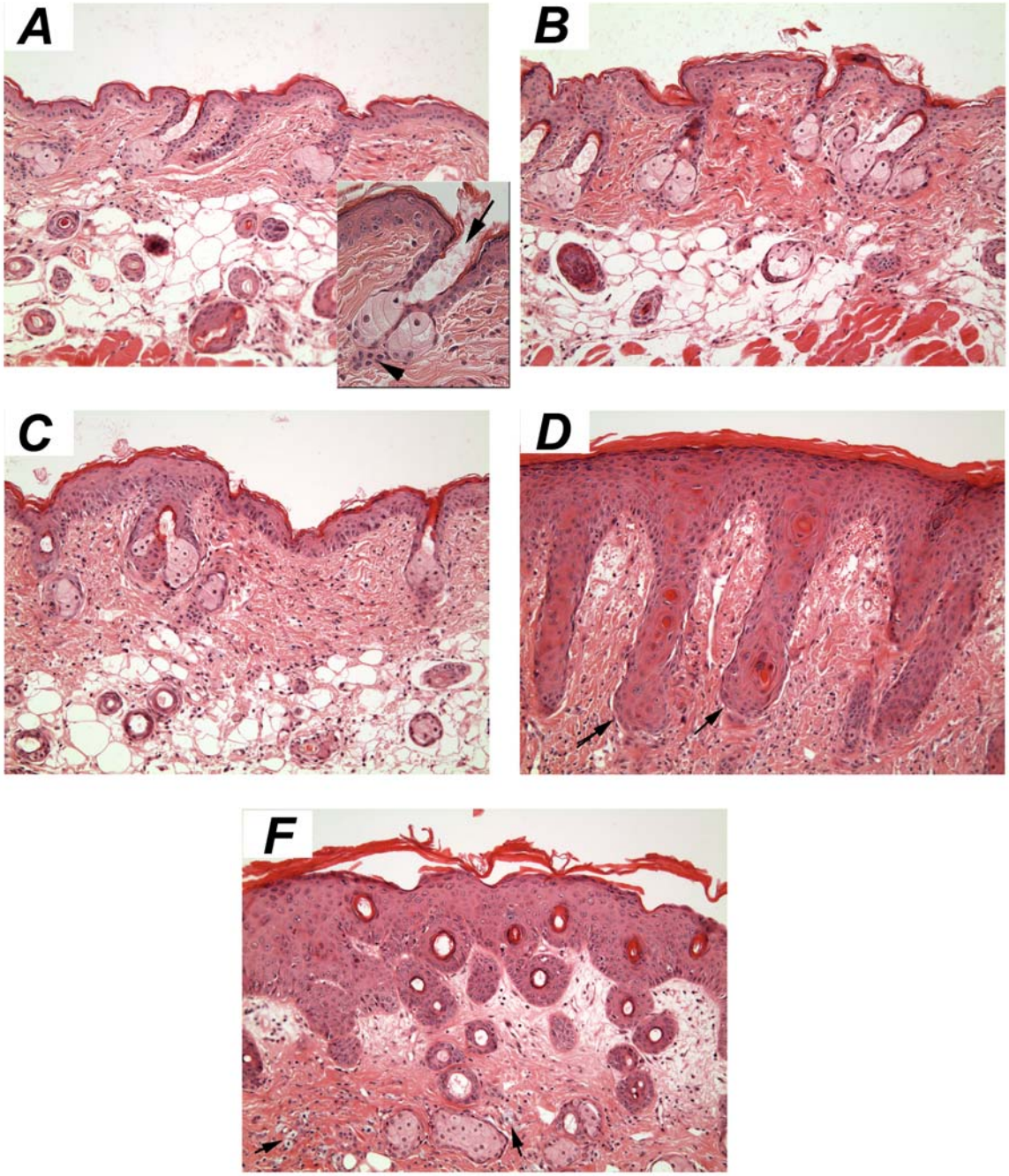

Figure 4.1

Figure 4.2. Immunochemical localization of pAkt in cutaneous tissue isolated from Skh/hr mice following exposure to UVB. pAkt immunoreactive protein was present in few cells in the epidermal and follicular compartments of non-irradiated dorsal skin ***(A)***. pAkt was present in all epidermal and follicular keratinocytes in dorsal skin of Skh/hr mice at 24 hr in response to UVB light ***(B)***. There was a significant increase in pAkt detected within the epidermis 48 hr following exposure to UVB ***(C)***. pAkt was also present within the putative bulge-derived cells of hair follicles of non-irradiated skin and skin isolated at 24 hr and 48 hr following exposure to UVB light ***(A-C, arrows)***. All epidermal and follicular keratinocytes within hyperplastic skin isolated at week 1 ***(D)*** and week 20 ***(E)*** following exposure to UVB light contained pAkt. The specificity of the immunoreactive pAkt localization was demonstrated by the lack of staining in skin tissue sections pre-incubated with anti-pAkt antibody and phospho-Akt-Ser-473 Blocking Peptide and ***(F)***. (A-F) original magnification 320x.

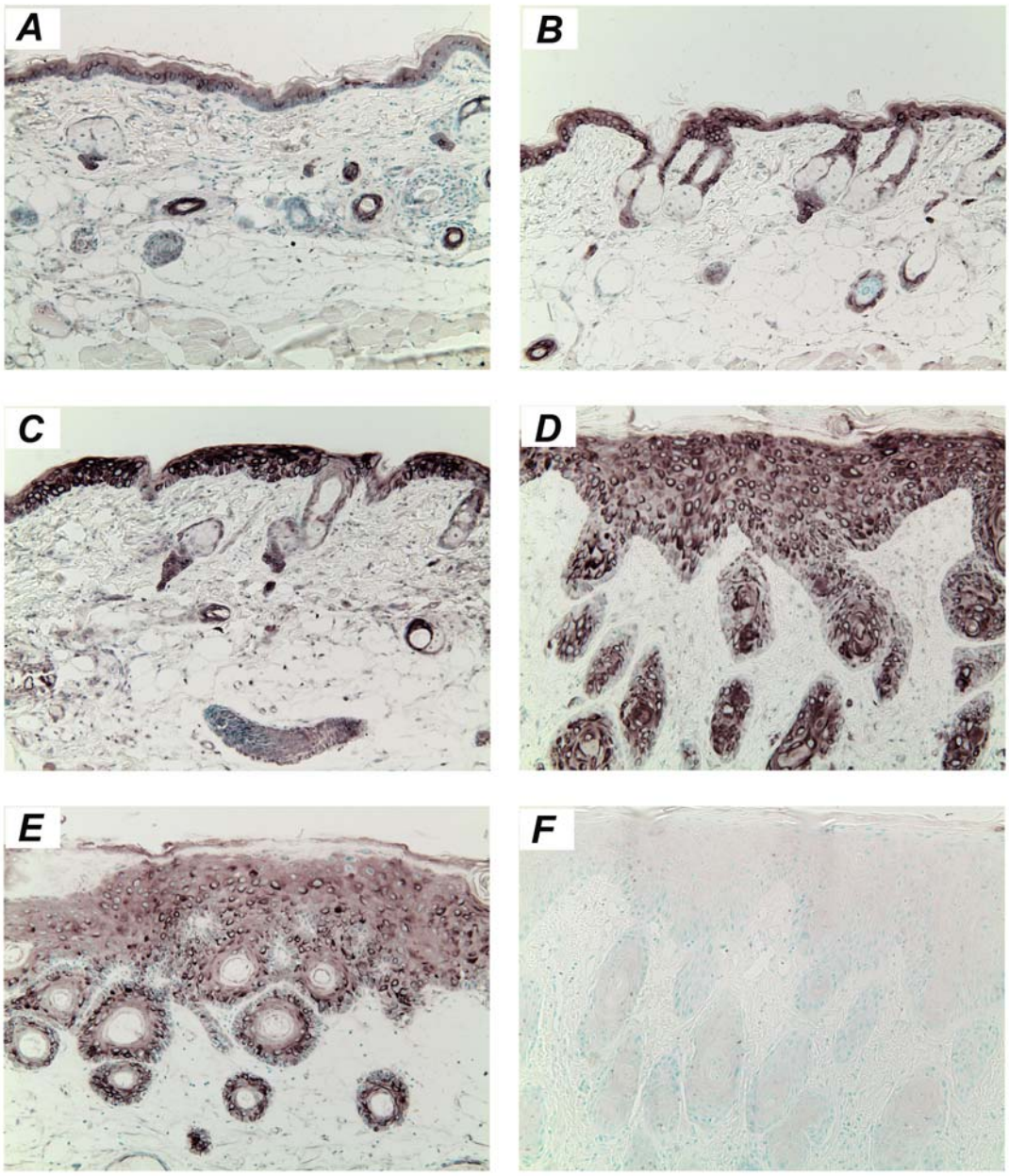

Figure 4.2

Figure 4.3. Immunochemical localization of pAkt and PCNA cutaneous tissue isolated from Skh/hr mice following exposure to UVB. Consecutive serial staining with anti-pAkt and anti-PCNA antibodies in sections of non-irradiated normal skin ***(A and A')*** and UVB-irradiated skin isolated from Skh/hr mice at 24 hr ***(B and B')***, 48 hr ***(C and C')***, week 1 ***(D and D')***, and week 20 ***(E and E')***. All images were taken at a 160x magnification. Insets are at an original magnification of 500x. Keratinocytes that contained pAkt were present within both the proliferative compartment, as defined by immunochemical detection of PCNA-positive populations, and within the non-proliferating cells population, which were PCNA-negative.

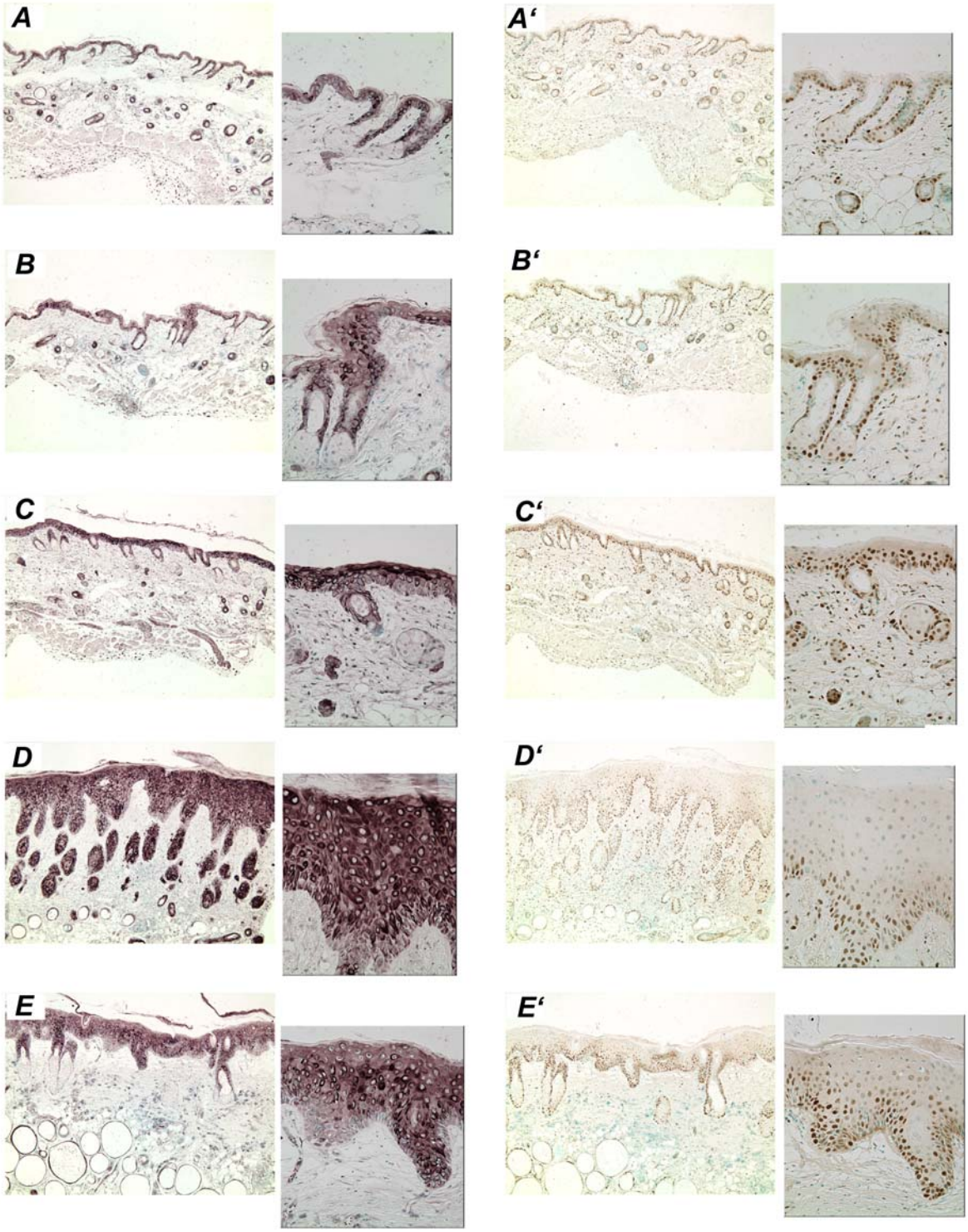

Figure 4.3

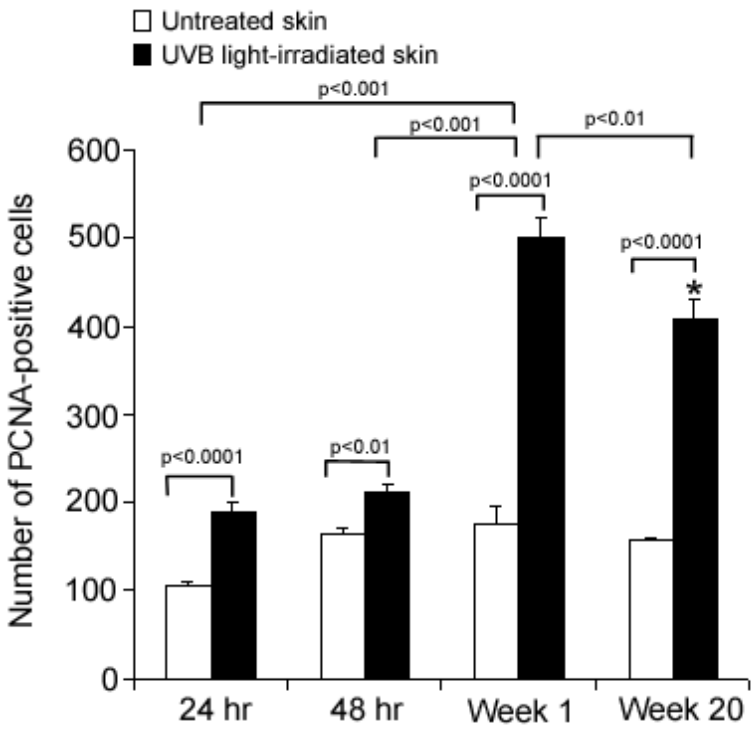

Figure 4.4. Quantitation of the effect of UVB light on epidermal proliferation. Kinetics of cell proliferation in UVB-irradiated skin was quantitated by counting cells within the epidermal layer that stained with anti-PCNA specific antibody in at least 5 high-power fields (250x). Quantitation of keratinocytes which stained with PCNA-positive antibody revealed that the number of PCNA-positive epidermal cells was maximal at week 1 following exposure to UVB. *, $p<0.001$ compared to 24 hr and 48 hr.

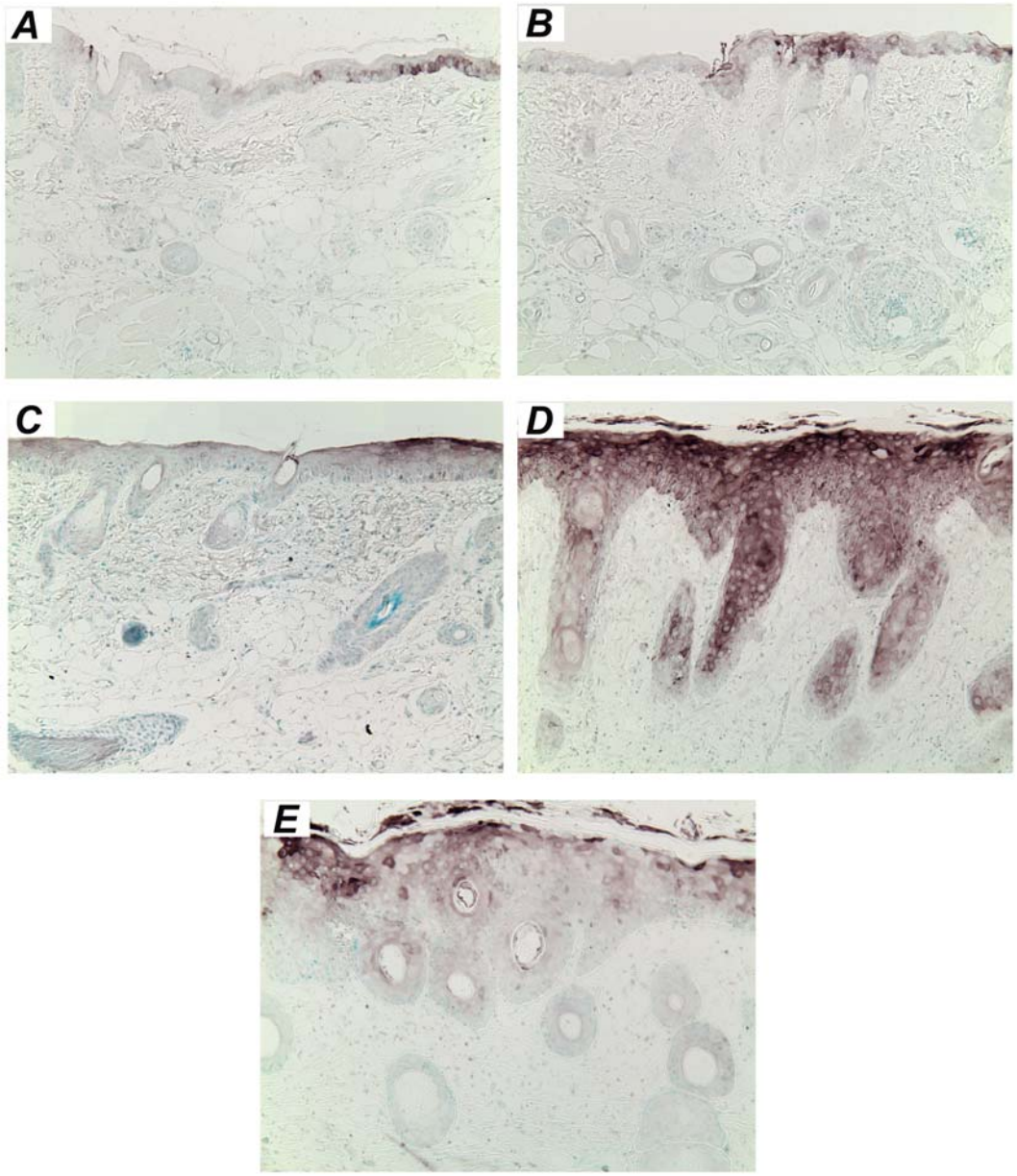

Figure 4.5. Immunochemical localization of pmTOR in cutaneous tissue isolated from Skh/hr mice following exposure to UVB. pmTOR immunoreactive protein was present in few cells scattered within the epidermal compartment in non-irradiated dorsal skin ***(A)*** and dorsal skin of Skh/hr mice at 24 hr ***(B)*** and 48 hr ***(C)*** in response to UVB light. At week 1 ***(D)*** and week 20 ***(E)*** following exposure to UVB light, all epidermal and follicular keratinocytes within hyperplastic skin isolated contained pmTOR. (A-E) original magnification at 320x.

Figure 4.6. Comparative analysis of pAkt, pmTOR, and PCNA immunlocalization in papillomas. (A-C) Consecutive serial sections of papillomas isolated of SENCAR mice initiated with a single topical application of 25 nmol DMBA and treated topically twice weekly with 2 μg of TPA in 0.2 ml acetone for 22 weeks stained with anti-pAkt ***(A)***, anti-pmTOR ***(B)***, and anti-PCNA ***(C)*** antibodies. ***(D-F)*** Consecutive serial sections of papillomas isolated from Skh/hr mice at 20 weeks of a regimen of 3 times weekly exposure to 2240 J/m^2 UVB light stained with anti-pAkt ***(D)***, anti-pmTOR ***(E)***, and anti-PCNA ***(F)*** antibodies. ***(G-H)*** Consecutive serial sections of pAkt ***(G)*** and pmTOR ***(H)*** staining in skin adjacent to papillomas isolated of SENCAR mice at week 22 of tumor promotion. ***(I-J)*** Consecutive serial sections of pAkt ***(I)*** and pmTOR ***(J)*** staining in skin adjacent to UVB-induced papillomas. All representative photomircographs are at 320x original magnification.

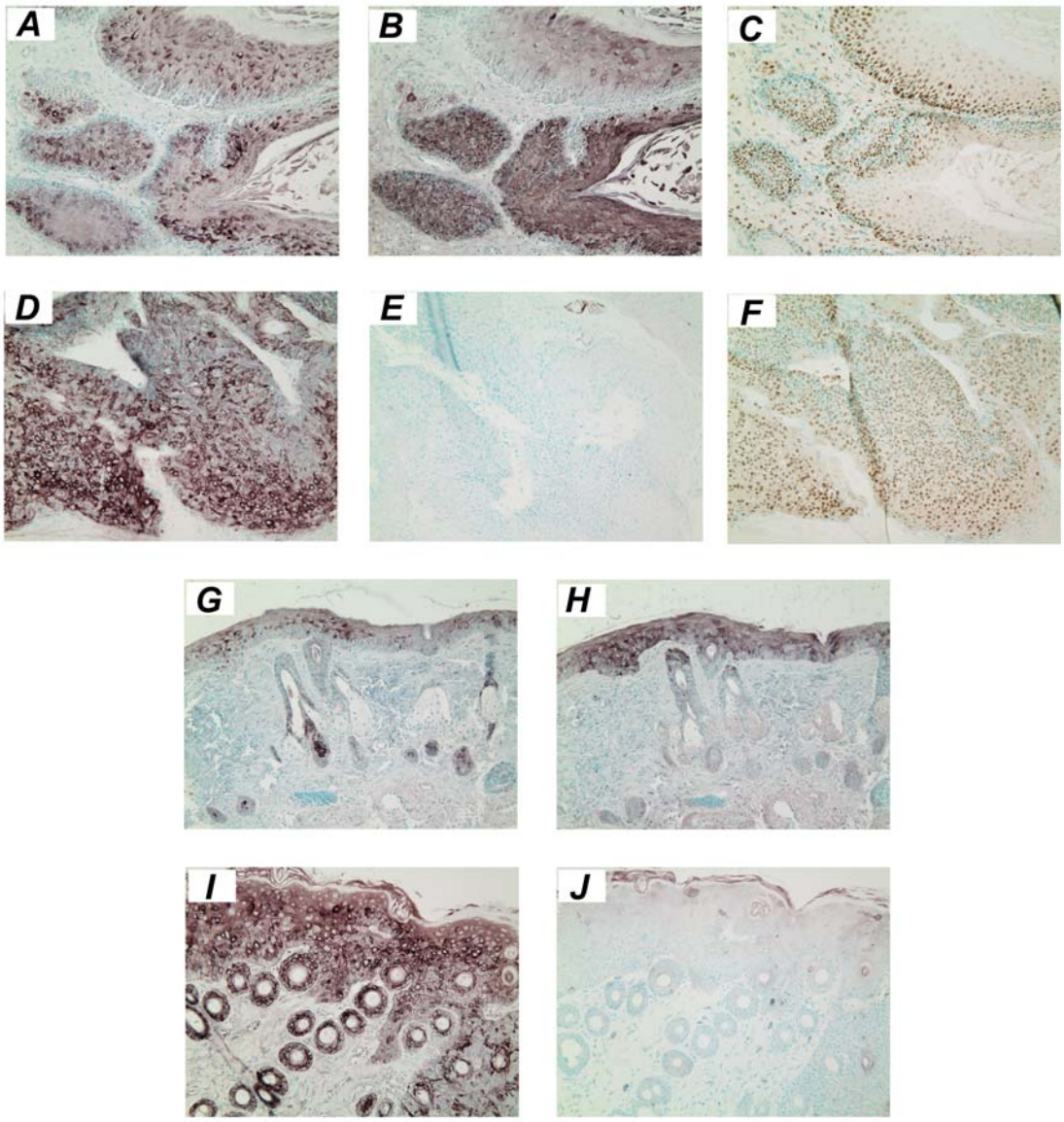

Figure 4.6

Figure 4.7. Immunochemical localization of VEGF in cutaneous tissue isolated from Skh/hr mice following exposure to UVB. There was no detectable VEGF protein present in skin isolated from non-irradiated Skh/hr mice ***(A)***. At 24 hr ***(B)*** and 48 hr ***(C)*** following exposure to UVB light, dorsal skin isolated from Skh/hr mice did not contain VEGF. At week 1 following exposure to UVB ***(D)***, few suprabasal cells produced VEGF protein ***(D, arrows)***. At week 20 following exposure to UVB ***(E)***, a large number of cells produced VEGF immunoreactive protein, including suprabasal and basal keratinocytes as well as follicular keratinocytes. The specificity of VEGF localization was demonstrated by the lack of staining in skin tissue sections pre-incubated with secondary antibody only and counterstained with methyl green ***(F)***. (A-F) original magnification 400x.

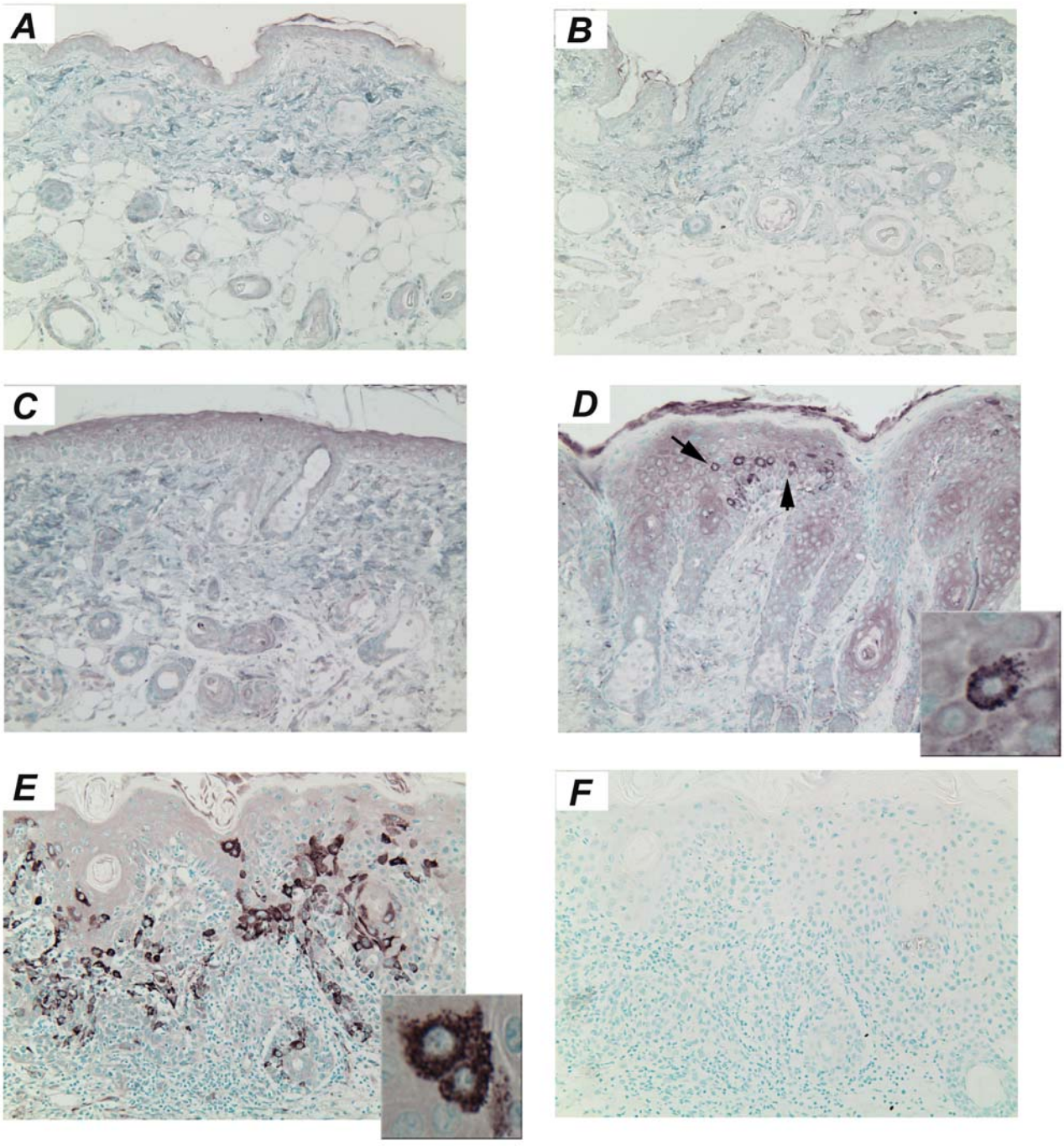

Figure 4.7

Figure 4.8. Neovascularization in cutaneous tissue isolated from Skh/hr mice following exposure to UVB. Immunochemical localization of CD31/PECAM-1 antibody was used to examine the formation of new blood vessels within the dermis of Skh/hr mice following exposure to UVB light. There were few blood vessels within the dermis of non-irradiated mice ***(A, arrows)***. These blood vessels were small in size ***(A, inset)***. At 24 hr and 48 hr following exposure to UVB light, there were fewer blood vessels within the dermis of Skh/hr mice ***(B and C, arrows)***. There was a significant increase in the number of blood vessels at week 1 following exposure to UVB light ***(D, arrows)***. These blood vessels ***(D, inset)*** were widely dilated compared to blood vessels in non-irradiated skin ***(A)***. At week 20 following exposure to UVB light, there was a significant increase in the number of widely dilated blood vessels ***(E, arrows)***. A significant number of blood vessels within the dermis of skin isolated from Skh/hr mice at week 20 were located at the dermal-epidermal junction ***(E)***. Blood vessels within the lower dermis of skin isolated at week 20 following UVB exposure were in close association with mast cells ***(E, inset, arrowheads)***. (A-E) original magnification at 400x.

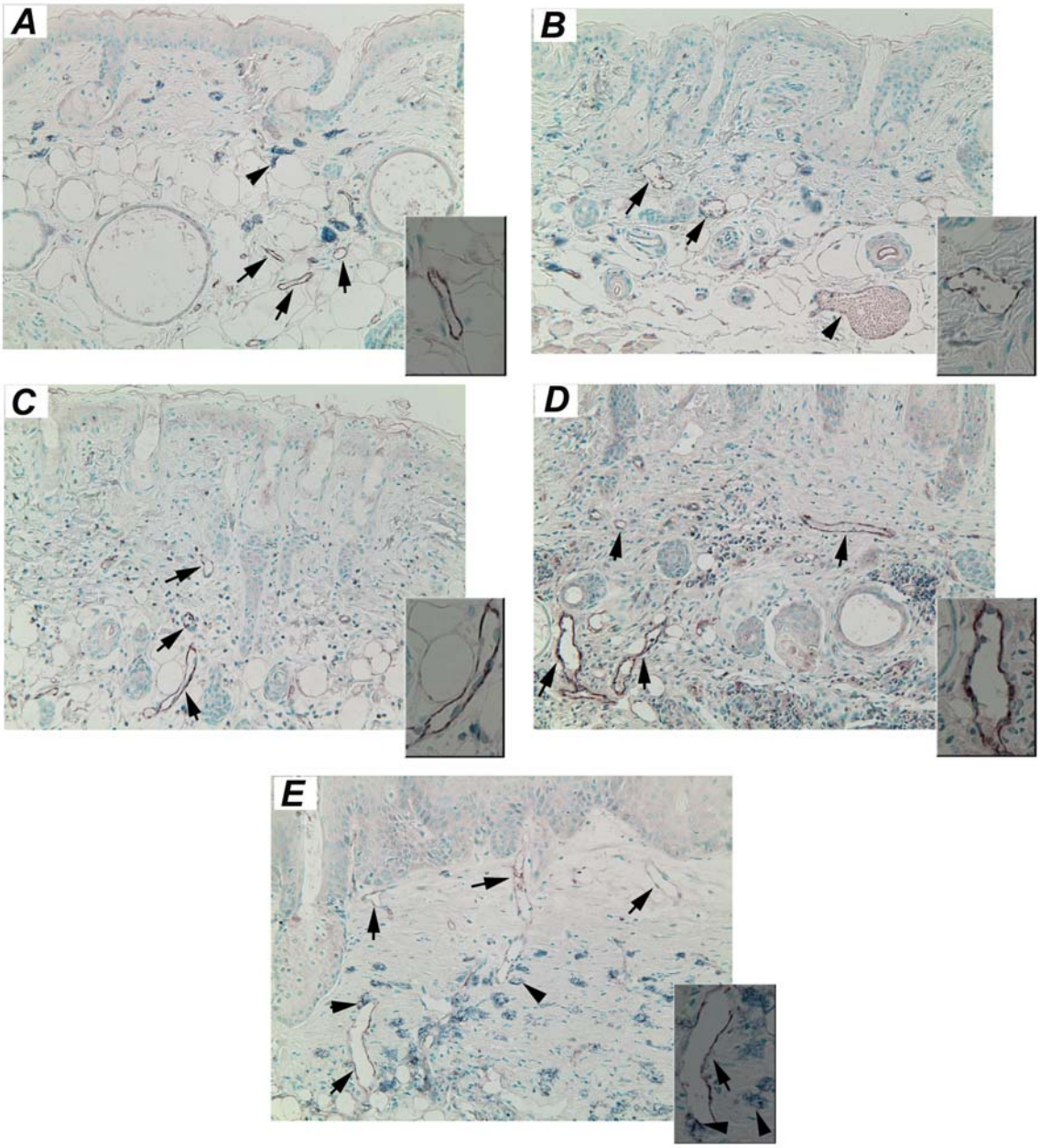

Figure 4.8

Figure 4.9. Quantitation of mast cell infiltration over the time course of UVB-skin carcinogenesis. Mast cells within the dermis were identified by Giemsa staining (*blue*) in dorsal skin of non-irradiated Skh/hr mice ***(A)*** and mice exposed to 2240 J/m2 UVB light for 24 hr ***(B)***, 48 hr ***(C)***, week 1 ***(D)***, and week 20 ***(E)***. (A-E) Original magnification at 150x. ***(F)*** Quantitative analysis of the number of mast cells within at least 10 high-power (200x) fields. The highest number of infiltrating mast cells occurred at week 20 following UVB exposure. *, $p<0.0001$ statistically significant difference from the corresponding control non-irradiated skin. ‡, $p<0.001$ significant increase in mast cell infiltration compared to any of the earlier time points.

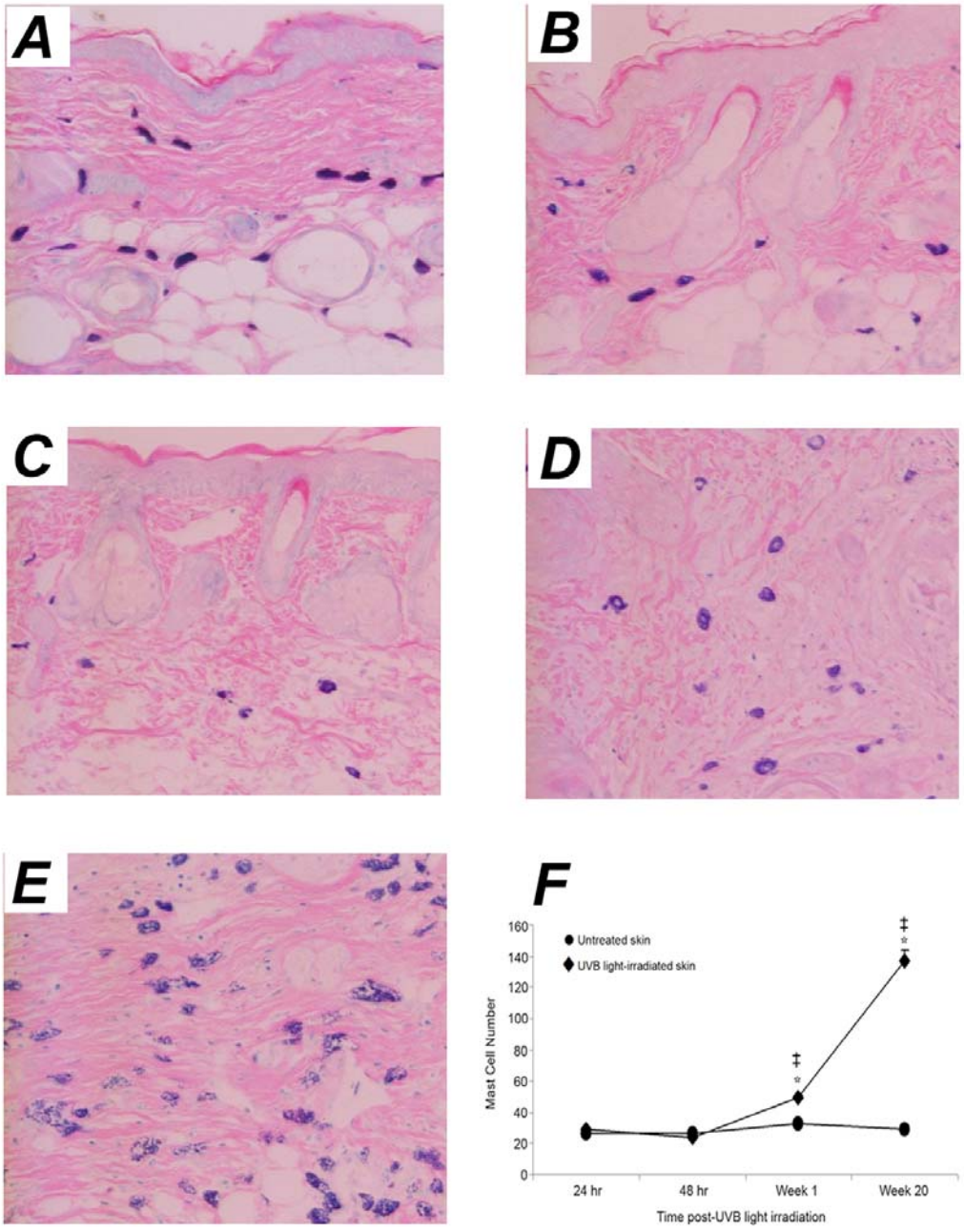
A
B
C
D
E
F
Untreated skin
UVB light-irradiated skin
Mast Cell Number
0
20
40
60
80
100
120
140
160
24 hr
48 hr
Week 1
Week 20
Time post-UVB light irradiation

Figure 4.9

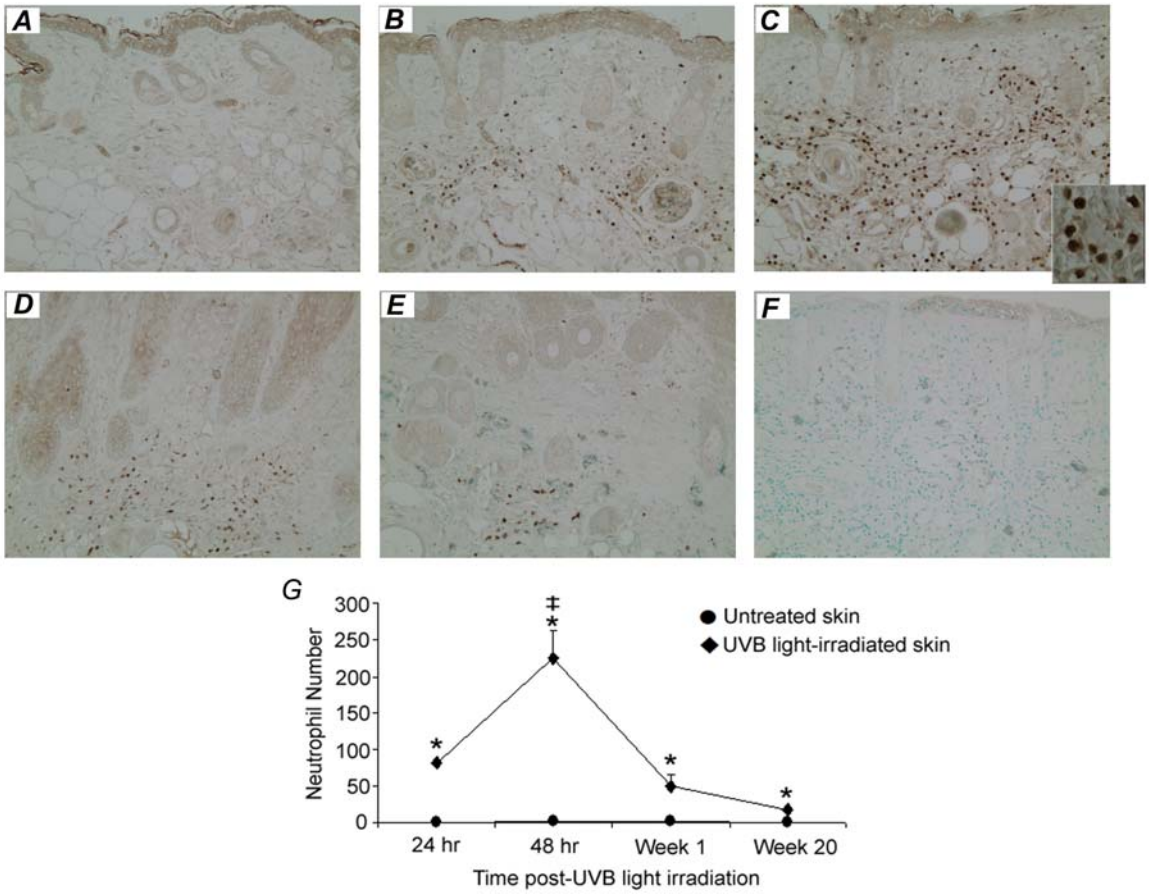

Figure 4.10. Quantitation of neutrophil infiltration over the time course of UVB-skin carcinogenesis. Neutrophils were identified using anti-Gr-1 antibody within the dermal area of non-irradiated skin isolated of Skh/hr mice ***(A)***, skin isolated at 24 hr ***(B)***, 48 hr ***(C)***, week 1 ***(D)***, and week 20 ***(E)*** following UVB exposure. The nonspecific isotypic control antibody binding confirmed that the immunolocalization was specific for neutrophils ***(F)***. (A-F) original magnification at 400x. ***(G)*** Quantitative analysis of the number of infiltrating neutrophils within at least 10 high-power (200x) fields. The highest number of infiltrating neutrophils occurred at 48 hr following UVB exposure. *, $p<0.01$ statistically significant difference from the corresponding control non-irradiated skin. ‡, $p<0.001$ significant increase in neutrophil infiltration compared to all other time points.

CHAPTER 5

LOCALIZATION OF ACTIVATED AKT AND MTOR IN SPECIFIC EPIDERMAL CELL POPULATIONS AND IN $CD34^+/K15^+$ KERATINOCYTE STEM CELLS DURING CUTANEOUS WOUND HEALING

5.1. Abstract

Akt, also known as Protein kinase B, acts as a multi-functional protein by regulating cell survival, size, and proliferation. Akt regulates cell cycle progression through mammalian target of rapamycin (mTOR)-dependent increases in protein translation. However, no studies have characterized the temporal activation of Akt (pAkt) and mTOR (pmTOR) over the time course of wound healing nor the specific types of cells that contain pAkt and pmTOR have been evaluated. In the present studies, a combination of immunohistochemistry and three-color immunoflourescence was used to examine the timing and spatial appearance of pAkt in specific skin cell populations in wound tissues isolated from FVB/N mice as well as the location of $CD34^+/K15^+$ KSC over a 21-day time course of full-thickness wound healing.

At 48 hr following wounding, all proliferating as well as non-proliferating epidermal keratinocytes localized to the wound edge contained pAkt, compared to the few epidermal keratinocytes that contained pAkt in skin distal to the wound site. Following complete closure of the epithelial layer at day 5, the highest levels of pAkt immunoreactive protein were detected within proliferating and non-proliferating epidermal keratinocytes located in the reepithelialized wound site, compared to the low levels of pAkt immunoreactive protein present in epidermal keratinocytes distal to the wound site. At day 21 following wounding, the epidermis had returned to a one-to-two cell layer thickness and the level of pAkt in epidermal keratinocytes along the wound healing line was comparable to that detected in keratinocytes distal to the wound site.

The rapid phosphorylation of Akt in epidermal keratinocytes within the leading edge of the wound during the initial homeostasis and inflammatory phase of wound healing was not followed with phosphorylation of mTOR. However, pmTOR was only detected during the reepithelialization phase in epidermal keratinocytes located in the reepithelialized wound site, which coincided with the presence of pAkt. pAkt was not only present within epidermal keratinocytes at the wound site, but was also present within $CD34^+$ KSC, which remained localized to the bulge niche of hair follicles in skin tissues adjacent to the wound site at all times during cutaneous wound healing. While pAkt was present within the outer root sheath (ORS) as well as the inner root sheath (IRS) of hair follicles, pmTOR was confined specifically to cells in the ORS.

Given the temporal sequence of Akt and mTOR activation in specific cell types following cutaneous injury, the present results suggest that pAkt and pmTOR may contribute to the proper healing of wounds. Activation of Akt and mTOR may serve as therapeutic strategies to enhance wound repair in chronic wounds that fail to heal, such as non-healing ulcers from patients with diabetes.

5.2. Introduction

Following skin injury, an exquisitely timed and spatial sequence of events results in the closure of the wound and the regeneration of tissue to restore the organization and strength of an undamaged skin tissue. Wound healing is a complex process that involves three sequential and distinct phases, including the homeostasis and inflammation, the reepithelialization, and the matrix and tissue remodeling [415-417]. Within 24 hr following wounding, the first phase involves a rapid influx of neutrophils to the wound site [418], the formation of a fibrin clot, and platelet aggregation to inhibit blood flow at the local site of the wound [417]. During this phase, resident fibroblasts and keratinocytes produce growth factors and chemotactic molecules that stimulate proliferation as well as migration of these cells along the cut margins of the dermis [419, 420]. In addition, expression of adhesion molecules aids in retention of these cells within the wound area [421]. At 48 hr following wounding, the reepithelialization and fibroplasia phase begins. This phase lasts until about 5-7 days after wounding. In response to the growth factors and chemotactic factors produced in the first phase of this process, epidermal keratinocytes undergo maximal proliferation during this second stage of healing, and then migrate inward from the leading edge of the wound. In addition, proliferating fibroblasts, i.e. fibroplasia, participate in forming granulation tissue by inducing synthesis of matrix proteins such as collagen [422]. Wound closure is mediated by the combination of epidermal keratinocyte and fibroblast proliferation with wound contracture. Following wound contracture, fibroblasts in the granulation tissue begin to mechanically force the wound margins together [423-425]. Neovascularization, or the development of new blood vessels, also occurs during this second phase of the healing process, which supports the regenerative process [426, 427]. The last stage of wound healing is the dermal remodeling phase, which begins after day 5-7, and lasts until the temporary matrix within the dermis is replaced with a true basement membrane [416].

In addition to the role of epidermal keratinocytes in mediating reepithelialization of the wound [428], growing evidence suggests that long-lived stem cells located to a special niche within hair follicles, which is defined as “the bulge” region [11, 19, 20], participate as well in the process of epidermal repair [42]. In the absence of differentiation and cellular markers, initial studies identified cutaneous stem cells using long-term pulse-chase experiments. Only mouse skin cells with slow-cycling nature retained the nucleoside analog labels, including methyl-[^{3}H]thymidine (^{3}H-T) and

bromodeoxyuridine (BrdU), which led to the definition of these cells in mouse skin as "label-retaining cells" (LRC) [11, 12, 14-16]. Given the high proliferative potential of LRC [26, 40, 41] as well as the ability of single isolated LRC to expand in culture and to grow as holoclones [25, 26, 40], these cells have been defined as mouse keratinocyte stem cells (KSC) [25, 26, 29, 32]. While an estimated 1-2% LRC were present in the basal layer of the interfollicular epidermis [11, 13-16], the majority of LRC have been shown to reside in the bulge region [11, 25, 26]. The bulge represents a well-protected [21] and "growth and differentiation-restricted" niche [19] within hair follicles, which not only contains KSC, but also has recently been shown to contain melanocyte stem cells [429].

Despite the higher clonogenic capacity of KSC located to the bulge region compared to epidermal KSC [25, 26], recent evidence indicate that KSC located to the bulge region do not migrate to the epidermis under homeostasis conditions [42]. In contrast, following skin injury, these bulge-derived stem cells are mobilized from the bulge niche and migrate along the infundibulum part of the hair follicle into the epidermal layer to participate in the reepithelialization process of wound healing [42]. Once in the epidermal layer, bulge KSC have been shown to acquire characteristics of suprabasal epidermal keratinocytes, such as expression of differentiation markers, including cytokeratin 10 (K10) and loricrin [42].

More recent studies have used CD34 [25], a cell surface glycoprotein that is expressed by hematopoietic progenitor cells and endothelial cells [22-24], as a selective marker to identify KSC localized to the outer root sheath of the bulge region of hair follicles in mice [25]; however, recent studies have documented the lack of CD34 expression in the bulge niche in human skin tissues [27, 359]. The cytoplasmic marker cytokeratin 15 (K15) has also been used to identify KSC in the bulge region [28]. While K15 is present in the least differentiated cells of neonatal epidermis, it is present in cells within both the outer and inner root sheaths of the bulge region of adult mouse and human hair follicles [28-31].

Physical wounding of the skin results in injury of epidermal keratinocytes, which become at risk of undergoing apoptosis [430]. However, wound closure depends on both migration and enhanced proliferation of epidermal keratinocytes [428]. To avoid delays in the process of wound healing, one mechanism that may confer resistance of epidermal keratinocytes to apoptotic signals is by activation of survival signaling pathways. Akt, also known as Protein kinase B, is an effector molecule downstream of

phosphoinositide 3-kinase (PI3-K) signaling pathway [302, 303], and has been shown to induce cell survival under conditions of cellular stresses [431]. Activation of PI3-K results in the generation of the membrane-bound lipid, phosphatidylinositol 3,4,5-triphosphate (PI-3,4,5-P_3), which binds with high affinity to Akt amino-terminal pleckstrin homology (PH) domain [231, 232]. Consequently, Akt is recruited to the inner surface of the plasma membrane, where it becomes activated by phosphorylation at two amino acid residues, serine-473 (Ser-473) [235, 306] and threonine-308 (Thr-308) [234].

Not only does Akt play a role in protecting cells from apoptosis [432], but Akt can also induce proliferation of cells by phosphorylating and activating mammalian target of rapamycin (mTOR) at Ser-2448 [256, 267, 309]. mTOR has been shown to regulate cell cycle progression by stimulating initiation of translation of proteins that are required for entry into the G1 phase of the cell cycle, such as cyclin D1 [365, 366]. Under adverse conditions, mTOR has recently been shown to coordinate cell size to progression through the cell cycle [282].

There are no studies thus far that have directly evaluated the role of Akt as well as mTOR during wound repair. Initial evidence for the potential importance of Akt during wound healing is based on studies which reported an association between the expression of nuclear receptor peroxisome-proliferator-activated receptorβ (PPARβ) in epidermal keratinocytes at the wound edge following cutaneous injury and increased survival of these keratinocytes [433, 434]. Further *in vitro* studies using human HaCaT keratinoytes and mouse BALB/MK keratinocytes suggested that PPARβ may mediate its anti-apoptotic effects by activating Akt-1 signaling pathway [435]. Although these previous studies suggested a role of Akt in survival of epidermal keratinocytes following skin injury, the type and location of cells that contain activated Akt and mTOR during cutaneous wound repair remain undefined.

The present study used a combination of immunohistochemistry and three-color immunoflourescence to examine the timing and spatial appearance of activated Akt, as determined by detection of phosphorylation of Akt at serine 473 (pAkt), in $CD34^+/K15^+$ KSC and specific epidermal skin cell populations over a 21-day time course of full-thickness wound healing.

5.3. Materials and Methods

5.3.1. Wound study: Female FVB/N mice (8-13 weeks old, 19-29g; Taconics Farms, Germantown, NY) were housed in vivarium facilities at The Ohio State University that meet American Association for Accreditation of Laboratory Animal Care requirements. All procedures were approved by The Ohio State University Institutional Animal Care Utilization Committee. Animals were fed Purina Pico Chow (Barnes Supply Co., Durham, NC) and basal Teklad 22/5 rodent diet (Harland Industries, Indianapolis, IN) *ad libitum* and kept in rooms maintained on a 12 hr light/dark cycle. Dorsal skin was carefully shaved 24 hr prior to wounding. Using a template to ensure accuracy and reproducibility, each mouse received a 2 cm full thickness wound using fine pointed scissors, which went completely through the epidermal and dermal layers of the skin. Mice that did not receive full-thickness wounds served as unwounded control animals. Wounds were closed with 9 mm stainless steel wound clips (Fisher Scientific, Pittsburgh, PA). These wounds remained closed with wound clips until repair of damaged tissue resulted in complete wound closure, as assessed visually. FVB/N mice were euthanized at 12, 24, and 48 hr and at day 5, 9, 12, 16, and 21 following wounding. Dorsal hair was removed using a depilatory agent. Sections of skin tissues isolated directly from the wound site as well as skin sections distal and proximal to the wound were isolated from both the left and right side of the wound. Tissue samples were fixed in 10% neutral buffered formalin (Shandon, Pittsburgh, PA) and embedded in paraffin for immunostaining analysis.

5.3.2. Masson's Trichome staining: 5 μm sections of paraffin-embedded skin tissues were mounted onto microscope slides (ProbeOn/Plus, Fisher Scientific, Pittsburgh, PA). Tissues sections were then deparaffinized using Histo-Clear (National Diagonistics, Atlanta, GA), and rehydrated in a graded series of alcohol. To examine collagen deposition, the Trichrome Stain (Masson) kit (Sigma, St. Louis, Pittsburgh, PA) and the Microprobe Manual Staining System (Fisher Scientific) were used. Briefly, slides were incubated with pre-heated Bouin's solution for 15 min at 56^{o}C, then cooled and rinsed for 2 min in tap water. Nuclei were stained with Weigert's Iron Hematoxylin solution for 5 min, followed by rinses in distilled water. Cytoplasm and muscle tissues were then stained with Biebrich Scarlet Fuchsin solution for 5 min, followed by rinsing with water. Following a 5 min incubation in Phosphotungstic/Phosphomolybdic Acid Solution, collagen was stained with Aniline Blue solution for 5 min, which was followed by

incubation with 1% acetic acid for 2 min. Following rinsing with water, the slides were then dehydrated, mounted, viewed, and photographed.

5.3.3. Immunochemical staining methods: 4 μm sections of paraffin-embedded skin tissues were mounted onto microscope slides (SuperFrost/Plus, Fisher Scientific, Pittsburgh, PA). Tissues sections were then deparaffinized using Histo-Clear (National Diagonistics, Atlanta, GA), and rehydrated in a graded series of alcohol. Endogenous peroxidase activity was quenched for 20 min using 3% H_2O_2 in methanol. Samples were then subjected to antigen retrieval by steam heating for 15 min in 10 mM citrate buffer (pH 6.0). Sections were then blocked for 1 hr in 1% bovine serum albumin (BSA) (Sigma) in Tris-Buffered Saline with Tween-20, pH 7.6 (TBST: Tris, 11.6 mM; Tris-HCl, 38 mM; NaCl, 150 mM; Tween 20, 0.05%). Tissues sections were then incubated in a humidified chamber with goat anti-CD34 (1:150; Santa Cruz Biotechnology, Santa Cruz, CA), chicken anti-keratin 15 (K15; 1:2000; Covance, Berkley, CA), rabbit anti-PCNA antibody (1:50, Santa Cruz) for 1 hr at room temperature, or rabbit anti-Akt-Ser-473-P (pAkt, 1:100; Santa Cruz), rabbit anti-phospho-mTOR-Ser-2448 (pmTOR; 1:50; Cell Signaling Technology, Beverly, MA) overnight at 4^{o}C in 1 % BSA in TBST. Sections were incubated for 20 min with biotinylated horse anti-goat IgG, goat anti-chicken, or goat anti-rabbit IgG (1:200; Vector Laboratories, Burlingame, CA), followed by incubation for 30 min with avidin-biotinylated horseradish peroxidase complex (ABC Elite) (Vector Laboratories). The presence of CD34, K15, pAkt, and pmTOR antigens was visualized with the chromagen VIP substrate (Vector Laboratories). The presence of PCNA antigen was visualized using 3,3-diaminobenzidine (DAB; Vector Laboratories). To stop the DAB and VIP development reactions, slides were washed with distilled water. The specificity of pAkt staining was determined by examining the extent of binding of anti-pAkt antibody by tissue sections that had been pre-incubated with Akt-Ser-473-P Blocking Peptide (Cell Signaling Technology, Beverly, MA) for 2 hr. Tissues were counterstained with Methyl Green for 5 min. Slides were then dehydrated, mounted, and digital images captured using a Diagnostic Instruments digital camera mounted on an Olympus research microscope.

5.3.4. Immunofluorescent staining: Sections of paraffin-embedded skin samples (4 μm) were rehydrated as described above. To reduce autofluorescence, sections were

treated with sodium borohydride (1 mg/ml; Sigma) in TBST. Sections were then incubated for 30 min at room temperature with Image-iT^{TM} FX Signal Enhancer (Molecular Probes, Eugene, OR) to block background staining. For double immunofluorescence staining, sections were incubated overnight at 4^{o}C with both anti-pAkt (1:50, Santa Cruz) and anti-CD34 (1:50, Santa Cruz). Tissues were then incubated at room temperature for 1 hr with Alexa Fluor-647-conjugated donkey anti-goat IgG, followed by Alexa Fluor-555-conjugated donkey anti-rabbit for 1 hr (1:500, Molecular Probes). For K15 immunofluorescence staining, tissue sections were incubated with chicken anti-K15 (1:2000) for 1 hr at room temperature. Sections were incubated with goat anti-chicken IgG, followed by incubation with avidin-biotinylated alkaline phosphatase complex. The slides were then incubated with the chromagen Vector Red alkaline phosphatase substrate, which was visualized as red fluorescence. Tissues were mounted using VectaShield Mounting Medium (Vector Laboratories) containing 4', 6-diamidino-2-phenylindole (DAPI), a DNA dye that specifically stains nucleated cells. Specificity of antibody binding was determined by incubation with only secondary antibodies followed by placement of coverslips using Vectashield containing DAPI.

5.3.5. Confocal microscopy and digital imaging: Digital images of stained tissues were captured using a Diagnostic Instruments digital camera (Insight camera; 1600 x 1200 resolution) mounted on an Olympus research microscope, using identical lighting and optical settings. Images were then transferred to digital image analysis software (Image Pro Plus, Media Cybernetics, Silver Spring, MD). Fluorescent images were obtained using a laser scanning confocal microscope (Zeiss LSM 510 Meta), with excitation wavelengths of 543 nm for Alexa Fluor-555 and Vector Red, 633 nm for Alexa Fluor-647, and 405 nm for DAPI-associated fluorescence. Emission signals were observed using a set of band-pass filters. Images were merged using Adobe Photoshop software (Adobe Systems, Inc., San Jose, CA).

5.4. Results

5.4.1. Histological evaluation of cutaneous alterations during wound healing. Sections of tissues isolated from FVB/N mice were evaluated for alterations in the dermis and epidermis over the 21-day time period following the receipt of a full-thickness wound using Masson's trichome stain, which allows visualization of collagen deposition (*dark blue*) and the proliferative epidermal cells (*pink*) (Figure 5.1). In unwounded skin, the epidermis was one-two cell layers thick composed of epidermal keratinocytes (Figure 5.1 A, arrow). At 12 hr and 48 hr following wounding, a visible fibrin clot started to form within the wound site, which was identified by the deeply stained fibrous material at the point of disruption of the dermal and epidermal layers (Figure 5.1 B and C, arrowheads). Epidermal keratinocytes adjacent to the wound site were hyperplastic (Figure 5.1 B and C, arrows). At day 5 following wounding, proliferating epidermal keratinocytes from the wound margin began to migrate into the wound site, which allowed reepithelialization (Figure 5.1 D, arrowhead) and complete closure of the wound site, as shown by the intact epidermal/dermal junction. Densely packed collagen was also present throughout the entire wound area at day 16 following wounding, as shown by the deep stained matrix within the dermal layer (Figure 5.1 E, arrowheads). At days 19 and 21, the epidermis had returned to one-to-two cell-layer thickness (Figure 5.1 F and G, arrows), as also seen in unwounded tissue (Figure 5.1 A, arrow), and the wound site was completely closed (Figure 5.1 F and G, arrows). Collagen within the lower dermis around the line of the wound was visible by the darkly stained collagen (Figure 5.1 F and G, arrowheads). There was a closure of the submuscular layer at day 21 (Figure 5.1 G, star). In addition, the hair follicles remained in a hyperplastic state at this time, indicating that the dermal layer continued to undergo remodeling.

5.4.2. Immunochemical localization of pAkt and proliferating cells during wound healing. Serial sections of skin isolated at 48 hr, day 5, and day 21 following wounding were examined to identify proliferating and/or non-proliferating keratinocytes which contained pAkt (Figure 5.2). At 48 hr following wounding (Figure 5.2 A-C), all basal (Figure 5.2 B, arrow) and suprabasal epithelial keratinocytes (Figure 5.2 B, arrowheads) that started to migrate along the cut margins of the dermis contained pAkt. In contrast, pAkt immunochemical localization was confined to suprabasal keratinocytes at sites

distal to the wound (Figure 5.2 C, arrowheads), with nominal staining of pAkt in basal keratinocytes (Figure 5.2 C, arrows).

Comparative analysis of serial sections at 48 hr following wounding demonstrated that keratinocytes localized to the wound edge and which contained pAkt (Figure 5.2 B) were present within both the proliferative compartment, as defined by the immunochemical localization of PCNA-positive populations (Figure 5.2 B', arrow), and the non-proliferating cell populations, which localized to suprabasal epidermal cells (Figure 5.2 B', arrowheads). pAkt-containing suprabasal keratinocytes distal to the wound site (Figure 5.2 C, arrowheads) were not undergoing proliferation, as assessed by their lack of PCNA staining (Figure 5.2 C', arrowheads).

At day 5 following wounding (Figure 5.2 D-F), there was a complete closure of the epithelial layer. High levels of pAkt immunoreactive protein were detected within epidermal keratinocytes that had migrated into the entire wound site (Figure 5.2 E) compared to the low levels of pAkt immunoreactive protein present in epidermal keratinocytes distal to the wound site (Figure 5.2 F). Comparative analysis of serial sections at day 5 following wounding indicate that pAkt (Figure 5.2 E) was present in both proliferating (Figure 5.2 E', arrow) as well as non-proliferating suprabasal (Figure 5.2 F', arrowhead) keratinocytes within the wound site. As the distance from the wound site increases, pAkt (Figure 5.2 F) was present within non-proliferating suprabasal keratinocytes (Figure 5.2 F', arrowhead).

At day 21 following wounding (Figure 5.2 G-I), the epidermis had returned to a one-to-two cell layer thickness and the level of pAkt in epidermal keratinocytes along the wound healing line (Figure 5.2 H) was comparable to that detected in keratinocytes distal to the wound site (Figure 5.2 I). pAkt staining in keratinocytes located within or distal to the wound site coincided with proliferating (Figure 5.2 H', arrow) as well as non-proliferating (Figure 5.2 H', arrowhead) keratinocytes.

5.4.3. Immunochemical localization of pmTOR during wound healing. At 12 hr following wounding (Figure 5.3 A-C), there was a nominal staining of pmTOR within epidermal keratinocytes along the cut edge of the wound tissue (Figure 5.3 B) as well as keratinocytes distal to the wound (Figure 5.3 C). At day 5 following wounding, all epidermal keratinocytes that migrated into the wound site contained pmTOR (Figure 5.3 E, arrows). In contrast, pmTOR was nominal in epidermal keratinocytes distal to the

wound site (Figure 5.3 F, arrowhead). At day 9 following wounding (Figure 5.3 G-I), pattern of pmTOR staining was similar to that observed at day 5 after wounding (Figure 5.3 D-F), with pmTOR immunoreactive protein present predominantly in epidermal keratinocytes within the reepithelialized wound site (Figure 5.3 H), compared to the low levels of pmTOR within epidermal keratinocytes distal to the wound (Figure 5.3 I). At 21 day following wounding (Figure 5.3 J-K), there were only few epidermal keratinocytes scattered throughout the epidermis which contained pmTOR (Figure 5.3 K).

5.4.4. Localization of $K15^+$ and $CD34^+$ cells during cutaneous wound healing. Immunofluorescent staining was used to evaluate the localization of $K15^+$ bulge cells (Vector-red associated fluorescence) at the wound site (Figure 5.4 A) and distal to the wound site (Figure 5.4 D) at day 5 following wounding (Figure 5.4 A-F). Nucleated cells within hair follicles were defined by DAPI-associated blue fluorescence (Figure 5.4 B and E). While $K15^+$ cells were not present within the epidermal compartment in the repithelialized wound site (Figure 5.4 A and C), $K15^+$ cells remained localized to the bulge niche of hair follicles that were adjacent to the wound site (Figure 5.4 A and D, arrows).

Immunochemical localization of CD34 expression during the process of wound healing demonstrated that $CD34^+$ cells were not detected at the wound site at 48 hr (Figure 5.4 G) and day 5 (Figure 5.4 I) following wounding. However, $CD34^+$ cells were located to the bulge niche of hair follicles adjacent to the wound site at both time points (Figure 5.4 H and J, arrows).

5.4.5. Localization of CD34, pAkt, and pmTOR in cells within the bulge niche during cutaneous wound healing. Double-immunofluorescence and confocal microscopy (Figure 5.5 A-D) were used to identify $CD34^+$ cells (Alexa-647 red-associated fluorescence), which localized to the outer root sheath (ORS) of the bulge (Bu) (Figure 5.5 A) and contained pAkt (Alexa-555 green-associated fluorescence) (Figure 5.5 B) in hair follicles adjacent to the wound site at 12 hr following wounding. Nucleated cells within hair follicles were defined by DAPI-associated blue fluorescence (Figure 5.5 C). Figure 5.5 D is a representative merged image of CD34, pAkt, and DAPI staining in hair follicles adjacent to the wound site at 12 hr following wounding showing co-localization of $CD34^+$ and $pAkt^+$ in nucleated cells within the Bu niche of hair follicles.

The presence of pAkt in the ORS of the Bu niche was also evident in hair follicles isolated from FVB/N mice at day 5 following wounding (Figure 5.5 E). While pAkt was present in both the ORS and the IRS of the Bu of hair follicles (Figure 5.5 E), pmTOR was present only in the ORS of hair follicles (Figure 5.5 F), which coincided with the presence of $CD34^{+}$ cells at this location (Figure 5.5 A).

5.5. Discussion

A highly regulated sequence of events is required for wound closure and for regeneration of the damaged skin tissue to its original strength. Little information is known about activation of Akt and mTOR during the process of cutaneous wound healing. The present studies are one of the first to evaluate the sequential activation and localization of pAkt and pmTOR in specific skin cells during the three phases of wound repair, including the initial homeostasis and inflammatory phase, the reepithelialization phase, and the dermal remodeling phase.

At the early stages of wound healing, all epidermal keratinocytes at the wound edge contained pAkt, compared to the fewer number of epidermal keratinocytes distal to the wound site that contained pAkt. Recent studies suggest that basal keratinocytes at the wound edge undergo apoptosis following skin injury. The current immunochemical studies suggest that the presence of pAkt in basal epidermal keratinocytes at the wound edge may be one mechanism by which basal epidermal cells survive following cutaneous injury.

In response to skin injury, epidermal keratinocytes at the wound site have the ability to withdraw from undergoing the process of terminal differentiation, and acquire further structural changes, which include down-regulation of cadherins and integrins, thus facilitating their migration. In addition, epidermal keratinocytes acquire a migratory phenotype by developing cellular projections and start “crawling” to re-establish the epidermal barrier. These changes in cell shape are controlled by reorganization of the cytoskeleton. Recent evidence suggests that Akt not only promotes cell survival, but also regulates cell motility in mammalian leukocytes [436, 437], fibroblasts [438], endothelial cells [439], and tumor cells [440]. Akt has been shown to localize to the leading edge of migrating fibroblast [438], and induces formation of lamellipodium by phosphorylating the structural protein Girdin, also known as Akt-phosphorylation enhancer (APE), in fibroblasts at the wound edge using a cell-based wound healing assay [326]. Collectively, the present results suggest that activation of Akt regulates early responses during wound healing, by providing epidermal keratinocytes with the ability to evade the normal process of terminal differentiation, and to subsequently acquire a migratory phenotype, allowing them to move along the dermal wound margins.

During the reepithelialization phase of wound healing, epidermal keratinocytes that had migrated into the entire wound site contained the highest levels of pAkt

compared to the low levels of pAkt immunoreactive protein present in epidermal keratinocytes as the distance from the wound site increases. Increases in pAkt levels within epidermal keratinocytes located in the wound site during the reepithelialization phase coincided with the presence of pmTOR in these cells. pmTOR staining was only confined to keratinocytes that migrated into the wound site, as the presence of pmTOR was nominal in keratinocytes distal to the wound site.

The present studies further demonstrate that basal keratinocytes that had migrated into the wound site continued to proliferate and contained both pAkt and pmTOR. pmTOR has been previously shown to stimulate entry of cells into the cell cycle by phosphorylating in parallel the 70 KDa ribosomal protein S6 kinase (p70 S6K) and eukaryotic initiation factor 4E (eIF4E)-binding protein 1 (4E-BP1). Once activated, p70 S6K induces translation of mRNAs that encode ribosomal proteins and translation elongation factors. On the other hand, mTOR, by phosphorylating 4E-BP1 at Thr-37/Thr-46 residues, inhibits the association between 4E-BP1 and eIF4E, therefore freeing eIF4E for initiation of translation of proteins that are required for entry into the G1-phase of the cell cycle, such as cyclin D1. The location of pAkt to keratinocytes within the basal layer of the reepithelialized wound site, which coincided with the presence of pmTOR, suggests that Akt/mTOR signaling pathway may be essential for the proliferation of basal cells during the reepithelialization phase.

On the other hand, the location of pAkt and pmTOR to suprabasal keratinocytes did not correlate with PCNA expression, a proliferative marker that is expressed in the G_1/S and G_2 phases of the cell cycle. Reepithelialization has previously been shown to involve the generation of a multi-layered epithelium, with different keratinocyte subtypes within the suprabasal compartment of the epidermis [428]. Recent evidence suggests that not only does pmTOR stimulate entry into the cell cycle, but also induced survival of primary AML cells [364]. Furthermore, inhibition of mTOR with the selective mTOR inhibitor, cell cycle inhibitor-779 (CCI-779), in the presence of constitutive activation of Akt induced apoptosis of glioblastoma tumor cells, indicating that pmTOR mediates pAkt-dependent survival pathways in these tumor cells [441]. Taken together, the present observations suggest that Akt and its downstream effector, mTOR, may act together or separately to induce survival and persistence of non-proliferating suprabasal keratinocytes during the reepithelialization phase following cutaneous wounding. Further

investigation is required to examine whether pmTOR may be an important factor that mediates Akt-dependent survival signaling.

Tissue regeneration following skin injury not only depends on proliferation and migration of epidermal keratinocytes into the wound site [428], but also requires participation of keratinocyte stem cells (KSC), in particular, KSC localized to the bulge region of hair follicles [42]. Although observations are conflicting regarding the contribution of KSC located to the bulge region to the self-renewal and maintenance of the epidermal compartment [38, 442], recent studies demonstrate that this cell population does participate in the regeneration of the epidermal compartment only in the presence of trauma, such as skin injury [42]. The present study localized $CD34^+$ and $K15^+$ KSC to the bulge region of hair follicles that were adjacent to the wound site and demonstrated that the location of KSC within this specific niche was not altered during the different stages of wound healing. Interestingly, expression of either K15 or CD34 was not detectable within keratinocytes at the wound site. These observations are in concert with recent studies [42], which demonstrated that bulge cells-derived KSC that migrated to the reepithelialized epidermis following cutaneous wounding did not express cytokeratin 17 (K17), a follicular marker; however, these bulge-derived cells expressed markers of epidermal differentiation, including cytokeratin 10 (K10) and loricrin [42]. These previous results suggest that KSC that are mobilized from the bulge niche after wounding acquire a “functional epidermal keratinocyte” phenotype [42], therefore, enhancing reepithelialization of the wound site.

There are no studies thus far that evaluated the presence of pAkt and pmTOR in KSC located to the bulge region of hair follicles during wound healing. $CD34^+$ cells within the ORS of the Bu niche in hair follicles adjacent to the wound site were observed to contain pAkt. The present results suggest that Akt activation in KSC during wound healing may contribute to the “growth and differentiation-restricted” [19] microenvironment of the bulge niche. Therefore, pAkt may represent one mechanism by which KSC resist undergoing differentiation when located to the bulge niche, which may be similar to the reported role of Akt in inducing long-term maintenance of human embryonic stem cells in their undifferentiated state [371, 372].

While pAkt was present within both the ORS as well as the IRS of hair follicles, pmTOR immunoreactive protein was confined only to the ORS of hair follicles, suggesting that pmTOR may serve as a cellular marker of cells located to the ORS of

the bulge region during the process of wound healing. The dual presence of pAkt and pmTOR in KSC localized to the ORS of the bulge region of hair follicles suggests that Akt/mTOR signaling pathway may play a role in tightly regulating the differentiation of KSC, thus maintaining a long-lived population of stem cells that has been to participate in skin regeneration following injury.

In summary, the present results suggest that the temporal sequence of Akt and mTOR activation in specific cell types following cutaneous injury may result in the proper healing of wounds. The present results suggest that activation of Akt and mTOR may serve as therapeutic strategies to enhance wound repair in chronic wounds that fail to heal, such as non-healing ulcers from patients with diabetes.

Figure 5.1. Histological evaluation of wound repair in FVB/N mice. Masson's Trichrome staining, which stains collagen *blue* and cytoplasm *red*, was used on paraffin embedded dorsal skin tissues isolated from FVB/N mice the 21-day time period following the receipt of a full-thickness wound. These representative photographs depict the trichrome staining for the responses of each of wound healing in unwounded skin ***(A)***, at the beginning of phase 1 at 12 hr ***(B)***, at the end of phase 1 and beginning of phase 2 at 48 hr ***(C)***, in the middle of phase 2 at day 5 ***(D)***, in the middle of phase 3 at day 16 ***(E)*** and day 19 ***(F)***, and at the end of phase 3 at day 21 ***(G)***. In the unwounded skin *(A)*, the epidermis was one-to-two cell-layers thick (arrow). At 12 hr *(B)*, there was a disruption of epidermis and dermis following wounding (arrowhead). By 48 hr *(C)*, a fibrin clot has formed to stop blood flow (arrowhead). Keratinocytes in the epidermis are in a hyperplastic state causing the epidermis to thicken (arrow) *(B and C)*. At day 5 *(D)*, keratinocytes had migrated into the entire wound site (arrowhead). At day 16 (E), densely packed collagen was present throughout the entire wound area (arrowheads). At days 19 *(F)* and 21 *(G)*, the epidermis (arrow) was comparable to unwounded tissue *(A)* and the collagen deposition along the wound healing line was visible (arrowheads). At day 21 *(G)*, there was a complete closure of the submuscular layer (star). All photographs are at an original magnification of 125x.

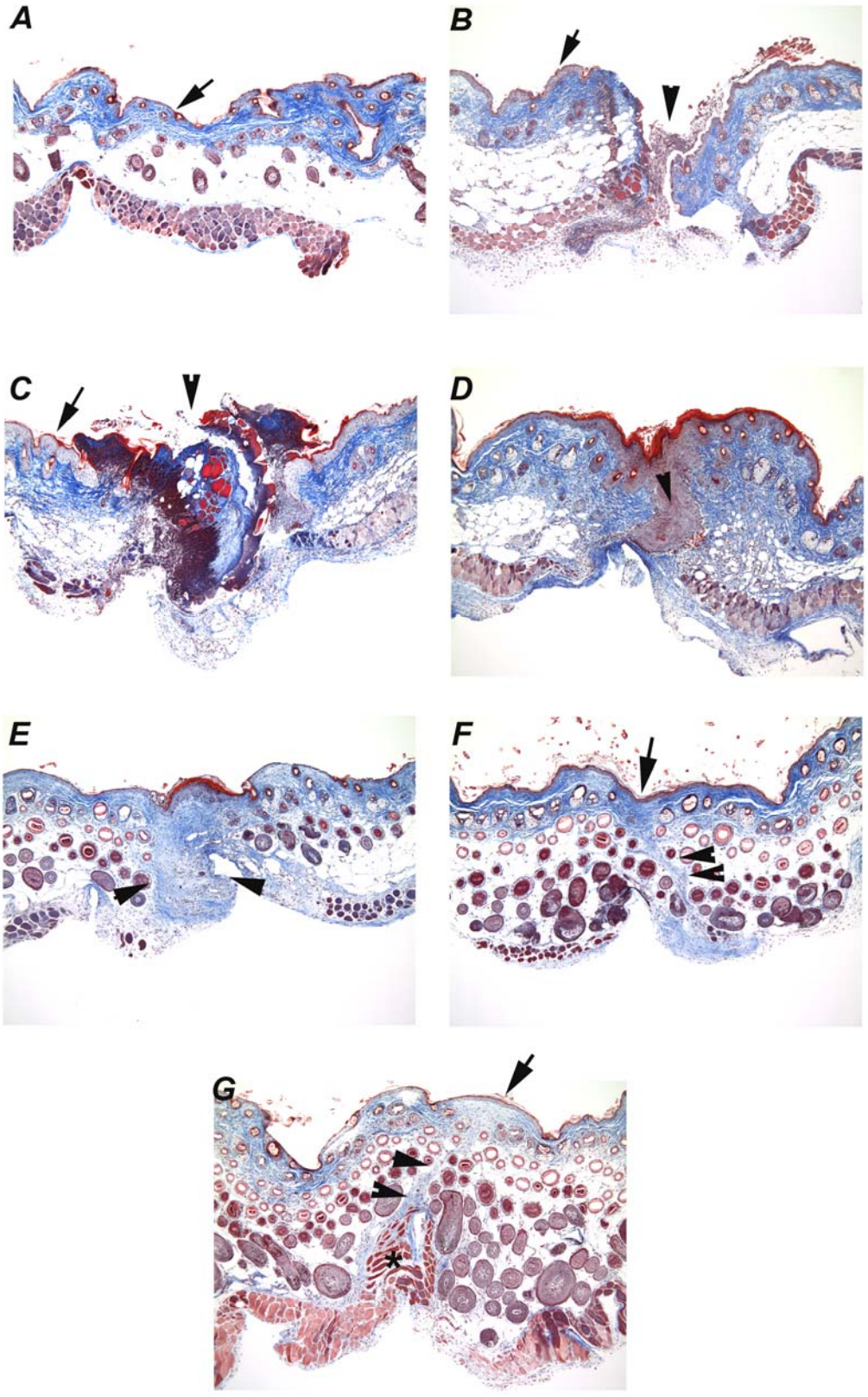

Figure 5.1

Figure 5.2. Immunochemical localization of pAkt and proliferating cells during cutaneous wound healing. Immunochemical localization of pAkt and PCNA were evaluated in serial sections of skin isolated from FVB/N mice at 48 hr ***(A-C; A'-C', respectively)***, at day 5 ***(D-F; D'-F', respectively)***, and day 21 ***(G-I; G'-I', respectively)***. *Arrows* indicate basal cell keratinocytes, whereas *arrowheads* indicate suprabasal keratinocytes. (A-A', D-D', G-G') photographs are at an original magnification of 160x. All other photographs are at a magnification of 500x.

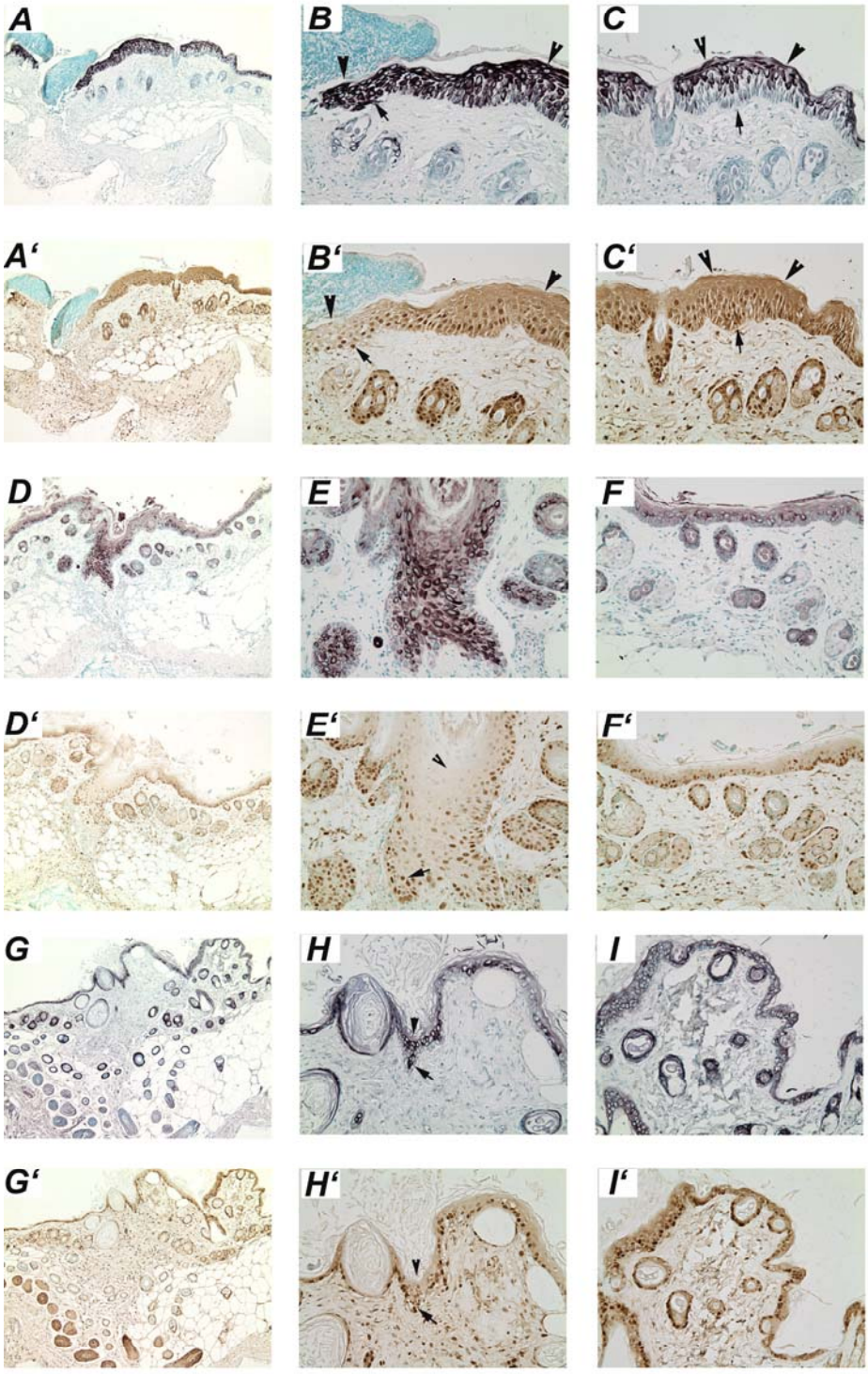

Figure 5.2

Figure 5.3. Localization pmTOR during cutaneous wound healing. At 12 hr following wounding ***(A-C)***, pmTOR staining was nominal within epidermal keratinocytes at the wound margins ***(B)*** and distal to the wound ***(C)***. At day 5 ***(D-F)*** and day 9 ***(G-I)*** following wounding, pmTOR immunoreactive protein was present in keratinocytes within the reepithelialized wound site ***(E, arrow; H)***. The intensity of pmTOR staining was reduced in keratinocytes that are distal to the wound site ***(F, arrowhead; I)***. At day 21 following wounding ***(J-K)***, only few epidermal keratinocytes contained pmTOR ***(K)***. (A, D, G, J) photographs are at an original magnification of 125x. All other photographs are at an original magnification of 320x.

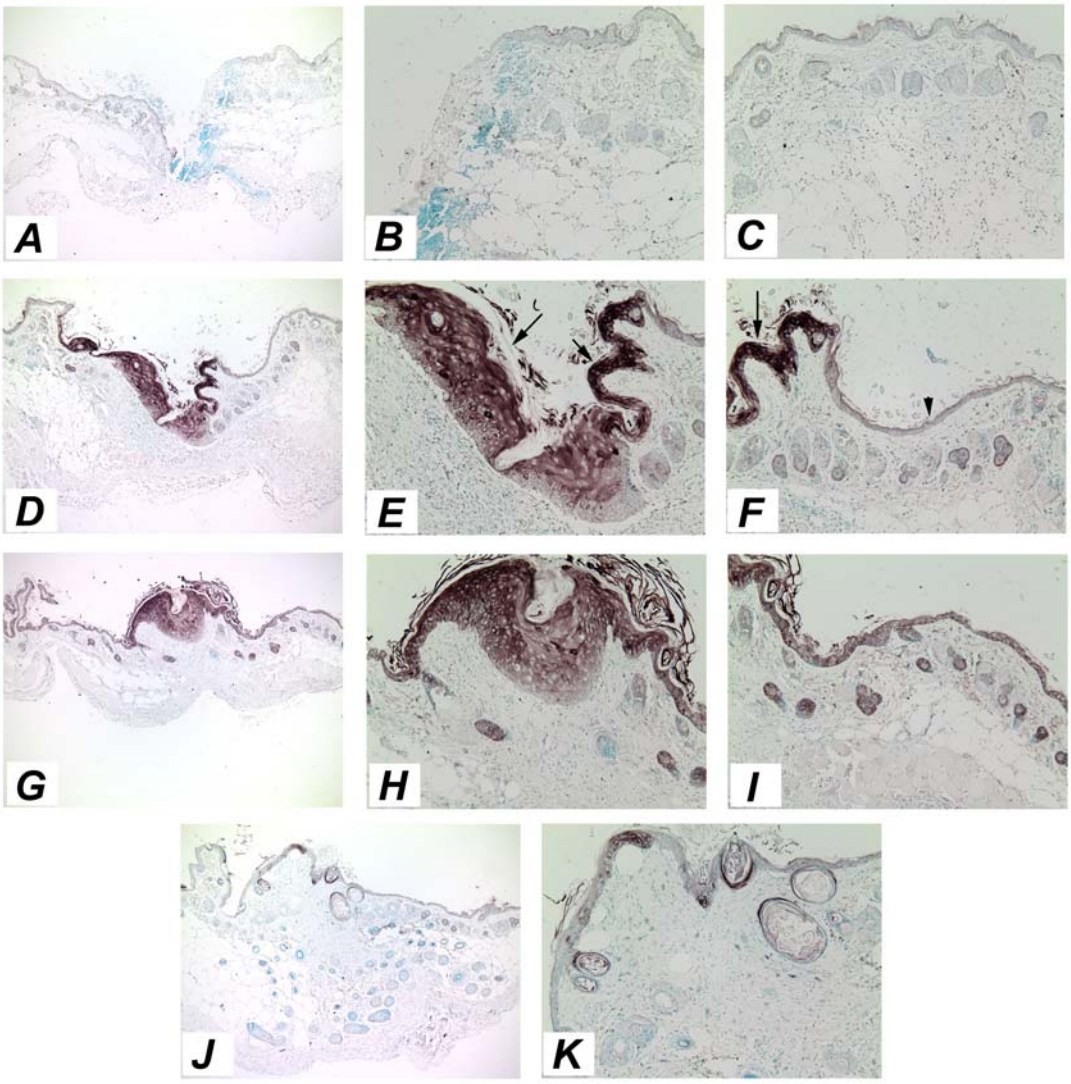

Figure 5.3

Figure 5.4. Localization of K15$^+$ and CD34$^+$ keratinocytes during cutaneous wound healing. Representative immunofluorescent photomicrographs of nucleated cells (DAPI-associated blue fluorescence) ***(B and E)*** that contain K15 ***(A and D)*** (vector red-associated red fluorescence) at the wound site *(A)* and in skin adjacent to the wound *(D)* in dorsal skin isolated from FVB/N mice at day 5 following wounding and subjected to confocal microscopy for imaging. ***(C and F)*** represents K15 staining merged with DAPI to highlight the location of nucleated cells in at the wound site (C) and in skin adjacent to the wound (F). (A-F) photographs are at 100x magnification). ***(G-J)*** Immunochemical localization of CD34$^+$ cells was evaluated in skin sections isolated at 48 hr *(G-H)* and day 5 *(I-J)* following wound healing at the wound site *(G and I)* and in hair follicles adjacent to the wound site *(H and J)*. (G-J) photographs are at 200x. Abbreviations: Bu, bulge; Blb, bulb; HS, hair shaft; Epi, epidermis; SG, sebaceous gland.

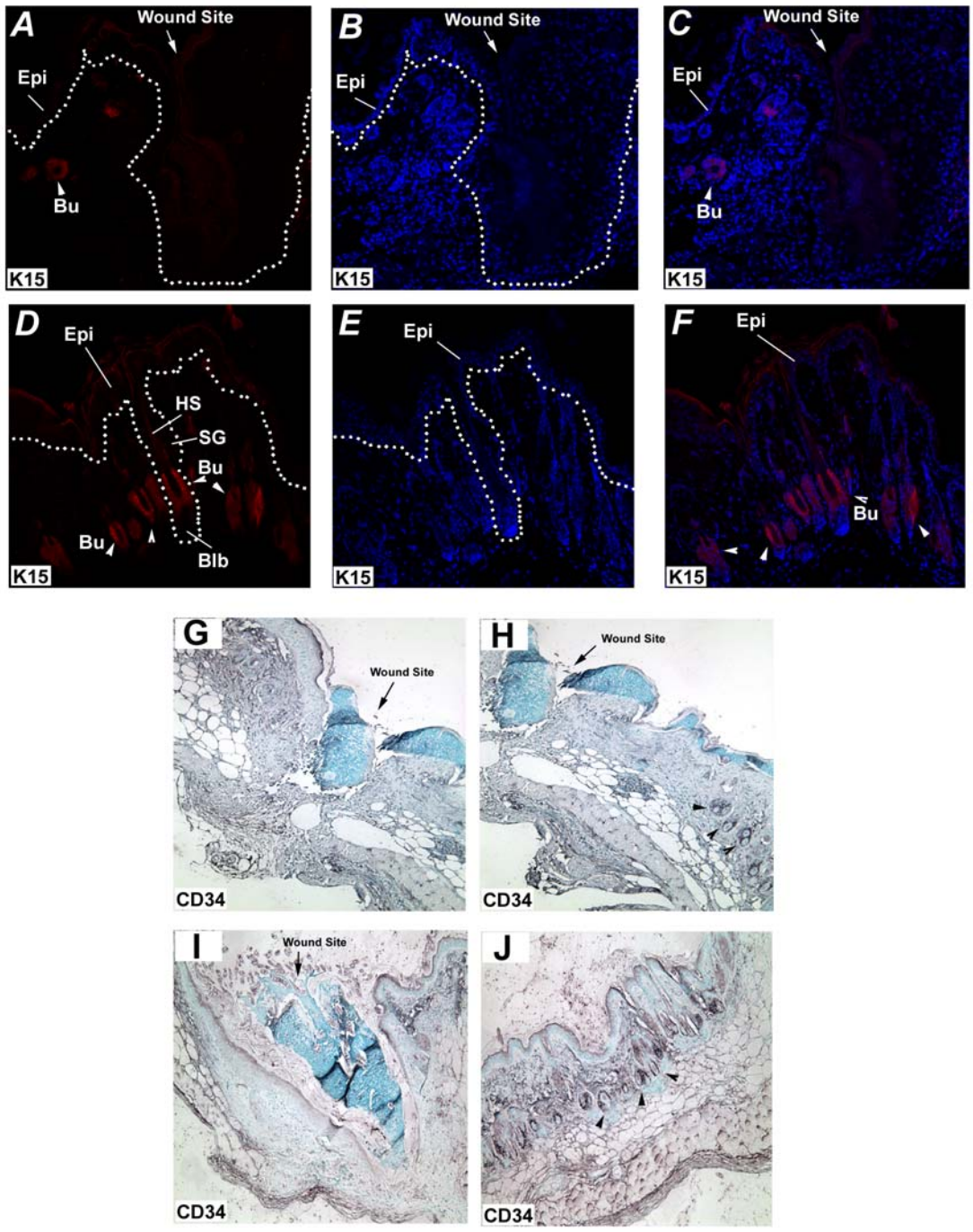
A
Wound Site
Epi
Bu
K15
B
Wound Site
Epi
K15
C
Wound Site
Epi
Bu
K15
D
Epi
HS
SG
Bu
Bu
BIb
K15
E
Epi
K15
F
Epi
Bu
K15
G
Wound Site
CD34
H
Wound Site
CD34
I
Wound Site
CD34
J
CD34

Figure 5.4

Figure 5.5. Localization of CD34, pAkt, and pmTOR in cells within the bulge niche during wound healing. Double immunofluorescence and confocal microscopy were used to identify nucleated cells (***C***; DAPI-associated blue fluorescence) that contained both CD34 (***A***; Alexa-647-associated red fluorescence) and pAkt (***B***, Alexa-555-associated green fluorescence) in hair follicles adjacent to the wound site in dorsal skin isolated from FVB/N mice at 12 hr following wounding. ***(D)*** CD34 *(red)* staining was merged with pAkt *(green)* and DAPI *(blue)* to reveal co-localization of CD34 and pAkt in KSC located in the outer root sheath of the bulge. (A-D) photographs are at 400x magnification. ***(E and F)*** Immunochemical localization of pAkt ***(E)*** and pmTOR ***(F)***, respectively, was evaluated in serial skin sections isolated at day 5 following wound healing in hair follicles adjacent to the wound site. While pAkt was present in both ORS and IRS of the Bu of hair follicles *(E)*, pmTOR localized to the ORS only *(F)*. (E-F) photographs are at 400x. *Abbreviations:* Bu, bulge; Blb, bulb; HS, hair shaft; Epi, epidermis; ORS/IRS, outer/inner root sheath.

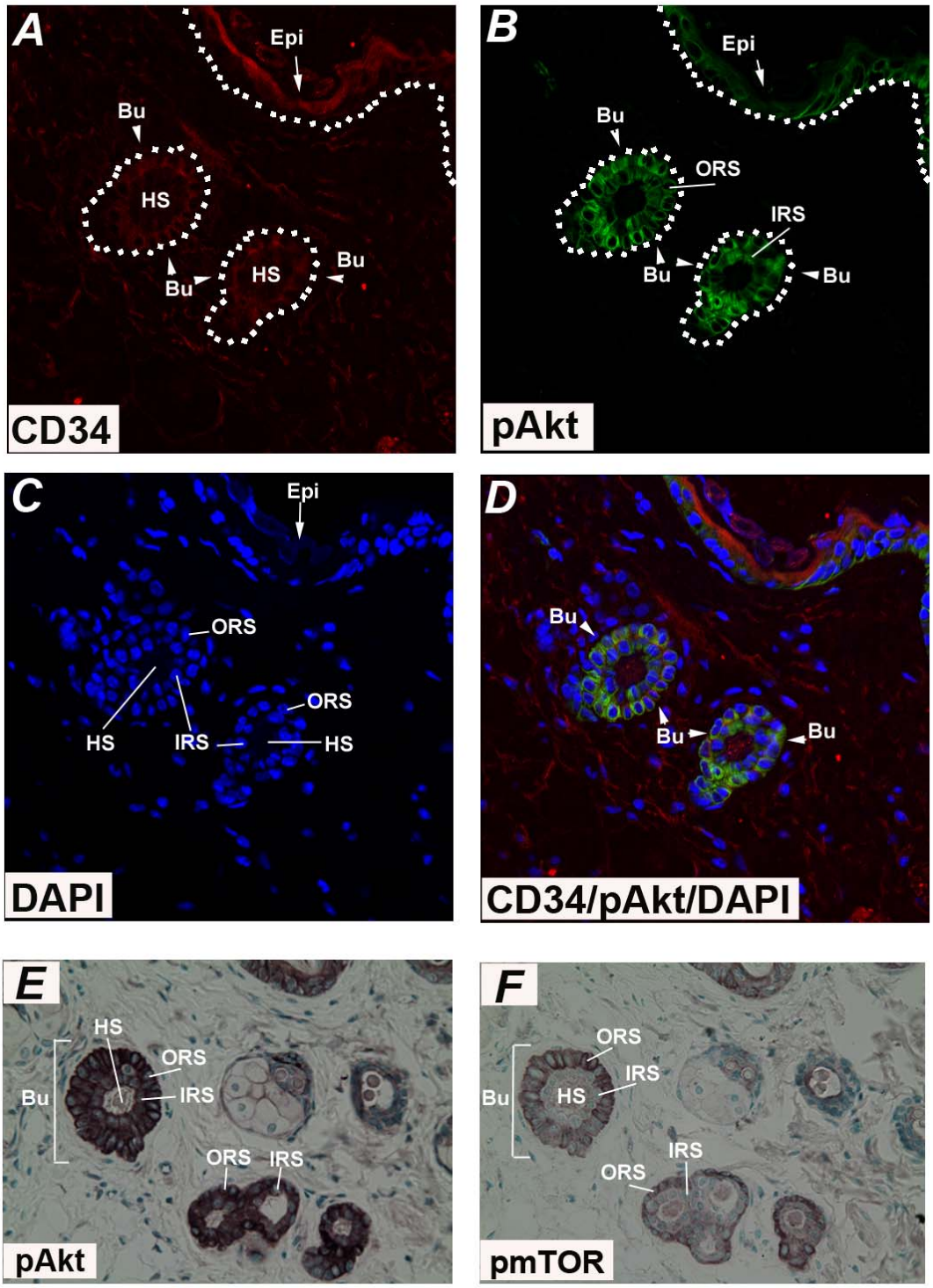
A
Epi
Bu
HS
Bu
HS
Bu
CD34
B
Epi
Bu
ORS
IRS
Bu
Bu
pAkt
C
Epi
ORS
ORS
HS
IRS
HS
DAPI
D
Bu
Bu
Bu
CD34/pAkt/DAPI
E
HS
ORS
Bu
IRS
ORS
IRS
pAkt
F
ORS
IRS
Bu
HS
IRS
ORS
pmTOR

Figure 5.5

CHAPTER 6

TARGETING HYPERPHOSPHORYLATION OF 4E-BP1 BY DUAL BLOCKADE OF PHOSPHOINOSITIDE 3-KINASE (PI3-K) AND MAMMALIAN TARGET OF RAPAMYCIN (MTOR) IN HUMAN BREAST TUMOR CELLS

6.1. Abstract

The present study compared the effects of the phosphoinositide 3-kinase(PI3K) selective inhibitor, LY294002, alone and in combination with the selective mammalian target of rapamycin (mTOR) inhibitor, rapamycin, on human Hs578T and MCF-7 breast tumor cell proliferation and phosphorylation of downstream targets of PI3K and mTOR, including, 4E-BP1 and cyclin D1. Using the highly invasive and metastatic human Hs578T breast tumor cell line and the slow growing and non-invasive human MCF-7 breast tumor cell line, the effects of LY294002 (25 μM) and rapamycin (1000 nM) were evaluated on the proliferation of these breast tumor cell lines at 72 and 96 hr. Western blot analysis was used to examine the effect of exposure of these agents on phosphorylation of Akt at serine-473, mTOR at serine-2448, 4E-BP1 at threonine-37/46, and total cyclin D1 protein levels. Cell proliferation of Hs578T and MCF-7 breast tumor cells was significantly ($p<0.001$) inhibited by the combination of LY294002 and rapamycin compared to the effect on proliferation by either agent alone. The combination of LY294002 and rapamycin also inhibited hyperphosphorylation of the slower migrating (δ, γ, β) species of phospho-4E-BP1, and significantly decreased cyclin D1 protein levels. These studies demonstrate that molecules downstream of PI3K/Akt and mTOR, including hyperphosphorylated forms (δ, γ) of 4E-BP1, may provide therapeutic targets for inhibition of breast tumor cell proliferation.

6.2. Introduction.

Akt, also known as protein kinase B (PKB), is a core component of the phosphoinositide 3-kinase (PI3K) signaling pathway [302, 303]. Activation of this signaling pathway has been shown to provide a survival advantage to cells under hypoxic and anoxic conditions [431]. Following activation of PI3K and generation of the membrane-bound lipid, phosphatidylinositol 3,4,5-triphosphate (PI-3,4,5-P_3), Akt is recruited to the inner surface of the plasma membrane [232], where Akt becomes fully activated by phosphorylation at two amino acid residues, serine-473 (Ser-473) [235, 306] and threonine-308 (Thr-308) [234]. 2-(4-morpholinyl)-8-phenylchrome (LY294002) is a competitive inhibitor for the ATP binding site of PI3K and leads to inhibition of Akt phosphorylation [239, 240]. Preclinical studies using human breast tumor cells demonstrated that LY294002 inhibits both their survival [443] and proliferation [444, 445].

The primary studies that have implicated the Akt signaling pathway in breast tumorigenesis have used murine mammary gland models. Under normal conditions, the process of mammary gland involution involves extensive apoptotic cell death and regression of the lobular structures in the terminal ducts [446]. Transfection of a constitutively active Akt, which contained an amino-terminal myristolation sequence (myr-Akt), into mouse mammary glands resulted in hyperplastic secretory epithelial cells and delayed mammary gland involution following cessation of lactation [447]. Other studies confirmed that constitutively active Akt can serve as an oncogene [448], suggesting that Akt promotes survival of cells that would otherwise undergo apoptosis. Other studies reporting that primary invasive breast cancer tissues have increased Akt phosphorylation and elevated Akt kinase activity are consistent with the hypothesis that Akt is involved in breast tumorigenesis [448, 449].

The ability of Akt to regulate cell proliferation is associated with its phosphorylation of the mammalian target of rapamycin (mTOR) at Ser-2448 [256, 267, 309, 329]. mTOR was initially identified as the cellular target of the pharmacological agent rapamycin [257], also known as sirolimus or Rapamune [258, 259]. Rapamycin is a lipophilic macrolide, which was first isolated from a strain of *Streptomyces hygroscopicus* that is indigenous to Easter Island (also known as Rapa Nui) [260]. Due to its ability to block T lymphocyte activation [450], rapamycin was initially approved as an immunosuppressant drug to prevent tissue rejection following organ transplantation

[451]. This agent was found to possess potent anti-tumor activity against spontaneous tumors that occur in transplant patients [452]. Rapamycin binds to a cytoplasmic receptor, FK506-binding protein-12 (FKBP12) [261], which interacts with the FKBP12-rapamycin binding (FRB) domain of mTOR [262], resulting in inhibition of mTOR kinase activity. In preclinical studies and human tumor xenograft models, rapamycin and its ester analog, cell cycle inhibitor-779 (CCI-779; Wyeth Pharmaceuticals, Collegeville, PA), was found to have significant anti-proliferative activity [453]. In a Phase II clinical study, CCI-779 was found to have potent anti-tumor activity in patients with locally advanced or metastatic breast cancer [454].

Although mTOR has been shown to act as a direct substrate for Akt [256, 267], the identity of upstream activator(s) of mTOR remains elusive [268, 272]. Akt and mTOR have been shown to be activated by parallel pathways, rather than being activated in a linear manner [453, 455]. Signaling molecules that have recently been shown to activate Akt and TOR in parallel include protein kinase C-η (PKCη) [263], a calcium-independent PKC isoform that is activated by the membrane bound lipids PI-3,4,5-P_3 following activation of PI3K [456, 457] (Figure 8).

Following its activation, mTOR stimulates phosphorylation of 70 KDa ribosomal protein S6 kinase (p70 S6K) enzyme at Thr-389. Once activated, p70 S6K stimulates entry of cells into the S-phase of the cell cycle by phosphorylating the 40S ribosomal protein, S6. This sequence of events leads to an increased rate of initiation of translation of mRNAs that encode ribosomal proteins and translation elongation factors [273, 311, 312]. In addition, mTOR phosphorylates a second isoform of p70 S6K, which has been defined as the 85 KDa ribosomal protein S6 kinase (p85 S6K), at Thr-412 [458]. These p70 S6K and p85 S6K isoforms are generated from alternative translation start sites on the same mRNA. While p70 S6K resides in the cytosol, p85 S6K is constitutively targeted to the nucleus due to the presence of additional 23 amino acid residues at its N-terminus [458]. Although the mechanism by which p85 S6K mediates cell cycle progression has not yet been completely defined, activation of p85 S6K is required for entry into the S-phase of the cell cycle [458].

In addition, mTOR initiates translation of proteins that are required for entry into the G1-phase of the cell cycle, such as cyclin D1, by regulating the activity of the eukaryotic initiation factor 4E, eIF4E [280]. The translational activity of eIF4E is negatively regulated by eIF4E-binding protein 1 (4E-BP1). mTOR stimulates eIF4E

activity by phosphorylating 4E-BP1 at Thr-37 and Thr-46 residues [278, 279, 313]. When 4E-BP1 is in its α form, which is hypophosphorylated, 4E-BP1 binds with high affinity to eIF4E. As a consequence, the α form of 4E-BP1 inhibits eIF4E-dependent mRNA translation. In contrast, the presence of δ and γ forms of 4E-BP1, which are hyperphosphorylated, inhibits the association between 4E-BP1 and eIF4E. This release of eIF4E by the δ and γ forms of 4E-BP1 leaves eIF4E free for initiation of protein translation [281].

The definition of the role(s) of hypophosphorylated α form of 4E-BP1 in inhibiting proliferation of breast tumor cells is only now emerging [459]. Human breast carcinomas have been reported to contain high protein levels of eIF4E [460-462]. Transfection of the human MCF-7 breast tumor cell line with a constitutively active form of 4E-BP1 that is resistant to mTOR-dependent phosphorylation resulted in cell cycle arrest and a decrease in cyclin D1 protein levels [463]. These results suggest that targeting mTOR, which controls phosphorylation of the hypophosphorylated α form of 4E-BP1, may be an effective means of inhibiting proliferation of human breast tumors.

Studies that have examined the effects of the combination of LY294002 and rapamycin have been limited to human prostate [464], human non-small cell lung cancer cells [465], and T-lymphocytes [466]. There have been no studies to date that have evaluated the effects of dual inhibition of PI3K/Akt and mTOR signaling pathways on proliferation of human breast tumor cells. In the present study, Hs578T cells were chosen as a representative of highly invasive and metastatic human breast tumor cells, which lost their expression of the cell adherence marker E-cadherin and acquired mesenchymal-like characteristics, including the expression of the intermediate filament protein vimentin and the acquisition of a fibroblast-like phenotype [467]. Hs578T cells have been shown to contain constitutively activated Akt in the absence of serum [449]. MCF-7 cells were chosen as a representative of slow-growing, and poorly invasive human breast tumor cells, and, in contrast to Hs578T cells, MCF-7 cells express E-cadherin and grow as interconnected colonies of polygonal cells [468]. MCF-7 breast tumor cells contained a low basal level of constitutive Akt kinase activity [469]. Stable transfection of MCF-7 cells with a constitutively active Akt resulted in a higher rate of proliferation and formation of significantly more colonies in soft agar compared to parental MCF-7 cells [470].

Taken together, these previous studies indicate that activated Akt regulates proliferation and may be involved in invasive activities in breast tumor cells. The goal of the present study was to define the roles of downstream effectors of Akt and mTOR, including hyperphospho-4E-BP1, in human Hs578T and MCF-7 breast tumor cells proliferation using the PI3K/Akt inhibitor LY294002 and the mTOR inhibitor, rapamycin.

6.3. Materials and Methods.

6.3.1. Cell lines and cultures. Human Hs578T and MCF-7 breast tumor cells were purchased from American Type Culture Collection (ATCC, Manassas, VA). Hs578T cells were maintained in DMEM-high glucose medium supplemented with 10% heat inactivated fetal bovine serum (FBS) (Invitrogen, Carlsbad, CA), 100 units/ml penicillin/streptomycin, and 10 μg/ml insulin (Invitrogen), in a 37°C humidified atmosphere with 5% CO_2. MCF-7 cells were maintained in DMEM-HEPES medium supplemented with 10% heat inactivated FBS, 0.1% gentamycin (Invitrogen), and 1% Nystatin (Sigma, St. Louis, MO), in a 37°C humidified atmosphere with 5% CO_2.

6.3.2. Quantitation of MCF-7 and Hs578T cell number. Hs578T and MCF-7 breast tumor cells were grown in 96-well tissue culture plates (1.25-80 x 10^3 cells per well) as described above and Alamar blue (10%; Biosource International, Carmarillo, CA) was added to the media. Following 24 hr of incubation of cells with Alamar blue, absorbance was measured as optical density (OD) at 570 nm and 600 nm. The percent of Alamar blue dye reduction was used as a measure of cell proliferation and was calculated according to manufacturer's instructions. Cell number was evaluated in at least 8 samples.

6.3.3. Cell treatment and analysis of cell number. Hs578T and MCF-7 cells were seeded in 24-well plates at a density of 3 x 10^4 cells per well. DMSO (< 1%) was used to dissolve both LY294002 and rapamycin, and served as the solvent control. At 24 hr following initial plating, medium was removed and cell monolayers were incubated with fresh medium that contained either LY294002 (25 μM; Sigma), rapamycin alone (1000 nM; Sigma), or the combination of LY294002 (25 μM) and rapamycin (1000 nM) for 72 hr or 96 hr in the presence of 10% FBS. Cells were washed with phosphate-buffered saline (PBS) and then harvested by gentle trypsinization. Cell number was determined by direct cell counts using a hemocytometer, with each sample assayed in triplicates.

6.3.4. Protein isolation. Hs578T and MCF-7 cells were seeded at a density of 1 x 10^5 cells per 100-mm plate and grown to 80% confluence prior to treatment with either LY294002 (25 μM), rapamycin (1000 nM), or the combination of LY294002 (25 μM) and rapamycin (1000 nM) for 96 hr in media containing 10% FBS. For serum-starvation

conditions, Hs578T and MCF-7 cells were incubated in serum-free medium for 96 hr. Cells were lysed with cold lysis buffer (150 mM NaCl, 10 mM Tris-HCl pH 7.5, 1% Triton X-100, 1 mM Na_3VO_4, 1 mM PMSF, 10 μg/ml leupeptin, 10 μg/ml aprotinin). Cells were scraped and whole lysates were clarified by centrifugation. Proteins were normalized using the BIO-RAD protein assay (BIO-RAD, Hercules, CA) and bovine serum albumin (BSA) as a standard. Samples were stored at -80^{o}C until Western blot analysis was performed.

6.3.5. Western blot analysis. Methods to analyze equal aliquots of total protein extracts (15-22 μg) by Western blotting were as previously described [363]. The following primary antibodies (Cell Signaling, Beverly, MA) were used in 1% BSA in PBS containing 0.1% (v/v) Tween-20 (PBST) overnight at 4^{o}C: rabbit anti-phospho-Akt-Ser-473 (1:500), anti-phospho-mTOR-Ser-2448 (1:500), anti-phospho-p70 S6K-Thr-389/phospho-p85 S6K-Thr-412 (1:500), anti-phospho-4E-BP1-Thr-37/Thr-46 (1:1500), and anti-cyclin D1 (1:1500). Blots were then incubated for 1 hr at room temperature with horseradish peroxidase (HRP)-linked goat anti-rabbit IgG (1:2000; Jackson ImmunoResearch Laboratories, West Grove, PA) in PBST containing 5% non-fat dried milk powder. Signals were visualized using the ECL+Plus Western Blotting Detection System (Amersham, Piscataway, NJ). Phospho-p70 S6K-Thr-389/phospho-p85 S6K-Thr-412 blots were incubated with ECL+Plus for 5 min, then exposed to Hyperfilm ECL (Amersham) for 1 sec or 10 sec as a short and long exposure times, respectively. Phospho-4E-BP1-Thr-37/Thr-46 blots were incubated with ECL+Plus for 40 sec and exposed to Hyperfilm ECL for 32 sec or 1 min 32 sec as a short and long exposure times, respectively. Blots were subsequently stripped and re-probed with rabbit anti-Akt (1:1000), anti-mTOR (1:500), anti-p70 S6K/p85 S6K (1:500), or anti-4E-BP1 (1:500). To verify equal loading, blots were re-probed with mouse anti-β-actin (1:5000, Sigma) for 1 hr at room temperature. Blots were then incubated with HRP-linked sheep anti-mouse IgG (1:4000, Amersham) for 30 min at room temperature. Western blots were scanned and band intensities analyzed using NIH Image 1.62 software, and each cell line was assayed in two different samples.

6.3.6. Statistical analysis. Significant differences between two groups were determined using unpaired one-tailed Student's *t*-test. Comparisons of three or more groups were

conducted using One-way Analysis of Variance (ANOVA) on ranks for non-parametric comparisons, with Student-Newman-Keuls *post-hoc* analysis (GraphPad Software, San Diego, CA). To evaluate significant comparisons between untreated cells and cells treated with LY294002 and/or rapamycin in Hs578T or MCF-7 cells, One-way ANOVA with *post-hoc* Dunnet test was used. Results were expressed as mean ± standard error of mean (SEM), and significance was defined as $p<0.05$.

6.4. Results.

6.4.1. Comparison of human Hs578T and MCF-7 breast tumor cell number. Number of human Hs578T and MCF-7 breast tumor cells was determined at 24 hr following incubation of cells using Alamar blue (Figure 6.1). At 24 hr after plating at an initial density of 20000-40000 cells per well, Hs578T cells were in the plateau phase of growth while MCF-7 cells were in the exponential phase of growth.

6.4.2. Effects of LY294002 and rapamycin on proliferation of human Hs578T and MCF-7 breast tumor cells. The combination of 25 μM LY294002 and 1000 nM rapamycin significantly ($p<0.001$) inhibited the proliferation of both Hs578T and MCF-7 cells at both 72 hr (Figure 6.2 A and B) and 96 hr (Figure 6.2 C and D) compared to control cells treated only with the vehicle DMSO. The most significant anti-proliferative effects were observed at 96 hr following exposure of MCF-7 cells to the combination of LY294002 and rapamycin compared MCF-7 cells treated with LY294002 alone ($p<0.05$) or rapamycin alone ($p<0.001$) (Figure 6.2 C). Exposure of both Hs578T and MCF-7 cells to 25 μM LY294002 for 96 hr resulted in significantly ($p<0.01$) decreased proliferation compared to treatment of Hs578T and MCF-7 cells with 1000 nM rapamycin alone (Figure 6.2 C and D).

6.4.3. Effects of LY294002 and rapamycin on phospho-Akt-Ser-473 in Hs578T and MCF-7 cells. Western blotting was performed to examine the effects of 25 μM LY294002, 1000 nM rapamycin, and the combination of these two agents on the ratio of phospho-Akt-Ser-473/Akt in Hs578T and MCF-7 cells (Figure 6.3). Untreated human Hs578T breast tumor cells contained 2.9-fold increase in the ratio of phospho-Akt-Ser-473/Akt ($p<0.05$) compared to untreated MCF-7 cells (Figure 6.3 A-C). Serum starvation had no effect on levels of phospho-Akt-Ser-473/Akt in either cell line (Figure 6.3 B and C).

Treatment of Hs578T cells with 25 μM LY294002 alone resulted in a 1.7-fold increase in the ratio of phospho-Akt-Ser-473/Akt compared to untreated Hs578T cells ($p<0.05$) (Figure 6.3 A and C). Treatment of Hs578T cells with 1000 nM rapamycin induced 2.8-fold increase in the ratio of phospho-Akt-Ser-473/Akt compared to untreated cells ($p<0.001$). The combination of 25 μM LY294002 and 1000 nM rapamycin induced a

3.5-fold increase in the ratio of phospho-Akt-Ser-473/Akt in Hs578T cells compared to untreated cells ($p<0.001$).

Treatment of MCF-7 cells with 25 μM LY294002 resulted in a 0.7-fold decrease in the ratio of phospho-Akt-Ser-473/Akt compared to untreated MCF-7 cells ($p<0.05$) (Figure 6.3 A and B). Treatment of MCF-7 cells with 1000 nM rapamycin did not change the ratio of phospho-Akt-Ser-473/Akt compared to untreated cells. The combination of LY294002 and rapamycin completely blocked phospho-Akt-Ser-473 in MCF-7 breast tumor cells (Figure 6.3 A and B).

The significant increase in the ratio of phospho-Akt-Ser-473/Akt induced by the combination of LY294002 and rapamycin in Hs578T cells (Figure 6.3 C) was accompanied by a significant ($p<0.05$) decrease in total Akt protein compared to untreated cells (Figure 6.3 E). Levels of total Akt protein in both Hs578T and MCF-7 cells did not change following exposure to either 25 μM LY294002 or 1000 nM rapamycin alone (Figure 6.3 D and E). Regardless of exposure to LY294002, rapamycin, or the combination of both agents, the amount of β-actin was constant in Hs578T and MCF-7 cells (Figure 6.3 A).

6.4.4. Effects of LY294002 and rapamycin on phospho-mTOR-Ser-2448 in human Hs578T and MCF-7 breast tumor cells. Western blotting was performed to examine the effects of 25 μM LY294002, 1000 nM rapamycin, and the combination of these two agents on the ratio of phospho-mTOR-Ser-2448/mTOR in Hs578T and MCF-7 cells (Figure 6.4). There was no significant difference in the ratio of phospho-mTOR-Ser-2448/mTOR in untreated Hs578T cells compared to untreated MCF-7 cells (Figure 6.4). Withdrawal of serum resulted in 2.8-fold increase ($p<0.01$) in the ratio of phospho-mTOR-Ser-2448/mTOR in Hs578T cells compared to the ratio of phospho-mTOR-Ser-2448/mTOR detected in the presence of serum (Figure 6.4 C). In contrast, withdrawal of serum caused a 0.7-fold decrease ($p<0.05$) in phospho-mTOR-Ser-2448/mTOR in MCF-7 cells compared to levels in the presence of serum (Figure 6.4 B).

Treatment of Hs578T cells with 25 μM LY294002, 1000 nM rapamycin, or the combination of both agents had no significant effects on the ratio of phospho-mTOR-Ser-2448/mTOR (Figure 6.4 C). Exposure of MCF-7 cells to 25 μM LY294002 resulted in a significant decrease ($p<0.01$) in the ratio of phospho-mTOR-Ser-2448/mTOR compared to untreated cells (Figure 6.4 B).

6.4.5. Effects of LY294002 and rapamycin on phospho-p70 S6K-Thr-389 and phospho-p85 S6K-Thr-412-P in human Hs578T and MCF-7 breast tumor cells. Untreated Hs578T cells contained significantly ($p<0.05$) higher levels of the ratio of phospho-p70 S6K-Thr-389/p70 S6K (Figure 6.5 C) compared to untreated MCF-7 cells (Figure 6.5 B), although untreated Hs578T cells contained 2-fold lower basal levels of p70 S6K (Figure 6.5 E) compared to the higher ($p<0.05$) basal levels of p70 S6K in untreated MCF-7 cells (Figure 6.5 D).

Treatment of Hs578T and MCF-7 cells with 25 μM LY294002 (Figure 5 A; long exposure) resulted in significantly decreased ratios of phospho-p70 S6K-Thr-389/S6K compared to untreated cells (Figure 6.5 B and C). Exposure to rapamycin (Figure 6 A; long exposure) resulted in a complete loss of phospho-p70 S6K-Thr-389 in both cell lines, which was similar to the effects of treatment of either of these breast tumor cell lines with the combination of 25 μM LY294002 and 1000 nM rapamycin (Figure 6.5 B and C). The loss of phospho-p70 S6K-Thr-389 in Hs578T cells following exposure to LY294002, rapamycin, or the combination of both agents was associated with an increase in the electrophoretic mobility of total p70 S6K (Figure 6.5 A). Treatment of Hs578T and MCF-7 cells with LY294002, rapamycin, or the combination of both agents resulted in the loss of phospho-p85 S6K-Thr-412 (Figure 6.5 A; long exposure). The combination of 25 μM LY294002 and 1000 nM rapamycin significantly decreased total p70 S6K protein in Hs578T ($p<0.01$; Figure 6.5 E) and MCF-7 cells compared to untreated cells ($p<0.05$; Figure 6.5 D).

6.4.6 Effects of LY294002 and rapamycin on hyperphospho-4E-BP1-Thr-37/46 in human Hs578T and MCF-7 breast tumor cells. Hyperphospho-4E-BP1 resolves into one to four bands during gel electrophoresis representing the phosphorylated α, β, γ, and δ forms of phospho-4E-BP1, with α representing the hypophosphorylated form of 4E-BP1 (Figure 6.6 A).

Untreated Hs578T cells contained high levels of the most hyperphosphorylated species of 4E-BP1, as defined by the presence of the slowest migrating band δ (Figure 6.6 A; short exposure). The presence of hyperphosphorylated δ band persisted in Hs578T cells grown under serum-free conditions (Figure 6.6 A; short exposure). Untreated MCF-7 cells contained lower levels of the hyperphosphorylated δ form of 4E-BP1 (Figure 6.6 A; long exposure) compared to untreated Hs578T cells (Figure 6.6 A;

short exposure). The presence of hyperphosphorylated δ band was completely lost in MCF-7 cells grown under serum-free conditions.

While 25 μM LY294002 induced a complete loss of the most hyperphosphorylated δ form of 4E-BP1 in Hs578T cells (Figure 6.6 A), treatment of Hs578T cells with 1000 nM rapamycin did not completely decrease levels of δ form of 4E-BP1 (Figure 6.6 A; short exposure). Treatment of MCF-7 cells with 25 μM LY294002 resulted in loss of both δ and γ species of 4E-BP1 (Figure 6.6 A; short exposure). Rapamycin also induced the loss of the δ form of 4E-BP1 and a decrease in the intensity of band γ of 4E-BP1 in MCF-7 cells (Figure 6.6 A; long exposure).

The combination of 25 μM LY294002 and 1000 nM rapamycin resulted in an overall complete loss of the hyperphosphorylated forms (δ and γ) of 4E-BP1, with hypophosphorylated α form of 4E-BP1 being the predominant isoform present in both Hs578T and MCF-7 breast tumor cell lines (Figure 6.6 A; long exposure).

6.4.7. Effects of LY294002 and rapamycin on cyclin D1 protein in human Hs578T and MCF-7 breast tumor cells. There was no significant difference in cyclin D1 protein levels in untreated Hs578T cells compared to untreated MCF-7 cells (Figure 6.7 A). Serum starvation had no effect on levels of cyclin D1 in either cell line (Figure 6.7 B-C).

Treatment with either LY294002 or rapamycin alone did not induce any significant changes in cyclin D1 protein levels in both cell lines. Treatment with the combination of 25 μM LY294002 and 1000 nM rapamycin resulted in a significant decrease in cyclin D1 protein in both Hs578T ($p<0.01$; Figure 6.7 C) and MCF-7 ($p<0.05$; Figure 6.7 B) cells compared to untreated cells.

6.5. Discussion

The goal of the present studies was to evaluate the effects of the combination of LY294002 and rapamycin on signaling molecules involved in the PI3K and mTOR pathways and on proliferation of human breast tumor cells. Although MCF-7 and Hs578T cells breast tumor cell lines grew at significantly different rates, exposure to the combination of LY294002 and rapamycin resulted in significant inhibition of proliferation of both these cell lines compared to the anti-proliferative effects of either agent alone. These results suggest that the combination of LY294002 and rapamycin may be able to effectively target a range of human breast tumors at different stages, including non-invasive and slow-growing breast tumor cells that are capable of growth as pleural effusion, as well as invasive and aggressive breast tumors in patients with advanced breast cancer.

Direct comparison of basal levels of the ratio of phospho-Akt at Ser-473/Akt revealed the presence of higher levels of phospho-Akt-Ser-473/Akt in Hs578T cells compared to the low levels of phospho-Akt-Ser-473/Akt in MCF-7 cells. Serum starvation mimics the metabolically stressed breast tumor microenvironment present in expanding breast tumors [471, 472]. Under conditions of serum deprivation, Hs578T and MCF-7 cells maintained phospho-Akt-Ser-473, which suggests that activated Akt may promote survival of both of these human breast tumor cell lines under adverse conditions. The presence of high levels of phospho-Akt-Ser-473/Akt in Hs578T cells did not increase the sensitivity of this cell line to rapamycin. This is in contrast to results from previous studies, which demonstrated that constitutive activation of Akt in BT-20, BT-549, SK-BR3, and MDA-MB-468 human breast tumor cells was associated with increased sensitivity to rapamycin [473].

The observation that LY294002 did not inhibit phosphorylation of Akt at Ser-473 and Thr-308 (Data not shown) in Hs578T cells suggests that the mechanism of Akt phosphorylation in Hs578T cells may occur as a consequence of constitutive activation of upstream kinases, including 3-phosphoinositide-dependent protein kinase-1 (PDK-1), which phosphorylates Thr-308 [234], and integrin-linked kinase-1 (ILK-1), which phosphorylates Ser-473 [307]. Constitutively active Ha-Ras oncogene also induces the constitutive activation of PI3K [474-476] (Figure 6.8). Hs578T cells have been shown to contain a single nucleotide substitution of adenine for guanine in the 12th codon of Ha-*ras* gene, rendering Ha-Ras constitutively active [477], which may explain the present observation of constitutive phosphorylation of Akt in the presence of LY294002,

rendering these cells less sensitive to inhibition of the PI3K/Akt pathway. Additional pathways that mediate phosphorylation of Akt through PI3K-independent mechanisms had been recently reported (Figure 6.8). Constitutively active Ha-Ras as well as PKC have been shown to induce the Raf/mitogen activated-extracellular regulated kinase (MEK)/mitogen-activated protein kinase (MAPK) signaling pathway [478], leading to phosphorylation of Akt through a mechanism that is independent of PI3K activation (Figure 6.8). Cyclic AMP (cAMP) has been also shown to activate Akt through an PI3K-independent mechanism [479]. Taken together, these observations indicate that phosphorylation of Akt in Hs578T cells may occur through mechanisms that are independent of PI3K signaling pathway. Further investigations may provide novel targets in invasive tumor breast cancers that contain constitutively active Akt.

Despite the presence of a constitutive active Akt (phospho-Akt-Ser-473) in Hs578T cells, treatment with LY294002 alone and in combination with rapamycin significantly decreased proliferation, suggesting that phospho-Akt-Ser-473 may play an important but non-essential role in the proliferation of the highly invasive Hs578T cells. In contrast, Akt phosphorylation was significantly inhibited in MCF-7 cells following treatment with LY294002, which confirms that Akt activation is mediated by PI3K signaling pathway in this cell line, as has previously been shown [444].

mTOR activation has recently emerged as a major effector of the IP3K/Akt signaling pathway that is known to regulate protein synthesis and cell cycle progression [267] (Figure 6.8). The present studies evaluated the effects of LY294002 and rapamycin on the ratio of phospho-mTOR-Ser-2448/mTOR. The presence of low basal levels of phospho-Akt-Ser-473/Akt in MCF-7 cells was associated with high levels of phospho-mTOR-Ser-2448/mTOR. Inhibition of phospho-Akt-Ser-473 following exposure of MCF-7 cells to the combination of LY294002 and rapamycin was not associated with inhibition of phospho-mTOR-Ser-2448. Recent evidence suggests that signaling molecules, including PKCη, activate Akt and mTOR in parallel [263] (Figure 6.8). Although phosphorylation of mTOR at Ser-2448 has been previously shown to be directly phosphorylated by Akt [256, 267], the nature of upstream kinase(s) that phosphorylate mTOR at this site remains elusive and requires further investigation [268-272] (Figure 6.8).

The effects of LY294002 and rapamycin on phosphorylation of mTOR downstream target, 4E-BP1, were also evaluated in Hs578T and MCF-7 cells.

Phosphorylation of 4E-BP1 results in a decrease in its electrophoretic mobility, giving rise to four different 4E-BP1 forms, which include the hyperphosphorylated and slowest migrating isoform (δ), the moderately phosphorylated isoforms (β and γ), and the hypophosphorylated and fast migrating species (α) [311]. Under conditions of serum starvation, Hs578T cells maintained the presence of the δ form of 4E-BP1, indicating for the first time the potential role of hyperphospho-4E-BP1 (δ) in stimulating cell cycle progression of breast tumor cells under adverse conditions.

There are no studies to date that have evaluated the effects of LY294002 and rapamycin on mTOR-dependent phosphorylation of 4E-BP1 at Thr-37/46 in human breast tumor cells. While rapamycin induced only a decrease in the δ form of 4E-BP1 in Hs578T cells and the loss of δ form and a decrease in γ form in MCF-7 cells, the combination of LY294002 and rapamycin resulted in complete loss of δ and γ forms of 4E-BP1 and a decrease in levels of β form compared to either agent alone in both cell lines. Previous studies reported that expression of a kinase inactive mutant form of mTOR enhanced the inhibitory effects of rapamycin on phospho-4E-BP1-Thr-37/46 [480]. These results suggest that the use of rapamycin in combination with a direct inhibitor of mTOR kinase domain may exert greater inhibitory effects on phosphorylation of 4E-BP1 than does rapamycin alone. LY294002 has been shown to bind to the catalytic domain of mTOR as well as PI3K (Figure 6.8), thus directly inhibiting mTOR kinase activity [377]. This dual activity of LY294002 may explain the present observation of inhibition of δ, γ, and β forms of 4E-BP1 by the combination of LY294002 and rapamycin.

The effects of LY294002 and rapamycin on phosphorylation of mTOR downstream target, p70 S6K, were also evaluated in Hs578T and MCF-7 cells. Once activated, p70 S6K stimulates entry of cells into the S-phase of the cell cycle by phosphorylating the 40S ribosomal protein, S6 [273, 311] (Figure 6.8). The loss of phospho-p70 S6K-Thr-389 in the presence of rapamycin alone was not associated with a decrease in the proliferation of Hs578T and MCF-7 cells to the diminished levels approaching those observed with the combination of LY294002 and rapamycin. While previous clinical studies used phosphorylation of p70 S6K as an indicative of responsiveness to mTOR inhibitors [481], the present study indicates that inhibition of δ, γ, and β forms of 4E-BP1 may define the effectiveness of PI3K and mTOR inhibitors in

preclinical and clinical studies more effectively than evaluating phoshorylation of p70 S6K.

Hyperphosphorylation and inactivation of 4E-BP1 causes its dissociation from eIF4E, which frees to initiate protein translation (Figure 6.8). The presence of hypophospho-4E-BP1 α isoform in Hs578T and MCF-7 cells following exposure to the combination of LY294002 and rapamycin was associated with a decrease in levels of total Akt protein. These results indicate that mTOR-mediated inactivation of 4E-BP1 may induce translation of Akt (Figure 6.8). Similar observations have been reported in recent studies demonstrating that protein levels of the epidermal growth factor receptor, ErbB3, were significantly reduced in the presence of hypophospho-4E-BP1 α form in human MD-MB-231 breast carcinoma cells following exposure to rapamycin [459]. Taken together, further investigations may provide evidence for the dependence of Akt protein synthesis on the translational activity of eIF4E.

Levels of cyclin D1 protein, an essential key regulator for progression into the G1-phase of the cell cycle [482], has also been shown to be regulated by the translational activity of eIF4E [280] (Figure 6.8). While eIF4E stimulates translation of cyclin D1 [280], glycogen synthase kinase-3β (GSK-3β), which is negatively regulated by Akt-dependent phosphorylation [406], has been shown to induce phosphorylation and subsequent proteolytic degradation of cyclin D1 [253] (Figure 6.8). There was a significant decrease in cyclin D1 protein levels in Hs578T and MCF-7 cells following exposure to the combination of LY294002 and rapamycin. This decrease in cyclin D1 may be a consequence of the abundance of the hypophosphorylated α form of 4E-BP1 following treatment with the combination of LY294002 and rapamycin, thus reducing the translation of cyclin D1 protein, as well as activation of GSK-3β kinase activity, resulting in proteolytic degradation of cyclin D1 protein (Figure 6.8).

In summary, the present study demonstrates that the strategy of dual inhibition of both the PI3K/Akt and mTOR signaling pathways results in maximal inhibition of hyperphosphorylation of 4E-BP1 and exerts a greater anti-proliferative effect on human breast tumor cells of different origins and metastatic activities than either of the agents alone. This finding represents a novel therapeutic strategy, especially in light of recent studies demonstrating the presence of common pathways of resistance that develop following use of endocrine-based therapies for treatment of breast tumors. One mechanism that has recently been shown to confer resistance in breast tumor cells to

estrogen antagonists such as tamoxifen or aromatase inhibitors is through up-regulation of phospho-Akt and phospho-mTOR [443, 444, 483, 484]. The present results indicate that inhibition of both PI3K and mTOR signaling pathways may provide means to counteract the resistance to the development of these endocrine therapies. Since estrogen has been shown to induce activation of the PI3K/Akt signaling pathway in a receptor-independent manner [485], the present observations suggest that this strategy of dual blockade of PI3K/Akt and mTOR may also be applicable to treatment of estrogen receptor (ER)-negative breast tumor cells, with effectiveness similar to that observed with treatment of the ER-negative Hs578T cells with the combination of LY294002 and rapamycin.

Future *in vivo* studies are necessary to evaluate the efficiency of treatment of breast tumors with the combination of LY294002 and rapamycin and the utility of using 4E-BP1 as well as cyclin D1 as biomarkers to predict the responsiveness of breast tumors to treatment with the combination of inhibitors of such signaling molecules as Akt, mTOR, and 4E-BP1.

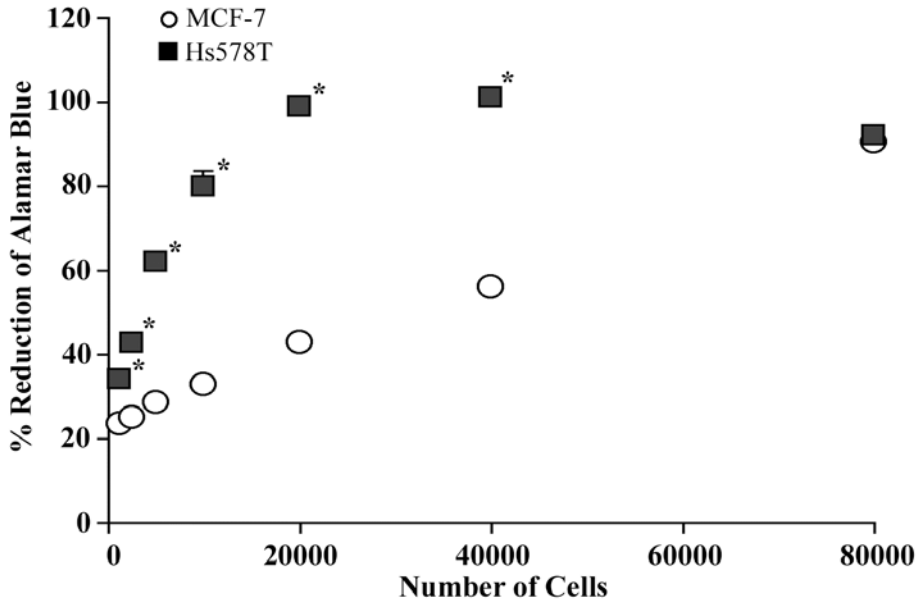

Figure 6.1. Comparison of cell number of Hs578T and MCF-7 cells at 24 hr. Hs578T and MCF-7 cells were plated at (1.25–80) x 10^3 cells in 96-well plates in the presence of 10% Alamar blue, and the percent of dye reduction was determined at 24 hr. Data were presented as mean ± SEM, n=9-10. *, $p<0.0001$ compared to MCF-7 cells at the same cell density.

Figure 6.2. Effects of LY294002 alone and in combination with rapamycin on proliferation of Hs578T and MCF-7 cells. Proliferation was assessed by direct cell count at 72 hr ***(A and B)*** and 96 hr ***(C and D)*** following treatment of Hs578T and MCF-7 cells with 25 μM LY294002 and/or 1000 nM rapamycin. DMSO was used as the vehicle control. Data were expressed as cell number x 10^4 ± SEM, n=3. $^{+}p<0.05$, *p<0.01, **p<0.001 versus same control cell line.

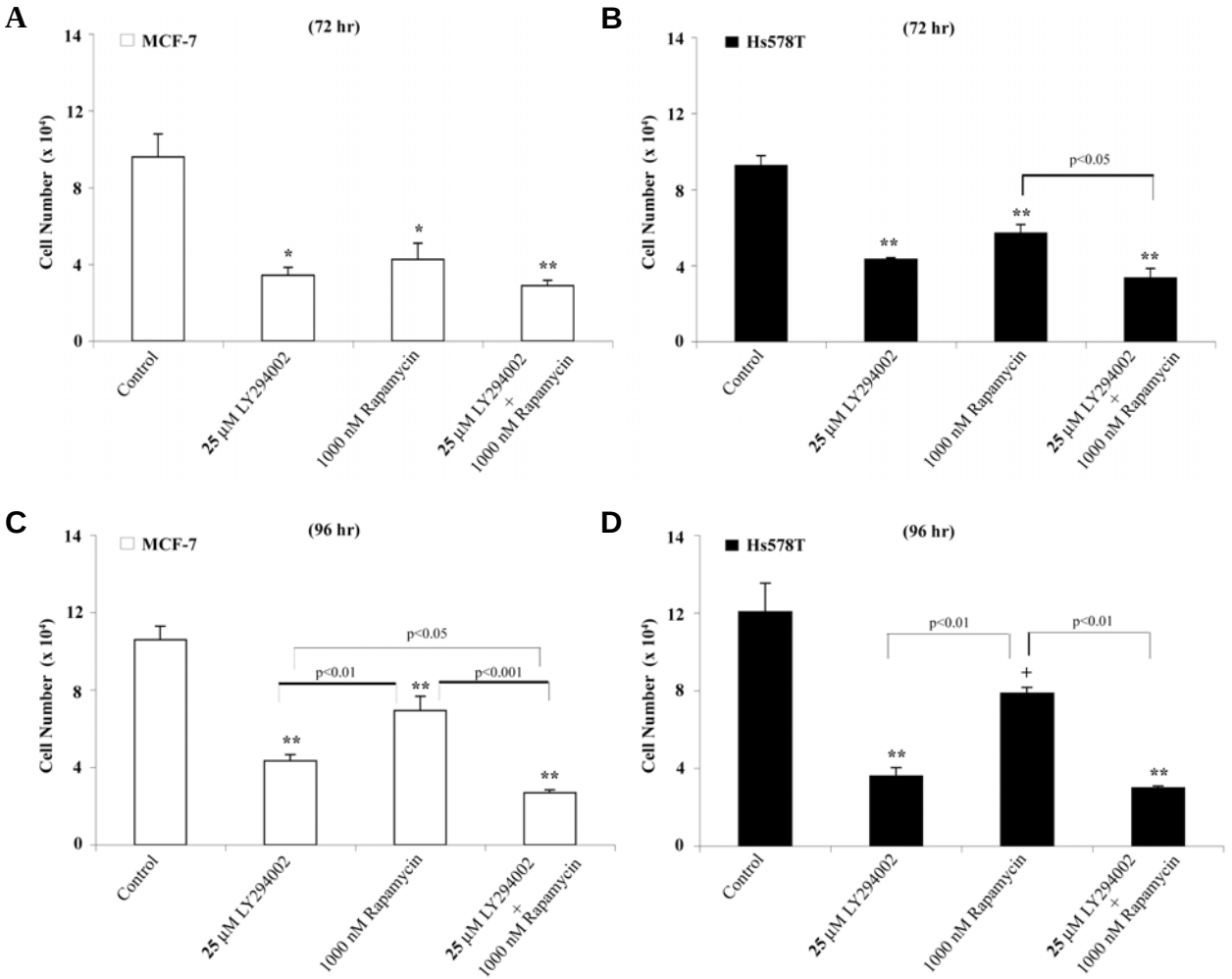
A
MCF-7
(72 hr)
Cell Number (x 10⁴)
14
12
8
4
0
*
*
**
Control
25 μM LY294002
1000 nM Rapamycin
25 μM LY294002 + 1000 nM Rapamycin
B
Hs578T
(72 hr)
p<0.05
**
**
**
C
MCF-7
(96 hr)
p<0.05
p<0.01
p<0.001
**
**
**
D
Hs578T
(96 hr)
p<0.01
p<0.01
+
**
**

Figure 6.2

Figure 6.3. Effects of LY294002 alone and in combination with rapamycin on phospho-Akt-Ser-473. (A) Hs578T and MCF-7 cells were treated with 25 μM LY294002 and/or 1000 nM rapamycin for 96 hr in the presence of 10% FBS. Equal aliquots of total proteins were resolved by 8% SDS-PAGE and immunobloted with anti-phospho-Akt-Ser-473 antibody. Blots were stripped and re-probed with anti-Akt. To verify equal loading of proteins, the blot was reprobed for β-actin. ***(B and C)*** Densitometric analysis of the ratio of phospho-Akt-Ser-473/Akt. Data represent mean ± SEM, n=2. *p<0.05, **p<0.001 versus untreated Hs578T or MCF-7 cells. ***(D and E)*** Densitometric analysis of the ratio of Akt/β-actin. Data represent mean ± SEM, n=2.

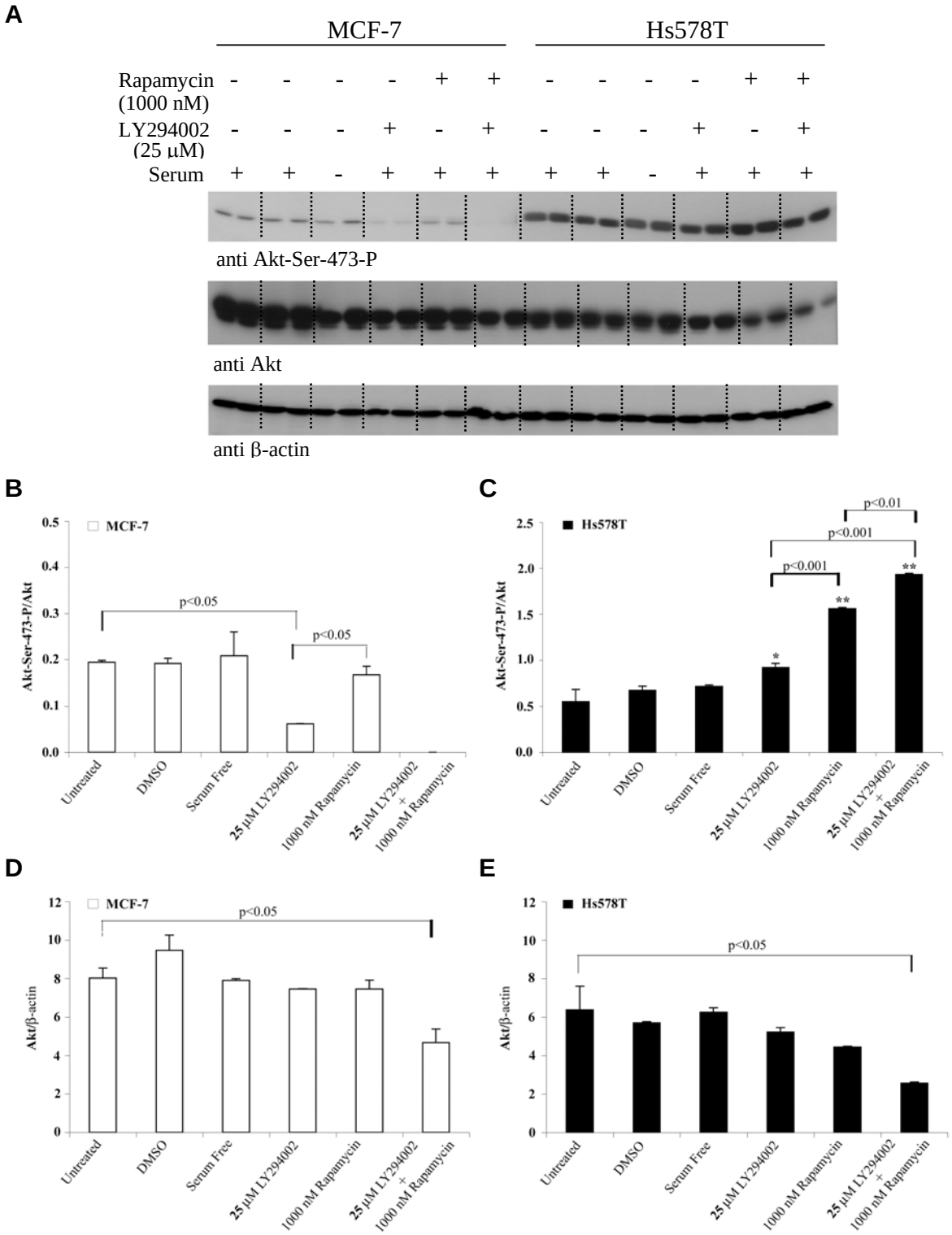
A
MCF-7
Hs578T
Rapamycin (1000 nM)
LY294002 (25 μM)
Serum
anti Akt-Ser-473-P
anti Akt
anti β-actin
B
MCF-7
Akt-Ser-473-P/Akt
p<0.05
p<0.05
C
Hs578T
Akt-Ser-473-P/Akt
p<0.01
p<0.001
p<0.001
D
MCF-7
Akt/β-actin
p<0.05
E
Hs578T
Akt/β-actin
p<0.05
Untreated
DMSO
Serum Free
25 μM LY294002
1000 nM Rapamycin
25 μM LY294002 + 1000 nM Rapamycin

Figure 6.3

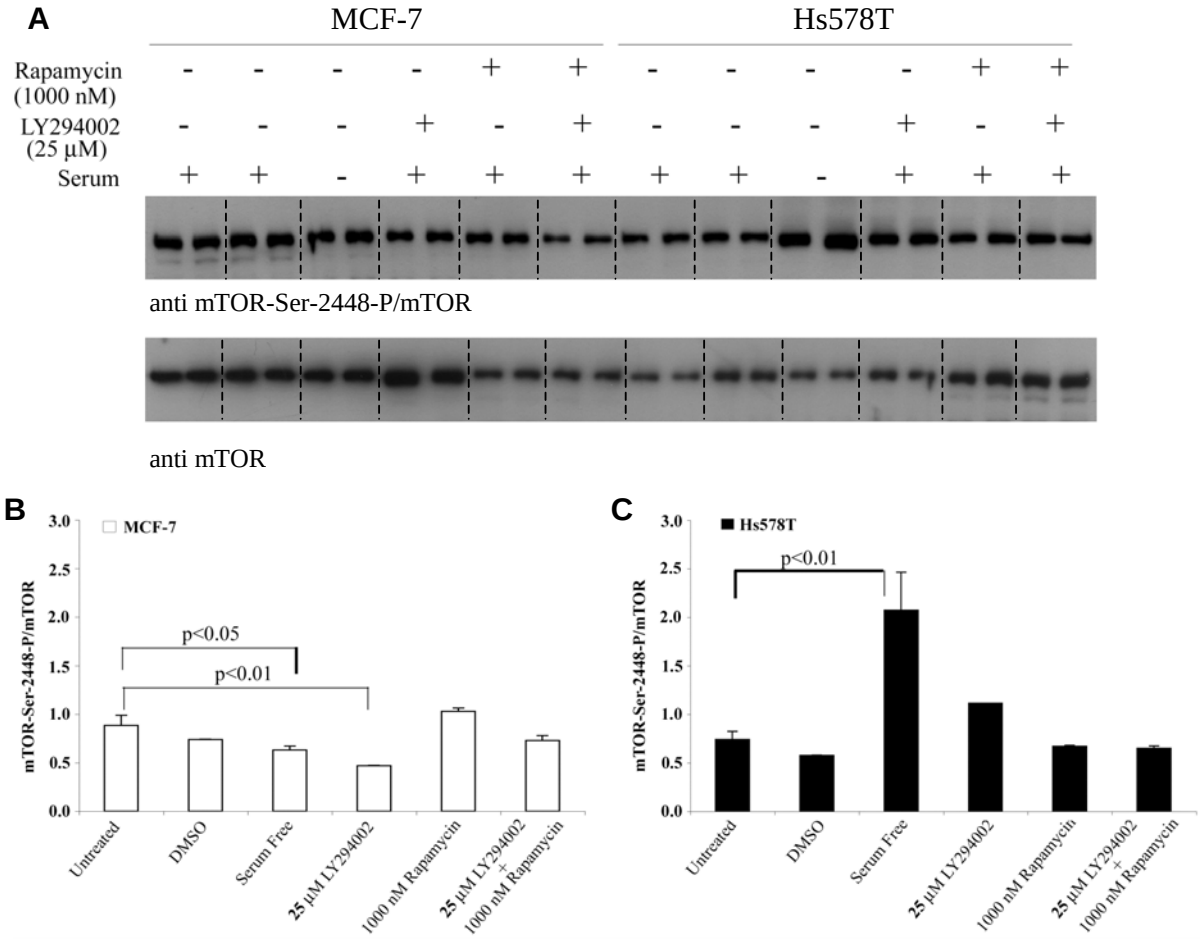

Figure 6.4. Effects of LY294002 alone and in combination with rapamycin on phospho-mTOR-Ser-2448. (A) Hs578T and MCF-7 cells were treated with 25 µM LY294002 and/or 1000 nM rapamycin for 96 hr in the presence of 10% FBS. Equal aliquots of total proteins were resolved by 8% SDS-PAGE and immunobloted with anti-phospho-mTOR-Ser-2448 antibody. Blots were stripped and re-probed with anti-mTOR. ***(B and C)*** Densitometric analysis of the ratio of phospho-mTOR-Ser-2448/mTOR. Data represent mean ± SEM, n=2.

Figure 6.5. Effects of LY294002 alone and in combination with rapamycin on phospho-p70 S6K. (A) Equal aliquots of total proteins of Hs578T and MCF-7 cells that were treated with 25 μM LY294002 and/or 1000 nM rapamycin for 96 hr in the presence of 10% FBS were separated on 8% SDS-PAGE. Blots were probed with anti-phospho-p70 S6K-Thr-389 antibody, stripped and re-probed with anti-p70 S6K. ***(B and C)*** Densitometric analysis of the ratio of phospho-S6K-Thr-389/S6K. Data represent mean ± SEM, n=2. ***(D and E)*** Densitometric analysis of the ratio of S6K/β-actin. Data represent mean ± SEM, n=2.

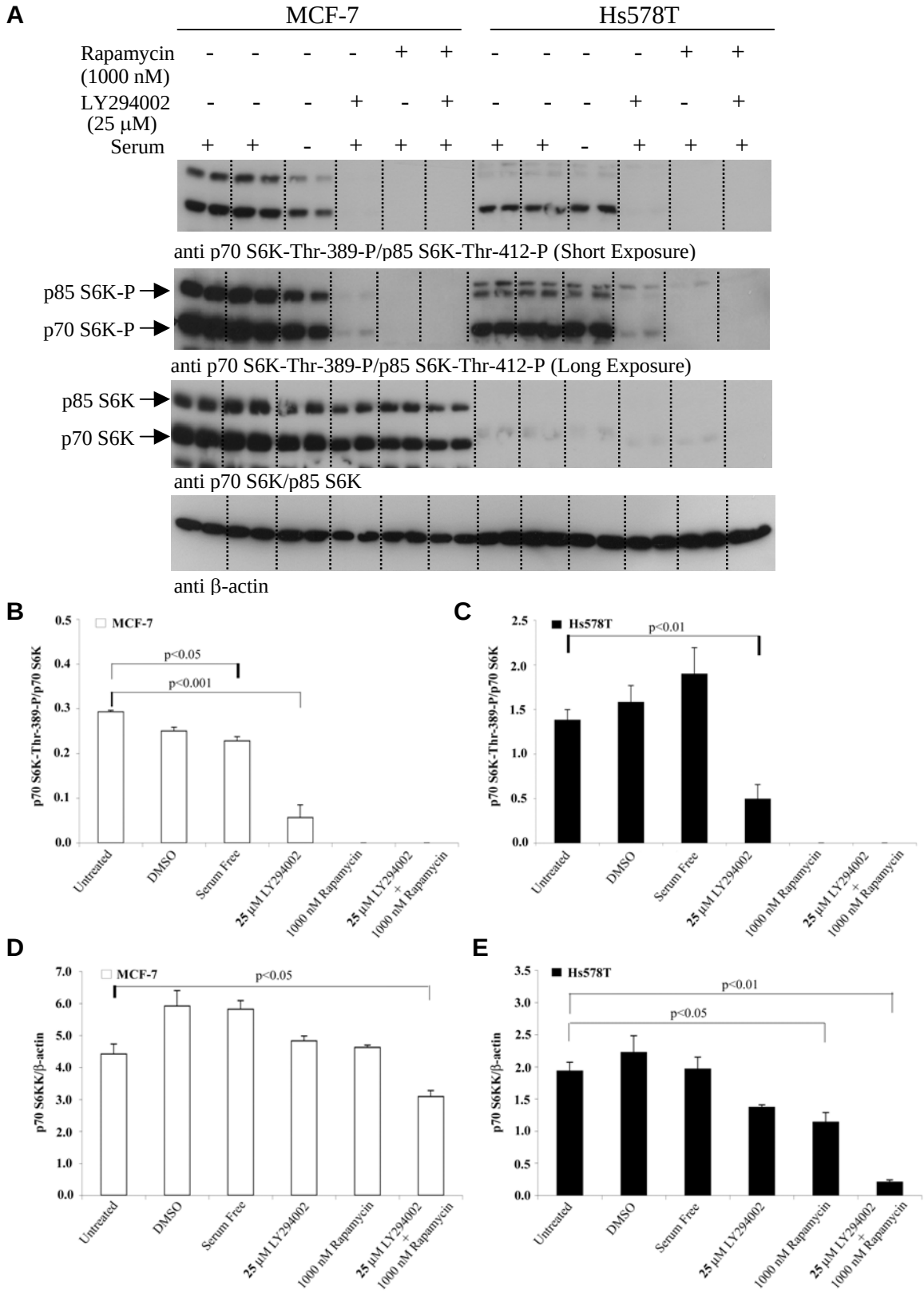
A
MCF-7
Hs578T
Rapamycin (1000 nM)
LY294002 (25 μM)
Serum
anti p70 S6K-Thr-389-P/p85 S6K-Thr-412-P (Short Exposure)
p85 S6K-P
p70 S6K-P
anti p70 S6K-Thr-389-P/p85 S6K-Thr-412-P (Long Exposure)
p85 S6K
p70 S6K
anti p70 S6K/p85 S6K
anti β-actin
B
MCF-7
p70 S6K-Thr-389-P/p70 S6K
p<0.05
p<0.001
C
Hs578T
p<0.01
D
MCF-7
p70 S6KK/β-actin
p<0.05
E
Hs578T
p<0.01
p<0.05
Untreated
DMSO
Serum Free
25 μM LY294002
1000 nM Rapamycin
25 μM LY294002 + 1000 nM Rapamycin

Figure 6.5

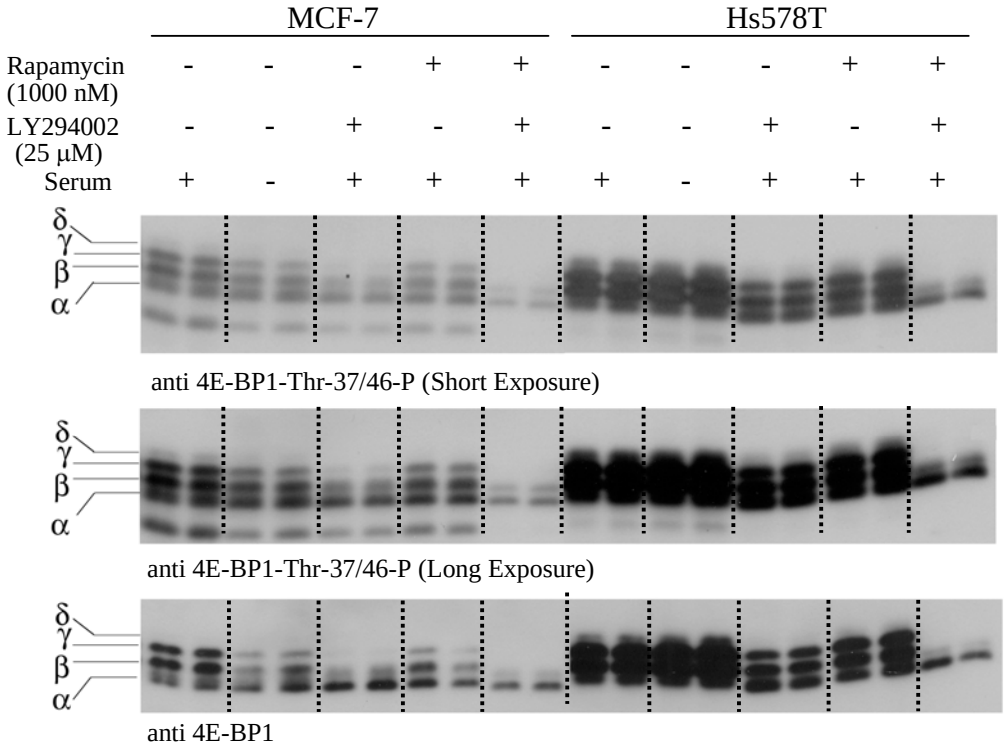

Figure 6.6. Effects of LY294002 alone and in combination with rapamycin on phospho-4E-BP1-Thr-37/46. Hs578T and MCF-7 cells were treated with 25 μM LY294002 and/or 1000 nM rapamycin for 96 hr in the presence of 10% FBS. Equal aliquots of total proteins (15 μg) were resolved by 15% SDS-PAGE and immunobloted with anti-phospho-4E-BP1-Thr-37/46 antibody, stripped and then re-probed with anti-4E-BP1 antibody. α, β, γ, δ are arbitrary designations for bands representing differently phosphorylated 4E-BP1, with band α being the hypophosphorylated form of 4E-BP1.

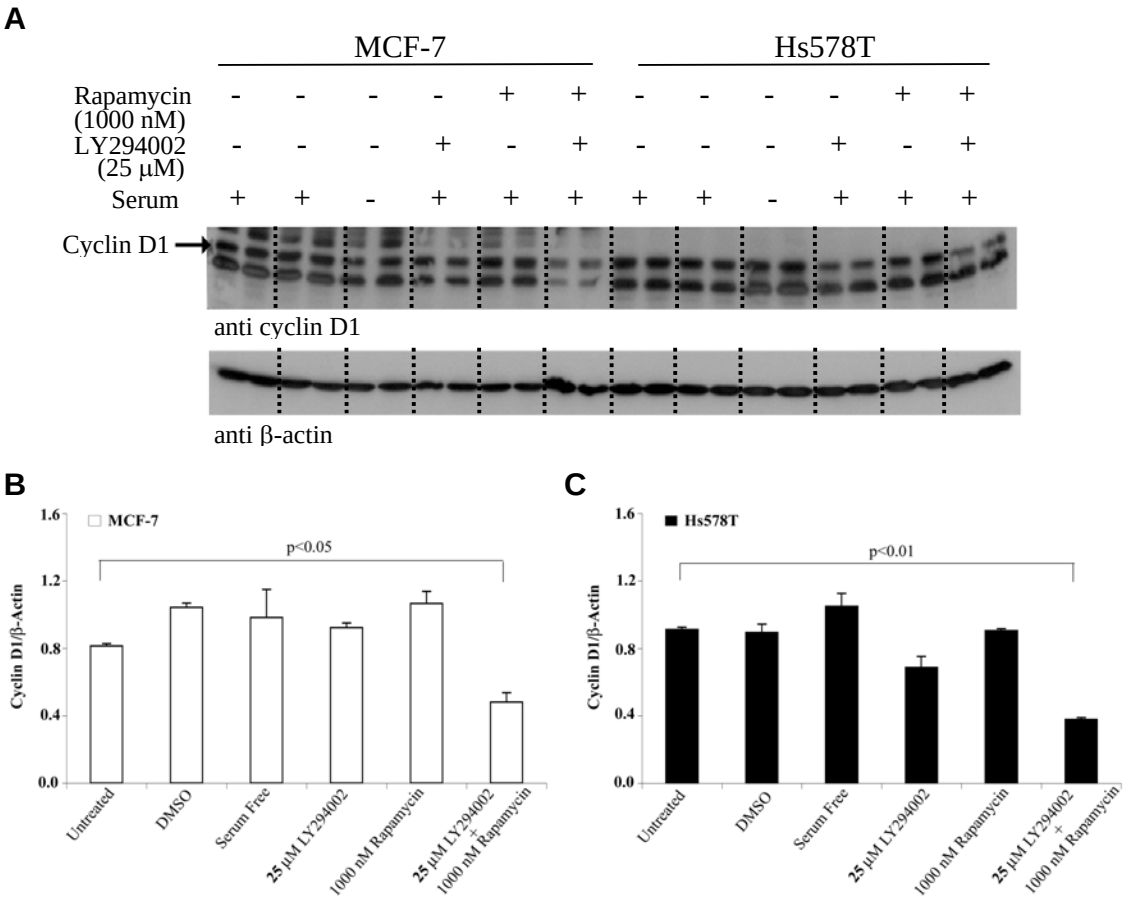

Figure 6.7. Effects of LY294002 alone and in combination with rapamycin on cyclin D1 protein. (A) Equal aliquots of total proteins were separated on 12% SDS-PAGE and immunobloted with anti-cyclin D1 antibody and re-probed for β-actin. ***(B and C)*** Densitometric analysis of the ratio of cyclin D1/β-actin. Data represent mean ± SEM, n=2.

Figure 6.8 Schematic diagram illustrating molecular targets of the combination of LY294002 and rapamycin in Hs578T and MCF-7 cells. While mTOR acts as a major effector of PI3K/Akt signaling pathway, PI3K-independent pathway(s) may induce activation of mTOR as well (The *dashed* lines indicate possible links). The combination of LY294002 and rapamycin was the most effective in inhibiting mTOR-dependent phosphorylation of 4E-BP1 than either agent alone. In its hypophosphorylated α form, 4E-BP1 binds to eIF4E, inhibiting initiation of translation of protein, such as cyclin D1, that are required for entry into the G1-phase of the cell cycle. LY294002 inhibits mTOR and PI3K kinase activities, while rapamycin is a selective inhibitor of mTOR.

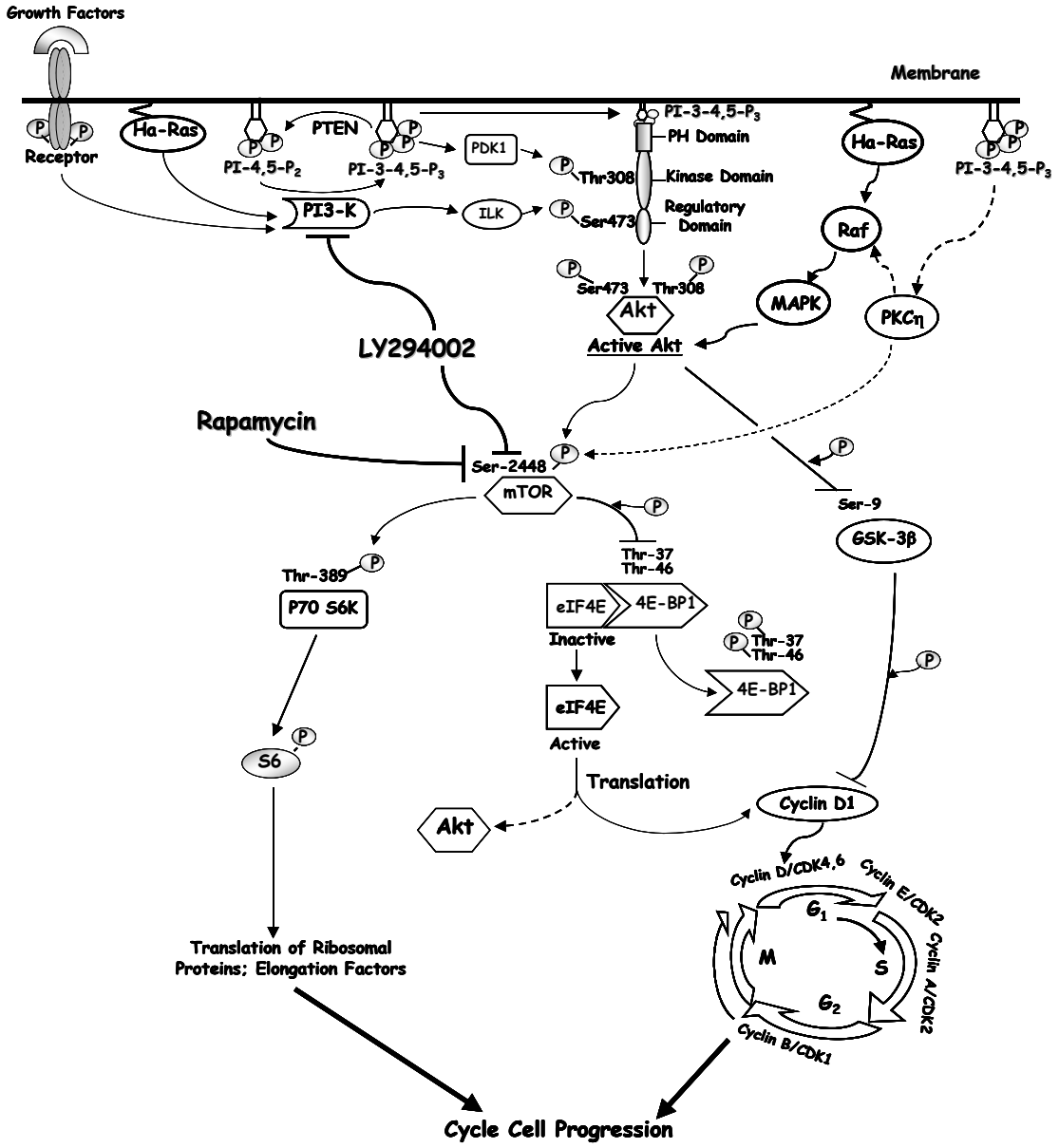
Growth Factors
Membrane
Receptor
Ha-Ras
PTEN
PI-4,5-P2
PI-3-4,5-P3
PDK1
PI3-K
ILK
PI-3-4,5-P3
PH Domain
Thr308
Kinase Domain
Ser473
Regulatory Domain
Ha-Ras
PI-3-4,5-P3
Raf
MAPK
PKCη
Ser473
Thr308
Akt
Active Akt
LY294002
Rapamycin
Ser-2448
mTOR
Ser-9
GSK-3β
Thr-37
Thr-46
Thr-389
P70 S6K
eIF4E
4E-BP1
Inactive
Thr-37
Thr-46
4E-BP1
eIF4E
Active
S6
Translation
Akt
Cyclin D1
Cyclin D/CDK4,6
Cyclin E/CDK2
Cyclin A/CDK2
Cyclin B/CDK1
G1
S
G2
M
Translation of Ribosomal
Proteins; Elongation Factors
Cycle Cell Progression

Figure 6.8

DISCUSSION

Akt has been shown to serve as a multi-functional protein, acting primarily as a survival factor to protect cells against apoptosis [241-249]. In addition, Akt regulates expansion in cell mass and stimulates entry of cells into the cell cycle by activating its downstream target mTOR [252, 256]. Over-expression of constitutive active Akt was sufficient to induce transformation of NIH3T3 [336], demonstrating that, upon its constitutive activation, Akt acts as an oncogene. Indeed, Akt kinase activity has been shown to be highly elevated in a wide range of tumor types [336, 486, 487] and associated with a tumorigenic phenotype [335, 337]. However, there are no studies to date that evaluated activation of Akt within specific cell types in normal skin, during multi-stage skin cacinogenesis, and tissue regeneration following skin injury. The goal of the present studies was to evaluate Akt signaling pathway using different cancer model systems, including chemically and UVB-induced skin carcinogenesis, breast tumorigenesis, as well as during cutaneous wound healing and tumor-associated angiogenesis. The present work also evaluated the utility of inhibiting target molecules within the Akt pathway using cultured human breast cancer cell lines.

In the present studies, we demonstrate that PI3K/Akt pathway is activated by specific VEGF splice variants, suggesting that these VEGF variants can selectively block apoptosis of endothelial cells involved in tumor-associated angiogenesis. Actively growing tumors have an absolute requirement for the development of new blood vessels, which support tumor growth, survival, as well as providing an avenue for tumor cells to enter the circulation and metastasize to distant organs. However, newly recruited endothelial cells are present within a hypoxic and nutrient-deprived microenvironment due to increases in tumor mass; therefore, endothelial cells are at risk of undergoing apoptosis. In the absence of blood vessel formation, apoptotic signal transduction pathways are activated, leading to tumor regression. In the current studies, we suggest

that tumor cells secrete survival factors to promote the persistence of the newly formed blood vessels.

Our laboratory previously reported the existence of a novel murine VEGF splice variant that contains an extended exon 6a, exon 6', which was termed $VEGF_{205}$*, that was preferentially expressed in mouse skin carcinomas, but not in normal skin [290]. Interestingly, $VEGF_{205}$* expression was prevalent in highly vascularized organs, including heart, lungs, liver, kidney, and brain of Tg.AC transgenic mice, which contain constitutively active v-Ha-*ras* that replaces the initiation step [290]. In contrast, there were no detectable levels of $VEGF_{205}$* in internal organs isolated from isogenic FVB/N mice [290]. These previous results suggested that constitutive activation of Ha-*ras* oncogene may be associated with alternative splicing of $VEGF_{205}$*.

The current studies demonstrate that exposure of vascular endothelial cells to $VEGF_{205}$* selectively stimulated phosphorylation of Akt at Ser-473 in a PI3K-dependent manner. The present results suggest that activation of PI3K/Akt signaling pathway in vascular endothelial cells is dependent upon the tumor microenvironment during which specific VEGF splice variants, such as $VEGF_{205}$*, are produced and secreted to stimulate phosphorylation of Akt at Ser-473. These results support a model for differential functions of VEGF splice variants during tumor-associated angiogenesis.

Not only was Akt activated in vascular endothelial cells undergoing angiogenesis, but the present studies also documented that specific populations of epidermal and follicular keratinocytes, which have been shown to ultimately form papillomas and carcinomas [17, 29, 356, 357], contained constitutively activated Akt during multi-stage skin carcinogenesis. Although previous studies have reported an association between increased Akt activation and development of skin tumors [334, 335, 337], the specific cell populations that contain activated Akt during multi-stage skin carcinogenesis have yet to be evaluated. Phospho-Akt staining was nominal within epidermal and follicular keratinocytes in dorsal skin isolated from SENCAR mice treated only with DMBA, which may be due to the very low number of initiated cells that contained pAkt. However, twice weekly topical applications of TPA for 15 weeks to dorsal skin of mice previously initiated with a single exposure to DMBA induced constitutive activation of Akt in epidermal and follicular keratinocytes. In contrast, treatment with TPA in the absence of tumor initiation with DMBA did not induce Akt activation in skin isolated at 15 weeks. Previous studies demonstrated that targeting insulin-like growth factor-1 (IGF-1) expression to basal

keratinocytes within the epidermis activated the PI3K/Akt pathway and was associated with a tumorigenic phenotype [334]. In contrast, twice weekly topical applications of the selective PI3K inhibitor, LY294002, significantly inhibited the development of skin tumors in IGF-1 transgenic mice [389]. These previous results suggest that inhibition of PI3K/Akt signaling pathway in initiated keratinocytes that contain activating mutations in the *ras* oncogene may block their clonal expansion. Taken together, the present observations suggest that one of the critical factors in stimulating constitutive activation of Akt is the clonal expansion of Ha-*ras* mutated cells during tumor promotion.

The present studies also demonstrate significant increases in pAkt immunohistochemical staining in papillomas isolated at week 22 from SENCAR mice initiated with DMBA and promoted with TPA, compared to pAkt in epidermal keratinocytes from the dorsal skin of mice treated topically with acetone. More specifically, pAkt localized to suprabasal keratinocytes within papilloma tissues, suggesting that pAkt may provide non-proliferating suprabasal cells in papillomas with the ability to resist undergoing terminal differentiation, thus conferring them with the ability to persist within the skin over long periods of time.

In addition to the presence of pAkt within epidermal and follicular keratinocytes during multi-stage skin carcinogenesis, infiltrating mast cells within the dermis of hyperplastic skin and in the stroma of papillomas contained activated Akt as well, suggesting that pAkt may provide mast cells with the ability to persist in the hyperplastic skin tissue during skin carcinogenesis, thus contributing to a pro-oxidant and pro-angiogenic microenvironment.

Using double-immunofluorescence staining in combination with confocal microscopy, the current results provide first time evidence of the presence of pAkt in $CD34^+$ cells within the outer root sheat (ORS) of the Bulge niche in hair follicles of dorsal skin treated only with acetone. There are no studies thus far which evaluated the mechanisms by which keratinocyte stem cells (KSC) persist in a quiescent state over the lifetime of the organism. The importance of pAkt in conferring $CD34^+$ cells with the ability to persist in the bulge region of hair follicles over the lifetime of the organism under homeostasis conditions may be similar to the recently reported role of pAkt in conferring long-term maintenance of human embryonic stem cells in their undifferentiated state [371, 372].

Cutaneous stem cells have also been shown to serve as targets for skin carcinogens [17, 374]. Studies that supported such role for KSC demonstrated that the number of papillomas did not significantly change in mice with lapses in time of greater than a year between initiation with DMBA and repetitive topical applications of the tumor promoter TPA [345, 488]. These previous results suggest that carcinogen-initiated cells are slow-cycling and long-lived, therefore share similar characteristics to KSC in the bulge region of hair follicles [375]. Although $CD34^+$ cells rarely divide, the present studies further demonstrate that $CD34^+$ cells do undergo proliferation in dorsal skin initiated with DMBA followed by repetitive topical applications of TPA for 15 weeks. Despite the proliferative potential of $CD34^+$ cells during multi-stage skin carcinogenesis, the present results show the persistence of this cell population to the ORS of the bulge region of hair follicles in hyperplastic skin during multi-stage skin carcinogenesis. These $CD34^+$ cells also retained their activation of Akt during tumor promotion. The findings of the present results suggest that following initiation with DMBA, bulge stem cells may represent the major cell population that acquires mutations in the Ha-*ras* oncogene. The presence of pAkt may induce persistence of these initiated cells, despite the presence of apoptotic mechanisms, which under normal conditions, would result in the removal of keratinocytes containing *ras* mutations. Following promotion with TPA, these carcinogen-retaining cells have the potential for clonal expansion. However, despite the proliferation of KSC, these cells remained precisely localized to the bulge region of hair follicles. The presence of pAkt in $CD34^+$ cells may prevent the loss of their undifferentiated morphology, and thus the depletion of this cell population during multi-stage skin carcinogenesis.

Although exposure to chemical carcinogens, including polycyclic hydrocarbons resulting from the incomplete combustion of fossil fuels, has been associated with the development of non-melanoma skin cancers, epidemiologic studies have consistently reported a strong association between exposure to UVB radiation and incidence of human skin cancers. There is little information available on the role of Akt-dependent signaling during UVB-induced skin carcinogenesis. One of the goals of the present studies was to determine the localization of activated Akt and mTOR in skin isolated from Skh/hr hairless mice following acute and chronic exposure to UVB light. In contrast to the chemical initiator DMBA, UVB light has been shown to act as both a tumor initiator and promoter. Acute exposure to UVB light induced activation of Akt within the

epidermal and follicular layers of the skin, while only few cells contained pAkt in non-irradiated skin. However, chronic exposure to UVB light induced clonal expansion of pAkt-containing keratinocytes. While chemical initiation with DMBA induces activating mutations in the Ha-*ras* oncogene [65, 66], exposure to UVB light results in mutations in *p53* tumor suppressor gene leading to a loss of p53 function [98]. In the absence of a functional p53 protein, chronic exposure to UVB light induces further mutations, which accumulate in critical proto-oncogenes and/or tumor suppressor genes. Collectively, results from the present studies demonstrate that one mechanism by which initiated keratinocytes may persist in the skin following exposure to chemical carcinogens such as DMBA or UVB light is by activation of Akt.

Interestingly, increases in pAkt staining at 24 hr and 48 hr following exposure to UVB preceded the induction of pmTOR, which was only prevalent at week 1 within epidermal and follicular keratinocytes. There were few cells that contained pmTOR at week 20 following UVB exposure compared to the higher number of keratinocytes which contained pmTOR at week 1 after UVB exposure. Activation of pmTOR in epidermal keratinocytes within hyperplastic skin at week 1 following UVB exposure coincided with production of VEGF by epidermal keratinocytes and an increase in the number of blood vessels within the dermal area. mTOR may be activated in a temporal manner during UVB-induced skin carcinogenesis and is associated with VEGF expression within epidermal keratinocytes. Future studies should focus on examining the potential role of pmTOR as a critical mediator of the angiogenic switch during UVB-induced skin carcinogenesis.

The present study is only one of few to characterize differences in localization of pAkt and pmTOR in papillomas isolated from SENCAR mice at week 22 following initiation with DMBA and repetitive topical applications of TPA and in papillomas isolated from Skh/hr mice at week 20 following a regimen of 3 times weekly exposure to 2240 J/m^2 UVB light. While proliferating cells were confined to the basal layer within papillomas isolated from SENCAR mice at 22 weeks of chemically-induced skin carcinogenesis, proliferating cells were present in all layers within papilloma tissues isolated from Skh/hr mice following UVB exposure. Examination of pAkt immunochemical localization revealed that while pAkt was present in non-proliferating suprabasal cells within chemically-induced papillomas, pAkt was present in all the proliferating cell layers in papillomas isolated from Skh/hr mice following UVB exposure.

In contrast to papillomas isolated from SENCAR mice, there were no detectable levels of pmTOR within UVB-induced papillomas. The present results suggest differential activation of Akt and mTOR signaling pathways during both processes. In UVB-induced papillomas, the presence of pAkt in proliferating cells in the absence of pmTOR suggest that pAkt may induce proliferation of keratinocytes during UVB-induced skin carcinogenesis independently of pmTOR. Studies been previously shown that Akt may regulate cell proliferation independently of mTOR activation by phosphorylating and consequently blocking the activity of glycogen synthase kinase-3β (GSK-3β) [406]. In its phosphorylated form, GSK-3β is inactive, therefore preventing phosphorylation and subsequent proteolytic degradation of cyclin D1 [253]. On the other hand, the presence of pAkt and pmTOR in non-proliferating suprabasal keratinocytes in chemically-induced papillomas tissues may confer this cell population with a survival advantage and the ability to resist terminal differentiation. Taken together, the present results suggest a model in which pAkt and pmTOR may act in concert to induce survival of suprabasal keratinocytes in chemically-induced papillomas, while the presence of pAkt may stimulate proliferation of the less-differentiated keratinocytes in UVB-induced papillomas independently of mTOR activation.

Given the hypothesis that tumors are wounds that do not heal [489], the present studies further prompted us to examine the role of pAkt and pmTOR in skin regeneration following injury. Wound closure and regeneration of the damaged tissue to its original strength requires a highly regulated sequence of events. The wound repair process consists of three phases, including the initial homeostasis and inflammatory phase, the reepithelialization phase, and the dermal remodeling phase.

During phase 1 of wound repair, all proliferating as well as non-proliferating epidermal keratinocytes localized to the wound edge contained pAkt, compared to the few epidermal keratinocytes that contained pAkt in skin distal to the wound site. In response to skin injury, epidermal keratinocytes at the wound site have the ability to withdraw from undergoing the process of terminal differentiation, and acquire a migratory phenotype. Recent evidence suggests that Akt not only promotes cell survival, but also regulates cell motility in a diversity of cell types [436, 437]. Taken together, the present results suggest that pAkt may provide epidermal keratinocytes with the ability to evade the normal process of terminal differentiation immediately following skin injury, and to

subsequently acquire a migratory phenotype, allowing them to move along the dermal wound margins.

Following complete closure of the epithelial layer at day 5, the highest levels of pAkt immunoreactive protein were detected within proliferating and non-proliferating epidermal keratinocytes located in the reepithelialized wound site, compared to the low levels of pAkt immunoreactive protein present in epidermal keratinocytes that were distal to the wound site. In contrast, the pattern of pmTOR distribution did not follow the same pattern of staining as pAkt. The presence of pmTOR was restricted to epidermal keratinocytes located in the reepithelialized wound site during phase 2 of wound repair. Given that basal keratinocytes that had migrated into the wound site continued to proliferate and contained both pAkt and pmTOR, the present results suggest that Akt/mTOR signaling pathway may be essential for the proliferation of basal cells during the reepithelialization phase. On the other hand, the location of pAkt and pmTOR to suprabasal keratinocytes within the reepethelialized wound site did not correlate with PCNA expression, a proliferative marker that is expressed in the G_1/S and G_2 phases of the cell cycle. Reepithelialization has previously been shown to involve the generation of a multi-layered epithelium, with different keratinocyte subtypes within the suprabasal compartment of the epidermis [428]. Taken together, the current observations suggest that pAkt and pmTOR may act together or separately to induce the survival and persistence of non-proliferating suprabasal keratinocytes during the reepithelialization phase. Further investigation is required to examine whether pmTOR may be an important factor that mediates Akt-dependent survival signaling.

Tissue regeneration following skin injury not only depends on proliferation and migration of epidermal keratinocytes into the wound site [428], but also requires participation of keratinocyte stem cells (KSC), in particular, KSC localized to the bulge region of hair follicles [42]. These previous results suggest that KSC that are mobilized from the bulge niche after wounding acquire a “functional epidermal keratinocyte” phenotype [42], therefore, enhancing reepithelialization of the wound site. In the present studies, pAkt was not only present within epidermal keratinocytes at the wound site, but was also present within $CD34^+$ KSC, which remained localized to the bulge niche of hair follicles in skin tissues adjacent to the wound site at all times during cutaneous wound healing. While pAkt was present within the ORS as well as IRS of hair follicles, pmTOR was confined specifically to cells in the ORS. The dual presence of pAkt and pmTOR in

KSC localized to the ORS of the bulge region of hair follicles suggests that Akt/mTOR signaling pathway may play a role in tightly regulating the differentiation of KSC, thus maintaining a long-lived population of stem cells that has been to participate in skin regeneration following injury. The present results further suggest that pmTOR may serve as a selective marker of cells located to the ORS of the bulge region during the process of wound healing.

Results from these series of studies indicate that activation of Akt and mTOR may regulate fundamental aspects during wound repair, thus serving as therapeutic strategies to enhance wound repair in chronic wounds that fail to heal, such as non-healing ulcers from patients with diabetes. We report that at day 21 following wounding, the level of pAkt in epidermal keratinocytes along the wound healing line was comparable to that detected in keratinocytes distal to the wound site. The current observations further predict that improper constitutive activation of pAkt and pmTOR within the wound site at phase 3 during wound repair may create a suitable environment favoring the development of chronic wounds.

While the present studies evaluated the localization of activated Akt and mTOR in specific epidermal, follicular, and dermal cell types during multi-stage skin carcinogenesis, little information is available about the effects of inhibiting Akt signaling pathway in development of malignant carcinomas. To evaluate the effects of the combination of the selective PI3K inhibitor, LY294002, and the selective mTOR inhibitor, rapamycin, on signaling molecules involved in the PI3K and mTOR pathways, a model of human breast cancer was used. Two human breast tumor cells, Hs578T and MCF-7 cell lines, were used to represent both highly invasive and metastatic and slow-growing, and poorly invasive human breast tumor cells, respectively. Despite their growth differences, the combination of LY294002 and rapamycin resulted in significant inhibition of proliferation of both these cell lines compared to the anti-proliferative effects of either agent alone. Results from chapter 5 suggest that inhibition of δ, γ, and β forms of 4E-BP1 following exposure of Hs578T cells to the combination of LY294002 and rapamycin was associated with a decrease in levels of cyclin D1, an essential regulator for progression of cells into the G1-phase of the cell cycle. Interestingly, inhibition of 4E-BP1 hyperphosphorylation occurred in the presence of constitutive active Akt in Hs578T cells, demonstrating the importance of using the combination of LY294002 and rapamycin to inhibit target molecules within the PI3K/Akt signaling pathway. Furthermore, we

demonstrate that inhibition of δ, γ, and β forms of 4E-BP1 may define the effectiveness of PI3K and mTOR inhibitors more effectively than evaluating phoshorylation of p70 S6K.

In summary, the present studies are the first to demonstrate localization of activated Akt in specific cell populations within the skin during multi-stage skin carcinogenesis and may play an important role during skin tumor development as well as during tumor-associated angiogenesis. Since Akt is activated in bulge stem cells, skin tumor cells, mast inflammatory cells, as well as vascular endothelial cells undergoing angiogenesis, the first approach to block skin tumor growth would be to simultaneously target all of these cell types. One such approach is to target Akt signaling pathway that is shared by all cell types involved in multi-stage skin carcinogenesis. Ultimately, this strategy would induce apoptosis in each of these cell types. Although these results show promise for the utility of Akt as a target molecule in skin tumor development, dual inhibition of Akt and mTOR by the combination of LY294002 and rapamycin induced maximal inhibition of hyperphosphorylation of 4E-BP1 and a greater anti-proliferative effect on human breast tumor cells of different origins and metastatic activities than either of the agents alone. The strategy of dual inhibition of Akt and mTOR may be applicable to skin tumor development as well, providing a novel therapeutic for the treatment of non-melanoma skin cancers, rather than using each agent alone. In contrast to the suggested tumor-promoting effects of Akt and mTOR presented in this study, the current observations suggest that activation of Akt/mTOR signaling pathway may provide utility as a therapeutic agent that may stimulate regeneration of blood vessels in tissues whose vascular supply has been insufficient, such as cardiovascular diseases, and would accelerate wound healing in patients with chronic wounds and non-healing ulcers

REFERENCES

1. Nelson WG and Sun TT: The 50- and 58-kdalton keratin classes as molecular markers for stratified squamous epithelia: cell culture studies. J Cell Biol 97: 244-251, 1983.

2. Barrandon Y and Green H: Three clonal types of keratinocyte with different capacities for multiplication. Proc Natl Acad Sci U S A 84: 2302-2306, 1987.

3. Fuchs E: Epidermal differentiation and keratin gene expression. J Cell Sci Suppl 17: 197-208, 1993.

4. Watt FM: Role of integrins in regulating epidermal adhesion, growth and differentiation. Embo J 21: 3919-3926, 2002.

5. Fuchs E and Raghavan S: Getting under the skin of epidermal morphogenesis. Nat Rev Genet 3: 199-209, 2002.

6. Potten CS: Surface epithelial tissue; your customised body bag. Biol Sci Rev 7: 23-27, 1994.

7. Leigh IM, Purkis PE, Whitehead P, and Lane EB: Monospecific monoclonal antibodies to keratin 1 carboxy terminal (synthetic peptide) and to keratin 10 as markers of epidermal differentiation. Br J Dermatol 129: 110-119, 1993.

8. Thacher SM and Rice RH: Keratinocyte-specific transglutaminase of cultured human epidermal cells: relation to cross-linked envelope formation and terminal differentiation. Cell 40: 685-695, 1985.

9. Eckert RL, Crish JF, and Robinson NA: The epidermal keratinocyte as a model for the study of gene regulation and cell differentiation. Physiol Rev 77: 397-424, 1997.

10. Allen TD and Potten CS: Ultrastructural site variations in mouse epidermal organization. J Cell Sci 21: 341-359, 1976.

11. Cotsarelis G, Sun TT, and Lavker RM: Label-retaining cells reside in the bulge area of pilosebaceous unit: implications for follicular stem cells, hair cycle, and skin carcinogenesis. Cell 61: 1329-1337, 1990.

12. Morris RJ and Potten CS: Highly persistent label-retaining cells in the hair follicles of mice and their fate following induction of anagen. J Invest Dermatol 112: 470-475, 1999.

13. Morris RJ, Fischer SM, and Slaga TJ: Evidence that the centrally and peripherally located cells in the murine epidermal proliferative unit are two distinct cell populations. J Invest Dermatol 84: 277-281, 1985.

14. Bickenbach JR and Chism E: Selection and extended growth of murine epidermal stem cells in culture. Exp Cell Res 244: 184-195, 1998.

15. Mackenzie IC and Bickenbach JR: Label-retaining keratinocytes and Langerhans cells in mouse epithelia. Cell Tissue Res 242: 551-556, 1985.

16. Bickenbach JR: Identification and behavior of label-retaining cells in oral mucosa and skin. J Dent Res 60 Spec No C: 1611-1620, 1981.

17. Morris RJ, Tryson KA, and Wu KQ: Evidence that the epidermal targets of carcinogen action are found in the interfollicular epidermis of infundibulum as well as in the hair follicles. Cancer Res 60: 226-229, 2000.

18. Potten CS: The epidermal proliferative unit: the possible role of the central basal cell. Cell Tissue Kinet 7: 77-88, 1974.

19. Tumbar T, Guasch G, Greco V, Blanpain C, Lowry WE, Rendl M, and Fuchs E: Defining the epithelial stem cell niche in skin. Science 303: 359-363, 2004.

20. Kobayashi K, Rochat A, and Barrandon Y: Segregation of keratinocyte colony-forming cells in the bulge of the rat vibrissa. Proc Natl Acad Sci U S A 90: 7391-7395, 1993.

21. Cotsarelis G, Kaur P, Dhouailly D, Hengge U, and Bickenbach J: Epithelial stem cells in the skin: definition, markers, localization and functions. Exp Dermatol 8: 80-88, 1999.

22. Nickoloff BJ: The human progenitor cell antigen (CD34) is localized on endothelial cells, dermal dendritic cells, and perifollicular cells in formalin-fixed normal skin, and on proliferating endothelial cells and stromal spindle-shaped cells in Kaposi's sarcoma. Arch Dermatol 127: 523-529, 1991.

23. Krause DS, Fackler MJ, Civin CI, and May WS: CD34: structure, biology, and clinical utility. Blood 87: 1-13, 1996.

24. Krause DS, Ito T, Fackler MJ, Smith OM, Collector MI, Sharkis SJ, and May WS: Characterization of murine CD34, a marker for hematopoietic progenitor and stem cells. Blood 84: 691-701, 1994.

25. Trempus CS, Morris RJ, Bortner CD, Cotsarelis G, Faircloth RS, Reece JM, and Tennant RW: Enrichment for living murine keratinocytes from the hair follicle bulge with the cell surface marker CD34. J Invest Dermatol 120: 501-511, 2003.

26. Blanpain C, Lowry WE, Geoghegan A, Polak L, and Fuchs E: Self-renewal, multipotency, and the existence of two cell populations within an epithelial stem cell niche. Cell 118: 635-648, 2004.

27. Ohyama M, Terunuma A, Tock CL, Radonovich MF, Pise-Masison CA, Hopping SB, Brady JN, Udey MC, and Vogel JC: Characterization and isolation of stem cell-enriched human hair follicle bulge cells. J Clin Invest 116: 249-260, 2006.

28. Lyle S, Christofidou-Solomidou M, Liu Y, Elder DE, Albelda S, and Cotsarelis G: The C8/144B monoclonal antibody recognizes cytokeratin 15 and defines the location of human hair follicle stem cells. J Cell Sci 111 (Pt 21): 3179-3188, 1998.

29. Morris RJ, Liu Y, Marles L, Yang Z, Trempus C, Li S, Lin JS, Sawicki JA, and Cotsarelis G: Capturing and profiling adult hair follicle stem cells. Nat Biotechnol 22: 411-417, 2004.

30. Liu Y, Lyle S, Yang Z, and Cotsarelis G: Keratin 15 promoter targets putative epithelial stem cells in the hair follicle bulge. J Invest Dermatol 121: 963-968, 2003.

31. Braun KM, Niemann C, Jensen UB, Sundberg JP, Silva-Vargas V, and Watt FM: Manipulation of stem cell proliferation and lineage commitment: visualisation of label-retaining cells in wholemounts of mouse epidermis. Development 130: 5241-5255, 2003.

32. Tani H, Morris RJ, and Kaur P: Enrichment for murine keratinocyte stem cells based on cell surface phenotype. Proc Natl Acad Sci U S A 97: 10960-10965, 2000.

33. Li A, Simmons PJ, and Kaur P: Identification and isolation of candidate human keratinocyte stem cells based on cell surface phenotype. Proc Natl Acad Sci U S A 95: 3902-3907, 1998.

34. Sonnenberg A, Calafat J, Janssen H, Daams H, van der Raaij-Helmer LM, Falcioni R, Kennel SJ, Aplin JD, Baker J, Loizidou M, and et al.: Integrin alpha 6/beta 4 complex is located in hemidesmosomes, suggesting a major role in epidermal cell-basement membrane adhesion. J Cell Biol 113: 907-917, 1991.

35. Jones PH and Watt FM: Separation of human epidermal stem cells from transit amplifying cells on the basis of differences in integrin function and expression. Cell 73: 713-724, 1993.

36. Jones PH, Harper S, and Watt FM: Stem cell patterning and fate in human epidermis. Cell 80: 83-93, 1995.

37. Watt FM: Stem cell fate and patterning in mammalian epidermis. Curr Opin Genet Dev 11: 410-417, 2001.

38. Ghazizadeh S and Taichman LB: Multiple classes of stem cells in cutaneous epithelium: a lineage analysis of adult mouse skin. Embo J 20: 1215-1222, 2001.

39. Rochat A, Kobayashi K, and Barrandon Y: Location of stem cells of human hair follicles by clonal analysis. Cell 76: 1063-1073, 1994.

40. Morris RJ, Tacker KC, Fischer SM, and Slaga TJ: Quantitation of primary in vitro clonogenic keratinocytes from normal adult murine epidermis, following initiation, and during promotion of epidermal tumors. Cancer Res 48: 6285-6290, 1988.

41. Morris RJ and Potten CS: Slowly cycling (label-retaining) epidermal cells behave like clonogenic stem cells in vitro. Cell Prolif 27: 279-289, 1994.

42. Ito M, Liu Y, Yang Z, Nguyen J, Liang F, Morris RJ, and Cotsarelis G: Stem cells in the hair follicle bulge contribute to wound repair but not to homeostasis of the epidermis. Nat Med 11: 1351-1354, 2005.

43. Levy V, Lindon C, Harfe BD, and Morgan BA: Distinct stem cell populations regenerate the follicle and interfollicular epidermis. Dev Cell 9: 855-861, 2005.

44. Panteleyev AA, Jahoda CA, and Christiano AM: Hair follicle predetermination. J Cell Sci 114: 3419-3431, 2001.

45. Stenn KS and Paus R: Controls of hair follicle cycling. Physiol Rev 81: 449-494, 2001.

46. Jahoda CA, Horne KA, and Oliver RF: Induction of hair growth by implantation of cultured dermal papilla cells. Nature 311: 560-562, 1984.

47. Johnson TM, Rowe DE, Nelson BR, and Swanson NA: Squamous cell carcinoma of the skin (excluding lip and oral mucosa). J Am Acad Dermatol 26: 467-484, 1992.

48. Miller DL and Weinstock MA: Nonmelanoma skin cancer in the United States: incidence. J Am Acad Dermatol 30: 774-778, 1994.

49. Clayman GL, Lee JJ, Holsinger FC, Zhou X, Duvic M, El-Naggar AK, Prieto VG, Altamirano E, Tucker SL, Strom SS, Kripke ML, and Lippman SM: Mortality risk from squamous cell skin cancer. J Clin Oncol 23: 759-765, 2005.

50. Einspahr JG, Stratton SP, Bowden GT, and Alberts DS: Chemoprevention of human skin cancer. Crit Rev Oncol Hematol 41: 269-285, 2002.

51. Kwa RE, Campana K, and Moy RL: Biology of cutaneous squamous cell carcinoma. J Am Acad Dermatol 26: 1-26, 1992.

52. De Fabo EC: Arctic stratospheric ozone depletion and increased UVB radiation: potential impacts to human health. Int J Circumpolar Health 64: 509-522, 2005.

53. Pott P: The chirurgical works of Percivall Pott, F.R.S., surgeon to St. Bartholomew's Hospital, a new edition, with his last corrections. 1808. Clin Orthop Relat Res: 4-10, 2002.

54. Boutwell RK: Some Biological Aspects of Skin Carcinogenisis. Prog Exp Tumor Res 19: 207-250, 1964.

55. DiGiovanni J: Multistage carcinogenesis in mouse skin. Pharmacol Ther 54: 63-128, 1992.

56. Berenblum I and Shubik P: The role of the croton oil applications, associated with a single painting of a carcinogen, in tumor induction of the mouse's skin. Br J Cancer 1, 1947.

57. Mottram JC: A developing factor in experimental blastogenesis. J Path Bact 56: 181-187, 1944.

58. Moschel RC, Pigott MA, Costantino N, and Dipple A: Chromatographic and fluorescence spectroscopic studies of individual 7,12-dimethylbenz[a]anthracene--deoxyribonucleoside adducts. Carcinogenesis 4: 1201-1204, 1983.

59. Dipple A, Pigott M, Moschel RC, and Costantino N: Evidence that binding of 7,12-dimethylbenz(a)anthracene to DNA in mouse embryo cell cultures results in extensive substitution of both adenine and guanine residues. Cancer Res 43: 4132-4135, 1983.

60. Cheng SC, Prakash AS, Pigott MA, Hilton BD, Lee H, Harvey RG, and Dipple A: A metabolite of the carcinogen 7,12-dimethylbenz[a]anthracene that reacts predominantly with adenine residues in DNA. Carcinogenesis 9: 1721-1723, 1988.

61. Bowden GT, Slaga TJ, Shapas BG, and Boutwell RK: The role of aryl hydrocarbon hydroxylase in skin tumor initiation by 7,12-dimethylbenz(a)anthracene and 1,2,5,6-dibenzanthracene using DNA binding and thymidine-3H incorporation into DNA as criteria. Cancer Res 34: 2634-2642, 1974.

62. RamaKrishna NV, Devanesan PD, Rogan EG, Cavalieri EL, Jeong H, Jankowiak R, and Small GJ: Mechanism of metabolic activation of the potent carcinogen 7,12-dimethylbenz[a]anthracene. Chem Res Toxicol 5: 220-226, 1992.

63. Chakravarti D, Pelling JC, Cavalieri EL, and Rogan EG: Relating aromatic hydrocarbon-induced DNA adducts and c-H-ras mutations in mouse skin papillomas: the role of apurinic sites. Proc Natl Acad Sci U S A 92: 10422-10426, 1995.

64. Feig LA: The many roads that lead to Ras. Science 260: 767-768, 1993.

65. Quintanilla M, Brown K, Ramsden M, and Balmain A: Carcinogen-specific mutation and amplification of Ha-ras during mouse skin carcinogenesis. Nature 322: 78-80, 1986.

66. Bizub D, Wood AW, and Skalka AM: Mutagenesis of the Ha-ras oncogene in mouse skin tumors induced by polycyclic aromatic hydrocarbons. Proc Natl Acad Sci U S A 83: 6048-6052, 1986.

67. Loehrke H, Schweizer J, Dederer E, Hesse B, Rosenkranz G, and Goerttler K: On the persistence of tumor initiation in two-stage carcinogenesis on mouse skin. Carcinogenesis 4: 771-775, 1983.

68. Slaga TJ, Fischer SM, Weeks CE, and Klein-Szanto AJP. Cellular and biochemical mechanisms of mouse skin tumor promoters. In: Reviews in Biochemical Toxicology, edited by Hodgson E, Bend J and Philpot RM. North-Holland, New-York: Elsevier, 1981, p. 231-281.

69. Budunova IV and Williams GM: Cell culture assays for chemicals with tumor-promoting or tumor-inhibiting activity based on the modulation of intercellular communication. Cell Biol Toxicol 10: 71-116, 1994.

70. Brissette JL, Kumar NM, Gilula NB, and Dotto GP: The tumor promoter 12-O-tetradecanoylphorbol-13-acetate and the ras oncogene modulate expression and phosphorylation of gap junction proteins. Mol Cell Biol 11: 5364-5371, 1991.

71. Raick AN: Ultrastructural, histological, and biochemical alterations produced by 12-O-tetradecanoyl-phorbol-13-acetate on mouse epidermis and their relevance to skin tumor promotion. Cancer Res 33: 269-286, 1973.

72. Janoff A, Klassen A, and Troll W: Local vascular changes induced by the cocarcinogen, phorbol myristate acetate. Cancer Res 30: 2568-2571, 1970.

73. Lewis JG and Adams DO: Early inflammatory changes in the skin of SENCAR and C57BL/6 mice following exposure to 12-O-tetradecanoylphorbol-13-acetate. Carcinogenesis 8: 889-898, 1987.

74. O'Brien TG, Megosh LC, Gilliard G, and Soler AP: Ornithine decarboxylase overexpression is a sufficient condition for tumor promotion in mouse skin. Cancer Res 57: 2630-2637, 1997.

75. O'Brien TG, Simsiman RC, and Boutwell RK: Induction of the polyamine-biosynthetic enzymes in mouse epidermis by tumor-promoting agents. Cancer Res 35: 1662-1670, 1975.

76. Pegg AE: Recent advances in the biochemistry of polyamines in eukaryotes. Biochem J 234: 249-262, 1986.

77. Castagna M, Takai Y, Kaibuchi K, Sano K, Kikkawa U, and Nishizuka Y: Direct activation of calcium-activated, phospholipid-dependent protein kinase by tumor-promoting phorbol esters. J Biol Chem 257: 7847-7851, 1982.

78. Dlugosz AA, Mischak H, Mushinski JF, and Yuspa SH: Transcripts encoding protein kinase C-alpha, -delta, -epsilon, -zeta, and -eta are expressed in basal and differentiating mouse keratinocytes in vitro and exhibit quantitative changes in neoplastic cells. Mol Carcinog 5: 286-292, 1992.

79. Fisher GJ, Tavakkol A, Leach K, Burns D, Basta P, Loomis C, Griffiths CE, Cooper KD, Reynolds NJ, Elder JT, and et al.: Differential expression of protein kinase C isoenzymes in normal and psoriatic adult human skin: reduced expression of protein kinase C-beta II in psoriasis. J Invest Dermatol 101: 553-559, 1993.

80. Takai Y, Kishimoto A, Kikkawa U, Mori T, and Nishizuka Y: Unsaturated diacylglycerol as a possible messenger for the activation of calcium-activated, phospholipid-dependent protein kinase system. Biochem Biophys Res Commun 91: 1218-1224, 1979.

81. Boyle WJ, Smeal T, Defize LH, Angel P, Woodgett JR, Karin M, and Hunter T: Activation of protein kinase C decreases phosphorylation of c-Jun at sites that negatively regulate its DNA-binding activity. Cell 64: 573-584, 1991.

82. Tseng CP, Kim YJ, Kumar R, and Verma AK: Involvement of protein kinase C in the transcriptional regulation of 12-O-tetradecanoylphorbol-13-acetate-inducible genes modulated by AP-1 or non-AP-1 transacting factors. Carcinogenesis 15: 707-711, 1994.

83. Imamoto A, Beltran LM, and DiGiovanni J: Evidence for autocrine/paracrine growth stimulation by transforming growth factor-alpha during the process of skin tumor promotion. Mol Carcinog 4: 52-60, 1991.

84. Oberyszyn TM, Sabourin CL, Bijur GN, Oberyszyn AS, Boros LG, and Robertson FM: Interleukin-1 alpha gene expression and localization of interleukin-1 alpha protein during tumor promotion. Mol Carcinog 7: 238-248, 1993.

85. Lee WY, Fischer SM, Butler AP, and Locniskar MF: Modulation of interleukin-1 alpha mRNA expression in mouse epidermis by tumor promoters and antagonists. Mol Carcinog 7: 26-35, 1993.

86. Robertson FM, Bijur GN, Oberyszyn AS, Pellegrini AE, Boros LG, Sabourin CL, and Oberyszyn TM: Granulocyte-macrophage colony stimulating factor gene expression and function during tumor promotion. Carcinogenesis 15: 1017-1029, 1994.

87. Wei L, Wei H, and Frenkel K: Sensitivity to tumor promotion of SENCAR and C57BL/6J mice correlates with oxidative events and DNA damage. Carcinogenesis 14: 841-847, 1993.

88. Robertson FM, Long BW, Tober KL, Ross MS, and Oberyszyn TM: Gene expression and cellular sources of inducible nitric oxide synthase during tumor promotion. Carcinogenesis 17: 2053-2059, 1996.

89. Inoue S and Kawanishi S: Oxidative DNA damage induced by simultaneous generation of nitric oxide and superoxide. FEBS Lett 371: 86-88, 1995.

90. Yermilov V, Rubio J, Becchi M, Friesen MD, Pignatelli B, and Ohshima H: Formation of 8-nitroguanine by the reaction of guanine with peroxynitrite in vitro. Carcinogenesis 16: 2045-2050, 1995.

91. Salgo MG, Bermudez E, Squadrito GL, and Pryor WA: Peroxynitrite causes DNA damage and oxidation of thiols in rat thymocytes [corrected]. Arch Biochem Biophys 322: 500-505, 1995.

92. Ohshima H, Friesen M, Brouet I, and Bartsch H: Nitrotyrosine as a new marker for endogenous nitrosation and nitration of proteins. Food Chem Toxicol 28: 647-652, 1990.

93. Ellison MJ and Childs JD: Pyrimidine dimers induced in Escherichia coli DNA by ultraviolet radiation present in sunlight. Photochem Photobiol 34: 465-469, 1981.

94. Chadwick CA, Potten CS, Nikaido O, Matsunaga T, Proby C, and Young AR: The detection of cyclobutane thymine dimers, (6-4) photolesions and the Dewar photoisomers in sections of UV-irradiated human skin using specific antibodies, and the demonstration of depth penetration effects. J Photochem Photobiol B 28: 163-170, 1995.

95. Miller JH: Mutagenic specificity of ultraviolet light. J Mol Biol 182: 45-65, 1985.

96. Brash DE, Rudolph JA, Simon JA, Lin A, McKenna GJ, Baden HP, Halperin AJ, and Ponten J: A role for sunlight in skin cancer: UV-induced p53 mutations in squamous cell carcinoma. Proc Natl Acad Sci U S A 88: 10124-10128, 1991.

97. lambert CW and Lambert MW. DNA repair deficiency and skin cancer in Xeroderma Pigmentosum. In: Sin cancer: Mechanisms and human relevance, edited by Mukhtar H. Boca Raton, Florida: CRC Press, 1995, p. 39-70.

98. Ouhtit A, Gorny A, Muller HK, Hill LL, Owen-Schaub L, and Ananthaswamy HN: Loss of Fas-ligand expression in mouse keratinocytes during UV carcinogenesis. Am J Pathol 157: 1975-1981, 2000.

99. Pierceall WE, Kripke ML, and Ananthaswamy HN: N-ras mutation in ultraviolet radiation-induced murine skin cancers. Cancer Res 52: 3946-3951, 1992.

100. Sato M, Nishigori C, Lu Y, Zghal M, Yagi T, and Takebe H: Far less frequent mutations in ras genes than in the p53 gene in skin tumors of xeroderma pigmentosum patients. Mol Carcinog 11: 98-105, 1994.

101. Berg RJ, van Kranen HJ, Rebel HG, de Vries A, van Vloten WA, Van Kreijl CF, van der Leun JC, and de Gruijl FR: Early p53 alterations in mouse skin carcinogenesis by UVB radiation: immunohistochemical detection of mutant p53 protein in clusters of preneoplastic epidermal cells. Proc Natl Acad Sci U S A 93: 274-278, 1996.

102. Rebel H, Mosnier LO, Berg RJ, Westerman-de Vries A, van Steeg H, van Kranen HJ, and de Gruijl FR: Early p53-positive foci as indicators of tumor risk in ultraviolet-exposed hairless mice: kinetics of induction, effects of DNA repair deficiency, and p53 heterozygosity. Cancer Res 61: 977-983, 2001.

103. Bremner R and Balmain A: Genetic changes in skin tumor progression: correlation between presence of a mutant ras gene and loss of heterozygosity on mouse chromosome 7. Cell 61: 407-417, 1990.

104. Bianchi AB, Aldaz CM, and Conti CJ: Nonrandom duplication of the chromosome bearing a mutated Ha-ras-1 allele in mouse skin tumors. Proc Natl Acad Sci U S A 87: 6902-6906, 1990.

105. Ruggeri B, Caamano J, Goodrow T, DiRado M, Bianchi A, Trono D, Conti CJ, and Klein-Szanto AJ: Alterations of the p53 tumor suppressor gene during mouse skin tumor progression. Cancer Res 51: 6615-6621, 1991.

106. Navarro P, Gomez M, Pizarro A, Gamallo C, Quintanilla M, and Cano A: A role for the E-cadherin cell-cell adhesion molecule during tumor progression of mouse epidermal carcinogenesis. J Cell Biol 115: 517-533, 1991.

107. Mukhtar H, Mercurio MG, and Agarwal R. Murine skin carcinogenesis: Relevance to humans. In: Skin cancer: Mechanisms and human relevance., edited by Mukhtar H. Boca Raton, Florida: CRC Press, 1995, p. 3-12.

108. Risau W: Embryonic angiogenesis factors. Pharmacol Ther 51: 371-376, 1991.

109. Torry RJ and Rongish BJ: Angiogenesis in the uterus: potential regulation and relation to tumor angiogenesis. Am J Reprod Immunol 27: 171-179, 1992.

110. Arnold F and West DC: Angiogenesis in wound healing. Pharmacol Ther 52: 407-422, 1991.

111. Pezzella F, Pastorino U, Tagliabue E, Andreola S, Sozzi G, Gasparini G, Menard S, Gatter KC, Harris AL, Fox S, Buyse M, Pilotti S, Pierotti M, and Rilke F: Non-small-cell lung carcinoma tumor growth without morphological evidence of neo-angiogenesis. Am J Pathol 151: 1417-1423, 1997.

112. Holash J, Maisonpierre PC, Compton D, Boland P, Alexander CR, Zagzag D, Yancopoulos GD, and Wiegand SJ: Vessel cooption, regression, and growth in tumors mediated by angiopoietins and VEGF. Science 284: 1994-1998, 1999.

113. Greenblatt M and Shubi P: Tumor angiogenesis: transfilter diffusion studies in the hamster by the transparent chamber technique. J Natl Cancer Inst 41: 111-124, 1968.

114. Folkman J: Anti-angiogenesis: new concept for therapy of solid tumors. Ann Surg 175: 409-416, 1972.

115. Holmgren L, O'Reilly MS, and Folkman J: Dormancy of micrometastases: balanced proliferation and apoptosis in the presence of angiogenesis suppression. Nat Med 1: 149-153, 1995.

116. Hlatky L, Hahnfeldt P, and Folkman J: Clinical application of antiangiogenic therapy: microvessel density, what it does and doesn't tell us. J Natl Cancer Inst 94: 883-893, 2002.

117. Bergers G and Benjamin LE: Tumorigenesis and the angiogenic switch. Nat Rev Cancer 3: 401-410, 2003.

118. Hanahan D and Folkman J: Patterns and emerging mechanisms of the angiogenic switch during tumorigenesis. Cell 86: 353-364, 1996.

119. Folkman J: Proceedings: Tumor angiogenesis factor. Cancer Res 34: 2109-2113, 1974.

120. Shing Y, Folkman J, Sullivan R, Butterfield C, Murray J, and Klagsbrun M: Heparin affinity: purification of a tumor-derived capillary endothelial cell growth factor. Science 223: 1296-1299, 1984.

121. Kandel J, Bossy-Wetzel E, Radvanyi F, Klagsbrun M, Folkman J, and Hanahan D: Neovascularization is associated with a switch to the export of bFGF in the multistep development of fibrosarcoma. Cell 66: 1095-1104, 1991.

122. Dono R, Texido G, Dussel R, Ehmke H, and Zeller R: Impaired cerebral cortex development and blood pressure regulation in FGF-2-deficient mice. Embo J 17: 4213-4225, 1998.

123. Senger DR, Perruzzi CA, Feder J, and Dvorak HF: A highly conserved vascular permeability factor secreted by a variety of human and rodent tumor cell lines. Cancer Res 46: 5629-5632, 1986.

124. Ferrara N and Henzel WJ: Pituitary follicular cells secrete a novel heparin-binding growth factor specific for vascular endothelial cells. Biochem Biophys Res Commun 161: 851-858, 1989.

125. Plouet J, Schilling J, and Gospodarowicz D: Isolation and characterization of a newly identified endothelial cell mitogen produced by AtT-20 cells. Embo J 8: 3801-3806, 1989.

126. Gospodarowicz D, Abraham JA, and Schilling J: Isolation and characterization of a vascular endothelial cell mitogen produced by pituitary-derived folliculo stellate cells. Proc Natl Acad Sci U S A 86: 7311-7315, 1989.

127. Ferrara N, Carver-Moore K, Chen H, Dowd M, Lu L, O'Shea KS, Powell-Braxton L, Hillan KJ, and Moore MW: Heterozygous embryonic lethality induced by targeted inactivation of the VEGF gene. Nature 380: 439-442, 1996.

128. Carmeliet P, Ferreira V, Breier G, Pollefeyt S, Kieckens L, Gertsenstein M, Fahrig M, Vandenhoeck A, Harpal K, Eberhardt C, Declercq C, Pawling J, Moons L, Collen D, Risau W, and Nagy A: Abnormal blood vessel development and lethality in embryos lacking a single VEGF allele. Nature 380: 435-439, 1996.

129. Olofsson B, Pajusola K, Kaipainen A, von Euler G, Joukov V, Saksela O, Orpana A, Pettersson RF, Alitalo K, and Eriksson U: Vascular endothelial growth factor B, a novel growth factor for endothelial cells. Proc Natl Acad Sci U S A 93: 2576-2581, 1996.

130. Joukov V, Pajusola K, Kaipainen A, Chilov D, Lahtinen I, Kukk E, Saksela O, Kalkkinen N, and Alitalo K: A novel vascular endothelial growth factor, VEGF-C, is a ligand for the Flt4 (VEGFR-3) and KDR (VEGFR-2) receptor tyrosine kinases. Embo J 15: 1751, 1996.

131. Orlandini M, Marconcini L, Ferruzzi R, and Oliviero S: Identification of a c-fos-induced gene that is related to the platelet-derived growth factor/vascular endothelial growth factor family. Proc Natl Acad Sci U S A 93: 11675-11680, 1996.

132. Ogawa S, Oku A, Sawano A, Yamaguchi S, Yazaki Y, and Shibuya M: A novel type of vascular endothelial growth factor, VEGF-E (NZ-7 VEGF), preferentially utilizes KDR/Flk-1 receptor and carries a potent mitotic activity without heparin-binding domain. J Biol Chem 273: 31273-31282, 1998.

133. Maglione D, Guerriero V, Viglietto G, Delli-Bovi P, and Persico MG: Isolation of a human placenta cDNA coding for a protein related to the vascular permeability factor. Proc Natl Acad Sci U S A 88: 9267-9271, 1991.

134. Petit AM, Rak J, Hung MC, Rockwell P, Goldstein N, Fendly B, and Kerbel RS: Neutralizing antibodies against epidermal growth factor and ErbB-2/neu receptor tyrosine kinases down-regulate vascular endothelial growth factor production by

tumor cells in vitro and in vivo: angiogenic implications for signal transduction therapy of solid tumors. Am J Pathol 151: 1523-1530, 1997.

135. Rak J, Mitsuhashi Y, Bayko L, Filmus J, Shirasawa S, Sasazuki T, and Kerbel RS: Mutant ras oncogenes upregulate VEGF/VPF expression: implications for induction and inhibition of tumor angiogenesis. Cancer Res 55: 4575-4580, 1995.

136. Arbiser JL, Moses MA, Fernandez CA, Ghiso N, Cao Y, Klauber N, Frank D, Brownlee M, Flynn E, Parangi S, Byers HR, and Folkman J: Oncogenic H-ras stimulates tumor angiogenesis by two distinct pathways. Proc Natl Acad Sci U S A 94: 861-866, 1997.

137. Mazure NM, Chen EY, Yeh P, Laderoute KR, and Giaccia AJ: Oncogenic transformation and hypoxia synergistically act to modulate vascular endothelial growth factor expression. Cancer Res 56: 3436-3440, 1996.

138. Ferrara N and Davis-Smyth T: The biology of vascular endothelial growth factor. Endocr Rev 18: 4-25, 1997.

139. Ferrara N and Gerber HP: The role of vascular endothelial growth factor in angiogenesis. Acta Haematol 106: 148-156, 2001.

140. Roberts WG and Palade GE: Increased microvascular permeability and endothelial fenestration induced by vascular endothelial growth factor. J Cell Sci 108 (Pt 6): 2369-2379, 1995.

141. Dvorak HF, Harvey VS, Estrella P, Brown LF, McDonagh J, and Dvorak AM: Fibrin containing gels induce angiogenesis. Implications for tumor stroma generation and wound healing. Lab Invest 57: 673-686, 1987.

142. Chung J, Bachelder RE, Lipscomb EA, Shaw LM, and Mercurio AM: Integrin (alpha 6 beta 4) regulation of eIF-4E activity and VEGF translation: a survival mechanism for carcinoma cells. J Cell Biol 158: 165-174, 2002.

143. Bachelder RE, Crago A, Chung J, Wendt MA, Shaw LM, Robinson G, and Mercurio AM: Vascular endothelial growth factor is an autocrine survival factor for neuropilin-expressing breast carcinoma cells. Cancer Res 61: 5736-5740, 2001.

144. Harmey JH and Bouchier-Hayes D: Vascular endothelial growth factor (VEGF), a survival factor for tumour cells: implications for anti-angiogenic therapy. Bioessays 24: 280-283, 2002.

145. Gerber HP, McMurtrey A, Kowalski J, Yan M, Keyt BA, Dixit V, and Ferrara N: Vascular endothelial growth factor regulates endothelial cell survival through the phosphatidylinositol 3'-kinase/Akt signal transduction pathway. Requirement for Flk-1/KDR activation. J Biol Chem 273: 30336-30343, 1998.

146. Bussolati B, Deambrosis I, Russo S, Deregibus MC, and Camussi G: Altered angiogenesis and survival in human tumor-derived endothelial cells. Faseb J 17: 1159-1161, 2003.

147. Suzuma K, Naruse K, Suzuma I, Takahara N, Ueki K, Aiello LP, and King GL: Vascular endothelial growth factor induces expression of connective tissue growth factor via KDR, Flt1, and phosphatidylinositol 3-kinase-akt-dependent pathways in retinal vascular cells. J Biol Chem 275: 40725-40731, 2000.

148. Ferroni P, Spila A, Martini F, D'Alessandro R, Mariotti S, Del Monte G, Graziano P, Buonomo O, Guadagni F, and Roselli M: Prognostic value of vascular endothelial growth factor tumor tissue content of colorectal cancer. Oncology 69: 145-153, 2005.

149. Ding S, Lin S, Dong X, Yang X, Qu H, Huang S, Liu W, Zhou L, and Liu D: Potential prognostic value of circulating levels of vascular endothelial growth factor-A in patients with gastric cancer. In Vivo 19: 793-795, 2005.

150. Kobayashi A, Yamaguchi T, Ishihara T, Ohshima T, Baba T, Shirai Y, Tadenuma H, Nakamura K, and Saisho H: Usefulness of plasma vascular endothelial growth factor in the diagnosis of pancreatic carcinoma: differential diagnosis, tumor progression, and patient survival. Pancreas 31: 74-78, 2005.

151. Bando H, Weich HA, Brokelmann M, Horiguchi S, Funata N, Ogawa T, and Toi M: Association between intratumoral free and total VEGF, soluble VEGFR-1, VEGFR-2 and prognosis in breast cancer. Br J Cancer 92: 553-561, 2005.

152. Suri C, Jones PF, Patan S, Bartunkova S, Maisonpierre PC, Davis S, Sato TN, and Yancopoulos GD: Requisite role of angiopoietin-1, a ligand for the TIE2 receptor, during embryonic angiogenesis. Cell 87: 1171-1180, 1996.

153. Davis S, Aldrich TH, Jones PF, Acheson A, Compton DL, Jain V, Ryan TE, Bruno J, Radziejewski C, Maisonpierre PC, and Yancopoulos GD: Isolation of angiopoietin-1, a ligand for the TIE2 receptor, by secretion-trap expression cloning. Cell 87: 1161-1169, 1996.

154. Maisonpierre PC, Suri C, Jones PF, Bartunkova S, Wiegand SJ, Radziejewski C, Compton D, McClain J, Aldrich TH, Papadopoulos N, Daly TJ, Davis S, Sato TN, and Yancopoulos GD: Angiopoietin-2, a natural antagonist for Tie2 that disrupts in vivo angiogenesis. Science 277: 55-60, 1997.

155. Tsigkos S, Koutsilieris M, and Papapetropoulos A: Angiopoietins in angiogenesis and beyond. Expert Opin Investig Drugs 12: 933-941, 2003.

156. Ellis LM, Ahmad S, Fan F, Liu W, Jung YD, Stoeltzing O, Reinmuth N, and Parikh AA: Angiopoietins and their role in colon cancer angiogenesis. Oncology (Williston Park) 16: 31-35, 2002.

157. Metheny-Barlow LJ and Li LY: The enigmatic role of angiopoietin-1 in tumor angiogenesis. Cell Res 13: 309-317, 2003.

158. Gamble JR, Drew J, Trezise L, Underwood A, Parsons M, Kasminkas L, Rudge J, Yancopoulos G, and Vadas MA: Angiopoietin-1 is an antipermeability and anti-inflammatory agent in vitro and targets cell junctions. Circ Res 87: 603-607, 2000.

159. Zhang L, Yang N, Park JW, Katsaros D, Fracchioli S, Cao G, O'Brien-Jenkins A, Randall TC, Rubin SC, and Coukos G: Tumor-derived vascular endothelial growth factor up-regulates angiopoietin-2 in host endothelium and destabilizes host vasculature, supporting angiogenesis in ovarian cancer. Cancer Res 63: 3403-3412, 2003.

160. Shih SC, Robinson GS, Perruzzi CA, Calvo A, Desai K, Green JE, Ali IU, Smith LE, and Senger DR: Molecular profiling of angiogenesis markers. Am J Pathol 161: 35-41, 2002.

161. Tse V, Xu L, Yung YC, Santarelli JG, Juan D, Fabel K, Silverberg G, and Harsh Gt: The temporal-spatial expression of VEGF, angiopoietins-1 and 2, and Tie-2 during tumor angiogenesis and their functional correlation with tumor neovascular architecture. Neurol Res 25: 729-738, 2003.

162. Larcher F, Franco M, Bolontrade M, Rodriguez-Puebla M, Casanova L, Navarro M, Yancopoulos G, Jorcano JL, and Conti CJ: Modulation of the angiogenesis response through Ha-ras control, placenta growth factor, and angiopoietin expression in mouse skin carcinogenesis. Mol Carcinog 37: 83-90, 2003.

163. Yu Q and Stamenkovic I: Angiopoietin-2 is implicated in the regulation of tumor angiogenesis. Am J Pathol 158: 563-570, 2001.

164. Jung YD, Ahmad SA, Liu W, Reinmuth N, Parikh A, Stoeltzing O, Fan F, and Ellis LM: The role of the microenvironment and intercellular cross-talk in tumor angiogenesis. Semin Cancer Biol 12: 105-112, 2002.

165. Jain RK and Booth MF: What brings pericytes to tumor vessels? J Clin Invest 112: 1134-1136, 2003.

166. Benjamin LE, Hemo I, and Keshet E: A plasticity window for blood vessel remodelling is defined by pericyte coverage of the preformed endothelial network and is regulated by PDGF-B and VEGF. Development 125: 1591-1598, 1998.

167. Leek RD, Hunt NC, Landers RJ, Lewis CE, Royds JA, and Harris AL: Macrophage infiltration is associated with VEGF and EGFR expression in breast cancer. J Pathol 190: 430-436, 2000.

168. Zhang H and Issekutz AC: Growth factor regulation of neutrophil-endothelial cell interactions. J Leukoc Biol 70: 225-232, 2001.

169. Gruber BL, Marchese MJ, and Kew R: Angiogenic factors stimulate mast-cell migration. Blood 86: 2488-2493, 1995.

170. Barbera-Guillem E, Nyhus JK, Wolford CC, Friece CR, and Sampsel JW: Vascular endothelial growth factor secretion by tumor-infiltrating macrophages essentially supports tumor angiogenesis, and IgG immune complexes potentiate the process. Cancer Res 62: 7042-7049, 2002.

171. Coussens LM, Raymond WW, Bergers G, Laig-Webster M, Behrendtsen O, Werb Z, Caughey GH, and Hanahan D: Inflammatory mast cells up-regulate angiogenesis during squamous epithelial carcinogenesis. Genes Dev 13: 1382-1397, 1999.

172. Pollard JW: Tumour-educated macrophages promote tumour progression and metastasis. Nat Rev Cancer 4: 71-78, 2004.

173. Taichman NS, Young S, Cruchley AT, Taylor P, and Paleolog E: Human neutrophils secrete vascular endothelial growth factor. J Leukoc Biol 62: 397-400, 1997.

174. Annabi B, Lee YT, Turcotte S, Naud E, Desrosiers RR, Champagne M, Eliopoulos N, Galipeau J, and Beliveau R: Hypoxia promotes murine bone-marrow-derived stromal cell migration and tube formation. Stem Cells 21: 337-347, 2003.

175. Hendrix MJ, Seftor EA, Hess AR, and Seftor RE: Vasculogenic mimicry and tumour-cell plasticity: lessons from melanoma. Nat Rev Cancer 3: 411-421, 2003.

176. Leung DW, Cachianes G, Kuang WJ, Goeddel DV, and Ferrara N: Vascular endothelial growth factor is a secreted angiogenic mitogen. Science 246: 1306-1309, 1989.

177. Poltorak Z, Cohen T, Sivan R, Kandelis Y, Spira G, Vlodavsky I, Keshet E, and Neufeld G: VEGF145, a secreted vascular endothelial growth factor isoform that binds to extracellular matrix. J Biol Chem 272: 7151-7158, 1997.

178. Lei J, Jiang A, and Pei D: Identification and characterization of a new splicing variant of vascular endothelial growth factor: VEGF183. Biochim Biophys Acta 1443: 400-406, 1998.

179. Houck KA, Ferrara N, Winer J, Cachianes G, Li B, and Leung DW: The vascular endothelial growth factor family: identification of a fourth molecular species and characterization of alternative splicing of RNA. Mol Endocrinol 5: 1806-1814, 1991.

180. Bates DO, Cui TG, Doughty JM, Winkler M, Sugiono M, Shields JD, Peat D, Gillatt D, and Harper SJ: VEGF165b, an inhibitory splice variant of vascular endothelial growth factor, is down-regulated in renal cell carcinoma. Cancer Res 62: 4123-4131, 2002.

181. Cui TG, Foster RR, Saleem M, Mathieson PW, Gillatt DA, Bates DO, and Harper SJ: Differentiated human podocytes endogenously express an inhibitory isoform of vascular endothelial growth factor (VEGF165b) mRNA and protein. Am J Physiol Renal Physiol 286: F767-773, 2004.

182. Shima DT, Kuroki M, Deutsch U, Ng YS, Adamis AP, and D'Amore PA: The mouse gene for vascular endothelial growth factor. Genomic structure, definition of the transcriptional unit, and characterization of transcriptional and post-transcriptional regulatory sequences. J Biol Chem 271: 3877-3883, 1996.

183. Matthews W, Jordan CT, Gavin M, Jenkins NA, Copeland NG, and Lemischka IR: A receptor tyrosine kinase cDNA isolated from a population of enriched primitive

hematopoietic cells and exhibiting close genetic linkage to c-kit. Proc Natl Acad Sci U S A 88: 9026-9030, 1991.

184. Quinn TP, Peters KG, De Vries C, Ferrara N, and Williams LT: Fetal liver kinase 1 is a receptor for vascular endothelial growth factor and is selectively expressed in vascular endothelium. Proc Natl Acad Sci U S A 90: 7533-7537, 1993.

185. de Vries C, Escobedo JA, Ueno H, Houck K, Ferrara N, and Williams LT: The fms-like tyrosine kinase, a receptor for vascular endothelial growth factor. Science 255: 989-991, 1992.

186. Terman BI, Dougher-Vermazen M, Carrion ME, Dimitrov D, Armellino DC, Gospodarowicz D, and Bohlen P: Identification of the KDR tyrosine kinase as a receptor for vascular endothelial cell growth factor. Biochem Biophys Res Commun 187: 1579-1586, 1992.

187. Terman BI, Carrion ME, Kovacs E, Rasmussen BA, Eddy RL, and Shows TB: Identification of a new endothelial cell growth factor receptor tyrosine kinase. Oncogene 6: 1677-1683, 1991.

188. Galland F, Karamysheva A, Pebusque MJ, Borg JP, Rottapel R, Dubreuil P, Rosnet O, and Birnbaum D: The FLT4 gene encodes a transmembrane tyrosine kinase related to the vascular endothelial growth factor receptor. Oncogene 8: 1233-1240, 1993.

189. Gille H, Kowalski J, Li B, LeCouter J, Moffat B, Zioncheck TF, Pelletier N, and Ferrara N: Analysis of biological effects and signaling properties of Flt-1 (VEGFR-1) and KDR (VEGFR-2). A reassessment using novel receptor-specific vascular endothelial growth factor mutants. J Biol Chem 276: 3222-3230, 2001.

190. Shalaby F, Rossant J, Yamaguchi TP, Gertsenstein M, Wu XF, Breitman ML, and Schuh AC: Failure of blood-island formation and vasculogenesis in Flk-1-deficient mice. Nature 376: 62-66, 1995.

191. Fong GH, Rossant J, Gertsenstein M, and Breitman ML: Role of the Flt-1 receptor tyrosine kinase in regulating the assembly of vascular endothelium. Nature 376: 66-70, 1995.

192. Zeng H, Sanyal S, and Mukhopadhyay D: Tyrosine residues 951 and 1059 of vascular endothelial growth factor receptor-2 (KDR) are essential for vascular permeability factor/vascular endothelial growth factor-induced endothelium migration and proliferation, respectively. J Biol Chem 276: 32714-32719, 2001.

193. Matsumoto T, Bohman S, Dixelius J, Berge T, Dimberg A, Magnusson P, Wang L, Wikner C, Qi JH, Wernstedt C, Wu J, Bruheim S, Mugishima H, Mukhopadhyay D, Spurkland A, and Claesson-Welsh L: VEGF receptor-2 Y951 signaling and a role for the adapter molecule TSAd in tumor angiogenesis. Embo J 24: 2342-2353, 2005.

194. Zeng H, Dvorak HF, and Mukhopadhyay D: Vascular permeability factor (VPF)/vascular endothelial growth factor (VEGF) peceptor-1 down-modulates VPF/VEGF receptor-2-mediated endothelial cell proliferation, but not migration,

through phosphatidylinositol 3-kinase-dependent pathways. J Biol Chem 276: 26969-26979, 2001.

195. Shibuya M: Structure and dual function of vascular endothelial growth factor receptor-1 (Flt-1). Int J Biochem Cell Biol 33: 409-420, 2001.

196. Hiratsuka S, Minowa O, Kuno J, Noda T, and Shibuya M: Flt-1 lacking the tyrosine kinase domain is sufficient for normal development and angiogenesis in mice. Proc Natl Acad Sci U S A 95: 9349-9354, 1998.

197. Meyer RD, Mohammadi M, and Rahimi N: A single amino acid substitution in the activation loop defines the decoy characteristic of VEGFR-1/FLT-1. J Biol Chem 281: 867-875, 2006.

198. Lohela M, Saaristo A, Veikkola T, and Alitalo K: Lymphangiogenic growth factors, receptors and therapies. Thromb Haemost 90: 167-184, 2003.

199. Van Trappen PO, Steele D, Lowe DG, Baithun S, Beasley N, Thiele W, Weich H, Krishnan J, Shepherd JH, Pepper MS, Jackson DG, Sleeman JP, and Jacobs IJ: Expression of vascular endothelial growth factor (VEGF)-C and VEGF-D, and their receptor VEGFR-3, during different stages of cervical carcinogenesis. J Pathol 201: 544-554, 2003.

200. Mukherjee P, Bhattacharya R, Wang P, Wang L, Basu S, Nagy JA, Atala A, Mukhopadhyay D, and Soker S: Antiangiogenic properties of gold nanoparticles. Clin Cancer Res 11: 3530-3534, 2005.

201. Cardones AR and Banez LL: VEGF inhibitors in cancer therapy. Curr Pharm Des 12: 387-394, 2006.

202. Mulkeen AL, Silva T, Yoo PS, Schmitz JC, Uchio E, Chu E, and Cha C: Short interfering RNA-mediated gene silencing of vascular endothelial growth factor: effects on cellular proliferation in colon cancer cells. Arch Surg 141: 367-374; discussion 374, 2006.

203. Soker S, Takashima S, Miao HQ, Neufeld G, and Klagsbrun M: Neuropilin-1 is expressed by endothelial and tumor cells as an isoform-specific receptor for vascular endothelial growth factor. Cell 92: 735-745, 1998.

204. Gluzman-Poltorak Z, Cohen T, Herzog Y, and Neufeld G: Neuropilin-2 is a receptor for the vascular endothelial growth factor (VEGF) forms VEGF-145 and VEGF-165 [corrected]. J Biol Chem 275: 18040-18045, 2000.

205. He Z and Tessier-Lavigne M: Neuropilin is a receptor for the axonal chemorepellent Semaphorin III. Cell 90: 739-751, 1997.

206. Chen H, Chedotal A, He Z, Goodman CS, and Tessier-Lavigne M: Neuropilin-2, a novel member of the neuropilin family, is a high affinity receptor for the semaphorins Sema E and Sema IV but not Sema III. Neuron 19: 547-559, 1997.

207. Migdal M, Huppertz B, Tessler S, Comforti A, Shibuya M, Reich R, Baumann H, and Neufeld G: Neuropilin-1 is a placenta growth factor-2 receptor. J Biol Chem 273: 22272-22278, 1998.

208. Makinen T, Olofsson B, Karpanen T, Hellman U, Soker S, Klagsbrun M, Eriksson U, and Alitalo K: Differential binding of vascular endothelial growth factor B splice and proteolytic isoforms to neuropilin-1. J Biol Chem 274: 21217-21222, 1999.

209. Rossignol M, Gagnon ML, and Klagsbrun M: Genomic organization of human neuropilin-1 and neuropilin-2 genes: identification and distribution of splice variants and soluble isoforms. Genomics 70: 211-222, 2000.

210. Wang L, Zeng H, Wang P, Soker S, and Mukhopadhyay D: Neuropilin-1-mediated vascular permeability factor/vascular endothelial growth factor-dependent endothelial cell migration. J Biol Chem 278: 48848-48860, 2003.

211. Soker S, Miao HQ, Nomi M, Takashima S, and Klagsbrun M: VEGF165 mediates formation of complexes containing VEGFR-2 and neuropilin-1 that enhance VEGF165-receptor binding. J Cell Biochem 85: 357-368, 2002.

212. Mac Gabhann F and Popel AS: Differential binding of VEGF isoforms to VEGF receptor 2 in the presence of neuropilin-1: a computational model. Am J Physiol Heart Circ Physiol 288: H2851-2860, 2005.

213. Oh H: [A novel molecular mechanism involving neuropilin-1 for vascular endothelial growth factor-induced retinal angiogenesis]. Nippon Ganka Gakkai Zasshi 107: 651-656, 2003.

214. Houck KA, Leung DW, Rowland AM, Winer J, and Ferrara N: Dual regulation of vascular endothelial growth factor bioavailability by genetic and proteolytic mechanisms. J Biol Chem 267: 26031-26037, 1992.

215. Park JE, Keller GA, and Ferrara N: The vascular endothelial growth factor (VEGF) isoforms: differential deposition into the subepithelial extracellular matrix and bioactivity of extracellular matrix-bound VEGF. Mol Biol Cell 4: 1317-1326, 1993.

216. Neufeld G, Cohen T, Gitay-Goren H, Poltorak Z, Tessler S, Sharon R, Gengrinovitch S, and Levi BZ: Similarities and differences between the vascular endothelial growth factor (VEGF) splice variants. Cancer Metastasis Rev 15: 153-158, 1996.

217. Jones PF, Jakubowicz T, Pitossi FJ, Maurer F, and Hemmings BA: Molecular cloning and identification of a serine/threonine protein kinase of the second-messenger subfamily. Proc Natl Acad Sci U S A 88: 4171-4175, 1991.

218. Coffer PJ and Woodgett JR: Molecular cloning and characterisation of a novel putative protein-serine kinase related to the cAMP-dependent and protein kinase C families. Eur J Biochem 201: 475-481, 1991.

219. Staal SP, Hartley JW, and Rowe WP: Isolation of transforming murine leukemia viruses from mice with a high incidence of spontaneous lymphoma. Proc Natl Acad Sci U S A 74: 3065-3067, 1977.

220. Bellacosa A, Testa JR, Staal SP, and Tsichlis PN: A retroviral oncogene, akt, encoding a serine-threonine kinase containing an SH2-like region. Science 254: 274-277, 1991.

221. Ahmed NN, Franke TF, Bellacosa A, Datta K, Gonzalez-Portal ME, Taguchi T, Testa JR, and Tsichlis PN: The proteins encoded by c-akt and v-akt differ in post-translational modification, subcellular localization and oncogenic potential. Oncogene 8: 1957-1963, 1993.

222. Altomare DA, Guo K, Cheng JQ, Sonoda G, Walsh K, and Testa JR: Cloning, chromosomal localization and expression analysis of the mouse Akt2 oncogene. Oncogene 11: 1055-1060, 1995.

223. Konishi H, Kuroda S, Tanaka M, Matsuzaki H, Ono Y, Kameyama K, Haga T, and Kikkawa U: Molecular cloning and characterization of a new member of the RAC protein kinase family: association of the pleckstrin homology domain of three types of RAC protein kinase with protein kinase C subspecies and beta gamma subunits of G proteins. Biochem Biophys Res Commun 216: 526-534, 1995.

224. Masure S, Haefner B, Wesselink JJ, Hoefnagel E, Mortier E, Verhasselt P, Tuytelaars A, Gordon R, and Richardson A: Molecular cloning, expression and characterization of the human serine/threonine kinase Akt-3. Eur J Biochem 265: 353-360, 1999.

225. Chen WS, Xu PZ, Gottlob K, Chen ML, Sokol K, Shiyanova T, Roninson I, Weng W, Suzuki R, Tobe K, Kadowaki T, and Hay N: Growth retardation and increased apoptosis in mice with homozygous disruption of the Akt1 gene. Genes Dev 15: 2203-2208, 2001.

226. Cho H, Mu J, Kim JK, Thorvaldsen JL, Chu Q, Crenshaw EB, 3rd, Kaestner KH, Bartolomei MS, Shulman GI, and Birnbaum MJ: Insulin resistance and a diabetes mellitus-like syndrome in mice lacking the protein kinase Akt2 (PKB beta). Science 292: 1728-1731, 2001.

227. Garofalo RS, Orena SJ, Rafidi K, Torchia AJ, Stock JL, Hildebrandt AL, Coskran T, Black SC, Brees DJ, Wicks JR, McNeish JD, and Coleman KG: Severe diabetes, age-dependent loss of adipose tissue, and mild growth deficiency in mice lacking Akt2/PKB beta. J Clin Invest 112: 197-208, 2003.

228. Tschopp O, Yang ZZ, Brodbeck D, Dummler BA, Hemmings-Mieszczak M, Watanabe T, Michaelis T, Frahm J, and Hemmings BA: Essential role of protein kinase B gamma (PKB gamma/Akt3) in postnatal brain development but not in glucose homeostasis. Development 132: 2943-2954, 2005.

229. Peng XD, Xu PZ, Chen ML, Hahn-Windgassen A, Skeen J, Jacobs J, Sundararajan D, Chen WS, Crawford SE, Coleman KG, and Hay N: Dwarfism, impaired skin development, skeletal muscle atrophy, delayed bone development, and impeded adipogenesis in mice lacking Akt1 and Akt2. Genes Dev 17: 1352-1365, 2003.

230. Chan TO, Rittenhouse SE, and Tsichlis PN: AKT/PKB and other D3 phosphoinositide-regulated kinases: kinase activation by phosphoinositide-dependent phosphorylation. Annu Rev Biochem 68: 965-1014, 1999.

231. James SR, Downes CP, Gigg R, Grove SJ, Holmes AB, and Alessi DR: Specific binding of the Akt-1 protein kinase to phosphatidylinositol 3,4,5-trisphosphate without subsequent activation. Biochem J 315 (Pt 3): 709-713, 1996.

232. Bellacosa A, Chan TO, Ahmed NN, Datta K, Malstrom S, Stokoe D, McCormick F, Feng J, and Tsichlis P: Akt activation by growth factors is a multiple-step process: the role of the PH domain. Oncogene 17: 313-325., 1998.

233. Milburn CC, Deak M, Kelly SM, Price NC, Alessi DR, and Van Aalten DM: Binding of phosphatidylinositol 3,4,5-trisphosphate to the pleckstrin homology domain of protein kinase B induces a conformational change. Biochem J 375: 531-538., 2003.

234. Alessi DR, James SR, Downes CP, Holmes AB, Gaffney PR, Reese CB, and Cohen P: Characterization of a 3-phosphoinositide-dependent protein kinase which phosphorylates and activates protein kinase Balpha. Curr Biol 7: 261-269, 1997.

235. Troussard AA, Mawji NM, Ong C, Mui A, St -Arnaud R, and Dedhar S: Conditional knock-out of integrin-linked kinase demonstrates an essential role in protein kinase B/Akt activation. J Biol Chem 278: 22374-22378. Epub 22003 Apr 22378., 2003.

236. Persad S, Attwell S, Gray V, Mawji N, Deng JT, Leung D, Yan J, Sanghera J, Walsh MP, and Dedhar S: Regulation of protein kinase B/Akt-serine 473 phosphorylation by integrin-linked kinase: critical roles for kinase activity and amino acids arginine 211 and serine 343. J Biol Chem 276: 27462-27469, 2001.

237. Stambolic V, Suzuki A, de la Pompa JL, Brothers GM, Mirtsos C, Sasaki T, Ruland J, Penninger JM, Siderovski DP, and Mak TW: Negative regulation of PKB/Akt-dependent cell survival by the tumor suppressor PTEN. Cell 95: 29-39, 1998.

238. Maehama T and Dixon JE: The tumor suppressor, PTEN/MMAC1, dephosphorylates the lipid second messenger, phosphatidylinositol 3,4,5-trisphosphate. J Biol Chem 273: 13375-13378, 1998.

239. Vlahos CJ, Matter WF, Hui KY, and Brown RF: A specific inhibitor of phosphatidylinositol 3-kinase, 2-(4-morpholinyl)-8-phenyl-4H-1-benzopyran-4-one (LY294002). J Biol Chem 269: 5241-5248., 1994.

240. Walker EH, Pacold ME, Perisic O, Stephens L, Hawkins PT, Wymann MP, and Williams RL: Structural determinants of phosphoinositide 3-kinase inhibition by wortmannin, LY294002, quercetin, myricetin, and staurosporine. Mol Cell 6: 909-919, 2000.

241. Suhara T, Mano T, Oliveira BE, and Walsh K: Phosphatidylinositol 3-kinase/Akt signaling controls endothelial cell sensitivity to Fas-mediated apoptosis via regulation of FLICE-inhibitory protein (FLIP). Circ Res 89: 13-19, 2001.

242. Abid MR, Guo S, Minami T, Spokes KC, Ueki K, Skurk C, Walsh K, and Aird WC: Vascular endothelial growth factor activates PI3K/Akt/forkhead signaling in endothelial cells. Arterioscler Thromb Vasc Biol 24: 294-300, 2004.

243. Rena G, Guo S, Cichy SC, Unterman TG, and Cohen P: Phosphorylation of the transcription factor forkhead family member FKHR by protein kinase B. J Biol Chem 274: 17179-17183, 1999.

244. Burgering BM and Medema RH: Decisions on life and death: FOXO Forkhead transcription factors are in command when PKB/Akt is off duty. J Leukoc Biol 73: 689-701, 2003.

245. Datta SR, Dudek H, Tao X, Masters S, Fu H, Gotoh Y, and Greenberg ME: Akt phosphorylation of BAD couples survival signals to the cell-intrinsic death machinery. Cell 91: 231-241, 1997.

246. del Peso L, Gonzalez-Garcia M, Page C, Herrera R, and Nunez G: Interleukin-3-induced phosphorylation of BAD through the protein kinase Akt. Science 278: 687-689, 1997.

247. Downward J: How BAD phosphorylation is good for survival. Nat Cell Biol 1: E33-35, 1999.

248. Cardone MH, Roy N, Stennicke HR, Salvesen GS, Franke TF, Stanbridge E, Frisch S, and Reed JC: Regulation of cell death protease caspase-9 by phosphorylation. Science 282: 1318-1321, 1998.

249. Kane LP, Shapiro VS, Stokoe D, and Weiss A: Induction of NF-kappaB by the Akt/PKB kinase. Curr Biol 9: 601-604, 1999.

250. Zong WX, Edelstein LC, Chen C, Bash J, and Gelinas C: The prosurvival Bcl-2 homolog Bfl-1/A1 is a direct transcriptional target of NF-kappaB that blocks TNFalpha-induced apoptosis. Genes Dev 13: 382-387, 1999.

251. Chu ZL, McKinsey TA, Liu L, Gentry JJ, Malim MH, and Ballard DW: Suppression of tumor necrosis factor-induced cell death by inhibitor of apoptosis c-IAP2 is under NF-kappaB control. Proc Natl Acad Sci U S A 94: 10057-10062, 1997.

252. Alvarez B, Garrido E, Garcia-Sanz JA, and Carrera AC: Phosphoinositide 3-kinase activation regulates cell division time by coordinated control of cell mass and cell cycle progression rate. J Biol Chem 278: 26466-26473, 2003.

253. Diehl JA, Cheng M, Roussel MF, and Sherr CJ: Glycogen synthase kinase-3beta regulates cyclin D1 proteolysis and subcellular localization. Genes Dev 12: 3499-3511, 1998.

254. Rossig L, Jadidi AS, Urbich C, Badorff C, Zeiher AM, and Dimmeler S: Akt-dependent phosphorylation of p21(Cip1) regulates PCNA binding and proliferation of endothelial cells. Mol Cell Biol 21: 5644-5657, 2001.

255. Zhou BP, Liao Y, Xia W, Spohn B, Lee MH, and Hung MC: Cytoplasmic localization of p21Cip1/WAF1 by Akt-induced phosphorylation in HER-2/neu-overexpressing cells. Nat Cell Biol 3: 245-252, 2001.

256. Nave BT, Ouwens M, Withers DJ, Alessi DR, and Shepherd PR: Mammalian target of rapamycin is a direct target for protein kinase B: identification of a convergence point for opposing effects of insulin and amino-acid deficiency on protein translation. Biochem J 344 Pt 2: 427-431., 1999.

257. Kunz J, Henriquez R, Schneider U, Deuter-Reinhard M, Movva NR, and Hall MN: Target of rapamycin in yeast, TOR2, is an essential phosphatidylinositol kinase homolog required for G1 progression. Cell 73: 585-596., 1993.

258. Abraham RT and Wiederrecht GJ: Immunopharmacology of rapamycin. Annu Rev Immunol 14: 483-510, 1996.

259. Vezina C, Kudelski A, and Sehgal SN: Rapamycin (AY-22,989), a new antifungal antibiotic. I. Taxonomy of the producing streptomycete and isolation of the active principle. J Antibiot (Tokyo) 28: 721-726., 1975.

260. Camardo J: The Rapamune era of immunosuppression 2003: the journey from the laboratory to clinical transplantation. Transplant Proc 35: 18S-24S, 2003.

261. Heitman J, Movva NR, and Hall MN: Targets for cell cycle arrest by the immunosuppressant rapamycin in yeast. Science 253: 905-909, 1991.

262. Sabatini DM, Erdjument-Bromage H, Lui M, Tempst P, and Snyder SH: RAFT1: a mammalian protein that binds to FKBP12 in a rapamycin-dependent fashion and is homologous to yeast TORs. Cell 78: 35-43, 1994.

263. Aeder SE, Martin PM, Soh JW, and Hussaini IM: PKC-eta mediates glioblastoma cell proliferation through the Akt and mTOR signaling pathways. Oncogene 23: 9062-9069, 2004.

264. Tee AR, Anjum R, and Blenis J: Inactivation of the tuberous sclerosis complex-1 and -2 gene products occurs by phosphoinositide 3-kinase/Akt-dependent and -independent phosphorylation of tuberin. J Biol Chem 278: 37288-37296, 2003.

265. Wlodarski P, Kasprzycka M, Liu X, Marzec M, Robertson ES, Slupianek A, and Wasik MA: Activation of mammalian target of rapamycin in transformed B lymphocytes is nutrient dependent but independent of Akt, mitogen-activated protein kinase/extracellular signal-regulated kinase kinase, insulin growth factor-I, and serum. Cancer Res 65: 7800-7808, 2005.

266. Fang Y, Vilella-Bach M, Bachmann R, Flanigan A, and Chen J: Phosphatidic acid-mediated mitogenic activation of mTOR signaling. Science 294: 1942-1945, 2001.

267. Sekulic A, Hudson CC, Homme JL, Yin P, Otterness DM, Karnitz LM, and Abraham RT: A direct linkage between the phosphoinositide 3-kinase-AKT signaling pathway and the mammalian target of rapamycin in mitogen-stimulated and transformed cells. Cancer Res 60: 3504-3513., 2000.

268. Holz MK and Blenis J: Identification of S6 kinase 1 as a novel mammalian target of rapamycin (mTOR)-phosphorylating kinase. J Biol Chem 280: 26089-26093, 2005.

269. Zhang Y, Gao X, Saucedo LJ, Ru B, Edgar BA, and Pan D: Rheb is a direct target of the tuberous sclerosis tumour suppressor proteins. Nat Cell Biol 5: 578-581, 2003.

270. Tee AR, Manning BD, Roux PP, Cantley LC, and Blenis J: Tuberous sclerosis complex gene products, Tuberin and Hamartin, control mTOR signaling by acting as a GTPase-activating protein complex toward Rheb. Curr Biol 13: 1259-1268, 2003.

271. Garami A, Zwartkruis FJ, Nobukuni T, Joaquin M, Roccio M, Stocker H, Kozma SC, Hafen E, Bos JL, and Thomas G: Insulin activation of Rheb, a mediator of mTOR/S6K/4E-BP signaling, is inhibited by TSC1 and 2. Mol Cell 11: 1457-1466, 2003.

272. Chiang GG and Abraham RT: Phosphorylation of mammalian target of rapamycin (mTOR) at Ser-2448 is mediated by p70S6 kinase. J Biol Chem 280: 25485-25490, 2005.

273. Jefferies HB, Fumagalli S, Dennis PB, Reinhard C, Pearson RB, and Thomas G: Rapamycin suppresses 5'TOP mRNA translation through inhibition of p70s6k. Embo J 16: 3693-3704, 1997.

274. Terada N, Patel HR, Takase K, Kohno K, Nairn AC, and Gelfand EW: Rapamycin selectively inhibits translation of mRNAs encoding elongation factors and ribosomal proteins. Proc Natl Acad Sci U S A 91: 11477-11481, 1994.

275. Pullen N, Dennis PB, Andjelkovic M, Dufner A, Kozma SC, Hemmings BA, and Thomas G: Phosphorylation and activation of p70s6k by PDK1. Science 279: 707-710, 1998.

276. Lane HA, Fernandez A, Lamb NJ, and Thomas G: p70s6k function is essential for G1 progression. Nature 363: 170-172, 1993.

277. Kawasome H, Papst P, Webb S, Keller GM, Johnson GL, Gelfand EW, and Terada N: Targeted disruption of p70(s6k) defines its role in protein synthesis and rapamycin sensitivity. Proc Natl Acad Sci U S A 95: 5033-5038, 1998.

278. Brunn GJ, Hudson CC, Sekulic A, Williams JM, Hosoi H, Houghton PJ, Lawrence JC, Jr., and Abraham RT: Phosphorylation of the translational repressor PHAS-I by the mammalian target of rapamycin. Science 277: 99-101., 1997.

279. Hara K, Yonezawa K, Kozlowski MT, Sugimoto T, Andrabi K, Weng QP, Kasuga M, Nishimoto I, and Avruch J: Regulation of eIF-4E BP1 phosphorylation by mTOR. J Biol Chem 272: 26457-26463., 1997.

280. Rosenwald IB, Lazaris-Karatzas A, Sonenberg N, and Schmidt EV: Elevated levels of cyclin D1 protein in response to increased expression of eukaryotic initiation factor 4E. Mol Cell Biol 13: 7358-7363, 1993.

281. Lin TA, Kong X, Haystead TA, Pause A, Belsham G, Sonenberg N, and Lawrence JC, Jr.: PHAS-I as a link between mitogen-activated protein kinase and translation initiation. Science 266: 653-656, 1994.

282. Fingar DC and Blenis J: Target of rapamycin (TOR): an integrator of nutrient and growth factor signals and coordinator of cell growth and cell cycle progression. Oncogene 23: 3151-3171, 2004.

283. Dennis PB, Jaeschke A, Saitoh M, Fowler B, Kozma SC, and Thomas G: Mammalian TOR: a homeostatic ATP sensor. Science 294: 1102-1105, 2001.

284. Cota D, Proulx K, Smith KA, Kozma SC, Thomas G, Woods SC, and Seeley RJ: Hypothalamic mTOR signaling regulates food intake. Science 312: 927-930, 2006.

285. Fulton D, Gratton JP, McCabe TJ, Fontana J, Fujio Y, Walsh K, Franke TF, Papapetropoulos A, and Sessa WC: Regulation of endothelium-derived nitric oxide production by the protein kinase Akt. Nature 399: 597-601, 1999.

286. Dimmeler S, Fleming I, Fisslthaler B, Hermann C, Busse R, and Zeiher AM: Activation of nitric oxide synthase in endothelial cells by Akt-dependent phosphorylation. Nature 399: 601-605, 1999.

287. Papapetropoulos A, Garcia-Cardena G, Madri JA, and Sessa WC: Nitric oxide production contributes to the angiogenic properties of vascular endothelial growth factor in human endothelial cells. J Clin Invest 100: 3131-3139, 1997.

288. Carmeliet P: VEGF as a key mediator of angiogenesis in cancer. Oncology 69 Suppl 3: 4-10, 2005.

289. Roth D, Piekarek M, Paulsson M, Christ H, Krieg T, Bloch W, Davidson JM, and Eming SA: Plasmin modulates vascular endothelial growth factor-A-mediated angiogenesis during wound repair. Am J Pathol 168: 670-684, 2006.

290. Tober KL, Cannon RE, Spalding JW, Oberyszyn TM, Parrett ML, Rackoff AI, Oberyszyn AS, Tennant RW, and Robertson FM: Comparative expression of novel vascular endothelial growth factor/vascular permeability factor transcripts in skin, papillomas, and carcinomas of v-Ha-ras Tg.AC transgenic mice and FVB/N mice. Biochem Biophys Res Commun 247: 644-653, 1998.

291. Rahimi N: VEGFR-1 and VEGFR-2: two non-identical twins with a unique physiognomy. Front Biosci 11: 818-829, 2006.

292. Rahimi N, Dayanir V, and Lashkari K: Receptor chimeras indicate that the vascular endothelial growth factor receptor-1 (VEGFR-1) modulates mitogenic activity of VEGFR-2 in endothelial cells. J Biol Chem 275: 16986-16992, 2000.

293. Lau SC, Rosa DD, and Jayson G: Technology evaluation: VEGF Trap (cancer), Regeneron/sanofi-aventis. Curr Opin Mol Ther 7: 493-501, 2005.

294. Kim WJ, Yockman JW, Lee M, Jeong JH, Kim YH, and Kim SW: Soluble Flt-1 gene delivery using PEI-g-PEG-RGD conjugate for anti-angiogenesis. J Control Release 106: 224-234, 2005.

295. Zhang Z, Zou W, Wang J, Gu J, Dang Y, Li B, Zhao L, Qian C, Qian Q, and Liu X: Suppression of tumor growth by oncolytic adenovirus-mediated delivery of an antiangiogenic gene, soluble Flt-1. Mol Ther 11: 553-562, 2005.

296. Luttun A, Autiero M, Tjwa M, and Carmeliet P: Genetic dissection of tumor angiogenesis: are PlGF and VEGFR-1 novel anti-cancer targets? Biochim Biophys Acta 1654: 79-94, 2004.

297. Dunk C and Ahmed A: Vascular endothelial growth factor receptor-2-mediated mitogenesis is negatively regulated by vascular endothelial growth factor receptor-1 in tumor epithelial cells. Am J Pathol 158: 265-273, 2001.

298. Ye C, Feng C, Wang S, Wang KZ, Huang N, Liu X, Lin Y, and Li M: sFlt-1 gene therapy of follicular thyroid carcinoma. Endocrinology 145: 817-822, 2004.

299. Hasumi Y, Mizukami H, Urabe M, Kohno T, Takeuchi K, Kume A, Momoeda M, Yoshikawa H, Tsuruo T, Shibuya M, Taketani Y, and Ozawa K: Soluble FLT-1 expression suppresses carcinomatous ascites in nude mice bearing ovarian cancer. Cancer Res 62: 2019-2023, 2002.

300. Ferrara N: Vascular endothelial growth factor as a target for anticancer therapy. Oncologist 9 Suppl 1: 2-10, 2004.

301. Castilla MA, Neria F, Renedo G, Pereira DS, Gonzalez-Pacheco FR, Jimenez S, Tramon P, Deudero JJ, Arroyo MV, Yague S, and Caramelo C: Tumor-induced endothelial cell activation: role of vascular endothelial growth factor. Am J Physiol Cell Physiol 286: C1170-1176, 2004.

302. Franke TF, Yang SI, Chan TO, Datta K, Kazlauskas A, Morrison DK, Kaplan DR, and Tsichlis PN: The protein kinase encoded by the Akt proto-oncogene is a target of the PDGF-activated phosphatidylinositol 3-kinase. Cell 81: 727-736, 1995.

303. Burgering BM and Coffer PJ: Protein kinase B (c-Akt) in phosphatidylinositol-3-OH kinase signal transduction. Nature 376: 599-602, 1995.

304. Guo D, Jia Q, Song HY, Warren RS, and Donner DB: Vascular endothelial cell growth factor promotes tyrosine phosphorylation of mediators of signal transduction that contain SH2 domains. Association with endothelial cell proliferation. J Biol Chem 270: 6729-6733, 1995.

305. Xia P, Aiello LP, Ishii H, Jiang ZY, Park DJ, Robinson GS, Takagi H, Newsome WP, Jirousek MR, and King GL: Characterization of vascular endothelial growth factor's effect on the activation of protein kinase C, its isoforms, and endothelial cell growth. J Clin Invest 98: 2018-2026, 1996.

306. Delcommenne M, Tan C, Gray V, Rue L, Woodgett J, and Dedhar S: Phosphoinositide-3-OH kinase-dependent regulation of glycogen synthase kinase 3

and protein kinase B/AKT by the integrin-linked kinase. Proc Natl Acad Sci U S A 95: 11211-11216, 1998.

307. Troussard AA, Mawji NM, Ong C, Mui A, St -Arnaud R, and Dedhar S: Conditional knock-out of integrin-linked kinase demonstrates an essential role in protein kinase B/Akt activation. J Biol Chem 278: 22374-22378, 2003.

308. Edinger AL and Thompson CB: Akt maintains cell size and survival by increasing mTOR-dependent nutrient uptake. Mol Biol Cell 13: 2276-2288, 2002.

309. Faridi J, Fawcett J, Wang L, and Roth RA: Akt promotes increased mammalian cell size by stimulating protein synthesis and inhibiting protein degradation. Am J Physiol Endocrinol Metab 285: E964-972. Epub 2003 Jul 2022., 2003.

310. Proud CG: Regulation of mammalian translation factors by nutrients. Eur J Biochem 269: 5338-5349, 2002.

311. Fingar DC, Richardson CJ, Tee AR, Cheatham L, Tsou C, and Blenis J: mTOR controls cell cycle progression through its cell growth effectors S6K1 and 4E-BP1/eukaryotic translation initiation factor 4E. Mol Cell Biol 24: 200-216., 2004.

312. Pause A, Belsham GJ, Gingras AC, Donze O, Lin TA, Lawrence JC, Jr., and Sonenberg N: Insulin-dependent stimulation of protein synthesis by phosphorylation of a regulator of 5'-cap function. Nature 371: 762-767., 1994.

313. Fadden P, Haystead TA, and Lawrence JC, Jr.: Identification of phosphorylation sites in the translational regulator, PHAS-I, that are controlled by insulin and rapamycin in rat adipocytes. J Biol Chem 272: 10240-10247., 1997.

314. Fiebich BL, Jager B, Schollmann C, Weindel K, Wilting J, Kochs G, Marme D, Hug H, and Weich HA: Synthesis and assembly of functionally active human vascular endothelial growth factor homodimers in insect cells. Eur J Biochem 211: 19-26, 1993.

315. Zhang HT, Scott PA, Morbidelli L, Peak S, Moore J, Turley H, Harris AL, Ziche M, and Bicknell R: The 121 amino acid isoform of vascular endothelial growth factor is more strongly tumorigenic than other splice variants in vivo. Br J Cancer 83: 63-68, 2000.

316. Peretz D, Gitay-Goren H, Safran M, Kimmel N, Gospodarowicz D, and Neufeld G: Glycosylation of vascular endothelial growth factor is not required for its mitogenic activity. Biochem Biophys Res Commun 182: 1340-1347, 1992.

317. Zachary I and Gliki G: Signaling transduction mechanisms mediating biological actions of the vascular endothelial growth factor family. Cardiovasc Res 49: 568-581, 2001.

318. Tamilarasan KP, Kolluru GK, Rajaram M, Indhumathy M, Saranya R, and Chatterjee S: Thalidomide attenuates nitric oxide mediated angiogenesis by blocking migration of endothelial cells. BMC Cell Biol 7: 17, 2006.

319. Ettenson DS and Gotlieb AI: Centrosomes, microtubules, and microfilaments in the reendothelialization and remodeling of double-sided in vitro wounds. Lab Invest 66: 722-733, 1992.

320. Ettenson DS and Gotlieb AI: Endothelial wounds with disruption in cell migration repair primarily by cell proliferation. Microvasc Res 48: 328-337, 1994.

321. Carmeliet P and Jain RK: Angiogenesis in cancer and other diseases. Nature 407: 249-257, 2000.

322. Bolontrade MF, Stern MC, Binder RL, Zenklusen JC, Gimenez-Conti IB, and Conti CJ: Angiogenesis is an early event in the development of chemically induced skin tumors. Carcinogenesis 19: 2107-2113, 1998.

323. Bootle-Wilbraham CA, Tazzyman S, Marshall JM, and Lewis CE: Fibrinogen E-fragment inhibits the migration and tubule formation of human dermal microvascular endothelial cells in vitro. Cancer Res 60: 4719-4724, 2000.

324. Grunstein J, Masbad JJ, Hickey R, Giordano F, and Johnson RS: Isoforms of vascular endothelial growth factor act in a coordinate fashion To recruit and expand tumor vasculature. Mol Cell Biol 20: 7282-7291, 2000.

325. Tan C, Cruet-Hennequart S, Troussard A, Fazli L, Costello P, Sutton K, Wheeler J, Gleave M, Sanghera J, and Dedhar S: Regulation of tumor angiogenesis by integrin-linked kinase (ILK). Cancer Cell 5: 79-90, 2004.

326. Enomoto A, Murakami H, Asai N, Morone N, Watanabe T, Kawai K, Murakumo Y, Usukura J, Kaibuchi K, and Takahashi M: Akt/PKB regulates actin organization and cell motility via Girdin/APE. Dev Cell 9: 389-402, 2005.

327. Irie HY, Pearline RV, Grueneberg D, Hsia M, Ravichandran P, Kothari N, Natesan S, and Brugge JS: Distinct roles of Akt1 and Akt2 in regulating cell migration and epithelial-mesenchymal transition. J Cell Biol 171: 1023-1034, 2005.

328. Ackah E, Yu J, Zoellner S, Iwakiri Y, Skurk C, Shibata R, Ouchi N, Easton RM, Galasso G, Birnbaum MJ, Walsh K, and Sessa WC: Akt1/protein kinase Balpha is critical for ischemic and VEGF-mediated angiogenesis. J Clin Invest 115: 2119-2127, 2005.

329. Scott PH, Brunn GJ, Kohn AD, Roth RA, and Lawrence JC, Jr.: Evidence of insulin-stimulated phosphorylation and activation of the mammalian target of rapamycin mediated by a protein kinase B signaling pathway. Proc Natl Acad Sci U S A 95: 7772-7777, 1998.

330. Balmain A, Ramsden M, Bowden GT, and Smith J: Activation of the mouse cellular Harvey-ras gene in chemically induced benign skin papillomas. Nature 307: 658-660, 1984.

331. Balmain A, Brown K, Akhurst RJ, and Fee FM: Molecular analysis of chemical carcinogenesis in the skin. Br J Cancer Suppl 9: 72-75, 1988.

332. Binder RL, Gallagher PM, Johnson GR, Stockman SL, Smith BJ, Sundberg JP, and Conti CJ: Evidence that initiated keratinocytes clonally expand into multiple existing hair follicles during papilloma histogenesis in SENCAR mouse skin. Mol Carcinog 20: 151-158, 1997.

333. Martinez LA, Chen Y, Fischer SM, and Conti CJ: Coordinated changes in cell cycle machinery occur during keratinocyte terminal differentiation. Oncogene 18: 397-406, 1999.

334. DiGiovanni J, Bol DK, Wilker E, Beltran L, Carbajal S, Moats S, Ramirez A, Jorcano J, and Kiguchi K: Constitutive expression of insulin-like growth factor-1 in epidermal basal cells of transgenic mice leads to spontaneous tumor promotion. Cancer Res 60: 1561-1570, 2000.

335. Segrelles C, Ruiz S, Perez P, Murga C, Santos M, Budunova IV, Martinez J, Larcher F, Slaga TJ, Gutkind JS, Jorcano JL, and Paramio JM: Functional roles of Akt signaling in mouse skin tumorigenesis. Oncogene 21: 53-64, 2002.

336. Sun M, Wang G, Paciga JE, Feldman RI, Yuan ZQ, Ma XL, Shelley SA, Jove R, Tsichlis PN, Nicosia SV, and Cheng JQ: AKT1/PKBalpha kinase is frequently elevated in human cancers and its constitutive activation is required for oncogenic transformation in NIH3T3 cells. Am J Pathol 159: 431-437, 2001.

337. Segrelles C, Ruiz S, Santos M, Martinez-Palacio J, Lara MF, and Paramio JM: Akt mediates an angiogenic switch in transformed keratinocytes. Carcinogenesis 25: 1137-1147, 2004.

338. Robertson FM, Ross MS, Tober KL, Long BW, and Oberyszyn TM: Inhibition of pro-inflammatory cytokine gene expression and papilloma growth during murine multistage carcinogenesis by pentoxifylline. Carcinogenesis 17: 1719-1728, 1996.

339. Mihm MJ, Coyle CM, Jing L, and Bauer JA: Vascular peroxynitrite formation during organic nitrate tolerance. J Pharmacol Exp Ther 291: 194-198, 1999.

340. Mihm MJ, Coyle CM, Schanbacher BL, Weinstein DM, and Bauer JA: Peroxynitrite induced nitration and inactivation of myofibrillar creatine kinase in experimental heart failure. Cardiovasc Res 49: 798-807, 2001.

341. Mihm MJ, Yu F, Weinstein DM, Reiser PJ, and Bauer JA: Intracellular distribution of peroxynitrite during doxorubicin cardiomyopathy: evidence for selective impairment of myofibrillar creatine kinase. Br J Pharmacol 135: 581-588, 2002.

342. Poladia DP and Bauer JA: Early cell-specific changes in nitric oxide synthases, reactive nitrogen species formation, and ubiquitinylation during diabetes-related bladder remodeling. Diabetes Metab Res Rev 19: 313-319, 2003.

343. Trush MA, Egner PA, and Kensler TW: Myeloperoxidase as a biomarker of skin irritation and inflammation. Food Chem Toxicol 32: 143-147, 1994.

344. Leis H, Segrelles C, Ruiz S, Santos M, and Paramio JM: Expression, localization, and activity of glycogen synthase kinase 3beta during mouse skin tumorigenesis. Mol Carcinog 35: 180-185, 2002.

345. Stenback F, Peto R, and Shubik P: Initiation and promotion at different ages and doses in 2200 mice. I. Methods, and the apparent persistence of initiated cells. Br J Cancer 44: 1-14, 1981.

346. Ariza ME, Oberyszyn AS, Robertson FM, and Williams MV: Mutagenic potential of peripheral blood leukocytes: in vivo exposure to the carcinogen 7,12-dimethylbenz[a]anthracene, and the tumor promoter 12-O-tetradecanoylphorbol acetate followed by in vitro co-culture with AS52 cells. Cancer Lett 106: 9-16, 1996.

347. Sirak AA, Beavis AJ, and Robertson FM: Enhanced hydroperoxide production by peripheral blood leukocytes following exposure of murine epidermis to 12-O-tetradecanoylphorbol-13-acetate. Carcinogenesis 12: 91-95, 1991.

348. Robertson FM, Beavis AJ, Oberyszyn TM, O'Connell SM, Dokidos A, Laskin DL, Laskin JD, and Reiners JJ, Jr.: Production of hydrogen peroxide by murine epidermal keratinocytes following treatment with the tumor promoter 12-O-tetradecanoylphorbol-13-acetate. Cancer Res 50: 6062-6067, 1990.

349. Perchellet EM, Abney NL, and Perchellet JP: Stimulation of hydroperoxide generation in mouse skins treated with tumor-promoting or carcinogenic agents in vivo and in vitro. Cancer Lett 42: 169-177, 1988.

350. Fischer SM, Cameron GS, Baldwin JK, Jasheway DW, and Patrick KE: Reactive oxygen in the tumor promotion stage of skin carcinogenesis. Lipids 23: 592-597, 1988.

351. Wang X, McCullough KD, Franke TF, and Holbrook NJ: Epidermal growth factor receptor-dependent Akt activation by oxidative stress enhances cell survival. J Biol Chem 275: 14624-14631, 2000.

352. Huang C, Li J, Ding M, Leonard SS, Wang L, Castranova V, Vallyathan V, and Shi X: UV Induces phosphorylation of protein kinase B (Akt) at Ser-473 and Thr-308 in mouse epidermal Cl 41 cells through hydrogen peroxide. J Biol Chem 276: 40234-40240, 2001.

353. Butts BD, Kwei KA, Bowden GT, and Briehl MM: Elevated basal reactive oxygen species and phospho-Akt in murine keratinocytes resistant to ultraviolet B-induced apoptosis. Mol Carcinog 37: 149-157, 2003.

354. Shaw M, Cohen P, and Alessi DR: The activation of protein kinase B by H2O2 or heat shock is mediated by phosphoinositide 3-kinase and not by mitogen-activated protein kinase-activated protein kinase-2. Biochem J 336 (Pt 1): 241-246, 1998.

355. Klotz LO, Schieke SM, Sies H, and Holbrook NJ: Peroxynitrite activates the phosphoinositide 3-kinase/Akt pathway in human skin primary fibroblasts. Biochem J 352 Pt 1: 219-225, 2000.

356. Potten CS and Booth C: Keratinocyte stem cells: a commentary. J Invest Dermatol 119: 888-899, 2002.

357. Morris RJ: Keratinocyte stem cells: targets for cutaneous carcinogens. J Clin Invest 106: 3-8, 2000.

358. Kaur P: Interfollicular Epidermal Stem Cells: Identification, Challenges, Potential. J Invest Dermatol, 2006.

359. Cotsarelis G: Gene expression profiling gets to the root of human hair follicle stem cells. J Clin Invest 116: 19-22, 2006.

360. Lavker RM and Sun TT: Epidermal stem cells: properties, markers, and location. Proc Natl Acad Sci U S A 97: 13473-13475, 2000.

361. Stenn KS and Cotsarelis G: Bioengineering the hair follicle: fringe benefits of stem cell technology. Curr Opin Biotechnol 16: 493-497, 2005.

362. Ito M, Kizawa K, Hamada K, and Cotsarelis G: Hair follicle stem cells in the lower bulge form the secondary germ, a biochemically distinct but functionally equivalent progenitor cell population, at the termination of catagen. Differentiation 72: 548-557, 2004.

363. Affara NI, Schanbacher BL, Mihm MJ, Cook AC, Pei P, Mallery SR, Trempus CS, Bauer JA, and Robertson FM: Activated Akt-1 in specific cell populations during multi-stage skin carcinogenesis. Anticancer Res 24: 2773-2781, 2004.

364. Xu Q, Thompson JE, and Carroll M: mTOR regulates cell survival after etoposide treatment in primary AML cells. Blood 106: 4261-4268, 2005.

365. Takuwa N, Fukui Y, and Takuwa Y: Cyclin D1 expression mediated by phosphatidylinositol 3-kinase through mTOR-p70(S6K)-independent signaling in growth factor-stimulated NIH 3T3 fibroblasts. Mol Cell Biol 19: 1346-1358, 1999.

366. Grewe M, Gansauge F, Schmid RM, Adler G, and Seufferlein T: Regulation of cell growth and cyclin D1 expression by the constitutively active FRAP-p70s6K pathway in human pancreatic cancer cells. Cancer Res 59: 3581-3587, 1999.

367. Burnworth B, Popp S, Stark HJ, Steinkraus V, Brocker EB, Hartschuh W, Birek C, and Boukamp P: Gain of 11q/cyclin D1 overexpression is an essential early step in skin cancer development and causes abnormal tissue organization and differentiation. Oncogene, 2006.

368. Segrelles C, Moral M, Lara MF, Ruiz S, Santos M, Leis H, Garcia-Escudero R, Martinez-Cruz AB, Martinez-Palacio J, Hernandez P, Ballestin C, and Paramio JM: Molecular determinants of Akt-induced keratinocyte transformation. Oncogene 25: 1174-1185, 2006.

369. Yamamoto H, Ochiya T, Takeshita F, Toriyama-Baba H, Hirai K, Sasaki H, Sakamoto H, Yoshida T, Saito I, and Terada M: Enhanced skin carcinogenesis in

cyclin D1-conditional transgenic mice: cyclin D1 alters keratinocyte response to calcium-induced terminal differentiation. Cancer Res 62: 1641-1647, 2002.

370. Di-Poi N, Ng CY, Tan NS, Yang Z, Hemmings BA, Desvergne B, Michalik L, and Wahli W: Epithelium-mesenchyme interactions control the activity of peroxisome proliferator-activated receptor beta/delta during hair follicle development. Mol Cell Biol 25: 1696-1712, 2005.

371. Kim SJ, Cheon SH, Yoo SJ, Kwon J, Park JH, Kim CG, Rhee K, You S, Lee JY, Roh SI, and Yoon HS: Contribution of the PI3K/Akt/PKB signal pathway to maintenance of self-renewal in human embryonic stem cells. FEBS Lett 579: 534-540, 2005.

372. Paling NR, Wheadon H, Bone HK, and Welham MJ: Regulation of embryonic stem cell self-renewal by phosphoinositide 3-kinase-dependent signaling. J Biol Chem 279: 48063-48070, 2004.

373. Alonso L, Okada H, Pasolli HA, Wakeham A, You-Ten AI, Mak TW, and Fuchs E: Sgk3 links growth factor signaling to maintenance of progenitor cells in the hair follicle. J Cell Biol 170: 559-570, 2005.

374. Morris RJ: A perspective on keratinocyte stem cells as targets for skin carcinogenesis. Differentiation 72: 381-386, 2004.

375. Morris RJ, Coulter K, Tryson K, and Steinberg SR: Evidence that cutaneous carcinogen-initiated epithelial cells from mice are quiescent rather than actively cycling. Cancer Res 57: 3436-3443, 1997.

376. Thrash BR, Menges CW, Pierce RH, and McCance DJ: AKT1 provides an essential survival signal required for differentiation and stratification on primary human keratinocytes. J Biol Chem, 2006.

377. Brunn GJ, Williams J, Sabers C, Wiederrecht G, Lawrence JC, Jr., and Abraham RT: Direct inhibition of the signaling functions of the mammalian target of rapamycin by the phosphoinositide 3-kinase inhibitors, wortmannin and LY294002. Embo J 15: 5256-5267, 1996.

378. Robles AI and Conti CJ: Early overexpression of cyclin D1 protein in mouse skin carcinogenesis. Carcinogenesis 16: 781-786, 1995.

379. Celis JE and Celis A: Cell cycle-dependent variations in the distribution of the nuclear protein cyclin proliferating cell nuclear antigen in cultured cells: subdivision of S phase. Proc Natl Acad Sci U S A 82: 3262-3266, 1985.

380. Jemal A, Tiwari RC, Murray T, Ghafoor A, Samuels A, Ward E, Feuer EJ, and Thun MJ: Cancer statistics, 2004. CA Cancer J Clin 54: 8-29, 2004.

381. Kripke ML: Latency, histology, and antigenicity of tumors induced by ultraviolet light in three inbred mouse strains. Cancer Res 37: 1395-1400, 1977.

382. Strickland PT: Tumor induction in Sencar mice in response to ultraviolet radiation. Carcinogenesis 3: 1487-1489, 1982.

383. de Gruijl FR: Photocarcinogenesis: UVA vs UVB. Methods Enzymol 319: 359-366, 2000.

384. Willis I, Menter JM, and Whyte HJ: The rapid induction of cancers in the hairless mouse utilizing the principle of photoaugmentation. J Invest Dermatol 76: 404-408, 1981.

385. Gervin CM, McCulla A, Williams M, and Ouhtit A: Dysfunction of p53 in photocarcinogenesis. Front Biosci 8: s715-717, 2003.

386. Campbell C, Quinn AG, Angus B, Farr PM, and Rees JL: Wavelength specific patterns of p53 induction in human skin following exposure to UV radiation. Cancer Res 53: 2697-2699, 1993.

387. Kress S, Sutter C, Strickland PT, Mukhtar H, Schweizer J, and Schwarz M: Carcinogen-specific mutational pattern in the p53 gene in ultraviolet B radiation-induced squamous cell carcinomas of mouse skin. Cancer Res 52: 6400-6403, 1992.

388. de Gruijl FR, van Kranen HJ, and Mullenders LH: UV-induced DNA damage, repair, mutations and oncogenic pathways in skin cancer. J Photochem Photobiol B 63: 19-27, 2001.

389. Wilker E, Lu J, Rho O, Carbajal S, Beltran L, and DiGiovanni J: Role of PI3K/Akt signaling in insulin-like growth factor-1 (IGF-1) skin tumor promotion. Mol Carcinog 44: 137-145, 2005.

390. Brenneisen P, Wenk J, Wlaschek M, Krieg T, and Scharffetter-Kochanek K: Activation of p70 ribosomal protein S6 kinase is an essential step in the DNA damage-dependent signaling pathway responsible for the ultraviolet B-mediated increase in interstitial collagenase (MMP-1) and stromelysin-1 (MMP-3) protein levels in human dermal fibroblasts. J Biol Chem 275: 4336-4344, 2000.

391. Shiojima I and Walsh K: Role of Akt signaling in vascular homeostasis and angiogenesis. Circ Res 90: 1243-1250, 2002.

392. Nijsten T, Colpaert CG, Vermeulen PB, Harris AL, Van Marck E, and Lambert J: Cyclooxygenase-2 expression and angiogenesis in squamous cell carcinoma of the skin and its precursors: a paired immunohistochemical study of 35 cases. Br J Dermatol 151: 837-845, 2004.

393. Howell BG, Wang B, Freed I, Mamelak AJ, Watanabe H, and Sauder DN: Microarray analysis of UVB-regulated genes in keratinocytes: downregulation of angiogenesis inhibitor thrombospondin-1. J Dermatol Sci 34: 185-194, 2004.

394. Yano K, Kajiya K, Ishiwata M, Hong YK, Miyakawa T, and Detmar M: Ultraviolet B-induced skin angiogenesis is associated with a switch in the balance of vascular

endothelial growth factor and thrombospondin-1 expression. J Invest Dermatol 122: 201-208, 2004.

395. Stein I, Itin A, Einat P, Skaliter R, Grossman Z, and Keshet E: Translation of vascular endothelial growth factor mRNA by internal ribosome entry: implications for translation under hypoxia. Mol Cell Biol 18: 3112-3119, 1998.

396. Larcher F, Robles AI, Duran H, Murillas R, Quintanilla M, Cano A, Conti CJ, and Jorcano JL: Up-regulation of vascular endothelial growth factor/vascular permeability factor in mouse skin carcinogenesis correlates with malignant progression state and activated H-ras expression levels. Cancer Res 56: 5391-5396, 1996.

397. Brauchle M, Funk JO, Kind P, and Werner S: Ultraviolet B and H2O2 are potent inducers of vascular endothelial growth factor expression in cultured keratinocytes. J Biol Chem 271: 21793-21797, 1996.

398. Yano K, Kadoya K, Kajiya K, Hong YK, and Detmar M: Ultraviolet B irradiation of human skin induces an angiogenic switch that is mediated by upregulation of vascular endothelial growth factor and by downregulation of thrombospondin-1. Br J Dermatol 152: 115-121, 2005.

399. Kevil CG, De Benedetti A, Payne DK, Coe LL, Laroux FS, and Alexander JS: Translational regulation of vascular permeability factor by eukaryotic initiation factor 4E: implications for tumor angiogenesis. Int J Cancer 65: 785-790, 1996.

400. Akiri G, Nahari D, Finkelstein Y, Le SY, Elroy-Stein O, and Levi BZ: Regulation of vascular endothelial growth factor (VEGF) expression is mediated by internal initiation of translation and alternative initiation of transcription. Oncogene 17: 227-236, 1998.

401. Panteleyev AA, Paus R, and Christiano AM: Patterns of hairless (hr) gene expression in mouse hair follicle morphogenesis and cycling. Am J Pathol 157: 1071-1079, 2000.

402. DeLisser HM, Newman PJ, and Albelda SM: Molecular and functional aspects of PECAM-1/CD31. Immunol Today 15: 490-495, 1994.

403. Saladi RN and Persaud AN: The causes of skin cancer: a comprehensive review. Drugs Today (Barc) 41: 37-53, 2005.

404. Bachelor MA, Cooper SJ, Sikorski ET, and Bowden GT: Inhibition of p38 mitogen-activated protein kinase and phosphatidylinositol 3-kinase decreases UVB-induced activator protein-1 and cyclooxygenase-2 in a SKH-1 hairless mouse model. Mol Cancer Res 3: 90-99, 2005.

405. Kanjilal S, Pierceall WE, Cummings KK, Kripke ML, and Ananthaswamy HN: High frequency of p53 mutations in ultraviolet radiation-induced murine skin tumors: evidence for strand bias and tumor heterogeneity. Cancer Res 53: 2961-2964, 1993.

406. Cross DA, Alessi DR, Cohen P, Andjelkovich M, and Hemmings BA: Inhibition of glycogen synthase kinase-3 by insulin mediated by protein kinase B. Nature 378: 785-789, 1995.

407. Yano K, Oura H, and Detmar M: Targeted overexpression of the angiogenesis inhibitor thrombospondin-1 in the epidermis of transgenic mice prevents ultraviolet-B-induced angiogenesis and cutaneous photo-damage. J Invest Dermatol 118: 800-805, 2002.

408. Levy AP, Levy NS, Wegner S, and Goldberg MA: Transcriptional regulation of the rat vascular endothelial growth factor gene by hypoxia. J Biol Chem 270: 13333-13340, 1995.

409. Bielenberg DR, Bucana CD, Sanchez R, Donawho CK, Kripke ML, and Fidler IJ: Molecular regulation of UVB-induced cutaneous angiogenesis. J Invest Dermatol 111: 864-872, 1998.

410. Grutzkau A, Kruger-Krasagakes S, Baumeister H, Schwarz C, Kogel H, Welker P, Lippert U, Henz BM, and Moller A: Synthesis, storage, and release of vascular endothelial growth factor/vascular permeability factor (VEGF/VPF) by human mast cells: implications for the biological significance of VEGF206. Mol Biol Cell 9: 875-884, 1998.

411. Bashkin P, Razin E, Eldor A, and Vlodavsky I: Degranulating mast cells secrete an endoglycosidase that degrades heparan sulfate in subendothelial extracellular matrix. Blood 75: 2204-2212, 1990.

412. Coussens LM and Werb Z: Matrix metalloproteinases and the development of cancer. Chem Biol 3: 895-904, 1996.

413. Azizkhan RG, Azizkhan JC, Zetter BR, and Folkman J: Mast cell heparin stimulates migration of capillary endothelial cells in vitro. J Exp Med 152: 931-944, 1980.

414. Mierke CT, Ballmaier M, Werner U, Manns MP, Welte K, and Bischoff SC: Human endothelial cells regulate survival and proliferation of human mast cells. J Exp Med 192: 801-811, 2000.

415. Hebda PA and Sandulache VC. The Biochemistry of Epidermal Healing. In: The epidermis in wound healing, edited by Rovee DT and Maibach HI: CRC Press, 2004, p. 59-86.

416. Yamaguchi Y and Yoshikawa K: Cutaneous wound healing: an update. J Dermatol 28: 521-534, 2001.

417. Kirsner RS and Eaglstein WH: The wound healing process. Dermatol Clin 11: 629-640, 1993.

418. Lundberg C, Lebel L, and Gerdin B: The inflammatory reaction in healing wounds: the role of polymorphonuclear leucocytes. Int J Tissue React 6: 477-483, 1984.

419. Rothe M and Falanga V: Growth factors. Their biology and promise in dermatologic diseases and tissue repair. Arch Dermatol 125: 1390-1398, 1989.

420. Gallucci RM, Simeonova PP, Matheson JM, Kommineni C, Guriel JL, Sugawara T, and Luster MI: Impaired cutaneous wound healing in interleukin-6-deficient and immunosuppressed mice. Faseb J 14: 2525-2531, 2000.

421. Hertle MD, Kubler MD, Leigh IM, and Watt FM: Aberrant integrin expression during epidermal wound healing and in psoriatic epidermis. J Clin Invest 89: 1892-1901, 1992.

422. Fathke C, Wilson L, Hutter J, Kapoor V, Smith A, Hocking A, and Isik F: Contribution of bone marrow-derived cells to skin: collagen deposition and wound repair. Stem Cells 22: 812-822, 2004.

423. Finesmith TH, Broadley KN, and Davidson JM: Fibroblasts from wounds of different stages of repair vary in their ability to contract a collagen gel in response to growth factors. J Cell Physiol 144: 99-107, 1990.

424. Darby I, Skalli O, and Gabbiani G: Alpha-smooth muscle actin is transiently expressed by myofibroblasts during experimental wound healing. Lab Invest 63: 21-29, 1990.

425. Grinnell F: Fibroblasts, myofibroblasts, and wound contraction. J Cell Biol 124: 401-404, 1994.

426. Zhang N, Fang Z, Contag PR, Purchio AF, and West DB: Tracking angiogenesis induced by skin wounding and contact hypersensitivity using a Vegfr2-luciferase transgenic mouse. Blood 103: 617-626, 2004.

427. Li J, Zhang YP, and Kirsner RS: Angiogenesis in wound repair: angiogenic growth factors and the extracellular matrix. Microsc Res Tech 60: 107-114, 2003.

428. Patel GK, Wilson CH, Harding KG, Finlay AY, and Bowden PE: Numerous keratinocyte subtypes involved in wound re-epithelialization. J Invest Dermatol 126: 497-502, 2006.

429. Nishimura EK, Granter SR, and Fisher DE: Mechanisms of hair graying: incomplete melanocyte stem cell maintenance in the niche. Science 307: 720-724, 2005.

430. Amendt C, Mann A, Schirmacher P, and Blessing M: Resistance of keratinocytes to TGFbeta-mediated growth restriction and apoptosis induction accelerates re-epithelialization in skin wounds. J Cell Sci 115: 2189-2198, 2002.

431. Datta SR, Brunet A, and Greenberg ME: Cellular survival: a play in three Akts. Genes Dev 13: 2905-2927, 1999.

432. Plas DR and Thompson CB: Akt-dependent transformation: there is more to growth than just surviving. Oncogene 24: 7435-7442, 2005.

433. Tan NS, Michalik L, Di-Poi N, Desvergne B, and Wahli W: Critical roles of the nuclear receptor PPARbeta (peroxisome-proliferator-activated receptor beta) in skin wound healing. Biochem Soc Trans 32: 97-102, 2004.

434. Michalik L, Desvergne B, Tan NS, Basu-Modak S, Escher P, Rieusset J, Peters JM, Kaya G, Gonzalez FJ, Zakany J, Metzger D, Chambon P, Duboule D, and Wahli W: Impaired skin wound healing in peroxisome proliferator-activated receptor (PPAR)alpha and PPARbeta mutant mice. J Cell Biol 154: 799-814, 2001.

435. Di-Poi N, Tan NS, Michalik L, Wahli W, and Desvergne B: Antiapoptotic role of PPARbeta in keratinocytes via transcriptional control of the Akt1 signaling pathway. Mol Cell 10: 721-733, 2002.

436. Chung CY, Potikyan G, and Firtel RA: Control of cell polarity and chemotaxis by Akt/PKB and PI3 kinase through the regulation of PAKa. Mol Cell 7: 937-947, 2001.

437. Merlot S and Firtel RA: Leading the way: Directional sensing through phosphatidylinositol 3-kinase and other signaling pathways. J Cell Sci 116: 3471-3478, 2003.

438. Higuchi M, Masuyama N, Fukui Y, Suzuki A, and Gotoh Y: Akt mediates Rac/Cdc42-regulated cell motility in growth factor-stimulated cells and in invasive PTEN knockout cells. Curr Biol 11: 1958-1962, 2001.

439. Morales-Ruiz M, Fulton D, Sowa G, Languino LR, Fujio Y, Walsh K, and Sessa WC: Vascular endothelial growth factor-stimulated actin reorganization and migration of endothelial cells is regulated via the serine/threonine kinase Akt. Circ Res 86: 892-896, 2000.

440. Kim D, Kim S, Koh H, Yoon SO, Chung AS, Cho KS, and Chung J: Akt/PKB promotes cancer cell invasion via increased motility and metalloproteinase production. Faseb J 15: 1953-1962, 2001.

441. Hu X, Pandolfi PP, Li Y, Koutcher JA, Rosenblum M, and Holland EC: mTOR promotes survival and astrocytic characteristics induced by Pten/AKT signaling in glioblastoma. Neoplasia 7: 356-368, 2005.

442. Taylor G, Lehrer MS, Jensen PJ, Sun TT, and Lavker RM: Involvement of follicular stem cells in forming not only the follicle but also the epidermis. Cell 102: 451-461, 2000.

443. Clark AS, West K, Streicher S, and Dennis PA: Constitutive and inducible Akt activity promotes resistance to chemotherapy, trastuzumab, or tamoxifen in breast cancer cells. Mol Cancer Ther 1: 707-717, 2002.

444. Jordan NJ, Gee JM, Barrow D, Wakeling AE, and Nicholson RI: Increased constitutive activity of PKB/Akt in tamoxifen resistant breast cancer MCF-7 cells. Breast Cancer Res Treat 87: 167-180, 2004.

445. DeGraffenried LA, Fulcher L, Friedrichs WE, Grunwald V, Ray RB, and Hidalgo M: Reduced PTEN expression in breast cancer cells confers susceptibility to inhibitors of the PI3 kinase/Akt pathway. Ann Oncol 15: 1510-1516, 2004.

446. Hutchinson J, Jin J, Cardiff RD, Woodgett JR, and Muller WJ: Activation of Akt (protein kinase B) in mammary epithelium provides a critical cell survival signal required for tumor progression. Mol Cell Biol 21: 2203-2212., 2001.

447. Schwertfeger KL, Richert MM, and Anderson SM: Mammary gland involution is delayed by activated Akt in transgenic mice. Mol Endocrinol 15: 867-881., 2001.

448. Sun M, Wang G, Paciga JE, Feldman RI, Yuan ZQ, Ma XL, Shelley SA, Jove R, Tsichlis PN, Nicosia SV, and Cheng JQ: AKT1/PKBalpha kinase is frequently elevated in human cancers and its constitutive activation is required for oncogenic transformation in NIH3T3 cells. Am J Pathol 159: 431-437., 2001.

449. Nicholson KM, Streuli CH, and Anderson NG: Autocrine signalling through erbB receptors promotes constitutive activation of protein kinase B/Akt in breast cancer cell lines. Breast Cancer Res Treat 81: 117-128., 2003.

450. Kuo CJ, Chung J, Fiorentino DF, Flanagan WM, Blenis J, and Crabtree GR: Rapamycin selectively inhibits interleukin-2 activation of p70 S6 kinase. Nature 358: 70-73, 1992.

451. Law BK: Rapamycin: an anti-cancer immunosuppressant? Crit Rev Oncol Hematol 56: 47-60, 2005.

452. Eng CP, Sehgal SN, and Vezina C: Activity of rapamycin (AY-22,989) against transplanted tumors. J Antibiot (Tokyo) 37: 1231-1237, 1984.

453. Yu K, Toral-Barza L, Discafani C, Zhang WG, Skotnicki J, Frost P, and Gibbons JJ: mTOR, a novel target in breast cancer: the effect of CCI-779, an mTOR inhibitor, in preclinical models of breast cancer. Endocr Relat Cancer 8: 249-258., 2001.

454. Chan S, Scheulen ME, Johnston S, Mross K, Cardoso F, Dittrich C, Eiermann W, Hess D, Morant R, Semiglazov V, Borner M, Salzberg M, Ostapenko V, Illiger HJ, Behringer D, Bardy-Bouxin N, Boni J, Kong S, Cincotta M, and Moore L: Phase II Study of Temsirolimus (CCI-779), a Novel Inhibitor of mTOR, in Heavily Pretreated Patients With Locally Advanced or Metastatic Breast Cancer. J Clin Oncol, 2005.

455. Gingras AC, Gygi SP, Raught B, Polakiewicz RD, Abraham RT, Hoekstra MF, Aebersold R, and Sonenberg N: Regulation of 4E-BP1 phosphorylation: a novel two-step mechanism. Genes Dev 13: 1422-1437, 1999.

456. Franke TF, Kaplan DR, and Cantley LC: PI3K: downstream AKTion blocks apoptosis. Cell 88: 435-437, 1997.

457. Toker A, Meyer M, Reddy KK, Falck JR, Aneja R, Aneja S, Parra A, Burns DJ, Ballas LM, and Cantley LC: Activation of protein kinase C family members by the novel polyphosphoinositides PtdIns-3,4-P2 and PtdIns-3,4,5-P3. J Biol Chem 269: 32358-32367, 1994.

458. Reinhard C, Fernandez A, Lamb NJ, and Thomas G: Nuclear localization of p85s6k: functional requirement for entry into S phase. Embo J 13: 1557-1565, 1994.

459. Liu M, Howes A, Lesperance J, Stallcup WB, Hauser CA, Kadoya K, Oshima RG, and Abraham RT: Antitumor activity of rapamycin in a transgenic mouse model of ErbB2-dependent human breast cancer. Cancer Res 65: 5325-5336, 2005.

460. DeFatta RJ, Turbat-Herrera EA, Li BD, Anderson W, and De Benedetti A: Elevated expression of eIF4E in confined early breast cancer lesions: possible role of hypoxia. Int J Cancer 80: 516-522., 1999.

461. Kerekatte V, Smiley K, Hu B, Smith A, Gelder F, and De Benedetti A: The proto-oncogene/translation factor eIF4E: a survey of its expression in breast carcinomas. Int J Cancer 64: 27-31., 1995.

462. Li BD, Gruner JS, Abreo F, Johnson LW, Yu H, Nawas S, McDonald JC, and DeBenedetti A: Prospective study of eukaryotic initiation factor 4E protein elevation and breast cancer outcome. Ann Surg 235: 732-738; discussion 738-739., 2002.

463. Jiang H, Coleman J, Miskimins R, and Miskimins WK: Expression of constitutively active 4EBP-1 enhances p27Kip1 expression and inhibits proliferation of MCF7 breast cancer cells. Cancer Cell Int 3: 2., 2003.

464. van der Poel HG: Mammalian target of rapamycin and 3-phosphatidylinositol 3-kinase pathway inhibition enhances growth inhibition of transforming growth factor-beta1 in prostate cancer cells. J Urol 172: 1333-1337, 2004.

465. Sun SY, Rosenberg LM, Wang X, Zhou Z, Yue P, Fu H, and Khuri FR: Activation of Akt and eIF4E survival pathways by rapamycin-mediated mammalian target of rapamycin inhibition. Cancer Res 65: 7052-7058, 2005.

466. Breslin EM, White PC, Shore AM, Clement M, and Brennan P: LY294002 and rapamycin co-operate to inhibit T-cell proliferation. Br J Pharmacol 144: 791-800, 2005.

467. Zajchowski DA, Bartholdi MF, Gong Y, Webster L, Liu HL, Munishkin A, Beauheim C, Harvey S, Ethier SP, and Johnson PH: Identification of gene expression profiles that predict the aggressive behavior of breast cancer cells. Cancer Res 61: 5168-5178, 2001.

468. Lacroix M and Leclercq G: Relevance of breast cancer cell lines as models for breast tumours: an update. Breast Cancer Res Treat 83: 249-289, 2004.

469. Liu W, Li J, and Roth RA: Heregulin regulation of Akt/protein kinase B in breast cancer cells. Biochem Biophys Res Commun 261: 897-903, 1999.

470. Stoica GE, Franke TF, Moroni M, Mueller S, Morgan E, Iann MC, Winder AD, Reiter R, Wellstein A, Martin MB, and Stoica A: Effect of estradiol on estrogen receptor-alpha gene expression and activity can be modulated by the ErbB2/PI 3-K/Akt pathway. Oncogene 22: 7998-8011, 2003.

471. Vaupel P and Hockel M: Blood supply, oxygenation status and metabolic micromilieu of breast cancers: characterization and therapeutic relevance. Int J Oncol 17: 869-879, 2000.

472. Gillies RJ, Raghunand N, Karczmar GS, and Bhujwalla ZM: MRI of the tumor microenvironment. J Magn Reson Imaging 16: 430-450, 2002.

473. Noh WC, Mondesire WH, Peng J, Jian W, Zhang H, Dong J, Mills GB, Hung MC, and Meric-Bernstam F: Determinants of rapamycin sensitivity in breast cancer cells. Clin Cancer Res 10: 1013-1023, 2004.

474. Murga C, Laguinge L, Wetzker R, Cuadrado A, and Gutkind JS: Activation of Akt/protein kinase B by G protein-coupled receptors. A role for alpha and beta gamma subunits of heterotrimeric G proteins acting through phosphatidylinositol-3-OH kinasegamma. J Biol Chem 273: 19080-19085, 1998.

475. Bommakanti RK, Vinayak S, and Simonds WF: Dual regulation of Akt/protein kinase B by heterotrimeric G protein subunits. J Biol Chem 275: 38870-38876, 2000.

476. Datta K, Bellacosa A, Chan TO, and Tsichlis PN: Akt is a direct target of the phosphatidylinositol 3-kinase. Activation by growth factors, v-src and v-Ha-ras, in Sf9 and mammalian cells. J Biol Chem 271: 30835-30839, 1996.

477. Kraus MH, Yuasa Y, and Aaronson SA: A position 12-activated H-ras oncogene in all HS578T mammary carcinosarcoma cells but not normal mammary cells of the same patient. Proc Natl Acad Sci U S A 81: 5384-5388, 1984.

478. Smit MJ, Verzijl D, Casarosa P, Navis M, Timmerman H, and Leurs R: Kaposi's sarcoma-associated herpesvirus-encoded G protein-coupled receptor ORF74 constitutively activates p44/p42 MAPK and Akt via G(i) and phospholipase C-dependent signaling pathways. J Virol 76: 1744-1752, 2002.

479. Sable CL, Filippa N, Hemmings B, and Van Obberghen E: cAMP stimulates protein kinase B in a Wortmannin-insensitive manner. FEBS Lett 409: 253-257, 1997.

480. Edinger AL, Linardic CM, Chiang GG, Thompson CB, and Abraham RT: Differential effects of rapamycin on mammalian target of rapamycin signaling functions in mammalian cells. Cancer Res 63: 8451-8460, 2003.

481. Chan S: Targeting the mammalian target of rapamycin (mTOR): a new approach to treating cancer. Br J Cancer 91: 1420-1424, 2004.

482. Baldin V, Lukas J, Marcote MJ, Pagano M, and Draetta G: Cyclin D1 is a nuclear protein required for cell cycle progression in G1. Genes Dev 7: 812-821, 1993.

483. deGraffenried LA, Friedrichs WE, Russell DH, Donzis EJ, Middleton AK, Silva JM, Roth RA, and Hidalgo M: Inhibition of mTOR activity restores tamoxifen response in breast cancer cells with aberrant Akt Activity. Clin Cancer Res 10: 8059-8067., 2004.

484. Mondesire WH, Jian W, Zhang H, Ensor J, Hung MC, Mills GB, and Meric-Bernstam F: Targeting mammalian target of rapamycin synergistically enhances chemotherapy-induced cytotoxicity in breast cancer cells. Clin Cancer Res 10: 7031-7042., 2004.

485. Tsai EM, Wang SC, Lee JN, and Hung MC: Akt activation by estrogen in estrogen receptor-negative breast cancer cells. Cancer Res 61: 8390-8392, 2001.

486. Tomita Y, Morooka T, Hoshida Y, Zhang B, Qiu Y, Nakamichi I, Hamada K, Ueda T, Naka N, Kudawara I, and Aozasa K: Prognostic significance of activated AKT expression in soft-tissue sarcoma. Clin Cancer Res 12: 3070-3077, 2006.

487. Gort EH, Groot AJ, Derks van de Ven TL, van der Groep P, Verlaan I, van Laar T, van Diest PJ, van der Wall E, and Shvarts A: Hypoxia-inducible factor-1alpha expression requires PI 3-kinase activity and correlates with Akt1 phosphorylation in invasive breast carcinomas. Oncogene, 2006.

488. Roe FJ, Carter RL, Mitchley BC, Peto R, and Hecker E: On the persistence of tumour initiation and the acceleration of tumour progression in mouse skin tumorigenesis. Int J Cancer 9: 264-273, 1972.

489. Dvorak HF: Tumors: wounds that do not heal. Similarities between tumor stroma generation and wound healing. N Engl J Med 315: 1650-1659, 1986.